# GÜMÜŞHANE ÜNİVERSİTESİ

# FEN BİLİMLERİ ENSTİTÜSÜ DERGİSİ

Gümüşhane University Journal of Science and Technology Institute

GÜMÜŞHANE ÜNİVERSİTESİ FEN BİLİMLERİ ENSTİTÜSÜ YAYINI

PUBLISHED BY GÜMÜŞHANE UNIVERSITY SCIENCE AND TECHNOLOGY INSTITUTE

ISSN 2146 - 538X CMES 2018 SEMPOZYUM EK SAYISI YIL / YEAR : KASIM 2018

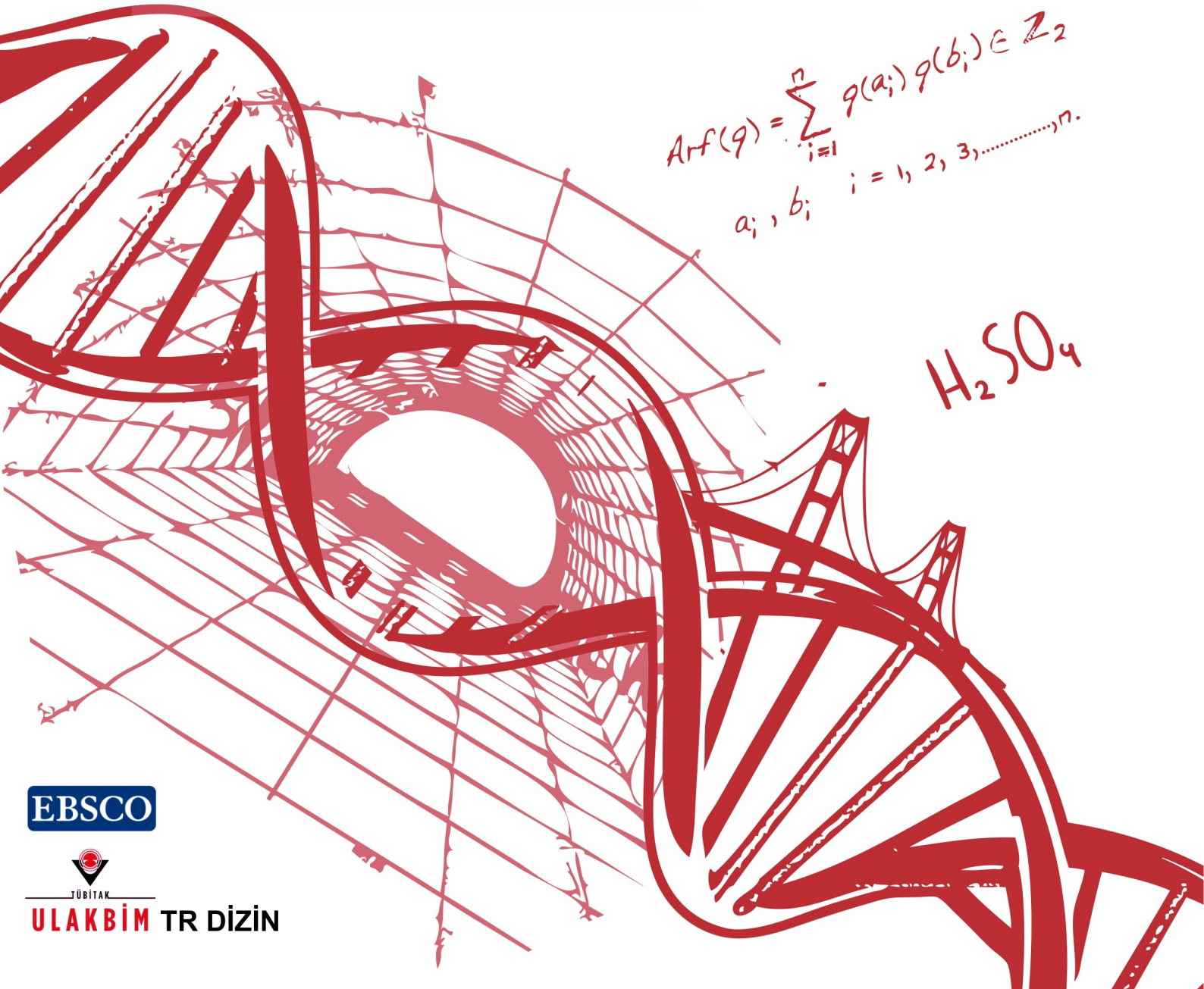


EBSCO

TÜBİTAK ULAKBİM TR DİZİN

*Gümüşhane University Journal of Science and Technology Institute*
**Gümüşhane Üniversitesi Fen Bilimleri Enstitüsü Dergisi**
*Published by Gümüşhane University Science and Technology Institute*
CMES 2018 Sempozyum Ek Sayısı / *CMES 2018 Special Issue*
Yıl/*Year*: Kasım 2018 / *November 2018*
Altı ayda bir yayımlanır/ *Published twice a year*
**ISSN 2146-538X**



**Yayın Türü / *Publication Type***
*Yaygın süreli ve hakemli/ Common term and refereed*

**Yayın Tarihi / *Publication Date***
**30 / 11 / 2018**

***Gümüşhane University Journal of Science and Technology Institute***
**Gümüşhane Üniversitesi Fen Bilimleri Enstitüsü Dergisi**
*Published by Gümüşhane University Science and Technology Institute*
CMES 2018 Sempozyum Ek Sayısı / *CMES 2018 Special Issue*
Yıl/*Year*: Kasım 2018 / *November 2018*
Altı ayda bir yayımlanır/ *Published twice a year*
**ISSN 2146-538X**

GÜMÜŞHANE ÜNİVERSİTESİ FEN BİLİMLERİ ENSTİTÜSÜ DERGİSİ
GÜMÜŞHANE UNIVERSITY JOURNAL OF SCIENCE AND TECHNOLOGY INSTITUTE
ISSN 2146 - 538X CMES 2018 SEMPOZYUM EK SAYISI YIL / YEAR: KASIM 2018

# İÇİNDEKİLER / *CONTENTS*

**Araştırma Makalesi** / *Research Article*

**GÜFBED/*GUSTIJ* (2018) CMES 2018 SEMPOZYUM EK SAYISI: 1-6**
DOI: 10.17714/gumusfenbil.430137 Araştırma Makalesi / *Research Article*

# Development of Internet Traffic Prediction Software Using Time-Series Multilayer Perceptron

## *Zaman Serili Çok Katmanlı Algılayıcı Kullanılarak Internet Trafik Tahmini Yazılımı Geliştirilmesi*

**Murat Can YÜKSEL[1,a], Mehmet Fatih AKAY[*1,b], Selami ÇİFTÇİ[2,c]**
[1]*Çukurova Üniversitesi, Mühendislik-Mimarlık Fakültesi, Bilgisayar Mühendisliği Bölümü, 01250, Adana*
[2]*Türk Telekom Araştırma ve Geliştirme Merkezi, 34394, İstanbul*

• Geliş tarihi / *Received*: 03.06.2018 • Düzeltilerek geliş tarihi / *Received in revised form*: 01.08.2018 • Kabul tarihi / *Accepted*: 12.09.2018

**Abstract**
Internet traffic prediction plays a fundamental role in network design, management, control and optimization. Although there exist several studies in litereture that focus on predicting Internet traffic using statistical and machine learning methods, to the best of our knowledge, a fully functional off-the-shelf software with different optimization capabilities has not been developed. The purpose of this study is to develop a new software for prediction of Internet traffic data based on time-series Multilayer Perceptron (MLP). The software includes features such as the optimization of the number of hidden layers and neurons in each layer and feedback delay optimization with respect to autocorrelations. The Internet traffic data from two different Internet Service Providers, varying by 1-hour and 5-minute time frequencies, have been used for testing the software. The datasets have been split into training and testing sets via 70-30% and 80-20% split ratios. The Mean Absolute Percentage Error (MAPE) has been utilized as the main error rate metric in order to evaluate the accuracy of the prediction models. It has been observed that the MAPE's of the Internet traffic prediction models change between 3.25 and 9.09. One can conclude that the developed software can be used for Internet traffic prediction within acceptable error rates.

**Keywords**: Multilayer perceptron, Traffic prediction, Time series

***Öz***
*Internet trafik tahmini ağ tasarımı, yönetimi, kontrolü ve optimizasyonunda temel bir rol oynamaktadır. Literatürde Internet trafiğinin istatistiksel ve makine öğrenme yöntemleri kullanılarak tahmin edilmesi üzerine odaklanan çeşitli çalışmalar bulunmasına rağmen, bilgimiz dahilinde farklı optimizasyon seçeneklerine sahip, tam işlevsel bir yazılım geliştirilmemiştir. Bu çalışmanın temel amacı, Internet trafik tahmini için zaman serili Çok Katmanlı Algılayıcı (Multilayer Perceptron, MLP) üzerine kurulu yeni bir yazılımın geliştirilmesidir. Yazılımın içerdiği özellikler arasında gizli katmanların ve her bir katman içerisindeki nöron sayısının optimize değerlerinin bulunmasının yanı sıra en uygun zaman gecikmesi değerlerinin otokorelasyonlara bağlı olarak optimize edilmesi de bulunmaktadır. Yazılımın test edilmesi amacıyla iki farklı İnternet Servis Sağlayıcısı'ndan tedarik edilen, zaman frekansları 1 saat ve 5 dakika şeklinde değişen Internet trafiği verileri kullanılmıştır. Veri setleri %70-30 ve %80-20 oranlarında eğitim ve test verileri olmak üzere iki kısma bölünmüştür. Tahmin modellerine ait performansın değerlendirilmesi amacıyla, ana metrik olarak Ortalama Mutlak Yüzde Hata (Mean Absolute Percentage Error, MAPE) hesaplanmıştır. Internet trafik tahmini modellerine ait MAPE değerlerinin 3.25 ve 9.09 arasında değiştiği gözlemlenmiştir. Elde edilen sonuçlara göre, geliştirilen yazılım kabul edilebilir hata oranları ile Internet trafiğinin tahmin edilmesi amacıyla kullanılabilir.*

***Anahtar kelimeler:*** *Çok katmanlı algılayıcı, Trafik tahmini, Zaman serileri*

[*b] Mehmet Fatih AKAY; mfakay@cu.edu.tr; Tel: (0322) 338 71 01; orcid.org/0000-0003-0780-0679
[a] orcid.org/0000-0003-4846-849X [c]orcid.org/0000-0003-0780-0679

## 1. Introduction

Internet traffic can be described as a general term including the transmission of any type of Internet data among different devices and systems. The timely and accurate prediction of Internet data usage is a topic which has great importance in both literature and industry. One of the most popular methods used for this purpose is Time Series Analysis, a research concept about processing data collected in certain time periods.

There exist several studies in literature about the prediction of the Internet data traffic with different methods. Table 1 displays a summary of these studies.

**Table 1.** Literature studies on network traffic prediction

| Study | Methods |
|---|---|
| Jiang et. al., 2009 | ARMA, |
| Chabaa et. al., 2010 | MLP, LM, |
| Liu et. al., 2011 | CTSA, SVM |
| Cortez et. al., 2012 | Naïve |
| Oliviera et. al., 2014 | MLP, SAE |
| Katris et. al., 2015 | FARIMA, |
| Daly, 2016 | NAR |
| Bian et. al., 2017 | LSTM |
| Sahrani et. al., 2017 | NARMA |
| Narejo et. al., 2018 | DBN |

**ANN**, Artificial Neural Network; **ARMA,** Auto-Regressive Moving Average; **CTSA**, Chaotic Time Series Analysis; **DBN,** Deep Belief Network; **FARIMA**, Autoregressive Fractionally Integrated Moving Average; **LM**, Levenberg-Marquardt; **LSTM,** Long-Short Term Memory, **MLP,** Multilayer Perceptron; **NAR,** Non-Linear Autoregressive Neural Networks; **NARMA,** Non-Linear Autoregressive Moving Average; **RBP**, Resilient Back Propagation; **SAE**, Stacked Autoencoder; **SVM**, Support Vector Machine;

Although there exist several academic studies on Internet traffic prediction, the efforts are limited to developing prediction models with various methods and doing comparisons. The main purpose of this study is to develop a standalone desktop application which can perform time-series prediction using MLP, a very common machine learning method that is often used for neural network-based studies in literature. It is also aimed to develop the software with a variety of options including customization of train/test ratio, optimization of the number of hidden layers, the amount of neurons in each layer, feedback delays and training functions.

Section 2 gives brief information about the datasets and software development. Section 3 presents the details of the software features and sample results. Section 4 concludes the paper.

## 2. Datasets and Software Development

### *2.1. Dataset Generation*

In this study, four data sets that have been obtained from two different Internet Service Providers have been used in order to create and evaluate prediction models. Two out of the four data sets (being referred to as A1H and B1H, respectively) consist of time-periodical data being measured in 1-hour time intervals while the time interval is 5 minutes for the other two data sets (being referred to as A5M and B5M, respectively). Table 2 shows the statistics of the data sets used for testing the prediction models generated by the software.

**Table 2.** Dataset statistics

| Name | Number of Samples | Time Interval | Data Format | Data Type |
|---|---|---|---|---|
| A1H | 1231 | 1 hour | Bit | Download |
| A5M | 14772 | 5 minutes | Bit | Download |
| B1H | 1657 | 1 hour | Bit | Download |
| B5M | 19888 | 5 minutes | Bit | Download |

### *2.2. Software Development*

The development of the software has been carried out using MATLAB programming language, MATLAB R2017a Compiler and Neural Network Toolbox. The design of the user interface has also been done in the same environment. The performance of the prediction models has been evaluated by calculating MAPE, the formula of which is given in (1).

$$MAPE = \frac{100}{N}\sum_{t=1}^{n}\left|\frac{A_t - P_t}{A_t}\right| \quad (1)$$

In (1), $A_t$ is the actual value, $P_t$ is the predicted value and N is the number of samples in the test set.

## 3. Features of the Software

### *3.1. Software Components*

The main features which have been developed are listed below.

#### *3.1.1. Train-Test ratio adjustment*

The amount of rows in the data set used for training and testing the network can be adjusted either with the exact amount or the percentage of the data set rows which are intented to be used as the training data whilst building the prediction models.

#### *3.1.2. The number of neurons in each hidden layer*

The amount of neurons in the hidden layers, which are the structures between the input and the output layers in an MLP network, can be adjusted either manually or by the optimization algorithms which are applied the training part of the data set when selected. Two main optimization options which have been provided by the software are 80-20% sequential data division and 10-fold cross validation. The software finds the optimum number of neurons in every hidden layer by creating sub-models and comparing the error rates produced by those sub-models. Afterwards, the optimized hidden layer size is used in order to build the main prediction model with the purpose of obtaining the best possible prediction accuracy.

#### *3.1.3. The number of hidden layers*

The option of using 1, 2 or 3 hidden layers in the neural network can be chosen by the user.

#### *3.1.4. The feedback delay values*

The feedback delays, being one of commonly-used criteria in time series analysis, can be decided with several options. The feedback delay optimization options are based on making use of dataset autocorrelation. The autocorrelation value of each row in the training data can be calculated by the software and displayed by clicking on the "Data Set AC" button. The main options for optimizing the feedback delays are using the indices which have a higher autocorrelation than a certain threshold, or sorting all autocorrelations in a descending order and using an array of best indices with the highest autocorrelations. These options also create an opportunity to test whether the autocorrelation has an effect on finding the optimum feedback delays.

#### *3.1.5. Network training function*

The activation function used for the neural network, which is also decided by the user.

#### *3.1.6. Save-Load option*

The user is able to create a brand-new prediction model and save the network settings after the prediction, then use the same settings in order to produce the same prediction results.

### *3.2. Prediction Steps*

The prediction steps followed by the software can be seen below.

- The neural network is created with respect to the initial parameters which are decided manually or automatically by the user's preference.
  - In the manual mode, the dataset is divided as training and testing sections. The neural network is created with respect the values entered manually on the user interface.
  - In the optimization mode, the training and testing data division is similar to the manual mode. In order to apply optimization, the training data is also divided into sections depending on the selected optimization option. The feedback delays are generated with respect to the training data indices with the best autocorrelations. Subsequent to the data preparation process and feedback delay selection, the software begins creating sub-networks, each of them built by a unique hidden layer size. Finally, the main network is created with the number of neurons that yielded the best performance in the sub-networks.
- The software opens a new window for displaying the comparison between the predicted values and the actual test data both in a table and a line graph, along with the calculated *MAPE*.
- The option to save the network settings is presented to the user in the results screen.

In order to test the software, eight different prediction models have been created using the given data sets with different train/test split ratios. Table 3 shows the testing results for each data set.

**Table 3.** *MAPE*'s for each data set

| Data Set | Train-Test Ratio | *MAPE* |
|---|---|---|
| A1H | 70-30 | 9.09 |
| A1H | 80-20 | 6.63 |
| A5M | 70-30 | 5.53 |
| A5M | 80-20 | 3.24 |
| B1H | 70-30 | 6.20 |
| B1H | 80-20 | 4.30 |
| B5M | 70-30 | 8.06 |
| B5M | 80-20 | 6.90 |

### *3.3. Screen Shots*

Figure 1 through Figure 5 show some screen shots of the developed software.

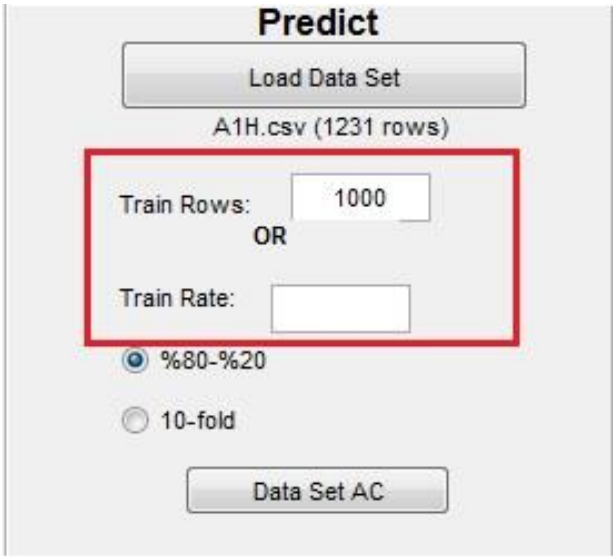


**Figure 1.** Adjustment of train-test ratio

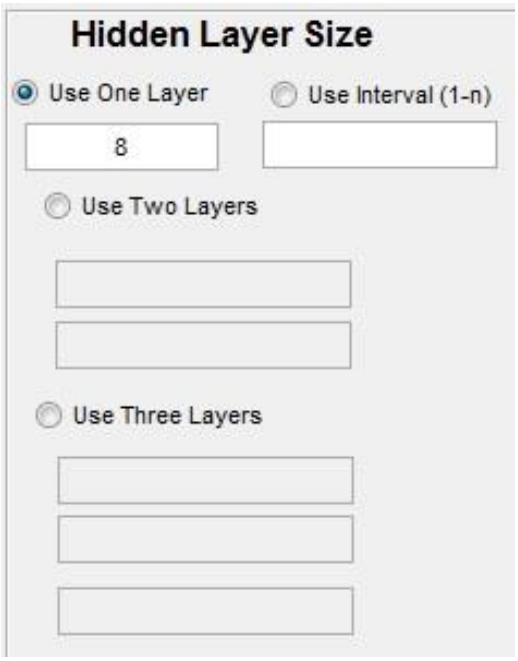


**Figure 2.** Number of hidden layers and neurons

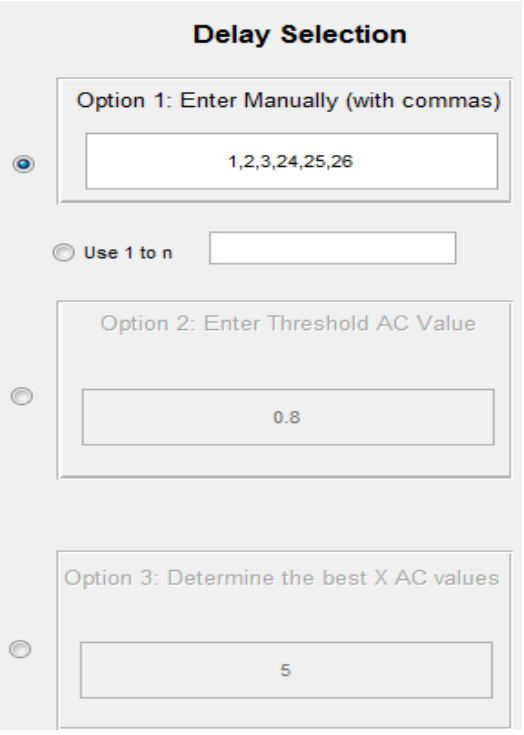


**Figure 3.** Feedback delay selection

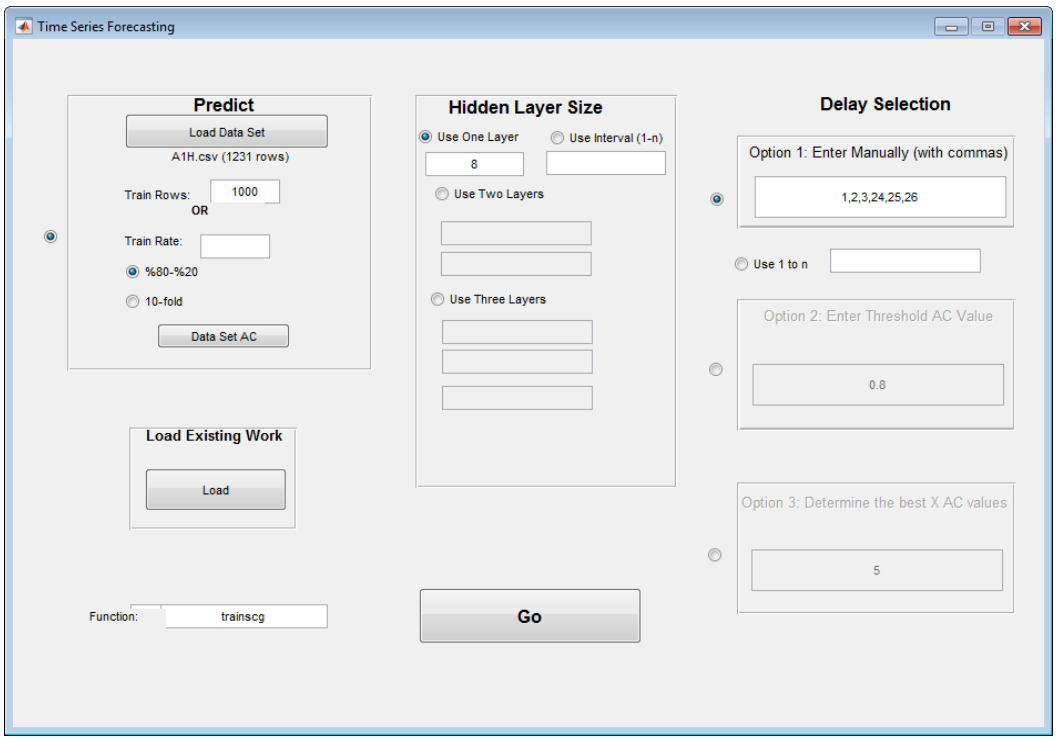


**Figure 4.** User interface - 1

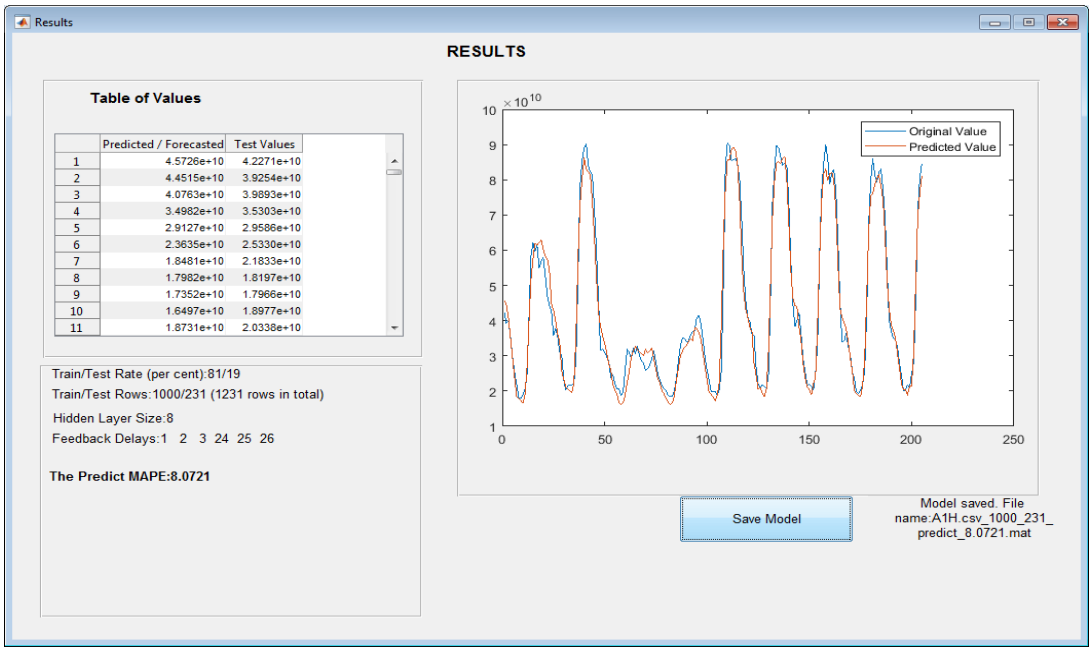


**Figure 5.** User interface - 2

## 4. Conclusion

The purpose of this study is the development of a new software based on machine learning and time series analysis, which can predict the Internet data traffic. The project has been developed using MATLAB programming language and the Neural Network Toolbox. The main options of the software include the optimization of hidden layer size, the number of hidden layers and the feedback delays. The performance of each prediction is calculated by using *MAPE*, which has been used as the main error metric. Using four different data sets consisting of time-series data, the models produce prediction *MAPE* values between 3.25 and 9.09. It can be concluded that the software can be used for the network traffic prediction within the acceptable error rates.

**Acknowledgment**

The authors would like to thank Cukurova University Scientific Research Projects Center for supporting this work under grant no. FYL-2018-10374.

**References**

Bian, G., Liu, J., ve Lin, W., 2017. Internet Traffic Forecasting using Boosting LSTM Method. DEStech Transactions on Computer Science and Engineering.

Chabaa, S., Zeroual, A. ve Antari, J., 2010. Identification and Prediction of Internet Traffic Using Artificial Neural Networks. Journal of Intelligent Learning Systems and Applications. 2(3), 147-155.

Cortez, P., Rio, M., Rocha, M. ve Sousa, P., 2012. Multi-scale Internet Traffic Forecasting Using Neural Networks and Time Series Methods. Expert Systems. 29(2), 143-155.

Daly, C., 2016. H. 265 Video Traffic Prediction Using Neural Networks. Georgia Southern University Research Symposium. s127.

Jiang, M., Wu, C. M., Zhang, M. ve Hu, D. M., 2009. Research on the Comparison of Time Series Models for Network Traffic Prediction. Acta Electronic Sinica. 37(1), 2353-2358.

Katris, C., ve Daskalaki, S., 2015. Comparing forecasting approaches for Internet traffic. Expert Systems with Applications, 42(21), 8172-8183.

Liu, X., Fang, X., Qin, Z., Ye, C., ve Xie, M., 2011. A Short-Term Forecasting Algorithm for Network Traffic Based on Chaos Theory and SVM. Journal of Network and Systems Management. 19(4), 427-447.

Narejo, S., ve Pasero, E., 2018. An Application of Internet Traffic Prediction with Deep Neural Network. In Multidisciplinary Approaches to Neural Computing. pp. 139-149. Springer, Cham.

Oliveira, T. P., Barbar, J. S. ve Soares, A. S., 2014. Multilayer Perceptron and Stacked Autoencoder for Internet Traffic Prediction. In Network and Parallel Computing. pp. 61-71.

Sahrani, M. N., Zan, M. M. M., Yassin, I. M., Zabidi, A., ve Ali, M. S. A. M., 2017. Artificial Neural Network Non-linear Auto Regressive Moving Average (NARMA) Model for Internet Traffic Prediction. Journal of Telecommunication, Electronic and Computer Engineering. 9(1-3), 145-149.

**GÜFBED/*GUSTIJ* (2018) CMES 2018 SEMPOZYUM EK SAYISI: 7-10**
DOI: 10.17714/gumusfenbil.435897 Araştırma Makalesi / *Research Article*

# Development of Physical Fitness Prediction Models for Turkish Secondary School Students Using Machine Learning Methods

## *Türk Ortaokul Öğrencileri için Makine Öğrenmesi Yöntemleri Kullanılarak Fiziksel Uygunluk Tahmin Modelleri Geliştirme*

**M.Fatih AKAY*[1,a], Ebru ÇETIN[2,b], İmdat YARIM[2,c], Özge BOZKURT[1,d], Sevtap ERDEM[1,e]**
[1] *Department of Computer Engineering, Çukurova University, Adana, Turkey*
[2] *School of Physical Education and Sport, Gazi University, Ankara, Turkey*

• Geliş tarihi / *Received*: 30.06.2018 • Düzeltilerek geliş tarihi / *Received in revised form*: 01.08.2018 • Kabul tarihi / *Accepted*: 12.09.2018

**Öz**
Fiziksel uygunluk, belirli testlerle ölçülebilen sağlık veya beceri ile ilgili bir dizi özelliktir. Fiziksel uygunluğu korumak sağlık ve esenlik için çok önemlidir. Ancak, fiziksel uygunluğun ölçülmesi profesyonel ekipman, deneyimli personel ve çok zaman gerektirdiğinden, araştırmacıların fiziksel uygunluğu belirlemek için farklı yollara ihtiyaçları vardır. Bu çalışmanın amacı, Destek Vektör Makineleri (SVM), Radyal Tabanlı Fonksiyon Sinir Ağı (RBFNN) ve Ağaç Artımı (TB) gibi makine öğrenme yöntemlerini kullanarak Türk ortaokul öğrencilerinin fiziksel uygunluğunu tahmin etmek için yeni tahmin modelleri geliştirmektir. Veri seti 30m hız, 20m aşama koşusu, denge ve çeviklik testlerinin sonuçlarından oluşan veriyi içermektedir. Tahmin modellerini geliştirmek için kullanılan tahmin değişkenleri cinsiyet, yaş, boy, kilo, vücut yağı, 30 saniyedeki mekik ve şınav sayılarından oluşmaktadır. Tahmin modellerinin performansı Ortalama Karesel Hata (*RMSE*) kullanılarak hesaplanmıştır. Sonuçlar, SVM tabanlı tahmin modellerinin, RBFNN ve TB'ye dayanan diğer modelleri geride bıraktığını göstermektedir. Ayrıca, fiziksel uygunluk tahmini için vücut yağı, mekik ve şınav gibi tahmin değişkenlerinin birlikte kullanılması durumunda sonuçlar üzerinde önemli bir rol oynadığını gösterilmiştir.

**Anahtar kelimeler:** Fiziksel uygunluk, Makine öğrenmesi, Tahmin.

***Abstract***
*Physical fitness is a set of attributes that are either health or skill-related which can be measured with specific tests. Maintaining physical fitness is essential for health and wellbeing. However, since measurement of physical fitness requires improved professional equipment, experienced staff and lots of time, researchers need different ways to determine physical fitness. The aim of this study is to develop new prediction models for predicting the physical fitness of Turkish secondary school students by using machine learning methods including Support Vector Machines (SVM), Radial Basis Function Neural Network (RBFNN) and Tree Boost (TB). The dataset comprises data of various number of subjects according to the target variables such as the test scores of the 30m speed, 20m stage run, balance and agility. The predictor variables used to develop the prediction models are gender, age, height, weight, body fat, number of curl-up and push-ups in 30 seconds. Root Mean Square Error (RMSE) has been utilized to assess the performance of the prediction models. Based on the results we can conclude that SVM based prediction models outperform other models based on RBFNN and TB. Also, the predictor variables body fat, push-up and curl-up play a significant role when used all together for physical fitness prediction.*

***Keywords**: Physical fitness, Machine learning, Prediction.*

*[a] Mehmet Fatih AKAY; makay@cu.edu.tr; Tel: (0322) 338 71 01; orcid.org/0000-0003-0780-0679
[b] orcid.org/0000-0001-7190-4929 [c] orcid.org/0000-0003-4794-129x [d] orcid.org/0000-0001-8633-6696
[e] orcid.org/0000-0002-9332-2070

## 1. Introduction

Physical fitness is a state of health and well-being and, more specifically, the ability to perform aspects of sports, occupations and daily activities. Physical fitness plays an important role in our lives and can improve our health and reduce the risk of developing several diseases like type 2 diabetes, cancer and cardiovascular disease. Fitness education and student fitness assessments offer students an opportunity to assess, track, and improve their fitness level (Hoffman, 2006). However, physical fitness assessment using test protocols requires improved professional equipment, experienced staff and lots of time. Therefore, several physical fitness prediction models using statistical and machine learning methods have been proposed in literature. In (Ahmed and Loutfi, 2013), Case-Based Reasoning (CBR) approach to identify physical activity of elderly based on pulse rate has been proposed. The CBR approach has been compared with the two popular classification techniques including SVM and Neural Network (NN) on 24 subjects. In (Dijkhuis, Blssuw, Ittersum and Aiello, 2018), an activity tracker to record participants' daily step count has been used as input for a coaching session. The gathered step count data was used to train eight different machine learning algorithms to make hourly estimations of the probability of achieving a personalized, daily steps threshold for the number of 48 subjects. In (Fergus et al., 2015), a supervised machine learning approach has been adopted by a set of activities and features suitable for measuring physical activity and evaluates the use of a Multilayer Perceptron neural network for the number of 28 subjects. In (Reichherzer et all., 2017), the data analysis methods have been used to train a classifier for records with the individuals, their physical activities, and conditions under which they were performed. Four different machine learning algorithms that Decision Tree (DT), Random Forest (RF), SVM, Naive Bayesian (NB) methods were used to make predictions for 29 participants.

The limitations of the studies in literature are as follows: All the studies concentrate on classifying physical activity levels rather than predicting the actual test results. As we can observe from literature reviews, the number of subject in the datasets is limited (less than 50) and the developed models require the subject to complete several exercises in order to have physical activity level rates.

In this study, the dataset which is covering approximately 400 subjects, was analyzed using rigorous data science techniques, which led to an improved understanding of activity types and features. A series of machine learning analyses were performed to develop improved prediction accuracy. Unlike previous studies, the predictor variables and the prediction methods were expanded to have more comprehensive prediction. This study proposes to develop new prediction models for Turkish secondary school students by using SVM, RBFNN and TB.

## 2. Dataset Generation

The dataset comprises of different number of subjects depending on the target variables of healthy secondary school students. Different physical exercise tests were applied on the subjects for measuring their physical fitness. A consent participant form was signed by all subjects participating in this study. Participants were assigned to perform the following core stabilization assessments 30 meter (m) Speed, 20m Stage Run, Balance and Agility Tests to predict physical fitness.

## 3. Results and Discussion

Three different machine learning methods including SVM, RBFNN and TB have been employed in order to develop physical fitness prediction models. SVM is a state-of-the-art regression method which is widely utilized in many application areas due to its high accuracy (Chuang et al., 2011; Wang, 2005; Abut et al., 2015). RBFNN is a particular type of neural network and is becoming an increasingly popular neural network with diverse applications. RBFNN consists of three layers: an input layer, a hidden (kernel) layer with a non-linear RBFNN activation function and a linear output layer. The nodes within each layer are fully connected to the previous layer (Hannan et al., 2010). The TB is a technique for improving the accuracy of a predictive function by applying the function repeatedly in a series and combining the output of each function with weighting so that the total error of the prediction is minimized.

Eight prediction models have been produced by using combinations of the predictor variables. *RMSE*, the equation which is given below, has been used to assess the performance of the prediction models.

$$RMSE = \sqrt{\frac{1}{n}\sum_{i=1}^{n}\left(Y - Y'\right)^2} \quad (1)$$

In (1), $Y$ is the measured value, $Y'$ is the predicted value, and $n$ is the number of samples in a test subset.

Table 1 shows the physical fitness prediction models. Table 2 shows the results for each model.

**Table 1.** Physical fitness prediction models

| Model Number | Predictor Variables |
|---|---|
| **1** | Gender, Age, Weight, Height |
| **2** | Gender, Age, Weight, Height, Curl-up |
| **3** | Gender, Age, Weight, Height, Push-up |
| **4** | Gender, Age, Weight, Height, Body Fat |
| **5** | Gender, Age, Weight, Height, Curl-up, Push-up |
| **6** | Gender, Age, Weight, Height, Curl-up, Body Fat |
| **7** | Gender, Age, Weight, Height, Push-up, Body Fat |
| **8** | Gender, Age, Weight, Height, Curl-up, Push-up, Body Fat |

**Table 2.** *RMSE* values of physical fitness prediction models

| Model No | 30m Speed (s) | | | 20m Stage Run (s) | | | Balance (s) | | | Agility (s) | | |
|---|---|---|---|---|---|---|---|---|---|---|---|---|
| | **SVM** | **RBF** | **TB** | **SVM** | **RBF** | **TB** | **SVM** | **RBF** | **TB** | **SVM** | **RBF** | **TB** |
| **1** | 0.51 | 0.55 | 0.58 | 2.11 | 2.17 | 2.17 | 6.65 | 7.41 | 9.85 | 1.76 | 1.83 | 1.86 |
| **2** | 0.47 | 0.53 | 0.50 | 2.06 | 2.13 | 2.14 | 6.60 | 6.99 | 9.83 | 1.63 | 2.48 | 1.72 |
| **3** | 0.49 | 0.50 | 0.53 | 2.07 | 2.17 | 2.11 | 6.62 | 7.10 | 9.82 | 1.68 | 1.87 | 1.75 |
| **4** | 0.48 | 0.51 | 0.54 | 2.06 | 2.22 | 2.22 | 6.70 | 6.94 | 9.80 | 1.74 | 1.87 | 1.85 |
| **5** | 0.44 | 0.47 | 0.46 | 2.04 | 2.14 | 2.09 | 6.62 | 7.65 | 9.81 | 1.58 | 1.69 | 1.64 |
| **6** | 0.44 | 0.48 | 0.47 | 2.04 | 2.14 | 2.16 | 6.67 | 7.43 | 9.84 | 1.61 | 1.76 | 1.72 |
| **7** | 0.46 | 0.58 | 0.49 | 2.05 | 2.18 | 2.15 | 6.62 | 7.44 | 9.81 | 1.68 | 1.84 | 1.76 |
| **8** | 0.43 | 0.49 | 0.45 | 2.03 | 2.22 | 2.12 | 6.63 | 9.69 | 9.80 | 1.59 | 1.90 | 1.65 |

SVM based models usually outperform RBFNN based and TB based models by yielding lower *RMSE*'s. The worst performance has been observed in TB based models. The predictor variables number of curl-up and push-ups in 30 seconds and body fat play a significant role in physical fitness prediction.

## 4. Conclusion

This is an initial study showing that SVM is a viable method that can be safely used to predict the physical fitness of Turkish secondary school students. In this context, several models have been developed to predict the results of 30m Speed, 20m Stage Run, Balance and Agility tests. However, future work is definitely required to improve the accuracy of physical fitness prediction models. Future work will include developing deep learning based physical fitness prediction models as well as integrating feature selection algorithms.

## Acknowledgment

The current study has been financed by Cukurova University Research Projects Center under grant no. FYL-2018-10430.

## References

Abut, F., Akay, M.F., Sow, B. and George, J., 2015. Support Vector Machines for Prediction of Endurance Times Involving Isometric Side Bridge Exercise Test, Third International Symposium on Engineering, Artificial Intelligence & Applications (ISEAIA2015), North Cyprus, pp. 7-9.

Ahmed, M.U., Loutfi, A., 2013. Pyhsical Activity Identification using Supervised Machine Learning and based on Pulse Rate, International Journal of Computer Science and Applications, Publication 4(7).

Chuang, C.C., Lee, Z.C., 2011. Hybrid robust support vector machines for regression without liers, Applied Soft Computing.

Dijkhuis, T.B., Blaauw, F., Ittersum, M. W., Aiello, M., 2018. Personalized Physical Activity Coaching : A Machine Learning Approach, in Sensors, 18(2), p.623.

Fergus, P., Hussain, A., Hearty, J., Fairclough, S., Boddy, L., Machintoch, K.A., Stratton,G., Ridgers, N.D. and Radi, N., 2015. A Machine Learning Approach to Measure and Monitor Physical Activity in Children to Help Fight Overweight and Obesity, Intelligent Computing Theories and Methodologies: 11th International Conference, ICIC 2015, Fuzhou, China, pp. 676-688.

Hannan, S.A., Manza, R.R., Ramteke, R.J., 2010. Generalized Regression Neural Network and Radial Basis Function for Heart Disease Diagnosis, International Journal of Computer Applications, Volume 13, Issue 2, ISBN: 10.5120/1325-1799.

Hoffman, J., 2006. Norms for Fitness, Performance and Health, Human Kinetics Publishers, ISBN-13: 9780736054836, 97–104.

Reichherzer, T., Timm, M., Earley, N., Reyes, N., 2017. Using Machine Learning Techniques to Track Individuals & Their Fitness Activities, In A. Bossard, G. Lee, & L. Miller (Eds.), Proceedings of 32nd International Conference on Computers and Their Applications, Honolulu, Hawaii, USA, pp. 119–124.

Wang, L., 2005. Support Vector Machines: Theory and Applications, Springer Science & Business Media, Volume 177, 1st Edition: ISBN: 978-3-540-32384-6.

**GÜFBED/*GUSTIJ* (2018) CMES 2018 SEMPOZYUM EK SAYISI: 11-14**
DOI: 10.17714/gumusfenbil.435854 Araştırma Makalesi / *Research Article*

# Prediction of Hamstring and Quadriceps Muscle Strength Using Multiple Linear Regression

## *Hamstring ve Kuadriseps Kas Gücünün Çoklu Doğrusal Regresyon Kullanılarak Tahmin Edilmesi*

**Mehmet Fatih AKAY*[1,a], Murat Can YÜKSEL[1,b], Sevtap ERDEM[1,c], Ebru ÇETİN[2,d], İmdat YARIM[2,e]**
[1]*Çukurova Üniversitesi, Mühendislik-Mimarlık Fakültesi, Bilgisayar Mühendisliği Bölümü, 01250, Adana*
[2]*Gazi Üniversitesi, Beden Eğitimi ve Spor Yüksekokulu, 06560, Ankara*

• Geliş tarihi / *Received*: 23.06.2018 • Düzeltilerek geliş tarihi / *Received in revised form*: 08.09.2018 • Kabul tarihi / *Accepted*: 17.09.2018

**Abstract**
The strength of hamstring and quadriceps muscles plays an important role for athletes and sportspeople in determining their performance. The purpose of this study is to predict the hamstring and quadriceps muscle strength using Multiple Linear Regression (MLR). The dataset used for this study includes the data of 70 athletes consisting of the features gender, sports branch, height, weight and age, as well as the hamstring and quadriceps muscle strength values measured with two types of activities (static training and classic training) used as the target variables. MLR has been used for the development of prediction models using different types of validation options including cross-validation and random percentage data split. The Root Mean Square Error (RMSE) has been utilized as the main error metric for evaluating the performance of the prediction models. The RMSE values of the prediction models range between 14.91 and 32.41 Nm, showing that in addition to machine learning methods, MLR can also be used for predicting the hamstring and quadriceps muscle strength with acceptable error rates.

**Keywords**: Multiple linear regression, Hamstring, Quadriceps, Prediction

***Öz***
*Hamstring ve Kuadriseps kas gruplarının gücü, atletler ve sporcuların performanslarının değerlendirilmesi için önemli bir rol oynamaktadır. Bu çalışmanın amacı, Hamstring ve Kuadriseps kas gücünün Çoklu Doğrusal Regresyon (Multiple Linear Regression, MLR) kullanılarak tahmin edilmesidir. Bu çalışma için kullanılan veri seti 70 sporcuya ait cinsiyet, spor dalı, boy, ağırlık ve yaş bilgilerinin yanı sıra hedef değişkenleri olarak iki tip fiziksel aktivite (statik antrenman ve klasik antrenman) ile ölçülen hamstring ve kuadriseps kas gücü değerlerinden oluşmaktadır. Tahmin modellerinin oluşturulmasında MLR ile birlikte çapraz doğrulama ve rastgele veri dağılımı olmak üzere farklı doğrulama seçenekleri kullanılmıştır. Tahmin modellerinin değerlendirilmesi amacıyla Ortalama Karesel Hata (Root Mean Square Error, RMSE) değerleri hesaplanmıştır. RMSE değerlerinin 14.91ve 32.41 Nm olarak değişmesi, MLR'nin kabul edilebilir hata oranlarıyla, hamstring ve kuadriseps kas gücünün tahmininde makine öğrenme yöntemlerine alternatif olarak kullanılabilirliğini göstermektedir.*

***Anahtar kelimeler:*** *Çoklu doğrusal regresyon, Hamstring, Kuadriseps, Tahmin*

*[a] Mehmet Fatih AKAY; mfakay@cu.edu.tr; Tel: (0322) 338 71 01; orcid.org/0000-0003-0780-0679
[b] orcid.org/0000-0003-4846-849X [c] orcid.org/0000-0002-9332-2070 [d] orcid.org/0000-0001-7190-4929
[e] orcid.org/0000-0003-4794-129X

## 1. Introduction

Muscular strength is a term that is used to explain the amount of force which can be applied by a muscle against a resistance in a single effort (Akay et. al., 2017). The strength that a muscle can produce during activities can be important in many cases such as athletism, team sports and any type of personal training or physical movement. Especially in sports, the strength of the hamstring and quadriceps muscles has a critical effect on the performance, speed and stamina of sportspeople (Sow et. al., 2017).

The absolute measurement of the strength of hamstring and quadriceps muscles can be made in the laboratories specifically designed for this purpose using advanced isometric devices called isokinetic dynamometers (Sow et. al., 2017). Although this method gives very accurate results, it requires expensive equipment, lots of time and trained staff while measuring the muscle strength. Therefore, the usage of prediction models would be a better choice than the direct measurement.

There have been several studies carried out in literature about the prediction of muscle strength using MLR or machine learning methods, as shown in Table 1.

**Table 1.** Literature review

| Study | Year | Method | Measured Strength | Metric | Value |
|---|---|---|---|---|---|
| Abadie et al. | 2000 | MLR | CPS, SPS, KES | *R* | 0.94 |
| Horvat et al. | 2003 | MLR | Bench Press | *R* | 0.91 |
| Harbo et al. | 2012 | MLR | Knee, Shoulder, Hip, Ankle, Elbow and | *R* | 0.79 |
| Muraki et al. | 2013 | MLR | KES | *R* | 0.57 |
| Sow et al. | 2017 | SVM | Hamstring & Quadriceps Muscles | *RMSE* | 15.19 |
| Akay et al. | 2017 | SVM | Hamstring & Quadriceps Muscles | *RMSE* | 15.55 |

**CPS,** Chest Press Strength; **KES,** Knee Extension Strength; **MLR,** Multiple Linear Regression; ***RMSE*,** Root Mean Square Error; ***R*,** Multiple Correlation Coefficient; **SVM,** Support Vector Machines; **SPS,** Shoulder Press Strength.

This study proposes to develop new prediction models for determination of hamstring and quadriceps muscle strength with the usage of MLR, with similar or better error rates as in the studies in literature. Eight different prediction models have been built using gender, sports branch, height, weight and age as predictor variables while the measured strength of hamstring and quadriceps muscles during different types of training as the target variables. The *RMSE*'s produced by the prediction models vary between 14.91 Nm and 32.41 Nm.

The rest of the paper is organized as follows. Section 2 describes dataset generation. Section 3 presents results and discussion. Finally, Section 4 concludes the paper.

## 2. Dataset Generation

In order to create prediction models, the data of 75 college-aged athletes has been used. The muscle strength values which have been used as the target variables are measured with the help of different physical activities including a light run for 5 minutes (classic training, CT), a 5-minute light run followed by 4-minute active stretching (static training, ST), as well as the static training followed by 5 and 15-minute resting periods (ST-5min and ST-15min).

Table 2 shows statistics of the dataset.

**Table 2.** Statistics of the dataset

| Feature | Minimum | Maximum | Mean | Standard Deviation |
|---|---|---|---|---|
| Gender | 0 | 1 | - | - |
| Sports branch | 0 | 16 | 5.94 | 4.67 |
| Height (m) | 1.57 | 2.02 | 1.71 | 0.07 |
| Weight (kg) | 45 | 93 | 62.04 | 11.27 |
| Age (Year) | 19 | 38 | 21.78 | 3.06 |
| M01 (Nm) | 50.10 | 195.90 | 111.84 | 36.10 |
| M11 (Nm) | 61.20 | 197.70 | 111.61 | 36.44 |
| M21 (Nm) | 56.70 | 202.20 | 112.59 | 36.53 |
| M31 (Nm) | 46.50 | 194.60 | 113.16 | 36.44 |
| M02 (Nm) | 72.20 | 285.20 | 154.77 | 54.80 |
| M12 (Nm) | 85.20 | 278.10 | 157.01 | 54.41 |
| M22 (Nm) | 85.70 | 301.20 | 161.76 | 56.62 |
| M32 (Nm) | 83.40 | 280.20 | 157.88 | 51.95 |

**M01,** Hamstring strength (CT)**; M11,** Hamstring strength (ST)**; M21,** Hamstring strength (ST-5min)**; M31,** Hamstring strength (ST-15min)**; M02,** Quadriceps strength (CT)**; M12,** Quadriceps strength (ST)**; M22,** Quadriceps strength (ST-5min)**; M32,** Quadriceps strength (ST-15min)

## 3. Results and Discussion

In this study, eight different prediction models have been built with respect to the muscle type (hamstring and quadriceps) and the type of physical activity (CT, ST, ST-5min and ST-15min). Five validation options including no validation, 5-fold cross-validation, 10-fold cross-validation, 70-30% random data division and 80-20% random data division have been applied, which yields a total number of 40 evaluations overall.

Comparison of the models has been made by calculating the *RMSE* of each model. Figure 1 and Figure 2 show the visual comparison of the *RMSE*'s of the prediction models.

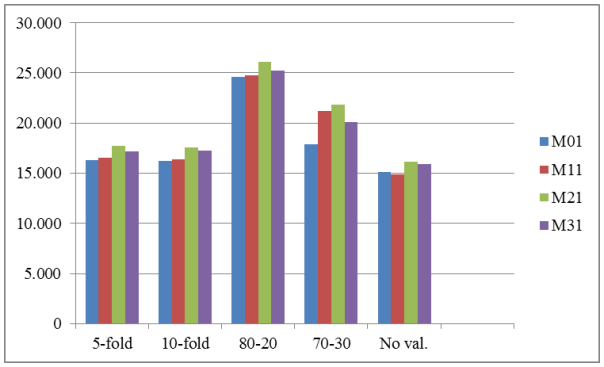


**Figure 1.** *RMSE* values of hamstring muscle strength prediction models

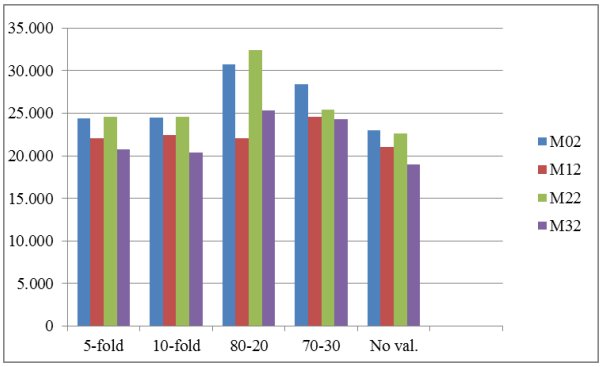


**Figure 2.** *RMSE* values of quadriceps muscle strength prediction models

- According to the *RMSE* of each prediction model, it has been observed that in general, the models which are used for prediction of hamstring muscle strength yield better results than the ones used for predicting quadriceps muscle strength. The models from M01 to M31 give a mean of *18.95 Nm* as *RMSE* for hamstring muscle strength prediction while the models from M02 to M32 give *24.13 Nm* for quadriceps muscle strength prediction.
- Among the prediction models, model M01 generates the lowest arithmetical mean *RMSE* with *18.03 Nm* while the highest arithmetical mean *RMSE* belongs to the model M02 with *26.19 Nm.*

- When the *RMSE'*s with the validation methods are compared to the ones with the No Validation option, the minimal shrinkage is caused by 10-fold cross-validation most frequently, in 5 out of the 8 models, ranging between 6.89% and 9.74%.
- The best prediction performance among the hamstring muscle strength models is given by model M01 with an average value of *18.03 Nm* while the average *RMSE* value, *21.95 Nm*, for the quadriceps strength is generated by model M32. This comparison shows that the type of training which leads to the best prediction performance is CT for hamstring muscle strength and ST-15min for quadriceps muscle strength.
- Among the models built by using the validation methods, M01 performs the most accurate prediction for hamstring muscle strength with the usage of 10-fold cross-validation and by classic training, with a mean *RMSE* of *16.194 Nm.*
- The highest *RMSE* values, *32.41*, *30.72* and *28.44 Nm* are produced by the models M22 (70-30%), M02 (70-30%) and M02 (80-20%), respectively, all built with the usage of random data division options.

## 4. Conclusion

This study has been carried out in order to create MLR-based models for prediction of hamstring and quadriceps muscle strength. Eight different models have been built with respect to the type of muscle group (hamstring and quadriceps) as well as the type of physical exercise (static or classic training, with or without rest). The study showed that the hamstring muscle strength prediction models are more accurate than the ones used for the quadriceps muscle strength, and also that the most favorable validation method for this purpose is 10-fold cross-validation while the target variables which yield more accurate predictions are CT and ST-15min for the hamstring and quadriceps muscle groups, respectively. The *RMSE'*s vary between *14.91 Nm* and *32.41 Nm*, which shows that the hamstring and quadriceps muscle strength can be predicted with the usage of MLR with acceptable error rates.

## References

Akay, M.F., Abut, F., Çetin, E., Yarım, İ. and Sow, B., 2017. Support Vector Machines for Predicting the Hamstring and Quadriceps Muscle Strength of College-Aged Athletes. Turkish Journal of Electrical Engineering and Computer Sciences. 25, 2567-2582.

Abadie, B. and Wentworth, M.C., 2000. Prediction of One Repetition Maximal Strength from a 5-10 Repetition Submaximal Strength Test in College-Aged Females. Journal of Exercise Physiology. 3, 1-6

Horvat, M., Ramsey, V., Franklin, C., Gavin, C., Palumbo, T. and Glass, L.A., 2003. A method for predicting maximal strength in collegiate women athletes. The Journal of Strength & Conditioning Research. 17, 324-328.

Harbo, T., Brincks, J. and Andersen, H., 2012. Maximal isokinetic and isometric muscle strength of major muscle groups related to age, body mass, height, and sex in 178 healthy subjects. European Journal of Applied Physiology. 112, 267-275.

Muraki, S., Fukumoto, K. and Fukuda, O., 2013. Prediction of the muscle strength by the muscle thickness and hardness using ultrasound muscle hardness meter. Springerplus. 2, 457.

Sow, B., 2017. Prediction of Hamstring and Quadriceps Muscle Strength of Athletes Using Machine Learning Methods. Yüksek Lisans Tezi, Çukurova Üniversitesi Fen Bilimleri Enstitüsü.

**GÜFBED/*GUSTIJ* (2018) CMES 2018 SEMPOZYUM EK SAYISI: 15-21**
DOI: 10.17714/gumusfenbil.443337 Araştırma Makalesi / *Research Article*

# Algorithm Design for Improving Performance of Microprocessor-Controlled Sonar Buoy Performing Surveillance of Underwater Objects

## *Sualtı Nesnelerinin Gözetimini Gerçekleştiren Mikroişlemci Kontrollü Sonar Şamandıra Performansını Artırmak İçin Algoritma Tasarımı*

**Eren KÜREN*[,a], Akın CELLATOĞLU[b]**
*Lefke Avrupa üniversitesi, Mühendislik Fakültesi, Bilgisayar Mühendisliği Bölümü, Lefke 99728, KKTC*

• Geliş tarihi / *Received*: 12.07.2018 • Düzeltilerek geliş tarihi / *Received in revised form*: 29.08.2018 • Kabul tarihi / *Accepted*: 17.09.2018

**Abstract**
An improved design software-based replica correlator method within the microprocessor-controlled sonar buoy systems has been proposed which improved the performance of detecting objects underwater. In the sea or ocean, the microprocessor-controlled buoy is provided to be automatically wirelessly scan for removal of underwater information and transmit it wirelessly to the main control station for additional processing and ultimate decision. In this study, sonar buoy performance and system design proposal with 7-31 cell replica correlation are presented. Although the digital delay lines are used to minimize the complexity of hardware-based replica correlator, the proposed software replica-correlated system within microprocessor-controlled buoys, has improved the performance.

**Keywords:** Buoy, microprocessor control, replica correlation, sonar, underwater surveillance

***Öz***
*Sualtında bulunan nesneleri gözetlemek amacıyla uygulanan mikroişlemci kontrollü sonar şamandıra sistemlerinin performansı için geliştirilmiş bir tasarım yaklaşımı önerilmiştir. Denize veya okyanus içerisinde, mikroişlemci kontrollü şamandıra, sualtı bilgisinin çıkarılması için otomatik olarak taranması ve daha ileri işlem ve nihai kontrol eylemi sağlanması amacıyla bir uzak yer istasyonuna kablosuz olarak iletilmesi sağlanır. Bu çalışmada, 7-31 hücre replika korelasyonunu içeren sonar şamandıra performansı ve sistem tasarım taslağı sunulmuştur. Donanımsal replika korelatörünün karmaşıklığı, dijital gecikme kanalları kullanılarak en aza indirilmesine rağmen, önerilen mikroişlemci kontrollü şamandıra, yazılım aracılığıyla replika korelasyonu gerçekleştirilmiş ve geliştirilmiş sistemle performans artırılmıştır.*

***Anahtar Kelimeler:*** *Şamandra, mikroişlemci kontroller, replika korolasyon, sonar, sualtı gözetim*

*[a] Eren KÜREN; ekuren@eul.edu.tr; Tel: (0533) 862 07 50; orcid.org/0000-0003-4279-9968
[b] orcid.org/0000-0001-8461-1308

## 1. Introduction

The sonar buoys systems, which is placed on the surface of the ocean is used to detect the object and get continuously present information for a long time. The noise types that affect the sonar system performances are impulse noise and colored noise. The presence of these noises affects the detection process in letting the systems to generate false alarms under different ambient conditions. The SNR values are decreased by the attenuation of the acoustic wave in the medium and the limited power output for wave transmitted by transducer. Detection of targets is an important concern in radars and sonars. In this aspect several approaches have been attempted (Skolnik, M.I., 2000; Sarkar, N., 2004; Taub, H., Saha, G. and Schilling, D. L., 2008) in the past. In pulse type systems, one approach to improve the detection process is to apply replica correlation (Balasubramanian, K. and Arica, S. ,1993; Balasubramanian, K., Camur, H. and Rajaravivarma, 1999; Balasubramanian, K., 2000, 2005, 2006). As a further attempt improving the design considerations of the replica correlation detection is now reported.

## 2. Replica Correlator

Replica correlation technique in radars and sonars is used to improve the probability of signal detection. The transmitted acoustic pulse consists *n* cells packet. In the proposed model '*n*' is chosen optimal pattern look-up table as lies between 7 and 31. The cells pattern is evaluated as a bit stream design + or 0 showing in-phase and – or 1 showing the out-phase of the Continuous Wave (CW) sinus wave incurring a phase shift of 180°. This technique involves in using binary phase shift keyed signal as a packet incorporated in the duration of the on-going pulse. Figure 1(a) shows the phase shift keyed signal pattern (Balasubramanian, K., 2000) present during the pulsing period. Figure 1(b) shows the block diagram of the replica correlator code encodes for carrier signal to receiver.

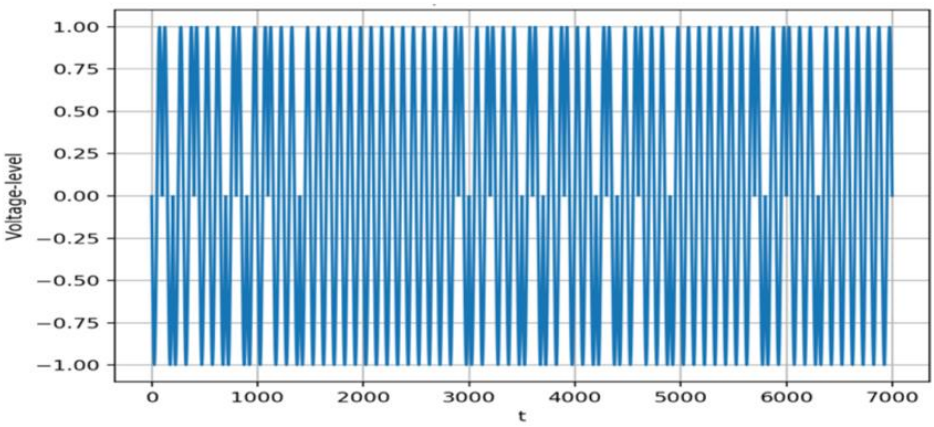


**(a)**

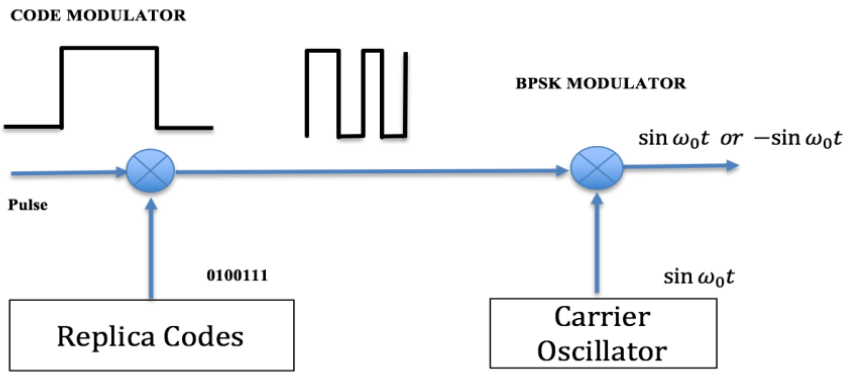


**(b)**

**Figure 1.** Replica correlation **(a)** CW coded signal binary phase shift keying. **(b)** block diagram of replica code encoded carrier signal.

The echo Binary phase shift keyed signal pass through and propagates up to the end of the delay channel (Balasubramanian, K. and Cihan, K., 1994; Balasubramanian, K., Gayathri,K.B. and Camur,H., 1999) with taps located at seven regular intervals. Each tap is connected with a DAC (Digital to Analogue Converter) to get the analogue equivalent of the delay produced in respective taps. Internally, analogue inverters are connected at taps 4, 5 and 7 such that inversion takes place in the reverse order {1 0 1 0 0 1 0} of the transmitted pattern. When the incoming signal reaches the last cell, at the instant of traversing it, the signal gets boosted up *n* times of the original amplitude. Figure 2 illustrates Replica correlated output for ΔT-7 Cell Pattern. The target is detected by comparing the signal amplitude with an appropriate threshold.

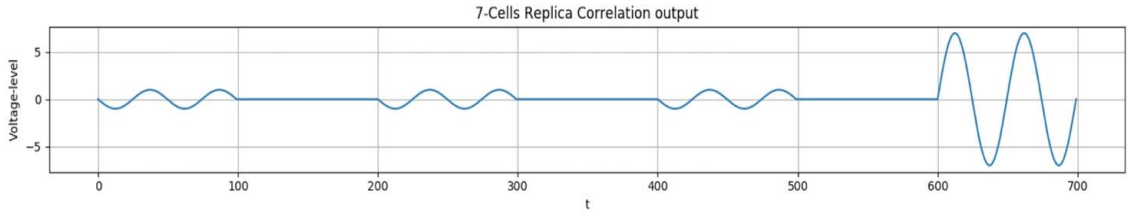


**Figure 2.** Replica correlated output for ΔT-7 cell pattern

## 3. Replica Correlator Algorithm Design

On the basis of replica correlation automatic cell pattern setting is an important concern for easy detection of targets. This pattern gets the signal boosted up in the last cell and suppresses it at lowest possible level in all other cells. The software finds the signal levels during *n*-pulse periods for all the set patterns and assesses the best pattern needed for the given *n*. Figure 3 and Figure 4 illustrate how to calculate the magnitude and cell pattern control function. Embedded software defined radio (SDR) module uses optimal pattern for given *n*-cells packet for SONAR buoys for custom needs.

$$K_i = \sum_{n=1}^{i} p_n \, x_{(i+1-n)} \quad (1)$$

if $x_i$ indicates the bi-phase worth of the received signal falling in $i^{th}$ cell and $p_n$ indicates the polarity of the amplifier connected to the $j^{th}$ faucet of the electrical circuit the output completed at the summing amplifier at numerous cells throughout the propagation of the signal within the electrical circuit is expressed in (1) whereby $K_i$ indicates the amplitude of the summing amplifier at the $i^{th}$ cell of the incoming signal. *n*-cell pattern $K_i$ calculation Lower Triangular Matrix algorithm is designed and implemented as given in Figure 5.

| | Amplitude Calculation | | | | | | | | | | |
|---|---|---|---|---|---|---|---|---|---|---|---|
| Sum of Cols | 1 | 0 | 0 | 0 | 0 | 0 | 0 | 0 | 0 | 0 | 0 |
| | 1 | 1 | 0 | 0 | 0 | 0 | 0 | 0 | 0 | 0 | 0 |
| | 1 | 1 | 1 | 0 | 0 | 0 | 0 | 0 | 0 | 0 | 0 |
| | 1 | -1 | -1 | -1 | 0 | 0 | 0 | 0 | 0 | 0 | 0 |
| | 1 | 1 | -1 | -1 | -1 | 0 | 0 | 0 | 0 | 0 | 0 |
| | 1 | 1 | 1 | -1 | -1 | -1 | 0 | 0 | 0 | 0 | 0 |
| | 1 | -1 | -1 | -1 | 1 | 1 | 1 | 0 | 0 | 0 | 0 |
| | 1 | -1 | 1 | 1 | 1 | -1 | -1 | -1 | 0 | 0 | 0 |
| | 1 | 1 | -1 | 1 | 1 | 1 | -1 | -1 | -1 | 0 | 0 |
| | 1 | -1 | -1 | 1 | -1 | -1 | -1 | 1 | 1 | 1 | 0 |
| | 1 | -1 | 1 | 1 | -1 | 1 | 1 | 1 | -1 | -1 | -1 |
| Ki = { | 11 | 0 | -1 | 0 | -1 | 0 | -1 | 0 | -1 | 0 | -1 } |

**Figure 3.** $K_i$ calculation by lower triangular matrix for 11-cells pattern

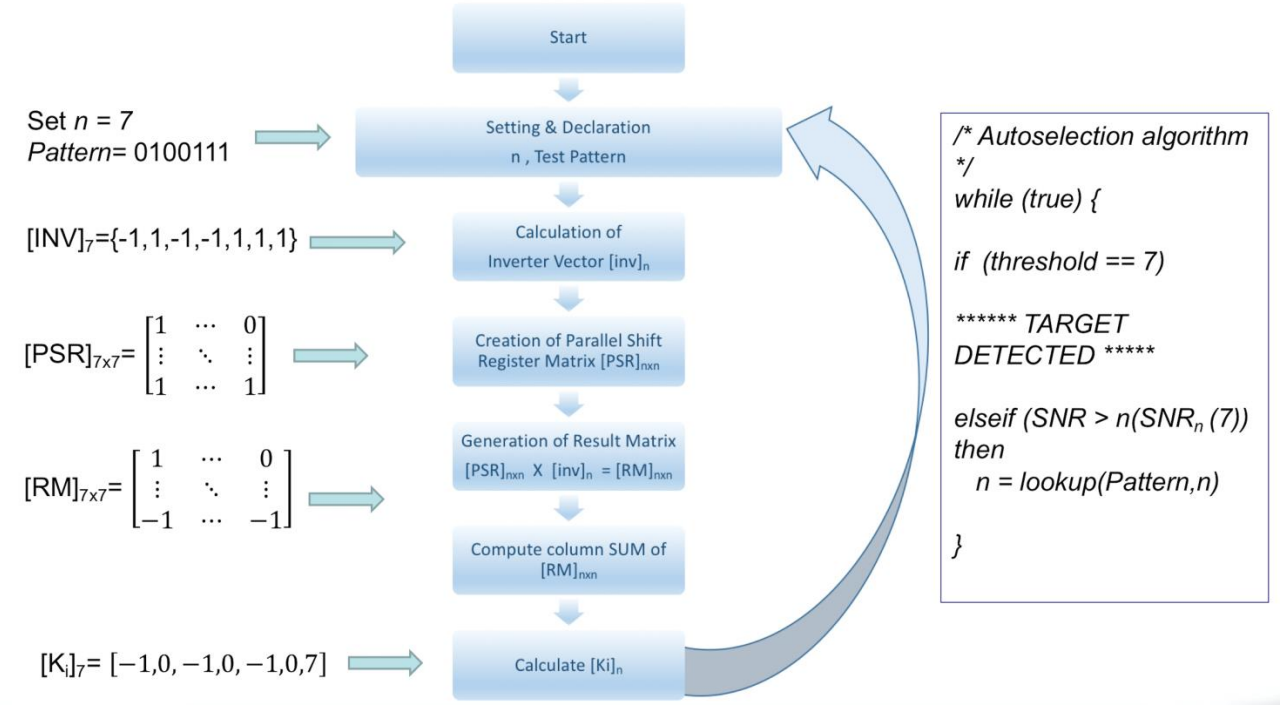


**Figure 4.** Sonar buoy SDR system block diagram and detection process.

```
Set _PATTERN_;
int N = _PATTERN_.Length ;
var _INV_ = new int[N + 1]; //InvereterVector
var _PSR_ = new int[N + 1, N + 1]; //ParallelShiftRegister Matrix
var _AMP_ = new int[N + 1, N + 1]; //Aplitude Matrix
var _Ki_ = new int[N + 1]; //Ki Result
int j=0, k=0;
for (int col = N-1; col >= 0; col--) {
  for (int row = (N-1) - col; row >= 0; row--) {
        _PSR_[j, k] = _INV_[row];
        if (_PSR_[j, k] == 0) _PSR_[j, k] = -1;
        k++; }
    k = 0,j = 0;
    j++; }
// Creating Lower Triangual Matrix
for (int col = N; col >= 0; col--) {
    for (int row = N - col; row >= 0; row--) {
        _AMP_[j, k] = _PSR_[j, k] * _INV_[N - col];
         k++; }
    k = 0;
    j++; }
// _Amplitude binnary Matrix calculation
for (int col = 0; col <= N; col++) {
    for (int row = 0; row <= N; row++)
        _Ki_[col] += _AMP_[row, col]; //calculated output levels Ki index voltage
  }
```

**Figure 5.** Algorithm for Ki replica pattern calculation

Table 1. gives optimum cell pattern for selected lengths ranging from 7 to 31 cells and presents the voltage level (Kuren, E., and Cellatoglu, A., 2017).

**Table 1.** Optimal cell patterns for look up table

| Cell Density *n* | Optimal-Cell Pattern | Voltage Level |
|---|---|---|
| 7 | 0100111 | 1 |
| 9 | 111001101 | 3 |
| 11 | 10110111000 | 1 |
| 13 | 1111100110101 | 1 |
| 15 | 101011001100000 | 3 |
| 17 | 11110001000100101 | 3 |
| 19 | 1000010000101110100 | 3 |
| 21 | 111111000110010010101 | 3 |
| 23 | 100001000010001011101000 | 3 |
| 25 | 111111000111001001001010 1 | 3 |
| 27 | 111000011101110111011010010 | 3 |
| 29 | 100010110001011000010011111011 | 3 |
| 31 | 111011100111000010110110010001 0 | 5 |

## 4. Dynamic Setting of Cells Length for Custom Needs References

Depending upon the requirements, as demanded by the situation, our software automatically finds the optimal pattern *n* and sets the packet as 7-cell pattern under low range and low noise environment or even 31-cell pattern under long range noisy environment. Considering an application of sonar buoys (Balasubramanian, K., 2006) launched in the sea or ocean for underwater exploration the selection of the value of *n* helps in optimizing the system performance. Figure 6. shows simplified block diagram of a sonar buoy.

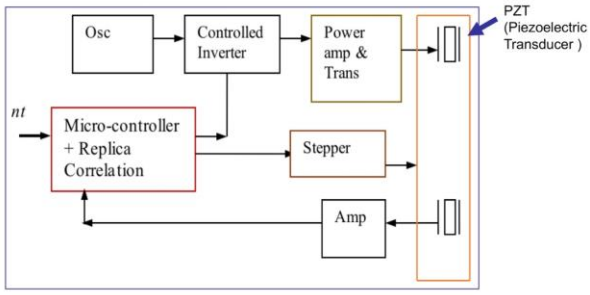


**Figure 6.** Simplified schematic of sonar transceiver

Herein *nt* indicating the type number of the buoy is given as an input to microcontroller, which in turn finds best cell density number (*n*) from a lookup table available in memory and calls the algorithm to set the cell pattern. The pattern is sending serially to a controlled inverter to generate the BPSK signal (Balasubramanian, K., 1998) accordingly. The source for CW input is a phase set oscillator (Osc). The BPSK generated is power amplified and fed to a transmitter Piezoelectric Transducer (PZT) for producing acoustic wave in under water medium. The reflected acoustic wave from a target is picked by receiver PZT and amplified. The processes of finding the envelope of the replica-correlation output, threshold detection and range estimation are all done in microcontroller. Also, the microcontroller issues drive signal to stepper motors driving the PZTs for producing angular sweeping of the acoustic beam. In reality, a set of buoys is thrown in sequence in a selected area for underwater exploration. Depending upon the distance from the shore, the buoy needs a particular cell density *n* for achieving optimal requirements. The value of *nt* need be fed into software in accordance with the type of buoy thrown at that instance.

## 5. Probability of Detection and Performance Analysis

The probability of detection depends on the probability of false alarm and the signal to noise ratio (Skolnik, M.I., 2000; Kuren, E., and Cellatoglu, A., 2017) of received signal. In addition, the level of the received signal plus noise depends on the number of cells *n* present in the transmitted pulse packet. The relationship between the probability of detection and *n* is almost linear. Therefore, with the larger *n* detecting the desired target on a threshold would be easy. This is seen in Figure 2. The sonar buoy works in underwater sea or ocean where the level of background noise is unknown. More noise would be added up with the signal when the

distance of the target increases. Therefore, detection performance of targets under the coverage of desired range would be important. Figure 7. and Figure 8. show the performance under different ranges of noisy environment. Gaussian Noise (AWGN) is added to the signal and performance is evaluated.

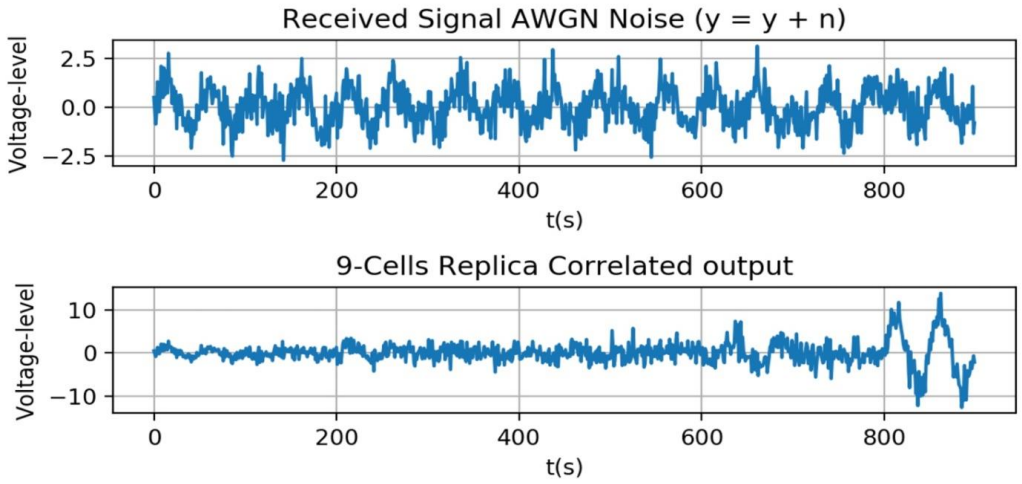


**Figure 7.** Performance evaluation with Gaussian noise (AWGN $SNR_{db}$=0) is added to transmitted signal.

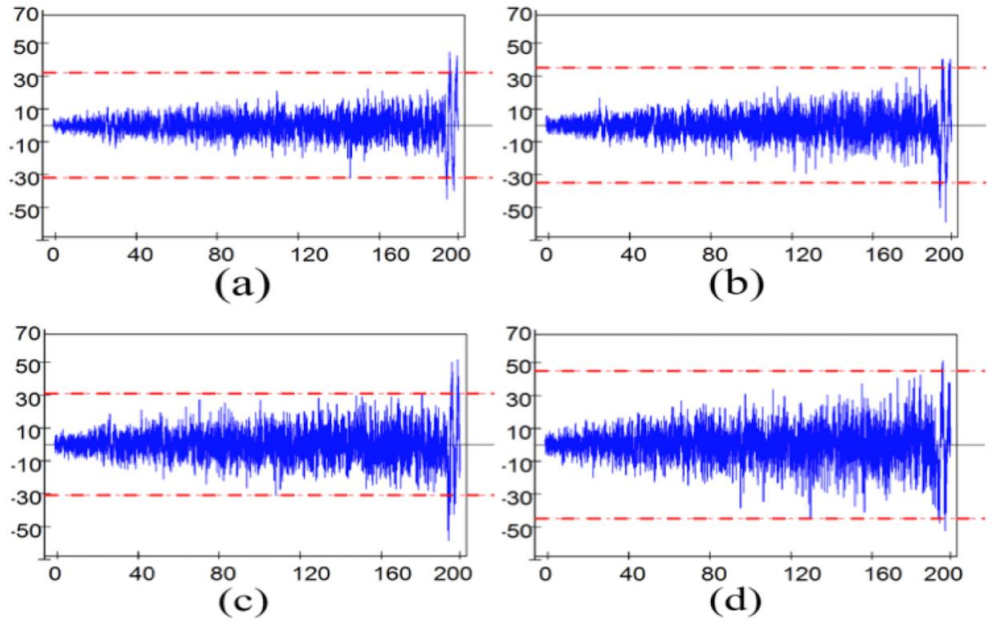


**Figure 8.** Performance analysis replica correlated output under different noise environment. **(a)** 31-cells pattern with 200% noise. **(b)** 31-cells pattern with 400% noise. **(c)** 31-cells pattern with 600% noise. **(d)** 31-cells pattern with 800% noise

## 6.Conclusion

In certain microprocessor-controlled target detection systems replica correlation technique is used with hardware-based control as well as software-based control. The hardware-based replica correlation employs digital delay line and becomes complex in complexity when the cell density *n* increases. The software replica correlation on the other hand uses FIFO memory to gather the data required for processing. While processing is performed almost instantaneously there is a very small delay is introduced in software method for processing. Nevertheless, with recent high-speed processors the time delay becomes negligible value. The complexity contributed in software method is mainly due to the growth size of FIFO memory occupying larger memory space. With the latest technological developments available in practice the complexity and cost factor would decrease well compared to hardware methods.

**References**

Balasubramanian, K., 1998.Binary phase shift keying generator. Electronics World, 104(1744), 300.

Balasubramanian, K., 2000. Replica correlation detection. Electronics World, Vol 106, No 1767, p. 238-240.

Balasubramanian, K., 2005. Design Considerations of Portable Sonar and Ground Station Sonar for Improved System Performance. The 3rd International Conference on Computing, Communications and Control Technologies, July 24-27, Austin, Abstract.

Balasubramanian, K., 2006. Sonar Buoys: an Improved Design Approach. Proceedings of the 3rd International Conference on Informatics in Control, Automation and Robotics. Setubal, Portugal, p. 161-167.

Balasubramanian, K. and Arica, S. ,1993. On the synthesis of a nine-point replica correlator for a sonar. Proceedings of the International Symposium on Signals Circuits and Systems, Iasi, Romania, 148-151.

Balasubramanian, K. and Camur, B. ,2002. On the development of replica correlation software for improving the probability of detection. Proceedings of the 6th World Multi conference on Systemics, Cybernetics and Informatics, Orlando, 9, p. 437-441.

Balasubramanian, K. and Cihan, K., 1994. An intelligent digital delay line for replica correlation. Proceedings of the International Conference on Robotics, Vision and Parallel Processing for Industrial Automation, Malaysia, p. 191-197.

Balasubramanian, K., Camur, H. and Rajaravivarma, 1999., Replica Correlation Technique for Improving the SNR of Digitally Transmitted signals. IEEE SoutheastCON Conference, Lexinton, Kentucky.

Balasubramanian, K., Gayathri, K.B. and Camur, H., 1999. Voltage Control for a Digital Delay Line. Electronics World, 105(1762), 826.

Kuren, E., and Cellatoglu, A., 2017. Optimal cell-pattern setting algorithm for communications systems. Electronics World, 123(1977), 32-34.

Sarkar, N., 2004. Elements of Digital signal processing: New Delhi, Khanna Publishers, 775p.

Skolnik, M.I., 2000. Introduction to Radar Systems: New York, McGraw Hill, 590p.

Taub, H., Saha, G. and Schilling, D. L., 2008. Principles of Communication systems: New Delhi, Tata Mc-Graw Hill, 884p.

**GÜFBED/*GUSTIJ* (2018) CMES 2018 SEMPOZYUM EK SAYISI: 22-30**
DOI: 10.17714/gumusfenbil.432302 Araştırma Makalesi / *Research Article*

# Karayolu Kaplamalarının Sonlu Elemanlar Yöntemi İle Analizinde Gerilme-Birim Şekil Değiştirme Davranışına Etki Eden Parametrelerin İncelenmesi

## *Investigation of Finite Element Method Parameters Affecting the Displacement Behaviour of Highway Pavements*

**Murat BOSTANCIOĞLU***
*İnşaat Mühendisliği Bölümü, Mühendislik Fakültesi, Cumhuriyet Üniversitesi, Sivas, TÜRKİYE*

• Geliş tarihi / *Received*: 08.06.2018 • Düzeltilerek geliş tarihi / *Received in revised form*: 27.09.2018 • Kabul tarihi / *Accepted*: 01.10.2018

**Öz**
Esnek kaplamalar bitüm ve granüler malzemeler ile inşa edilen bir üst yapı türüdür. Esnek üst yapıların projelendirilmesinde kullanılan yöntemler; ampirik yöntemler, kayma göçmesi sınırlama yöntemi, deplasman sınırlama yöntemi, regresyon yöntemi ve mekanistik ampirik yöntemler olarak beş kategoriye ayrılabilir. Bu yöntemler arasından geleneksel ampirik yöntemlerden mekanistik ampirik dizayn yöntemlerine doğru bir yönelme söz konusudur. Kaplama tabakalarının heterojenliği, dinamik ve tekrarlı yükleme koşulları gibi sebeplerle araştırmacılar çalışmalarını sonlu elemanlar yöntemi ile yapmayı tercih etmektedir ancak sonlu elemanlar modelinin 2 veya 3 boyutlu olarak tanımlanması, yükleme koşulları, tabakalar arası temas durumları ve formülasyonları, ızgara boyutları, sınır koşulları ve model boyutları gibi parametreler sonuçlar üzerinde önemli bir etkiye sahiptir. Bu çalışmada kaplama, temel ve alt temel tabakalarından oluşan geleneksel bir üst yapı kesiti üzerinde statik yükleme koşulları altında kaplama tepkilerini etkileyen parametreler incelenmiştir.

**Anahtar kelimeler:** Esnek üst yapılar, Kaplama tepkileri, Mekanistik-ampirik dizayn, Sonlu elemanlar yöntemi

***Abstract***
*Flexible pavements are a type of superstructure constructed using bitumen and granular materials. The methods used in the design of flexible pavements can be examined in five categories. Empirical methods, limiting shear failure methods, limiting deflection methods, regression methods and mechanistic-empirical methods. There has been a dramatic change in the design methods for flexible pavements from the early purely empirical methods to the modern mechanistic-empirical methods. Due to the heterogeneous pavement layers and dynamic and cycling loading instead of static loading, researchers diverted their research to the finite element method, which provides a better solution in the dynamic analysis of pavements while considering the heterogeneity. However, in finite element method, parameters such as the definition of the model as 2D or 3D, the loading condition, the types and formulation of contact between layers, size of mesh, boundary conditions and dimensions of the model have a significant effect on the results. In this study, finite element model parameters affecting the pavement responses under static loading were investigated on a typical superstructure configuration consists pavement, base and subgrade layers.*

***Keywords****: Flexible pavements, Pavement responses, Mechanistic-empirical design, Finite element model*

*Murat BOSTANCIOĞLU, bostancioglu@cumhuriyet.edu.tr, Tel: (0346) 219 10 10; orcid.org/0000-0001-6820-2213

## 1. Giriş

Esnek kaplamalar bitüm ve granüler malzemeler kullanılarak inşa edilen bir üst yapı tipidir. Esnek üst yapıların tasarımında kullanılan yöntemler beş kategoride incelenebilir. Bunlar; kaplama kalınlığını tabakaların Kaliforniya taşıma gücü oranı (CBR) ile ilişkilendiren ampirik yöntemler, kaplama kalınlığı hesabında kayma göçmesini ve taban zemini veya yüzey deplasmanını sınırlamayı prensip olarak alan "kayma göçmesi sınırlama" ve "deplasman sınırlama" yöntemleri, ülkemizde Karayolları Genel Müdürlüğü tarafından esnek üst yapıların projelendirilmesinde kullanılan AASHTO yönteminin de içinde yer aldığı kaplama performansına veya yol testlerine bağlı regresyon yöntemleri ve mekanistik-ampirik yöntemler olarak sıralanabilir. Günümüzde kaplama tasarımında, sadece sınırlı sayıda malzeme, yük ve çevresel etkiler ile yapılan yol testlerinden elde edilen verileri kullanan ampirik yöntemlerden mevcut trafik ve çevre etkileri altındaki kaplamanın tepkilerini (gerilme, şekil değiştirme, deplasman) mekanik teoriler ile hesaplayan mekanistik-ampirik yöntemlere bir yönelme söz konusudur (Huang, 2004; Zheng vd., 2012; Lu vd., 2014; Ahmed ve Erlingsson, 2016).

Burmister'ın elastik teorisi mekanistik-amprik yöntemler arasında en pratik ve sıklıkla kullanılan yöntem olarak bilinmektedir. Bu teorinin amacı kaplama tabakası altındaki yatay çekme birim şekil değiştirmelerini ve taban zemini üzerindeki düşey basınç birim şekil değiştirmelerini sınırlamaktır (Huang, 2004; Ahmed ve Erlingsson, 2016). Yöntemde tabakaların sabit bir elastisite modülü (E) ve poisson oranına sahip (ν) homojen, izotropik ve lineer elastik olduğu, malzemelerin ağırlıksız, tabakaların en alt tabaka hariç sonlu kalınlıkta (en alt tabaka yarı sonsuz) ve yükün dairesel bir alana uniform olarak etki ettiği kabulleri yapılmaktadır. Burmister yöntemi modifiye edilerek viskoelastik veya non-lineer elastik malzemelerden oluşan tabakalı yapıların analizinde de kullanılmaktadır (Huang, 2004; Zheng vd., 2012).

Karayolu üst yapı tabakalarının idealden uzak heterojen davranışları, trafik yüklerinin dairesel yerine farklı geometrideki temas yüzeyleri üzerine etki etmesi ve bu yüklerin statik yerine dinamik ve tekrarlı olması, dikdörtgensel kesitler yerine daha kompleks geometriler ve sınır koşulları ile çalışma zorunlulukları ve gelişen ve hızlanan bilgisayar teknolojisinin bir sonucu olarak, sonlu elemanlar metodu (SEM) son dönemde kaplama tepkilerini belirlemek için yaygın olarak kullanılan bir yöntem haline gelmiştir (Hadi ve Bodhinayake, 2003; Abd Alla, 2006; Yoo vd., 2006; Ambassa vd., 2013; Beskou vd., 2016; Sarkar, 2016).

SEM metodu 2 ve 3 boyutlu üst yapı modellerinin statik ve dinamik analizlerinde, lineer elastik ve viskoelastik olarak tanımlanan malzeme tiplerinde, farklı yükleme hızlarında, tek veya çift tekerlek yükü ve tekil, tandem, tridem aks yükleri altında, geogrid ile güçlendirilmiş kaplamaların analizlerinde başarıyla uygulanmıştır (Al-Azzawi, 2012; Beskou vd., 2016; Ahmed ve Erlingsson, 2016; Sarkar, 2016; Ahirwar ve Mandal, 2017). Ancak SEM metodunda modelin 2 boyutlu veya 3 boyutlu olarak tanımlanması, yükleme durumu, tabakalar arasındaki yüzeylerin temas tipleri, sonlu eleman ızgarasının sıklığı (mesh) ve oluşturulan modelin boyutları gibi parametreler sonuca önemli ölçüde etki etmekte ve metodun etkin kullanımı için uygun bir şekilde düzenlenmelidir.

Bu çalışmada taban zemini, temel ve kaplama tabakalarından oluşan tipik bir esnek üst yapı kesiti SEM metodu ile modellenmiş ve modelin kaplama tepkilerini doğru tahmin etmesi için gerekli değişkenlerin optimize edilmesi sağlanmıştır. Modelleme için ticari ANSYS 18.2 Workbench yazılımı kullanılmıştır. Hesaplanan gerilme ve birim şekil değiştirme değerlerine göre dönüşüm fonksiyonları yardımıyla yol ömrü hesabı yapılarak SEM metodu değişkenlerinin bir esnek üst yapının ömrüne olan etkisi de ayrıca incelenmiştir.

## 2. Materyal ve Yöntem

### *2.1. Model Geometrisi ve Sınır Koşulları*

Çalışmada eksenel simetrik geometride, taban zemini, temel ve kaplama tabakalarından oluşan bir üst yapı kesiti seçilmiştir (Huang, 2004). Malzemeler lineer elastik olarak tanımlanmış ve özellikleri Şekil 1-a'da verilmiştir. Kaplama yüzeyine etki eden yük 122 mm yarıçapında dairesel bir alan üzerine 0.83 MPa tekerlek iç basıncı ile uniform olarak etki etmektedir. 3 boyutlu modelde simetriden dolayı ¼ dairesel alan üzerine yükleme yapılarak analizler çalıştırılmıştır (Şekil 1-b). Kesiti oluşturan tüm tabakalar için herhangi bir süreksizlik olmadığı (çatlaksız tabaka) ve tabaka ara yüzeylerinin tamamen yapışık (bonded) olduğu değerlendirilmiştir (Hadi ve Bodhinayake, 2003).

Modelin sınır koşullarının tanımlanmasında aşağıdaki koşullar dikkate alınmıştır (Şekil 2'ye referansla);

- Taban düzlemindeki (bcde) düğüm noktalarının düşey deplasmanları engellenmiştir
- (abcf) düzlemi, simetri düzlemi olduğu için yüke dik doğrultulardaki deplasmanlar engellenmiş, düşey deplasmanlar serbest bırakılmıştır.
- (cefg) düzlemi tekerleğin tam ortasından geçen düşey düzlem olduğundan yüke dik doğrultulardaki deplasmanlar engellenmiş, düşey deplasmanlar serbest bırakılmıştır (Hadi ve Bodhinayake, 2003).

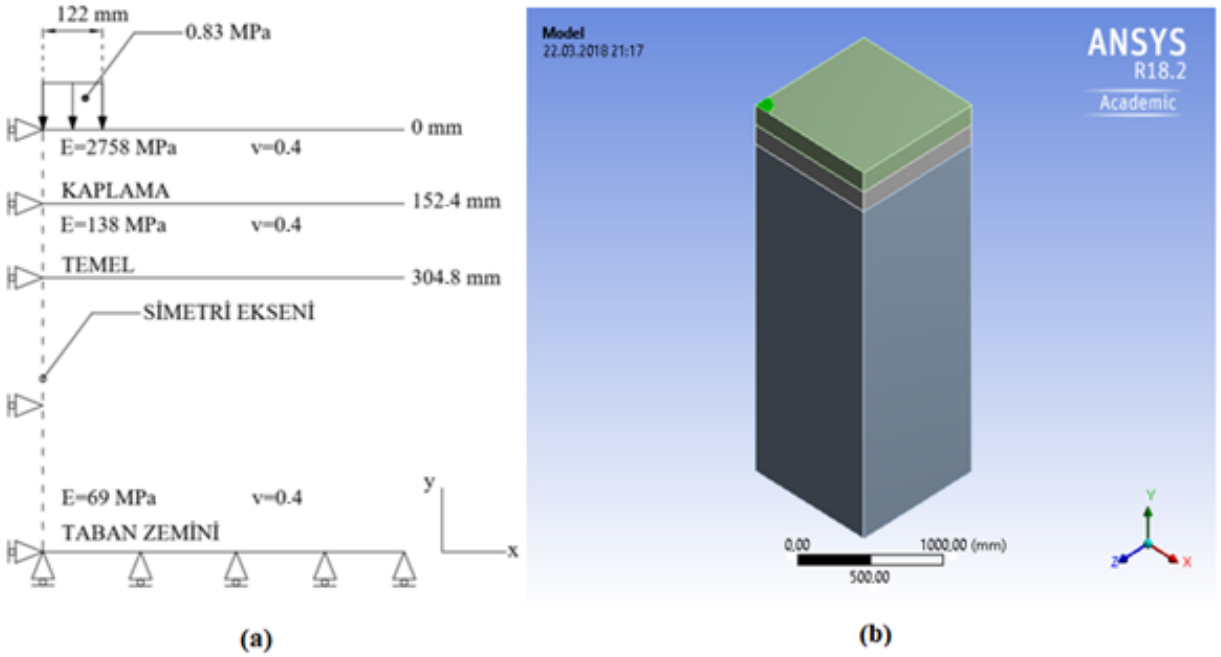


**Şekil 1.** (a) Üst yapı en kesiti, (b) 3 boyutlu model ve yükleme alanı

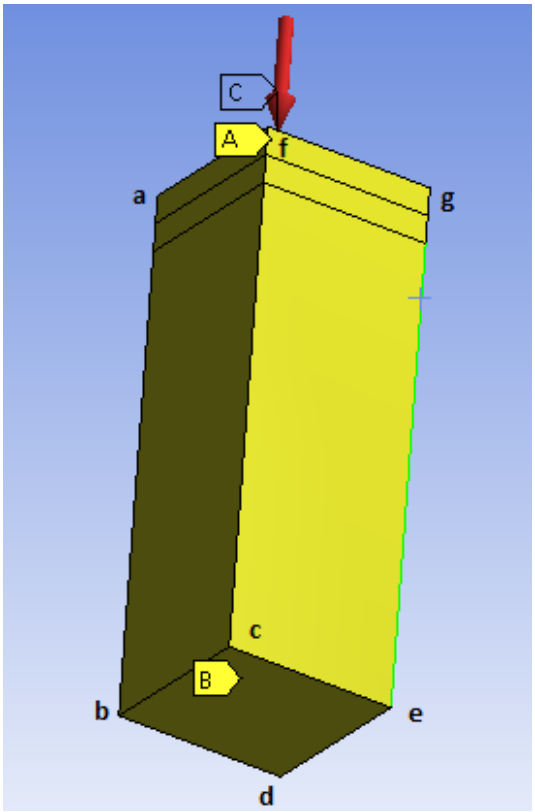


**Şekil 2.** Sınır koşulları

Modelden elde edilen sonuçların doğrulanması amacıyla Huang (2004) tarafından geliştirilen ve mekanistik-ampirik kaplama analizlerinde referans kabul edilen (Muniandy vd., 2013; Sarkar, 2016; Chegenizadeh vd., 2016; Hafeez vd., 2017) Kenlayer paket programı kullanılmıştır. Belirlenen kesitin Kenlayer ile çözümünde kaplama tabakası üst yüzeyi için elde edilen deplasman değeri (0.56 mm) oluşturulan modelde plan boyutları 950x950 mm ve taban zemini derinliği 2540 mm olarak seçildiğinde 0.55 mm olarak bulunmuş ve %98 oranında bir uyumluluk elde edilmiştir.

### *2.2. Yol Hizmet Ömrünün Tahmin Edilmesi*

Mekanistik-ampirik dizayn yöntemlerinin kullanılabilmesi için elde edilen gerilme, birim şekil değiştirme veya deplasman değerlerinin kaplama davranışını (çatlama, tekerlek izinde oturma, pürüzlülük vd.) yansıtan bir parametreye dönüştürülmesi gerekmektedir (Ekwulo ve Eme, 2009). Yorulma çatlakları kaplamada tekrarlı yüklemeye bağlı olarak ortaya çıkan bir bozulma tipidir. Mekanistik-ampirik dizayn yönteminde

yorulma kriteri olarak asfalt betonu tabakası altında meydana gelen çekme birim şekil değiştirmeleri kullanılmaktadır. Bu birim şekil değiştirme değerlerinin belirli bir sınırı aşması durumunda kaplamada çatlaklar meydana gelmektedir. Asfalt Enstitüsü ve Shell yöntemleri ile yorulmaya bağlı göçmeyi sağlayan yük tekrar sayısı formülleri sırasıyla aşağıda belirtilmiştir (Ekwulo ve Eme, 2009; Adhikari vd., 2009).

$$N_f = 0.0796\ (\varepsilon_t)^{-3.291}(E_1)^{-0.854} \quad (1)$$

$$N_f = 0.0685\ (\varepsilon_t)^{-5.671}(E_1)^{-2.363} \quad (2)$$

Formüllerde $N_f$ göçmeyi meydana getiren yük tekrar sayısını, $\varepsilon_t$ kaplama tabakası altındaki yatay birim şekil değiştirmeyi, $E_1$ ise kaplama tabakasının elastisite modülünü (psi) belirtmektedir.

Asfalt Enstitüsü ve Shell tarafından önerilen ve kaplamada meydana gelen tekerlek izinde oturmaya bağlı göçme ile taban zemini üzerindeki düşey basınç birim şekil değiştirmesi arasındaki ilişki Formül 3 ve 4'te belirtilmiştir.

$$N_f = 1.365x10^{-9}(\varepsilon_c)^{-4.477} \quad (3)$$

$$N_f = 6.15x10^{-7}(\varepsilon_c)^{-4} \quad (4)$$

Formüllerde $N_f$ tekerlek izinde oturma göçmesini meydana getiren yük tekrar sayısını, $\varepsilon_c$ ise taban zemini üzerindeki basınç birim şekil değiştirmesini göstermektedir (Hesham ve Shiraz, 1998; Ekwulo ve Eme, 2009).

## 3. Bulgular ve Tartışma

Sonlu elemanlar yönteminde plan ve kesit boyutlarının (Şekil 3) seçimi sonuca önemli ölçüde etki etmektedir. Plan boyutlarının etkinliğini incelemek amacıyla farklı kenar uzunlukları için analizler yapılarak üst yapıdaki maksimum deplasman değerleri hesaplanmış ve sonuçlar Tablo 1'de verilmiştir.

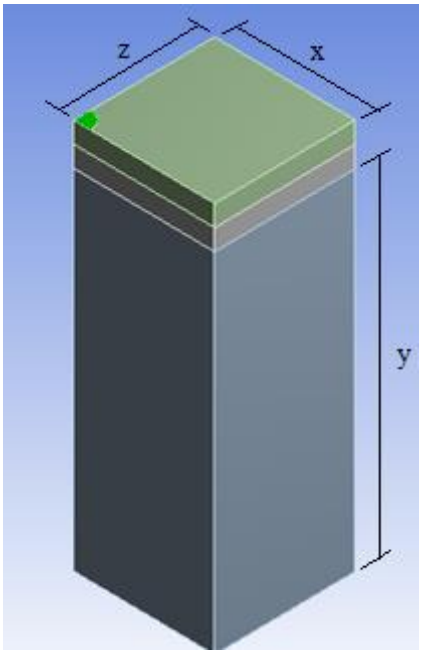


**Şekil 3.** Model boyutları

**Tablo 1.** Plan boyutlarına bağlı deplasman değerleri

| Yükleme yarıçapı (r)(mm) | Plan boyutları (x-z)(mm) | r/x | Maksimum deplasman (mm) |
|---|---|---|---|
| 122 | 1350x1350 | 0.090 | 0.41 |
| 122 | 1100x1100 | 0.111 | 0.48 |
| 122 | 1050x1050 | 0.116 | 0.50 |
| 122 | 1000x1000 | 0.122 | 0.52 |
| 122 | 950x950 | 0.128 | 0.55 |
| 122 | 900x900 | 0.135 | 0.58 |

Tablo 1 incelendiğinde kenar boyutlarının artışına bağlı olarak deplasman değerlerinin düştüğü gözlenmektedir. Kenar uzunluklarındaki artışın yükleme noktası etrafındaki yanal desteği artırması düşen deplasman değerlerini açıklamaktadır.

Taban zemini derinliği 2540 mm sabit olmak üzere farklı plan boyutlarının yol ömrü üzerindeki etkisinin sayısal değerler ile kıyaslanmasını sağlamak amacıyla taban zemini üzerinde meydana gelen düşey birim şekil değiştirme ($\varepsilon_c$) ve buna bağlı Shell yöntemi ile hesaplanan yol ömrü değerleri ($N_f$) Tablo 2'de verilmiştir. $N_f$ değerleri incelendiğinde plan boyutlarının artmasına bağlı olarak düşey birim şekil değiştirme değerlerinde bir azalma ve buna bağlı olarak yol ömründe yaklaşık %25 bir artış söz konusudur. Bu sonuçlara göre plan boyutlarının seçimi yol ömrüne bağlı analizlerde mutlaka göz önünde bulundurulması gereken önemli bir parametre olarak değerlendirilmelidir.

**Tablo 2.** Plan boyutlarına bağlı düşey birim şekil değiştirme ve yol ömrü değerleri

| Plan boyutları (x-z)(mm) | $\varepsilon_c$ | $N_f$ |
|---|---|---|
| 900x900 | $5.14x10^{-4}$ | 8.81E+06 |
| 950x950 | $5.04x10^{-4}$ | 9.53E+06 |
| 1000x1000 | $4.96x10^{-4}$ | 1.02E+07 |
| 1050x1050 | $4.91x10^{-4}$ | 1.06E+07 |
| 1100x1100 | $4.86x10^{-4}$ | 1.10E+07 |

Şekil 4'te verilen ve yarı sonsuz tabaka derinliği (y) olarak adlandırılan taban zemini kalınlığı değişimine bağlı deplasman değerleri incelendiğinde taban zemini kalınlığı azaldıkça deplasman değerlerinin de azaldığı görülmektedir. Plan boyutlarının 950x950 olarak belirlendiği bu analizde deplasman değerlerinin azalmasını sağlayan en önemli parametre sınır koşullarında düşey deplasmanı engellenmiş olan taban düzlemine olan mesafenin kısalmasıdır. Düşey doğrultuda rijit davranış gösteren yüzeye olan mesafe kısaldıkça deplasman değerleri de düşmüştür. Kenlayer programı ile elde edilen deplasman değerini sağlayan temel derinliği/taban zemini derinliği oranı grafikten 0.06 olarak okunmaktadır. Buna bağlı olarak hesaplanan taban zemini derinliği ise 2540 mm dir. Boyutsal analizden elde edilen bu değerler ışığında yarı sonsuz tabaka derinliğinin plan boyutlarına oranla 2.67 kat fazla olması gerektiği söylenebilir.

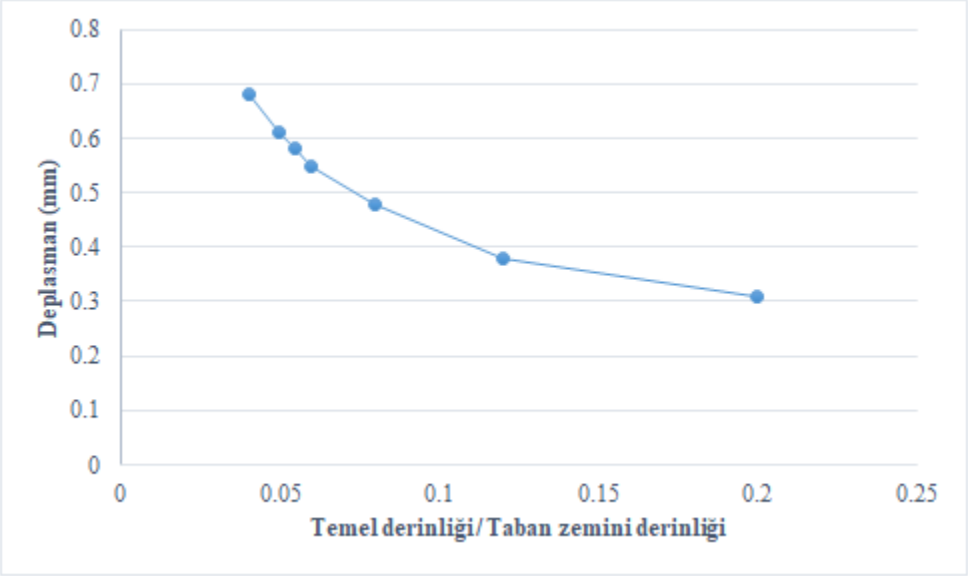


**Şekil 4.** Taban zemini derinliğine bağlı deplasman değişimi

Sınır koşullarının tanımlanması sonlu elemanlar yönteminde sonuçlara etki eden bir diğer önemli parametredir, çalışmada daha önceden de tanımlandığı gibi taban düzlemi, simetri düzlemi ve tekerlek ortasından geçen düzlem düşeyde deplasman yapmayacak şekilde tanımlanmıştır bu sınır koşullarına ilave olarak yolun trafik akış yönündeki derinliğinin fazla olması sebebiyle bu akış yönünde dikey olan düzlemin de (Şekil 2'ye referans ile (cefg) düzlemine paralel karşı düzlem)

düşey deplasmanları sınırlanarak analizler yapılmıştır. Bu kapsamda çalışmanın başlangıcındaki sınır koşulları (boundary condition) 3 düzlemi kapsadığından "3BC", trafik doğrultusuna dik düzlemin de kısıtlanması ile oluşan yeni model "4BC" olarak tanımlanmış ve bu iki farklı durumda oluşan deplasman değerleri plan boyutlarının değişimine bağlı olarak Şekil 5'te verilmiştir.

Şekil 5 incelendiğinde trafik doğrultusuna dik olan düzlemde ek bir sınır koşulu tanımlamak deplasman değerlerinde %18-22 arasında bir düşüşe sebep olmaktadır, rijit düğüm noktası sayısının artması deplasman değerlerinde önemli bir fark ortaya koymaktadır ve şekilden de görüleceği gibi plan boyutlarının azalması deplasman değerlerinin daha fazla düşmesini sağlamaktadır. 3BC modeli ile 4BC modeli arasındaki farkların beton yollar gibi daha rijit kaplama tiplerinde birbirine yakın sonuçlar vereceği değerlendirilebilir. Ancak esnek kaplamalar üzerlerine gelen tekerlek iç basınçlarını beton yollara nazaran daha az bir alana yayabildikleri için 4BC modeli ile çalışmak yerine 3BC modeli ile çalışmak daha uygun bir çözüm olarak ifade edilebilir.

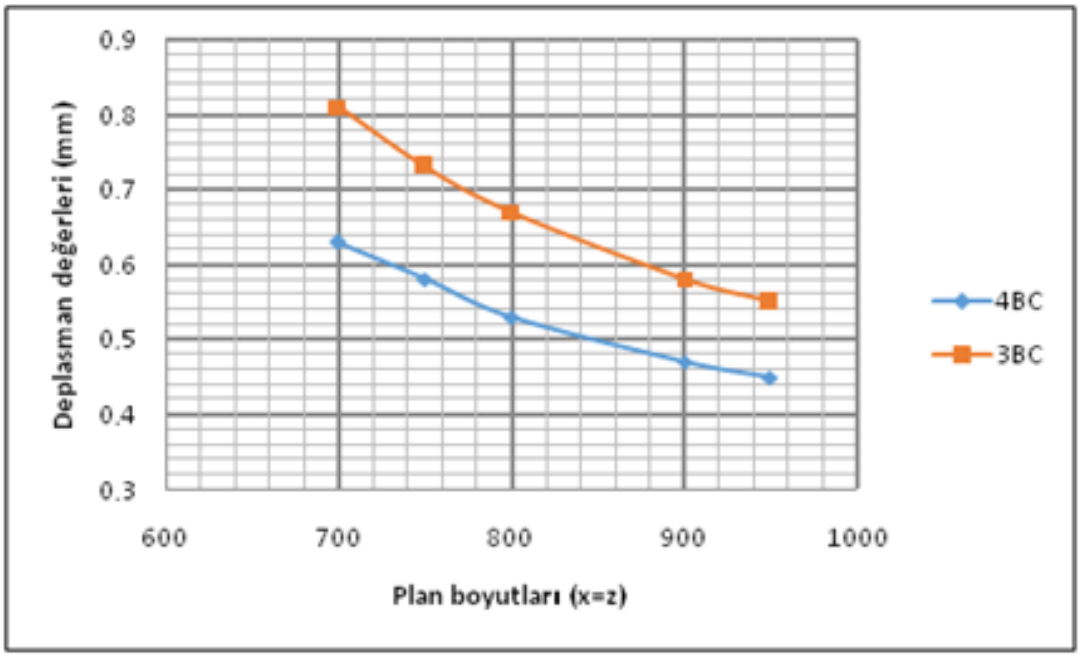


**Şekil 5.** Sınır koşullarına bağlı deplasman değerleri

Izgara (mesh) boyutlarının seçimi sonlu elemanlar yönteminin sonuçlara etki eden en önemli parametrelerinden birisidir, büyük ızgara boyutları yakınsak olmayan sonuçlar verirken küçülen ızgara boyutları ise çözüm süresinin oldukça uzamasına sebebiyet vermekte ve özellikle birden çok analizin yapılacağı problemlerde büyük zaman kayıplarına yol açmaktadır. Çalışmada karayolu kaplamasının deplasman değerlerine ızgara boyutlarının etkisini değerlendirmek amacıyla 3 farklı çalışma yapılmıştır (Şekil 6). Bu çalışmalarda yükün uygulandığı ¼ daire alandaki ızgara boyutları, kaplama tabakasının ızgara boyutları ve temel tabakasının ızgara boyutları üzerindeki değişimlerin sonuca etkileri araştırılmıştır. Izgara analizi yapılırken plan boyutları 950x950 mm, yarı sonsuz tabaka derinliği 2540 mm ve boyut fonksiyonu "uniform" olarak çalışılmıştır. Yük altındaki bölgede yapılan inceltme işlemine ve kaplama tabakasını oluşturan dikdörtgen prizmanın maksimum yüzey boyutuna bağlı deplasman sonuçları Tablo 3'te, temel tabakası kalınlığının (152.4 mm) bölünme boyutuna bağlı deplasman değerleri ise Tablo 4'te özetlenmiştir.

Sonuçlar incelendiğinde yük altındaki bölgede ızgara boyutlarının incelmesi sonuçlar üzerinde çok etkili değilken kaplama tabakası yüzey boyutları sonuçlar üzerinde %0.4 oranında etki göstermiştir. Yükü doğrudan almayan temel tabakasındaki ızgara boyutu değişimi ise sonuçlar hiçbir farklılık ortaya çıkartmamıştır. Bu sonuçlara göre ızgara boyutları seçiminin, çalışılan modelin etkin sonuçlar vermesi açısından birinci derece öneme sahip bir parametre olmadığı belirtilebilir.

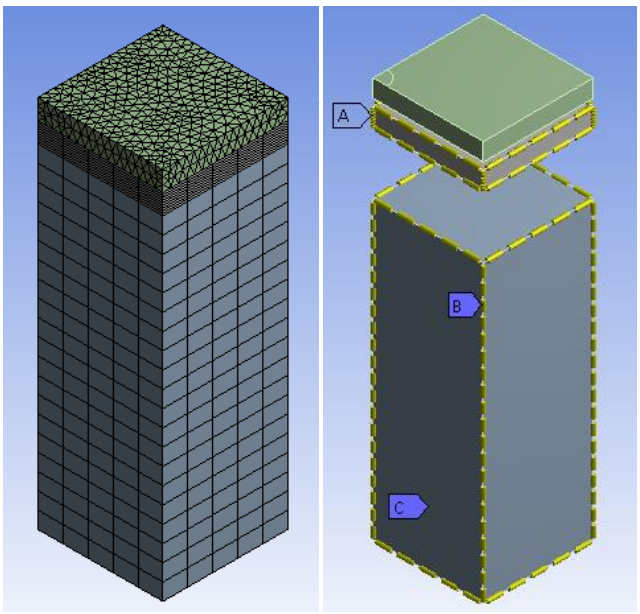


**Şekil 6.** Model ızgara analizi

**Tablo 3.** Izgara boyutlarına bağlı deplasman değerleri (mm)

| Analiz bölgesi | Izgara inceltme seviyesi / Maksimum yüzey boyutu (mm) | | | | | | | | |
|---|---|---|---|---|---|---|---|---|---|
| | İnceltme 1 (Kalın) | İnceltme 2 (Orta) | İnceltme 3 (İnce) | 60 | 50 | 40 | 30 | 20 | 10 |
| ¼ daire | 0.55049 | 0.55062 | 0.55069 | | | | | | |
| Kaplama | | | | 0.5497 | 0.55023 | 0.55128 | 0.55138 | 0.55169 | 0.55198 |

**Tablo 4.** Temel tabakası kalınlığı bölme boyutuna bağlı deplasman değerleri (mm)

| Analiz bölgesi | Temel tabakası kalınlığı bölme boyutu (mm) | | | |
|---|---|---|---|---|
| | 50 | 38 | 4.75 | 9.5 |
| Temel | 0.54969 | 0.54969 | 0.5497 | 0.5497 |

Sonlu elemanlar yönteminde birbirinden farklı malzeme özelliklerine sahip yüzeyler arasında temas denklemleri kurulması gerekmektedir. Eğer uygun temas denklemi seçilmez ise yük altında, bir kütlenin kendisinden farklı mekanik özellikteki kütle içerisine girmesi/batması sonucu ortaya çıkmaktadır (Şekil 7). Bu durum üst yapı analizlerinde tekerlek-kaplama veya kaplama-temel ara yüzeylerinde gerçekleşebilir ancak fiziksel olarak mümkün olmayan bu durumun engellenmesi için ANSYS paket programında temas formülasyonu olarak "Multi Point Constraint (MPC)" seçimi yapılmalıdır. Bu formülasyon temas yüzeyleri arasında deplasmanları birbirine bağlayan kısıt denklemleri ekleyerek temas yüzeyindeki iki düğüm noktasının deplasmanlarını birbirine eşitlemektedir.

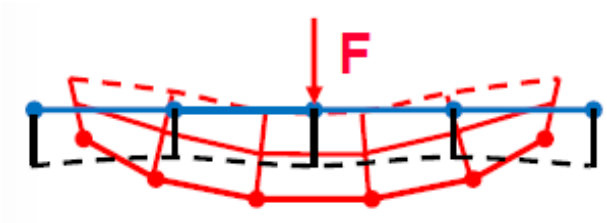


**Şekil 7.** Temas kütlesinin hedef kütle içerine batması

## 4. Sonuçlar ve Öneriler

Karayolu esnek üst yapı tabakalarının sonlu elemanlar yöntemi ile analiz edilmesinde model sonuçlarına etki eden parametrelerin incelendiği bu çalışmaya ait bulgular ışığında aşağıdaki sonuçlar ifade edilebilir;

- Plan boyutlarının seçimi sonlu elemanlar analizinde önemli parametrelerden bir tanesidir ve bu boyutların fazla veya eksik olarak tanımlanması elde edilen deplasman değerlerini önemli ölçüde etkilemektedir. Çalışmada yükleme yarıçapı/plan boyutu oranının optimum değeri 0.128 olarak bulunmuştur.
- Plan boyutlarının yol ömrü hesaplarına etkisini değerlendirmek amacıyla yapılan analizlerde 900x900 mm yerine 1100x1100 mm kare kesitli bir model ile çalışıldığında tekerlek izinde oturma kriterine bağlı yol ömrü değerinde %25 oranında bir artış olduğu belirlenmiştir. Bu sonuçlar birim şekil değiştirme ve buna bağlı dönüşüm formülleri ile yol ömrü hesaplamalarında plan boyutları seçiminin çok önemli bir kriter olduğunu ortaya koymaktadır.
- Modeli oluşturan tabakalardan en altta yer alan ve yarı sonsuz tabaka olarak adlandırılan taban zemini derinliği, taban düzleminin düşey deplasmanlarının engellenmesi sebebiyle sonuçlar üzerinde önemli bir etkiye sahiptir. Bu tabakanın derinliğinin az seçilmesi deplasman değerlerini azaltırken fazla seçiminde ise deplasman değerleri önemli ölçüde artmaktadır. Temel tabakası derinliği / taban zemini derinliği oranında optimum değerin %6 olduğu belirtilebilir.
- Kare prizma olarak tanımlanan modeli meydana getiren 6 yüzeyden 3 veya 4 tanesinde düşey sınır koşulu tanımlayarak çalıştırılan analizlerde trafik yönüne dik doğrultudaki yüzeyin de düşey deplasmanlarının sınırlandırılması elde edilen deplasman değerlerinde %18-22 arasında bir düşüşe sebep olduğu ancak bu kısıtın esnek kaplamalar yerine rijit kaplamalar için daha uygun bir sınır koşulu olacağı değerlendirilmiştir.
- Izgara boyutlarının değerlendirilmesi için yapılan çalışmalarda yüke doğrudan temas eden kaplama tabakasındaki düğüm noktası sayısının artmasının modelin yakınsaması üzerinde çok az bir etkiye sahip olduğu belirlenmiş ancak yükü doğrudan almayan temel tabakasındaki ızgara boyutlarının sonuçlara bir etkisinin olmadığı gözlenmiştir. Izgara boyutlarındaki azalmanın ve düğüm noktası sayısındaki artışın çözüm süresini de artırdığı göz önüne alındığında çok ince ızgaralar ile çalışmanın gerekli olmadığı söylenebilir.
- Kaplama analizlerinde fiziksel olarak tabakaların veya kaplama üzerindeki tekerleğin birbirleri içerisine batma durumu düşünülmediğinden beraber hareket eden yüzeylere ortak düğüm noktaları tanımlamayı sağlayan MPC temas formülasyonunun uygun bir analiz parametresi olduğu düşünülmektedir.

## Teşekkür

Bu çalışma, Cumhuriyet Üniversitesi Bilimsel Araştırma Projeleri (CÜBAP) tarafından M-682 proje numarası ile desteklenmiştir.

## Kaynakça

Abd Alla, E.M., 2006. The rational use of finite element method in the analysis of flexible pavements. Journal of Engineering Sciences, Assiut University, 34, 1185-1211.

Adhikari, S., Shen, S. ve You, Z., 2009. Evaluation of fatigue models of hot-mix asphalt through laboratory testing. Transportation Research Record Journal of the Transportation Research Board, 2127, 36-42.

Ahirwar, S.K. ve Mandal, J.N., 2017. Finite element analysis of flexible pavement with geogrids. Procedia Engineering, 189, 411-416.

Ahmed, A. ve Erlingsson, S., 2016. Viscoelastic response modelling of a pavement under moving load. Transportation Research Procedia, 14, 748-757.

Al-Azzawi, A.A., 2012. Finite element analysis of flexible pavements strenghted with geogrid. ARPN Journal of Engineering and Applied Sciences, 7, 1295-1299.

Ali, H.A. ve Tayabji, S.D., 1998. Mechanistic evaluation of test data from LTPP flexible pavement test sections, US Department of Transportation Federal Highway Administration, Report no. FHWA-RD-98-012

Ambassa, Z., Allou, F., Petit, C. ve Eko, R.M., 2013. Fatigue life prediction of an asphalt pavement subjected to multiple axle loadings with viscoelastic FEM. Constrğuction and Building Materials, 43, 443-452.

Beskou, N.D., Tsinopoulos, S.V. ve Theodorakopoulos, D.D., 2016. Dynamic elastic analysis of 3-D flexible pavements under moving vehicles: A unified FEM

treatment. Soil Dynamics and Earthquake Engineering, 82, 63-72.

Chegenizadeh, A., Keramatikerman, M. ve Nikraz, H., 2016. Flexible pavemet modelling using Kenlayer. EJGE, 21, 2467-2479.

Ekwulo, E.O. ve Eme, D.B., 2009. Fatigue and rutting strain analysis of flexible pavements designed using CBR methods. African Journal of Environmental Science and Technology, 3, 412-421.

Hadi, M.N.S. ve Bodhinayake, B.C., 2003. Non-linear finite element analysis of flexible pavements. Advances in Engineering Software, 34, 657-662.

Hafeez, I., Shan, A., Ali, A. ve Ahmed, I., 2017. Flexible pavement design evaluation using mechanistic-empirical approaches. Technical Journal, University of Engineering and Technology, 22, 27-33.

Huang, Y.H., 2004. Pavement Analysis and Design, Pearson Prentice Hall, New Jersey.

Lu, P., Bratlien, A. ve Tolliver, D., 2014. North Dakota Implementation of Mechanistic-Empirical Pavement Design Guide (MEPDG), Mountain-Plains Consortium, North Dakota.

Muniandy, R., Aburkaba, E. ve Thamer, N., 2013. Comparison of flexible pavement performance using Kenlayer and Chev PC software program. Australian Journal of Basic and Applied Sciences, 7, 112-119.

Sarkar, A., 2016. Numerical comparison of flexible pavement dynamic response under different axles. International Journal of Pavement Engineering, 17, 377-387.

Yoo, P.J., Al-Qadi, L.L., Elseifi, M.A. ve Janajreh, I., 2006. Flexible pavement responses to different loading amplitudes considering layer interface condition and lateral shear forces. The International Journal of Pavement Engineering, 7, 73-86.

Zheng, L., Hai-lin, Y., Wan-ping, W. ve Ping, C., 2012. Dynamic stres and deformation of a layered road structure under vehicle traffic loads: Experimental measurements and numerical calculations. Soil Dynamics and Earthquake Engineering, 39, 100-112.

**GÜFBED/*GUSTIJ* (2018) CMES 2018 SEMPOZYUM EK SAYISI: 31-36**
DOI: 10.17714/gumusfenbil.440949 Araştırma Makalesi / *Research Article*

# Üç Boyutlu Riemannian Heisenberg Grubunda Paralel Faktorable Yüzeylerin Bazı Karakterizasyonları

## *Some New Characterizations of Parallel Factorable Surface in Riemannian Three Dimensional Heisenberg Group*

**Gülden ALTAY SUROĞLU**[a]
*Fırat University, Faculty of Science, Department of Mathematics, 23000, Elazığ*

• Geliş tarihi / *Received*: 05.07.2018 • Düzeltilerek geliş tarihi / *Received in revised form*: 27.9.2018 • Kabul tarihi / *Accepted*: 01.10.2018

**Abstract**
*In this paper, we give some properties of parallel factorable surface which is obtained by group operations in Riemannian three dimensional Heisenberg Group $H_3$. Then, we obtain some characterizetions of parallel factorable surface according to Levi- Civita connections of $H_3$.*

**Keywords**: *Factorable surface, Heisenberg group, parallel surface, Riemannian metric*

***Öz***
*Bu çalışmada üç boyutlu Riemannian Heisenberg grubunda grup işlemiyle elde edilen paralel faktörlenebilen yüzeylerin bazı özellikleri verildi. Daha sonra $H_3$ te Levi- Civita konneksiyonlarına göre paralel faktörlenebilen yüzeylerin bazı karakterizasyonları elde edildi.*

***Anahtar kelimeler:*** *Faktörlenebilen yüzey, Heisenberg grup, paralel yüzey, Riemannian metrik*

[a] Gülden ALTAY SUROĞLU; guldenaltay23@hotmail.com; Tel: (0424) 237 00 00; orcid.org/0000-0003-1976-3465

## 1. Introduction

A surface S in the Euclidean 3-space is r(u,v)={x(u,v),y(u,v),z(u,v)}.
A surface of factorable S in E³ can be given as z=f(x)g(y) or y=f(x)g(z) or x=f(y)g(z), where f and g are smooth functions on some interval of $\mathbb{R}$.

In Yu and Liu (2007), a classification and some fundamental formulas were given for factorable surfaces in the Euclidean space and in the Minkowski space. In Meng and Liu (2009), factorable surfaces in 3- dimensional Minkowski space studied and some classification of such surfaces are given.

A surface $M^r$ is parallel to M if points of $M^r$ are at a constant distance along the normal from the surface M. So, there are infinite numbers of parallel surfaces (Yoon, 2008).

Kızıltuğ and Yaylı studied timelike curves on timelike parallel surfaces in Minkowski 3-spaces $E_1^3$. They find images of timelike curve which lie on timelike surface in $E_1^3$. Then, they gave some characterization for its image curve in (Kızıltuğ and Yaylı, 2012). Unluturk and Ekici (2003), obtain parallel surfaces of timelike ruled surfaces which are developable are timelike ruled Weingarten surfaces. Then, some properties of that kind parallel surfaces are obtained in Minkowski 3-space in (Unluturk and Ekici, 2003). Safiulina investigate the existence and geometry of such two-dimensional Riemannian submanifolds (surfaces) and she gives their complete classification. Moreover, it is shown that in E_{s}^n with s>0 do exist not totally geodesic minimal semiparallel space-like surfaces in (Safiulina, 2001). Calvaruso and Van der Veken completely classified surfaces with parallel second fundamental form in all non-symmetric homogeneous Lorentzian three manifolds in (Calvaruso and Veken, 2010). In Yılmaz (2010), they investigate singularities of all parallel surfaces to a given regular surface.

## 2. Method

The Heisenberg group $Heis_3$ is defined as $R^3$ with the group operation

$$(x,y,z)*(x_1,y_1,z_1)=x+x_1,y+y_1z+z_1+\frac{1}{2}(xy_1-x_1y \quad (1)$$

The left invariant Riemannian metric given by

$$g=ds^2=dx^2+dy^2+\left(dz+\frac{1}{2}(ydx-xdy)\right)^2 \quad (2)$$

Then we have for the left invariant Riemann metric $g$:

$$e_1=\frac{\partial}{\partial x}-\frac{y}{2}\frac{\partial}{\partial z},e_2=\frac{\partial}{\partial y}+\frac{x}{2}\frac{\partial}{\partial z},e_3=\frac{\partial}{\partial z} \quad (3)$$

These vector fields are dual to the coframe

$$w^1=dx,w^2=dy,w^3=dz+\frac{y}{2}dx-\frac{x}{2}dy \quad (4)$$

Then, Levi- Civita connections are

$$2\nabla_{e_i}e_j=\begin{bmatrix}0 & e_3 & -e_2\\ -e_3 & 0 & e_1\\ -e_2 & e_1 & 0\end{bmatrix} \quad (5)$$

also, we have the Heisenberg bracket relations.

$$[e_1,e_2]=e_3,[e_3,e_1]=[e_2,e_3]=0 \quad (6)$$

In this paper, we used Riemannian metric and Levi- Civita connections for obtain mean curvature.

## 3. Parallel Surface of the Factorable Surface in $H_3$

### 3.1. *Parallel Surfaces of Type 1 Factorable Surface*

Let $\alpha(x)=(\alpha_1(x),\alpha_2(x),\alpha_3(x))$ and $\beta(y)=(\beta_1(y),\beta_2(y),\beta_3(y))$ be differentiable nongeodesic curves in $Heis_3$ which is endowed with left invariant Riemannian metric $g$. Type 1 of the factorable surface parameterized as

$$\varphi(x,y)=(\alpha_1(x),0,c)*(0,\beta_2(y),d)=(\alpha_1(x),\beta_2(y),\tfrac{1}{2}\alpha_1(x)\beta_2(y)) \quad (7)$$

Then, the parallel surface of factorable surface $\varphi(x,y)=\alpha(x)*\beta(y)$ is defined as

$$\theta(x,y)=\varphi(x,y)+N(x,y) \quad (8)$$

where N is the unit normal vector field of the factorable surface.

**Theorem 3.1**. If the parallel surface of the factorable surface of type 1 θ(x,y) in the $H_3$ is a minimal surface, then

$$\beta_2'(\frac{a^2}{(1+\beta_2^2)^2}+(\frac{\alpha_1}{2}-\frac{\beta_2}{(1+\beta_2^2)^{3/2}})^2+1)(-\beta_2\alpha_1''+\frac{1}{2}\alpha_1'^2_1\beta_2(\alpha_1+\frac{\beta_2(a+2)}{(1+\beta_2^2)^{3/2}})+2\alpha_1''\beta_2)$$
$$-\frac{\beta_2'}{2}(\alpha_1'(-\beta_2^2+(\alpha_1+\frac{\beta_2(a+2)}{(1+\beta_2^2)^{3/2}})(\frac{\alpha_1}{2}+\frac{\beta_2(a+1)}{(1+\beta_2^2)^{3/2}})+2(\alpha_1'-1))-\beta_2^2$$
$$-(\beta_2+\frac{\alpha_1}{2}-\frac{\beta_2}{(1+\beta_2^2)^{3/2}})(\alpha_1+\frac{\beta_2(a+2)}{(1+\beta_2^2)^{3/2}})+2(\beta_2'-1)+\alpha_1'\beta_2'(1+\frac{1}{4}\beta_2^2) \quad (9)$$
$$(-\beta_2\frac{\alpha_1}{2}-\frac{\beta_2 a}{(1+\beta_2^2)^{3/2}}+A)-\frac{a}{(1+\beta_2^2)^{3/2}}(\frac{\alpha_1}{2}-\frac{\beta_2}{(1+\beta_2^2)^{3/2}})$$
$$\alpha_1+\frac{\beta_2(a+2)}{(1+\beta_2^2)^{3/2}})+2B=0$$

where

$$A=\frac{a(-3\beta_2\beta_2'+(1+\beta_2^2)\beta_2'')}{(1+\beta_2^2)^{5/2}} \quad (10)$$

$$B=\frac{\beta_2'(1-2\beta_2^2)+\beta_2\beta_2''(1+\beta_2^2)}{(1+\beta_2^2)^{5/2}} \quad (11)$$

**Proof.** The parameterization of the parallel factorable suface

$$\theta(x,y)=(\alpha_1(x)-\frac{a\beta_2(y)}{\sqrt{1+\beta_2(y)^2}})e_1+\beta_2(y)e_2+(\frac{1}{2}\alpha_1(x)\beta_2(y)+\frac{a}{\sqrt{1+\beta_2(y)^2}})e_3 \quad (12)$$

where a is a non-zero constant. If we take derivatives of the parallel surface of the factorable surface according to x and y, then we have

$$\theta_x=\alpha_1'(e_1+\frac{1}{2}\beta_2 e_3) \quad (13)$$

$$\theta_y=\beta_2'(\frac{a}{(1+\beta_2^2)^{3/2}}e_1+e_2+(\frac{1}{2}\alpha_1+\frac{a\beta_2}{(1+\beta_2^2)^{3/2}})e_3) \quad (14)$$

An orthogonal vector at each point of the surface is

$$N=\frac{1}{\rho}(-\beta_2 e_1+(\alpha_1+\frac{3\beta_2 a}{(1+\beta_2^2)^{3/2}})e_2+2e_3) \quad (15)$$

where

$$\rho=\sqrt{\beta_2^2+(\alpha_1+\frac{3\beta_2 a}{(1+\beta_2^2)^{3/2}})^2+4} \quad (16)$$

The coefficients of the first fundamental form are

$$E=\alpha_1'^2(1+\frac{1}{4}\beta_2^2) \quad (17)$$

$$F=\alpha_1'\beta_2'^2(\frac{a}{(1+\beta_2^2)^{3/2}}+\frac{1}{2}\beta_2(\frac{\alpha_1}{2}-\frac{a\beta_2}{(1+\beta_2^2)^{3/2}})) \quad (18)$$

$$G = \beta_2{}'^2\left(\frac{a^2}{(1+\beta_2{}^2)^3} + \left(\frac{1}{2}\alpha_1 + \frac{a\beta_2}{(1+\beta_2{}^2)^{3/2}}\right)^2 + 1\right) \tag{19}$$

Then, components of the second fundamental form are

$$h_{11} = \frac{\alpha_1{}'}{\rho}\left(-\beta_2\alpha_1{}'' + \frac{1}{2}\left(\alpha_1{}'^2\beta_2\left(\alpha_1 + \frac{\beta_2(a+2)}{(1+\beta_2{}^2)^{3/2}}\right) + 2\alpha_1{}''\beta_2\right)\right. \tag{20}$$

$$h_{12} = \frac{\alpha_1{}'\beta_2{}'}{2\rho}\left(-\beta_2{}^2 + \alpha_1\left(\frac{\alpha_1}{2} + \frac{\beta_2(1+a)}{(1+\beta_2{}^2)^{3/2}} + 2(\alpha_1{}'-1)\right)\right. \tag{21}$$

$$h_{21} = \frac{\beta_2{}'}{2\rho}\left(-\beta_2{}^2 - \left(\beta_2 + \frac{\alpha_1}{2} - \frac{a\beta_2}{(1+\beta_2{}^2)^{3/2}}\left(\alpha_1 + \frac{\beta_2(2+a)}{(1+\beta_2{}^2)^{3/2}} + 2(\beta_2{}'-1)\right)\right.\right. \tag{22}$$

$$\begin{aligned} h_{22} &= \frac{\beta_2{}'}{2\rho}\left(-\beta_2(y)\left(\frac{\alpha_1}{2} - \frac{a\beta_2}{(1+\beta_2{}^2)^{3/2}} + A\right) - \frac{a}{(1+\beta_2{}^2)^{3/2}}\left(\frac{\alpha_1}{2} - \frac{a\beta_2}{(1+\beta_2{}^2)^{3/2}}\right)\right. \\ &\left.\left(\alpha_1 + \frac{\beta_2(2+a)}{(1+\beta_2{}^2)^{3/2}} + 2B\right),\right. \end{aligned} \tag{23}$$

So, if θ(x,y) is minimal, we have the equation (17).

### 3.2. *Parallel Surfaces of Type 2 Factorable Surface*

Let $\alpha(x)$ and $\beta(y)$ be differentiable nongeodesic curves in $Heis_3$ which is endowed with left invariant Riemannian metric $g$. Type 1 of the factorable surface parameterized as

$$\varphi(x,y) = (0,\alpha_2(x),c) * (\beta_1(y),0,-c) = (\beta_1(y),\alpha_2(x),\frac{1}{2}\beta_1(y)\alpha_2(x)) \tag{24}$$

Then, the parallel surface of factorable surface $\phi(x,y) = \alpha(x) * \beta(y)$ is defined as

$$\xi(x,y) = (\beta_1(y),\alpha_2(x),\frac{1}{2}\beta_1(y)\alpha_2(x)) + bN(x,y) \tag{25}$$

where N is the unit normal vector field of the factorable surface and b is a non-zero constant.

**Theorem 3.2**. If the parallel surface of the factorable surface of type 2 ξ(x,y) in the $H_3$ is a minimal surface, then

$$
\begin{aligned}
&\alpha_2{}'^2\,\beta_1{}'((1+\frac{\beta_1^2}{4})(\frac{b}{(1+\beta_1^2)^{3/2}}(\beta_1{}''+\frac{1}{2}(\frac{\alpha_2}{2}-\frac{b\beta_1}{(1+\beta_1^2)^{3/2}})(\frac{\alpha_2}{2}-\frac{\beta_1(b+1)}{(1+\beta_1^2)^{3/2}})\\
&+(\frac{1}{4}\beta_1(\frac{\alpha_2}{2}-\frac{b\beta_1}{(1+\beta_1^2)^{3/2}})(\frac{b\beta_1}{(1+\beta_1^2)^{3/2}}-1)-\frac{3b\beta_1\beta_1{}'}{(1+\beta_1^2)^{5/2}}-\frac{\beta_1}{2}))\\
&-\alpha_2{}'\beta_1^2(1+\frac{\beta_1}{2}(\frac{\alpha_2}{2}-\frac{b\beta_1}{(1+\beta_1^2)^{3/2}}))((\frac{\alpha_2}{2}-\frac{b\beta_1}{(1+\beta_1^2)^{3/2}})(\frac{\alpha_2}{2}-\frac{\beta_1(b+1)}{(1+\beta_1^2)^{3/2}})\\
&-\frac{3b\beta_1\beta_1{}'}{2(1+\beta_1^2)^{5/2}}+b(\frac{3\beta_1\beta_1{}'^2-(1+\beta_1^2)\beta_1{}''}{(1+\beta_1^2)^{5/2}}+\frac{1}{2})+\frac{\alpha_2{}'}{2}(\frac{\alpha_2}{2}-\frac{b\beta_1}{(1+\beta_1^2)^{3/2}})(\frac{\alpha_2}{2}-\frac{\beta_1(b+1)}{(1+\beta_1^2)^{3/2}})\\
&+\frac{1}{2}\beta_1(\alpha_2{}''-\frac{1}{4}\alpha_2{}'\beta_1)+\frac{1}{2}(\beta_1\alpha_2{}''+\alpha_2{}'\beta_1{}'(\frac{b}{(1+\beta_1^2)^{3/2}}+1)))\\
&+\beta_1{}'^2\alpha_2{}'^2(1+\frac{b^2}{(1+\beta_1^2)^3}+(\frac{\alpha_2}{2}-\frac{b\beta_1}{(1+\beta_1^2)^{3/2}})^2)((\frac{\alpha_2}{2}-\frac{\beta_1(b+1)}{(1+\beta_1^2)^{3/2}})+\beta_1{}'=0.
\end{aligned}
\tag{26}
$$

*Proof.* The proof can be shown similarly to Theorem 1.

**Example 3.3.** Let the factorable surface given with

$$\varphi(x,y)=\cos y e_1+\sin x e_2+\frac{1}{2}\sin x\cos y e_3 \quad (27)$$

and the unit normal vector fied of this surface is

$$
\begin{aligned}
&N=-\frac{\sin x}{\sqrt{\cos^2 y+\sin^2 x+4}}e_1-\frac{\cos y}{\sqrt{\cos^2 y+\sin^2 x+4}}e_2+\frac{2}{\sqrt{\cos^2 y+\sin^2 x+4}}e_3.\\
&\cos y e_1+\sin x e_2+\frac{1}{2}\sin x\cos y e_3
\end{aligned}
\tag{28}
$$

Then, the parallel factorable surface of type 2 is

$$
\begin{aligned}
&\xi(x,y)=(\cos y-\frac{\sin x}{\sqrt{\cos^2 y+\sin^2 x+4}})e_1+(\sin x-\frac{\cos y}{\sqrt{\cos^2 y+\sin^2 x+4}})e_2\\
&+(\frac{\sin x\cos y}{2}+\frac{2}{\sqrt{\cos^2 y+\sin^2 x+4}}e_3.
\end{aligned}
\tag{29}
$$

## 4. Conclusion

In this paper, we deduce conditions of minimal parallel factorable surface in three dimensional Riemannian Heisnberg group.

## References


Calvaruso, G. and Van der Veken, J., 2010. Parallel Surfaces in Three Dimensional Lie Groups. Taiwanese Journal of Mathematics, 14(1), 223-250.

Kızıltuğ, S. and Yaylı, Y., 2012. Timelike Curves on Timelike Parallel Surfaces in Minkowski 3-space $E_1^3$. Mathematica Aeterna, 2(8), 689 – 700.

Meng, H. and Liu, H., 2009. Factorable Surfaces in 3- Minkowski Space. Bulletin of the Korean Mathematical Society. 46(2), 155-169.

Safiulina, E., 2001. Parallel and Semi-parallel Space-like Surfaces in Pseudo-Euclidean Spaces. Proceedings of the

Estonian Academy of Sciences. Physics. Mathematics, 50(1), 16-33.

Unluturk, Y. and Ekici, C., 2003. On Parallel Surfaces of Timelike Ruled Weingarten Surfaces. Balkan Journal of Mathematics, 1, 72-91.

Yılmaz, S., 2010. Bishop spherical images of a spacelike curve in Minkowski 3-space. International Journal of the Physical Sciences, 5(6), 898-905.

Yoon, D.W., 2008. Some properties of parallel surfaces in Euclidean 3-spaces. Honam Mathematical Journal, 30(4), 637-644.

Yu, Y. and Liu, H., 2007. The factorable minimal surfaces. Proceedings of The Eleventh International Workshop on Differential Geometry, 11, 33-39.

**GÜFBED/*GUSTIJ* (2018) CMES 2018 SEMPOZYUM EK SAYISI: 37-45**
DOI: 10.17714/gumusfenbil.429431 Araştırma Makalesi / *Research Article*

# Yıldızıl Fonksiyonların $P(j, \lambda, \alpha, n, z_0)$ Alt Sınıfının Özellikleri

## *On Properties of the Subclass $P(j,\lambda,\alpha,n,z_0)$ of Starlike Functions*

**Hüseyin BABA***
*Hakkâri Üniversitesi, Çölemerik Meslek Yüksekokulu, Matematik Bölümü, 30000, Hakkâri*

• Geliş tarihi / *Received*: 01.06.2018 • Düzeltilerek geliş tarihi / *Received in revised form*: 18.09.2018 • Kabul tarihi / *Accepted*: 03.10.2018

**Öz**
Bu makalede, açık birim diskte analitik olan $f(z) = z - \sum_{k=j+1}^{\infty} a_k z^k$ biçimindeki fonksiyonlar ve $D^n$ diferansiyel operatörü kullanılarak negatif katsayılı yıldızıl fonksiyonların $P(j, \lambda, \alpha, n)$ alt sınıfına çalışıldı. $a_k \geq 0$ , $z_0 \in \mathbb{R}$ ve $f(z_0) = z_0$ olan $P(j, \lambda, \alpha, n, z_0)$ sınıfını göz önüne alındı. $P(j, \lambda, \alpha, n, z_0)$ sınıfına ait bazı özellikler elde edildi.

**Anahtar kelimeler:** Ünivalent fonksiyon, Sabit nokta, Yıldızıl, Konveks, Sălăgean operatörü

***Abstract***
*In this paper, we study the subclass $P(j, \lambda, \alpha, n)$ of starlike functions and with negative coefficients by using the differential $D^n$ operator and functions of the form $f(z) = z - \sum_{k=j+1}^{\infty} a_k z^k$ which are analytic in the open unit disk. We consider the class $P(j, \lambda, \alpha, n, z_0)$ for which $(z_0) = z_0$ , $z_0$ real where $a_k \geq 0$. Some properties belonging to the class $P(j, \lambda, \alpha, n, z_0)$ are obtained.*

***Keywords:*** *Univalent function, Fixed point, Starlike, Convex, Sălăgean operator*

*Hüseyin BABA, huseyinbaba@hakkari.edu.tr, Tel: (0438) 211 83 56 -1434; 0(531) 7186412; orcid.org/0000-0001-9749-2299

## 1. Giriş

***1.1. Tanım*** $f$, $\mathcal{U}=\{z: z\in\mathbb{C}\ ve\ |z|<1\}$ açık birim diskinde analitik olan

$$f(z)=z+\sum_{n=2}^{\infty}a_n z^n \qquad (1)$$

formundaki $f$ fonksiyonlar ailesi $\mathcal{A}$ ile tanımlıdır. $f\in\mathcal{A}$ fonksiyonunun $\alpha$. mertebeden yıldızıl olduğunu söyleyebilmemiz için gerek ve yeter şart

$$Re\left\{\frac{zf'(z)}{f(z)}\right\}>\alpha \qquad (0\le\alpha<1;\ z\in\mathcal{U}) \qquad (2)$$

olmasıdır. Bütün böyle fonksiyonların sınıfı $S^*(\alpha)$ olarak adlandırılır. Ayrıca $f\in\mathcal{A}$ fonksiyonunun $\alpha$. mertebeden konveks olduğunu söyleyebilmemiz için gerek ve yeter şart

$$Re\left\{1+\frac{zf''(z)}{f'(z)}\right\}>\alpha \quad (0\le\alpha<1;\ z\in\mathcal{U}) \qquad (3)$$

olmasıdır. Bütün böyle fonksiyonların sınıfı $C(\alpha)$ olarak adlandırılır. $\mathcal{U}$ açık birim diskinde yıldızıl ve konveks fonksiyonların sınıfı sırasıyla $S^*(0)=S$ ve $C(0)=C$ ile gösterilir.

Silverman (1976), $a_n\ge 0$ ve $-1<z_0<1$ olmak üzere $f$ fonksiyonunun $f(z_0)=z_0$ olan yıldızıl fonksiyonların alt sınıflarını $S_0^*(\alpha,z_0)$ şeklinde ve $f'(z_0)=1$ olan yıldızıl fonksiyonların alt sınıflarını da $S_1^*(\alpha,z_0)$ şeklinde tanımladı (Silverman, 1976).

***1.2. Tanım***

$D^0f(z)=f(z)$

$D^1f(z)=Df(z)=zf'(z)=z+\sum_{k=j+1}^{\infty}ka_kz^k$

.

.

.

$\mathrm{D^nf(z)=D\left(D^{n-1}f(z)\right)=z+\sum_{k=j+1}^{\infty}k^na_kz^k}\qquad(\mathrm{n}\in\mathbb{N})$

şeklindeki $D$ operatörüne Sălăgean Operatörü denir (Sălăgean, 1983).

***1.3. Tanım*** $\mathcal{U}=\{z: z\in\mathbb{C}\ ve\ |z|<1\}$ açık birim diskinde analitik olan

$$\mathrm{f(z)=z+\sum_{k=j+1}^{\infty}a_kz^k}\qquad(\mathrm{j}\in\mathbb{N}=\{1,2,3,\dots\}) \qquad (4)$$

şeklindeki fonksiyonların sınıfı $\mathcal{A}(j)$ olarak tanımlanır (Sălăgean, 1983).

***1.4. Tanım*** $\mathcal{A}(j)$ sınıfında olan $f$ fonksiyonunun pozitif katsayılı $Q(j,\lambda,\alpha,n)$ sınıfında olması için gerek ve yeter şart

$$Re\left\{\frac{(1-\lambda)z\left(D^nf(z)\right)'+\lambda z\left(D^{n+1}f(z)\right)'}{(1-\lambda)D^nf(z)+\lambda D^{n+1}f(z)}\right\}>\alpha \qquad (5)$$

$(j\in\mathbb{N};0\le\alpha<1;0\le\lambda<1;n\in\mathbb{N}_0;\ \forall z\in\mathcal{U})$ olmasıdır. Burada, $D^n$ Sălăgean operatörüdür (Aouf ve Srivastava, 1996).

***1.5. Tanım*** $\mathcal{U}$ açık birim diskinde analitik olan

$$f(z)=z-\sum_{k=j+1}^{\infty}a_kz^k \qquad (a_k\ge 0;n\in\mathbb{N}) \qquad (6)$$

biçimindeki fonksiyonların sınıfı $T(j)$ olarak tanımlanır (Aouf ve Srivastava, 1996).

***1.6. Tanım*** $P(j,\lambda,\alpha,n)=Q(j,\lambda,\alpha,n)\cap T(j)$ ile negatif katsayılı olarak $P(j,\lambda,\alpha,n)$ sınıfı olarak tanımlanır (Aouf ve Srivastava, 1996). $P(j,\lambda,\alpha,n)$ sınıfındaki bir $f$ fonksiyonu

$D^0f(z)=f(z)$

$D^1f(z)=Df(z)=zf'(z)=z-\sum_{k=j+1}^{\infty}ka_kz^k$

ve $n=1,2,3,..$ için

$D^nf(z)=D\left(D^{n-1}f(z)\right)=z-\sum_{k=j+1}^{\infty}k^na_kz^k$

$(n\in\mathbb{N})$

yazabiliriz.

$P(j,\lambda,\alpha,n)$ sınıfına ait fonksiyonlar için katsayı eşitsizliklerini, ayrık teoremlerini, kapalılık teoremlerini ve bazı özelliklerini Aouf ve Srivastava (1996) elde etmişlerdir. Onlar birde $P(j,\lambda,\alpha,n)$ sınıfının konvekslik, yıldızıllık, yakın konvekslik yarıçapını belirlemişlerdir.

Teoremimizin ispatı için aşağıdaki üç lemma gereklidir.

***1.1. Lemma*** $f(z)=z-\sum_{k=j+1}^{\infty}a_kz^k$ şeklinde tanımlı fonksiyonun $P(j,\lambda,\alpha,n)$ sınıfında olması için gerek ve yeter şart

$$\sum_{k=j+1}^{\infty}k^n(k-\alpha)\{1+(k-1)\lambda\}a_k\le 1-\alpha \qquad (7)$$

olmasıdır. Burada, $a_k\ge 0$, $n\in\mathbb{N}_0$, $0\le\alpha<1$, $z\in\mathcal{U}$ $ve$ $0\le\lambda<1$ dır (Aouf ve Srivastava, 1996).

***1.2. Lemma*** Her $n\in\mathbb{N}$ için $a_n\ge 0$ olmak üzere $f(z)=a_1z-\sum_{n=2}^{\infty}a_nz^n$ fonksiyonunun $S_0^*(\alpha,z_0)$ olması için gerek ve yeter şart

$$\sum_{n=2}^{\infty}a_n\left[\frac{n-\alpha}{1-\alpha}-z_0^{n-1}\right]\le 1 \qquad (8)$$

olmasıdır. Burada, $z_0 \in \mathbb{R}$ sabit nokta, $a_1 \neq 0$ ve $0 \leq \alpha < 1$ dır (Silverman, 1976).

***1.1. Sonuç*** (Silverman, 1975) makalesindeki, 3. Teoreminin ispatında küçük bir değişik ile Teorem 3.1.3'ün şartları altında $f(z)$ fonksiyonunun ünivalent olması için gerek ve yeter şart $\sum_{n=2}^{\infty} a_n(n - {z_0}^n) \leq 1$ durumunu ortaya koymuştur ($\alpha = 0$ olduğuna dikkat edelim). Dolayısıyla, Silverman'nın yukarıdaki gibi tanımladığı fonksiyonların ünivalent olması için gerek ve yeter şart yıldızıl olmasıdır sonucu çıkarılır (Silverman, 1976).

***1.2. Sonuç (Ekstremal fonksiyon)*** Eğer $f(z) = a_1 z - \sum_{n=2}^{\infty} a_n z^n$ fonksiyonu $S_0^*(\alpha, z_0)$ sınıfında olursa, o zaman her $n \in \mathbb{N}$ için $a_n \leq \frac{1-\alpha}{(n-\alpha)-(1-\alpha)z_0^{n-1}}$ olduğundan ekstremal fonksiyonu

$$f(z) = \frac{(n-\alpha)z-(1-\alpha)z^n}{(n-\alpha)-(1-\alpha)z_0^{n-1}} \quad (9)$$

dir (Silverman, 1976).

***1.3. Lemma*** $f(z) = z - \sum_{k=j+1}^{\infty} a_k z^k$ şeklinde tanımlı fonksiyonun $P(j, \lambda, \alpha, n, z_0)$ sınıfında olması için gerek ve yeter şart

$$\sum_{k=j+1}^{\infty} \left[k^n \left(\frac{k-\alpha}{1-\alpha}\right)\{1 + (k-1)\lambda\} - z_0^{k-1}\right] a_k \leq 1 \quad (10)$$

olmasıdır. Burada $a_k \geq 0, j \in \mathbb{N}, n \in \mathbb{N}_0, 0 \leq \alpha < 1, z \in \mathcal{U},\ 0 \leq \lambda < 1$ ve $z_0 \in \mathbb{R}$ sabit noktadır (Kızıltunc ve Baba, 2012).

Herhangi bir sabit noktaya sahip $P(j, \lambda, \alpha, n, z_0)$ alt sınıfını tanımlandı ve bu sınıfa ait katsayı eşitsizlikleri belirlendi (Kızıltunç ve Baba, 2012). Baba (2018), çalışmamda $P(j, \lambda, \alpha, n, z_0)$ sınıfının konveks olduğunu ve bu sınıfa ait fonksiyonların Modified Hadamard çarpımı elde edildi. Bu makaledeki sonuçlar, (Silverman, 1976) makalesiyle sonuç kesinleştirildi.

## 2. $P(j, \lambda, \alpha, n, z_0)$ Sınıfının Bazı Özellikleri

$P(j, \lambda, \alpha, n, z_0)$ sınıfı için örnekler ve bazı sonuçlar verildi. (Aouf ve Srivastava, 1996) tarafından kullanılan yöntemlerle $P(j, \lambda, \alpha, n, z_0)$ sınıfının bazı özellikleri elde edildi.

***2.1. Örnek*** Öncelikle $z \in \mathcal{U}$ olmak üzere, Lemma 1.1 yardımıyla $P(j, \lambda, \alpha, n)$ sınıfına ait $f(z)$ fonksiyonunu tanımlayalım. $j = 1,\ \alpha = 0$ ve $\lambda = 1$ değerleri için, (7) eşitsizliğinden $\sum_{k=2}^{\infty} k^{n+2} a_k \leq 1$ elde edilir ve bu son eşitsizlikte $a_k = \frac{1}{k^{n+6}}$ alınırsa,

$\sum_{k=2}^{\infty} k^{n+2} a_k = \sum_{k=2}^{\infty} k^{n+2} \frac{1}{k^{n+6}} = \sum_{k=2}^{\infty} \frac{1}{k^4} = \frac{31\pi^4}{1440} - 1 \cong 0{,}082323 < 1$

olur ve dolayısıyla

$$f(z) = z - \sum_{k=2}^{\infty} \frac{1}{k^{n+6}} z^k \quad (11)$$

fonksiyonu elde edilir. Ayrıca, bu $f(z)$ fonksiyonu reel eksen boyunca $z \to 1$ iken,

$$Re\left\{\frac{(1-\lambda)z\left(D^n f(z)\right)' + \lambda z\left(D^{n+1} f(z)\right)'}{(1-\lambda)D^n f(z) + \lambda D^{n+1} f(z)}\right\} > \alpha \Longrightarrow Re\left\{\frac{z\left(D^n f(z)\right)'}{D^{n+1} f(z)}\right\} > 0 \Longrightarrow \frac{1+\sum_{k=2}^{\infty}\frac{1}{k^4}}{1+\sum_{k=2}^{\infty}\frac{1}{k^3}} > 0 \quad (12)$$

olduğundan dolayı $P(j, \lambda, \alpha, n, z)$ sınıfındadır. Şimdi de, (11) deki $f(z)$ fonksiyonu için (10) eşitsizliği kullanılarak,

$$\sum_{k=2}^{\infty} \left[k^{n+2} - {z_0}^{k-1}\right] \frac{1}{k^{n+6}} \leq 1 \Longrightarrow \sum_{k=2}^{\infty} \frac{1}{k^{n+6}} z_0^{k-1} \geq \sum_{k=2}^{\infty} \frac{1}{k^4} - 1 = \frac{31\pi^4}{1440} - 2$$

eşitsizliği elde edilir. Bu da, $f(z)$ fonksiyonun $P(j, \lambda, \alpha, n, z_0)$ sınıfında olması demektir. Bu son eşitsizliğin sol tarafı sıfıra eşit olacağından fonksiyonun sabit noktası bulunabilir. Yine, son eşitsizliğin sağ tarafı negatif olduğundan, $z_0 = 0$ noktası $f(z)$ fonksiyonunun bir sabit noktasıdır. Birim diskin $f(z)$ fonksiyonu altındaki görüntüsü Şekil 1'de gösterildiği gibidir.

***2.1. Not*** Genel olarak, her $z_0 \in \mathbb{R}$ sabit noktası için uygun bir $a_k$ katsayısı bulunarak, $P(j, \lambda, \alpha, n, z_0)$ sınıfına ait $f(z)$ fonksiyonunun sabit noktası bulunabilir. Bunun için Lemma 1.3'ün şartlarını ve bu teoremin bir sonucu olan $\sum_{k=j+1}^{\infty} a_k z_0^{k-1} = 0$ eşitliğini sağlaması yeterli olacaktır.

***2.2. Örnek*** $z_0 = \frac{1}{2}$ sabit nokta olmak üzere, $P(j, \lambda, \alpha, n, z_0)$ sınıfına ait herhangi bir $f(z)$ fonksiyonu bulalım. Lemma 1.1 yardımıyla $n = 0$, $j = 1$, $\alpha = 0$ ve $\lambda = 1$ değerleri için, (7) eşitsizliğinden $\sum_{k=2}^{\infty} k a_k \leq 1$ elde edilir. Bunun için uygun bir $a_k$ katsayısı,

$$\sum_{k=2}^{\infty} k a_k = \sum_{k=2}^{\infty} k \left( \frac{2{,}3413}{k^2(k-1)} - \left(\frac{1}{2}\right)^{k-1} \right) = \sum_{k=2}^{\infty} \left( \frac{2{,}3413}{k(k-1)} - k\left(\frac{1}{2}\right)^{k-1} \right) \cong 2{,}3 - 3 \leq 1$$

eşitsizliğini sağlayacak şekilde $a_k = \frac{2{,}3413}{k^2(k-1)} - \left(\frac{1}{2}\right)^{k-1}$ olarak bulunabilir.

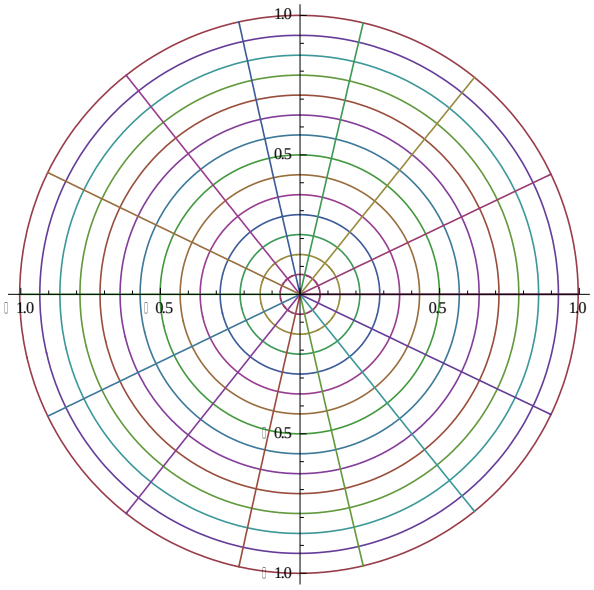


**Şekil 1.** Birim diskin $f(z) = z - \sum_{k=2}^{\infty} \frac{1}{k^{n+6}} z^k$ fonksiyonu altındaki görüntüsü ($z_0 = 0$ sabit noktası için).

Şimdi de,

$$f(z) = z - \sum_{k=2}^{\infty} \left[ \frac{2{,}3413}{k^2(k-1)} - \left(\frac{1}{2}\right)^{k-1} \right] z^k \tag{13}$$

fonksiyonu için (1.10) eşitsizliği kullanılarak,

$$\sum_{k=2}^{\infty} \left[ k - z_0{}^{k-1} \right] a_k \leq 1 \Longrightarrow \sum_{k=2}^{\infty} a_k z_0^{k-1} \geq \sum_{k=2}^{\infty} k a_k = 2{,}3413 - 3 = -0{,}6587$$

elde edilir. Son eşitsizliğin sol tarafı sıfıra eşit olacağından fonksiyonun sabit noktasını bulunabilir. Burada Lemma 1.3'ün şartlarının sağlandığı görülebilir. Yine, $z_0 = 0$ noktası bu elde edilen fonksiyonun bir sabit noktasıdır.

Aynı şekilde, $z_0 = \frac{1}{2}$ noktasının bir sabit nokta olması için (13)'deki fonksiyonun $\sum_{k=j+1}^{\infty} a_k z_0^{k-1} = 0$ eşitliğini sağlaması gerekir. O halde,

$$\sum_{k=2}^{\infty} \left[ \frac{2{,}3413}{k^2(k-1)} - \left(\frac{1}{2}\right)^{k-1} \right] = \sum_{k=2}^{\infty} \frac{2{,}3413 \left(\frac{1}{2}\right)^{k-1}}{k^2(k-1)} = 2{,}3413.0{,}14237 - \frac{1}{3} = \frac{1}{3} - \frac{1}{3} = 0$$

olacağından $z_0 = \frac{1}{2}$ noktası bu $f(z)$ fonksiyonunun bir sabit noktadır. Burada, birim diskin $f(z) = z - \sum_{k=2}^{\infty}\left[\frac{2,3413}{k^2(k-1)} - \left(\frac{1}{2}\right)^{k-1}\right]z^k$ fonksiyonu altındaki görüntüsü Şekil 2'de verilmiştir.

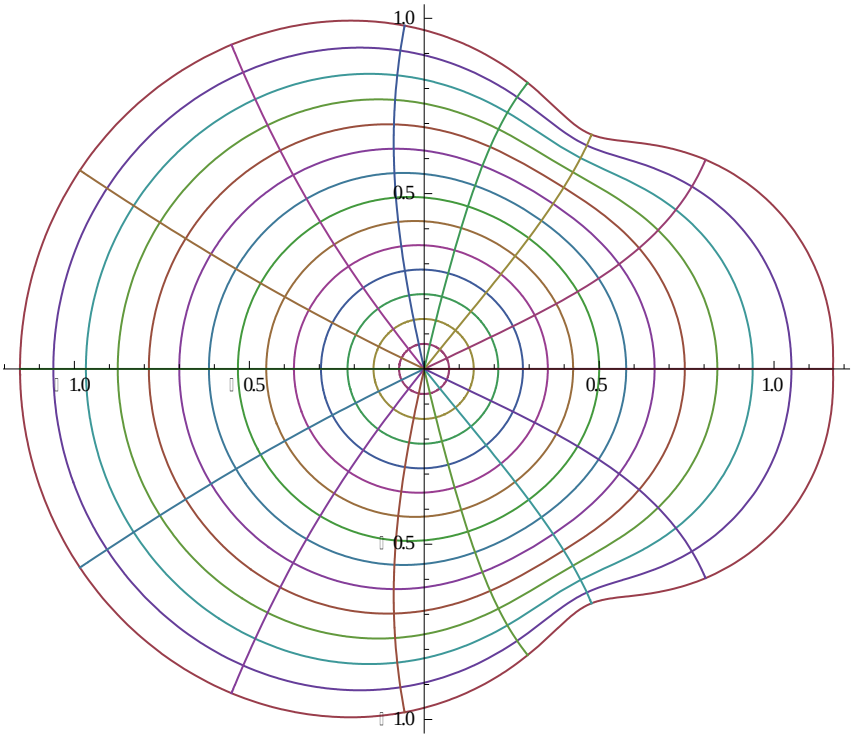


**Şekil 2.** Birim diskin $f(z) = z - \sum_{k=2}^{\infty}\left[\frac{2,3413}{k^2(k-1)} - \left(\frac{1}{2}\right)^{k-1}\right]z^k$ fonksiyonu altındaki görüntüsü ($z_0 = \frac{1}{2}$ için).

***2.1. Sonuç*** Lemma 1.1 için ekstremal fonksiyonu,

$$f(z) = z - \frac{(1-\alpha)(j+1)^m}{(j+1)^n(j+1-\alpha)(1+j\lambda) - (1-\alpha){z_0}^{k-1}}z^{j+1} \tag{14}$$

şeklindedir. Burada $a_k \geq 0, j \in \mathbb{N}, n \in \mathbb{N}_0, 0 \leq \alpha < 1, z \in \mathcal{U},\ 0 \leq \lambda < 1$ ve $z_0 \in \mathbb{R}$ sabit noktadır.

***2.2. Sonuç*** $f(z) \in P(j, \lambda, \alpha, n, z_0)$ ise

$$a_k \leq \frac{(1-\alpha)(j+1)^m}{(j+1)^n(j+1-\alpha)(1+j\lambda) - (1-\alpha){z_0}^{k-1}} \tag{15}$$

dır.

***2.3. Sonuç*** Eğer, $j = 1, \lambda = 0, n = 0$ alınırsa $P(j, \lambda, \alpha, n, z_0) = P(1, \alpha, z_0)$ olur. Dolayısıyla,

$$\sum_{k=2}^{\infty}\left[\left(\frac{k-\alpha}{1-\alpha}\right) - z_0^{k-1}\right]a_k \leq 1 \tag{16}$$

olur ki, $P(1, \alpha, z_0) = S_0^*(\alpha, z_0)$ elde edilir (Kiziltunc ve Baba, 2012).

***2.4. Sonuç*** $f(z) \in P(j, \lambda, \alpha, n, z_0)$ sınıfının ünivalent olması için gerek ve yeter şart

$$\sum_{k=j+1}^{\infty}\left[k^{n+1}\{1+(k-1)\lambda\}-z_0^{k-1}\right]a_k \leq 1 \tag{17}$$

olmasıdır. $j=1, \lambda=1, n=0$ alınırsa Sonuç 1.1 elde edilir.

***2.5. Sonuç*** Eğer, $j=1, \lambda=1, n=0$ alınırsa $P(j,\lambda,\alpha,n,z_0)=P(1,1,\alpha,z_0)$ olur. Dolayısıyla,

$$\sum_{k=2}^{\infty}\left[\frac{k(k-\alpha)}{1-\alpha}-z_0^{k-1}\right]a_k \leq 1 \tag{18}$$

olur ki, $P(1,1,\alpha,z_0)=K_0^*(\alpha,z_0)$'dır (Kiziltunc ve Baba, 2012).

***2.1. Teorem*** $0\leq \alpha_1 \leq \alpha_2$, $0\leq \lambda \leq 1$, $n \in \mathbb{N}_0$ ve j ∈ ℕ olmak üzere

$$P(j,\lambda,\alpha_1,n,z_0) \supseteq P(j,\lambda,\alpha_2,n,z_0) \tag{19}$$

dir.

*İspat.* $0\leq \alpha_1 \leq \alpha_2 < 1$ ve $\delta > 0$ olmak üzere, $P(j,\lambda,\alpha_1,n,z_0) \supseteq P(j,\lambda,\alpha_2,n,z_0)$ olduğunu gösterelim. $f(z) \in P(j,\lambda,\alpha_2,n,z_0)$ ve $\alpha_1=\alpha_2-\delta$ olsun. Lemma 1.3 kullanılarak

$$\sum_{k=j+1}^{\infty}\left[k^n\left(\frac{k-\alpha_2}{1-\alpha_2}\right)\{1+(k-1)\lambda\}-z_0^{k-1}\right]a_k \leq 1$$

elde edilir ve $\sum_{k=j+1}^{\infty} a_k z_0^{k-1}=0$ olduğundan,

$$\sum_{k=j+1}^{\infty}\left[k^n(k-\alpha_2)\{1+(k-1)\lambda\}-z_0^{k-1}\right]a_k \leq 1-\alpha_2$$

dır. Lemma 1.1'den,

$$\sum_{k=j+1}^{\infty}[k^n\{1+(k-1)\lambda\}]a_k \leq 1$$

olur. Sonuç olarak,

$$\begin{aligned}
&\sum_{k=j+1}^{\infty}\left[k^n(k-\alpha_1)\{1+(k-1)\lambda\}-z_0^{k-1}\right]a_k \\
&=\sum_{k=j+1}^{\infty}\left[k^n(k-\alpha_2+\delta)\{1+(k-1)\lambda\}-z_0^{k-1}\right]a_k \\
&\leq \sum_{k=j+1}^{\infty}\left[k^n(k-\alpha_2)\{1+(k-1)\lambda\}-z_0^{k-1}\right]a_k+\delta\sum_{k=j+1}^{\infty}k^n\{1+(k-1)\lambda\}\,a_k \\
&\leq 1-\alpha_2+\delta=1-\alpha_1<1
\end{aligned}$$

olduğundan, $f(z) \in P(j,\lambda,\alpha_1,n,z_0)$ olur.

***2.2. Teorem*** $0\leq \alpha < 1$, $0\leq \lambda_1 \leq \lambda_2 \leq 1$ olmak üzere

$$P(j,\lambda_1,\alpha,n,z_0) \supseteq P(j,\lambda_2,\alpha,n,z_0) \tag{20}$$

dir.

*İspat.* $0\leq \lambda_1 \leq \lambda_2 \leq 1$ ve $\delta > 0$ olmak üzere, $P(j,\lambda_1,\alpha,n,z_0) \supseteq P(j,\lambda_2,\alpha,n,z_0)$ olduğunu gösterelim. $f(z) \in P(j,\lambda_1,\alpha,n,z_0)$ ve $\lambda_1=\lambda_2-\delta$ olsun. Lemma 1.3 kullanılarak

$$\sum_{k=j+1}^{\infty}\left[k^n\left(\frac{k-\alpha}{1-\alpha}\right)\{1+(k-1)\lambda_1\}-z_0^{k-1}\right]a_k$$
$$\leq \sum_{k=j+1}^{\infty}\left[k^n\left(\frac{k-\alpha}{1-\alpha}\right)\{1+(k-1)\lambda_2\}-z_0^{k-1}\right]a_k < 1$$

elde edilir. Dolayısıyla, $f(z) \in P(j,\lambda_2,\alpha,n,z_0)$ olur.

***2.3. Teorem:*** $0\leq \alpha < 1$, $0\leq \lambda <1$, $n \in \mathbb{N}_0$ ve j $\in \mathbb{N}$ olmak üzere

$$P(j,\lambda,\alpha,n+1,z_0) \subseteq P(j,\lambda,\alpha,n,z_0) \tag{21}$$

dür.

*İspat.* $f(z) \in P(j,\lambda,\alpha,n,z_0)$ olsun. Lemma 1.3 kullanılarak

$$\sum_{k=j+1}^{\infty}\left[k^n\left(\frac{k-\alpha}{1-\alpha}\right)\{1+(k-1)\lambda\}-z_0^{k-1}\right]a_k$$
$$\leq \sum_{k=j+1}^{\infty}\left[k^{n+1}\left(\frac{k-\alpha}{1-\alpha}\right)\{1+(k-1)\lambda\}-z_0^{k-1}\right]a_k < 1$$

elde edilir. Dolayısıyla, $f(z) \in P(j,\lambda,\alpha,n+1,z_0)$ olur.

***2.4. Teorem*** (6) ile tanımlı $f(z)$ fonksiyonu $P(j,\lambda,\alpha,n,z_0)$ sınıfında olsun. Bu durumda $|z| = r < 1$ için,

$$|D^m f(z)| \geq r - \frac{(1-\alpha)(j+1)^m}{(j+1)^n\big(j+1-\alpha)(1+j\lambda)\big)-(1-\alpha){z_0}^{k-1}}r^{j+1} \tag{22}$$

ve

$$|D^m f(z)| \leq r + \frac{(1-\alpha)}{(j+1)^n\big(j+1-\alpha)(1+j\lambda)\big)-(1-\alpha){z_0}^{k-1}}r^{j+1} \tag{23}$$

şeklindedir. Burada, z$\in \mathcal{U}$ ve $0 \leq m \leq n$ dir.

(22) ve (23) eşitsizliklerindeki eşitlik durumları,

$$f(z) = z - \frac{1-\alpha}{(j+1)^n(j+1-\alpha)(1+j\lambda)}z^{j+1} \qquad (z=\pm r) \tag{24}$$

şeklindeki ekstremal fonksiyonu ile sağlanır.

*İspat.* $|z| = r < 1$ olmak üzere $f(z) \in P(j,\lambda,\alpha,n,z_0)$ olması için gerek ve yeter şart
$$D^m f(z) \in P(j,\lambda,\alpha,n-m,z_0)$$
olmasıdır. Ayrıca,

$$D^m f(z) = z - \sum_{k=j+1}^{\infty} k^m a_k z^k \tag{25}$$

eşitliği ve Lemma 1.3 kullanılarak

$$\sum_{k=j+1}^{\infty} \left[k^n (k-\alpha)\{1+(k-1)\lambda\} - (1-\alpha) z_0^{k-1}\right] a_k \leq 1-\alpha$$

olur. Bu son eşitsizlik yardımıyla,

$$\begin{aligned}
1-\alpha &\geq \sum_{k=j+1}^{\infty} \left[k^n (k-\alpha)\{1+(k-1)\lambda\} - (1-\alpha) z_0^{k-1}\right] a_k \\
&= (j+1)^n (j+1-\alpha)(1+j\lambda) a_{j+1} + \cdots - (1-\alpha) \sum_{k=j+1}^{\infty} \frac{k^m}{k^m} a_k z_0^{k-1} \\
&\geq (j+1)^{m+(n-m)} (j+1-\alpha)(1+j\lambda) a_{j+1} + \cdots - \frac{(1-\alpha) z_0^j}{(j+1)^m} \sum_{k=j+1}^{\infty} k^m a_k \\
&\geq (j+1)^{n-m} (j+1-\alpha)(1+j\lambda)(j+1)^m a_{j+1} + \cdots - \frac{(1-\alpha) z_0^j}{(j+1)^m} \sum_{k=j+1}^{\infty} k^m a_k \\
&\geq (j+1)^{n-m} (j+1-\alpha)(1+j\lambda) \sum_{k=j+1}^{\infty} k^m a_k - \frac{(1-\alpha) z_0^j}{(j+1)^m} \sum_{k=j+1}^{\infty} k^m a_k
\end{aligned}$$

elde edilir ve buradan da

$$\sum_{k=j+1}^{\infty} k^m a_k \leq \frac{(1-\alpha)(j+1)^m}{(j+1)^n (j+1-\alpha)(1+j\lambda) - (1-\alpha) z_0^j} \tag{26}$$

bulunur. (26) ifadesi, (25)'de yerine yazılırsa,

$$\begin{aligned}
r - \frac{(1-\alpha)(j+1)^m}{(j+1)^n (j+1-\alpha)(1+j\lambda) - (1-\alpha) z_0^{k-1}} r^{j+1} &\leq |D^m f(z)| \\
&\leq r + \frac{(1-\alpha)(j+1)^m}{(j+1)^n (j+1-\alpha)(1+j\lambda) - (1-\alpha) z_0^{k-1}} r^{j+1}
\end{aligned}$$

elde edilir. Böylece ispat tamamlanmış olur.

Teorem 2.4 de $m = 0$ alınırsa aşağıdaki sonuç elde edilir.

***2.6. Sonuç*** (6) ile tanımlı $f(z)$ fonksiyonu $P(j, \lambda, \alpha, n, z_0)$ sınıfında olsun. Bu durumda $|z| = r < 1$ için,

$$|f(z)| \geq r - \frac{(1-\alpha)}{(j+1)^n (j+1-\alpha)(1+j\lambda) - (1-\alpha) z_0^{k-1}} r^{j+1} \tag{27}$$

ve

$$|f(z)| \geq 1 + \frac{(1-\alpha)}{(j+1)^n (j+1-\alpha)(1+j\lambda) - (1-\alpha) z_0^{k-1}} r^j \qquad (z \in \mathcal{U}) \tag{28}$$

olur.

(27) ve (28) eşitsizliklerindeki eşitlik durumları (24) da tanımlı ekstremal fonksiyonu için sağlanır.
Teorem 4.4.13'de $m = 1$ alınırsa aşağıdaki sonuç elde edilir.

***2.7. Sonuç*** (6) ile tanımlı $f(z)$ fonksiyonu $P(j,\lambda,\alpha,n,z_0)$ sınıfında olsun. Bu durumda $|z|=r<1$ için,

$$|f'(z)| \geq 1-\frac{(1-\alpha)(j+1)}{(j+1)^n(j+1-\alpha)(1+j\lambda)-(1-\alpha)z_0^{k-1}}r^j \tag{29}$$

ve

$$|f'(z)| \geq 1+\frac{(1-\alpha)(j+1)}{(j+1)^n(j+1-\alpha)(1+j\lambda)-(1-\alpha)z_0^{k-1}}r^j \qquad (z\in\mathcal{U}) \tag{30}$$

olur. (29) ve (30) eşitsizliklerindeki eşitlik durumları (24)'da tanımlı ekstremal fonksiyonu için sağlanır.

**Kaynaklar**


Aouf, M.K. ve Srivastava, H.M., 1996. Some families of starlike functions with negative coefficients. Journal of Mathematical Analysis and Applications, 203, 762-790.

Baba, H., 2018. The Modified Hadamard Products of Functions Belonging to the Class $P(j,\lambda,\alpha,n,z_0)$. International Journal of Scientific and Technological Research, 4(3), 19-26.

Kiziltunc, H. ve Baba, H., 2012. Inequalities for Fixed Points of the Subclass P(j,λ,α,n) of Starlike Functions with Negative Coefficients. Advances in Fixed Point Theory, 2, 197-202.

Sălăgean, G.Şt., 1983. Subclasses of univalent functions: "Complex Analysis: Fifth Romanian-Finnish Seminar." Part I, Lecture Notes in Mathematics, 1013, Springer-Verlag, Berlin/Newyork, pp. 362-372.

Silverman, H., 1975. Univalent functions with negative coefficients. Proceedings of the American Mathematical Society, 51, 109-116.

Silverman, H., 1976. Extreme points of univalent functions with two fixed points. Transactions of the American Mathematical Society, 219, 387-395.

**GÜFBED/*GUSTIJ* (2018) CMES 2018 SEMPOZYUM EK SAYISI: 46-52**
DOI: 10.17714/gumusfenbil.430034 Araştırma Makalesi / *Research Article*

# Morphological Disambiguation of Turkish with Free-order Co-occurrence Statistics

## *Serbest Sırada Birliktelik İstatistiklerinin Kullanımıyla Türkçe'nin Biçimbirimsel Belirsizliği'nin Giderilmesi*

**Enis ARSLAN*[1,a], Umut ORHAN[1,b], B. Tahir TAHİROĞLU[2,c]**
[1]*Çukurova Üniversitesi, Mühendislik Mimarlık Fakültesi, Bilgisayar Mühendisliği Bölümü, 01130, Adana*
[2]*Çukurova Üniversitesi, Türk Dili ve Edebiyatı Bölümü, 01130, Adana*

• Geliş tarihi / *Received*: 02.06.2018 • Düzeltilerek geliş tarihi / *Received in revised form*: 12.09.2018 • Kabul tarihi / *Accepted*: 09.10.2018

**Abstract**
In this article, a solution to the morphological ambiguity problem which occurs frequently in morphologically complex languages like Turkish is proposed. Generally, statistical methods are applicable for these tasks which maximize the information, obtained for a probable word order sequence in a sentence. The decision in selection of the method for calculation of the probabilities and the sequence selection method depends on the nature of the language. By using the co-occurrence statistics obtained from a semantic graph network which represents the lemmas of the sentences, the best word order sequence is selected from the alternatives. The non-ambiguous and free-word-order character of this network is helpful in determining the statistics independently. The probability values are obtained by using the Naive Bayes (NB) method and the selection of each word sequence is achieved by maximization, in the inspiration of the Viterbi algorithm.

***Keywords:*** *Co-occurrence, Morphological ambiguity, Naive Bayes, the Viterbi algorithm*

***Öz***
*Bu makalede, Türkçe gibi biçimsel olarak karmaşık yapıda olan dillerde sıklıkla karşılaşılan biçimbirimsel belirsizlik problemi için bir çözüm önerilmiştir. Genellikle, bu tipte bir problemin çözümü için bir cümledeki muhtemel kelime sıralarından uygun olanın seçilmesi için bilgiyi maksimuma çıkaran istatistiksel yöntemler uygulanmaktadır. Olasılıkların hesaplanması ve uygun sıranın seçilmesi için tercih edilecek metot uygulanacak dilin doğasına bağlıdır. Cümlelerde geçen kelimelerin madde başlarının oluşturduğu bir anlamsal çizgeden elde edilen birliktelik istatistikleri kullanılarak alternatifler arasından uygun olan kelime sıra dizilimi seçilmektedir. Bu çizge ağının belirsizlik içermeyen serbest sıralı karakteri istatistiklerin bağımsız olarak hesaplanmasında oldukça faydalıdır. Olasılıksal değerler Naive Bayes (NB) yöntemi kullanılarak elde edilmekte ve her kelime sıraları arasından uygun olanının, Viterbi algoritmasından esinlenilerek, maksimumu seçilmektedir.*

***Anahtar kelimeler:*** *Birliktelik, Biçimbirimsel belirsizlik, Naive Bayes, Viterbi algoritması*

*[a] Enis ARSLAN; enisarslan@gmail.com; Tel: (0322) 338 60 60; orcid.org/0000-0002-2609-3925
[b] orcid.org/0000-0003-1882-6567 [c] orcid.org/0000-0002-7956-3257

## 1. Introduction

Natural languages, ambiguity occurs according to the researched language's nature. In morphologically simple languages, especially like English, polysemous words can have different senses according to their usage purposes in texts. This kind of ambiguity problem is solved by Word Sense Disambiguation (WSD) methods. On the other hand, for the morphologically complex languages like Turkish, Finnish and Hungarian the output of the morphological analyser can cause more than one solution for a word which causes ambiguity. Lexical or syntactical disambiguation methods help in removing this kind of ambiguities. Recently graphs are getting more popular in the application of lexical disambiguation and WSD in many research (Sinha and Mihalcea, 2007; Minkov et al., 2006; Fan et al., 2011; Hessami et al., 2011).

The complex structure of the languages causes the new words to be included and the useless ones to be removed from usage. Sometimes, some relations between words are stronger and sometimes weaker as time goes by. Complex networks are ideal for modelling these languages according to the necessity. In general, the simplest design is created by using the co-occurrence relations between words in a text (Borge-Holthoefer and Arenas, 2010). It is possible to produce a co-occurrence graph by applying a fixed-width window in a sentence or document (Beliga et al., 2015). Co-occurrence graphs are used in Natural language processing (NLP) fields like text summarization (Mihalcea and Tarau, 2004), indexing (Matsuo et al., 2001), keyword and keyphrase extraction (Lahiri et al., 2014; Litvak et al., 2011), disambiguation (Duque et al., 2018; Martinez-Romo et al., 2011).

In this study, a directed and weighted graph is composed by ignoring the neighbouring sequences, in an unsupervised fashion. This graph is used in morphological disambiguation of Turkish sentences which have at least one ambiguous word. The second section of the study summarizes the related work for this field, the third section describes the methodology, the fourth section gives the experimental results and the fifth section concludes the study.

## 2. Related Work

Using co-occurrence of words in WSD takes place in many NLP studies. In (Niwa and Nitta, 1994), they have concluded that using co-occurrence vectors instead of distance vectors is advantageous. In machine translation field, query disambiguation tests provide better results when co-occurrence statistics is applied (Ballesteros and Croft, 1998). In (Duque et al., 2018), the paper abstracts of bio-medical science are used to construct a co-occurrence network of concepts for WSD and the study achieved a 10% improvement in accuracy. In another study (Martinez-Romo et al., 2011), a co-occurrence graph is established to cluster words with similar meanings and by assigning weight values of statistical significance using in WSD and Word Sense Induction (WSI). When morphological disambiguation of Turkish is considered, (Sak et al., 2007) provide the best reported accuracy value in their study. They collect the trigram statistics of the word features and roots in the sentences and select the n-best sequences by using the Viterbi algorithm.

## 3. Methodology

In this study, a semantic graph of Turkish lemmas is composed by using the co-occurrence relations existing in the sentence level. These relationship statistics are used as an input to the Naive Bayes (NB) method to be used in the selection of the correct sequence in an ambiguous sentence.

Lemma is the dictionary form of a word in a natural language. Lemmatization is used as a term to discover the lemmas of the words. In the first stage of the study, lemmas of Turkish Language Association (TLA) are added to a graph database to be used in lemmatization. For the lemmatization of words in corpus, we have used the finite state automatas which are described in (Eryiğit, 2012). In the second stage, the sentences in the corpus (Tahiroğlu et al., 2014) are lemmatized and lemmas are used as the main component of the semantic graph by establishing connections in-between. Co-occurrence provides frequency increases of the graph. As a corpus, 57,000 sentences of Turkish newspaper texts are processed.

### 3.1 *Composition of the Semantic Graph*

A semantic graph which has unambiguous character is composed by connecting the lemmas (If it is a lemma connect itself) of a sentence with a relation property named 'COOCCUR'. This property is used to calculate co-occurrence frequencies for further processing.

In the beginning, during the process of each sentence, a tokenization is applied. Following the

tokenization, all lemmas occurred in the sentence are collected as a list. The inflected words which have more than one lemma alternative (ambiguity) are ignored to obtain a non-ambiguous semantic graph. All the lemmas collected in the list are connected to each other with 'COOCCUR' relation type.

Co-occurrence graph is trained as follows:

1. Take a sentence from the sentence dataset
2. Select a token from the sentence.
   i. If the token is an inflected word lemmatize it. If there is only one lemma candidate of the inflected word (non-ambiguity) add this lemma to the sentence lemma list. If there is more than one candidate (ambiguity) do nothing.
   ii. If the token is a lemma add it to the lemma list
3. Connect all the lemmas in the lemma list with a 'COOCCUR' relation type in the graph. relFreq=1 (If this relation occurs only increment relFreq value)
4. Go to 1
5. End function

'relFreq' value of 'COOCCUR' relationship represents the lemma pairs which co-occur in a sentence. Each lemma node name in the list is checked with the others for a sentence and if there does not exist a relation between lemmas a 'COOCCUR' relation with type 'relFreq=1' is established. If there exists a relation 'relFreq' frequency value is incremented.

In Figure 1, other lemmas connected to the lemma node named 'festival' (fest in English) in the semantic graph can be seen. As seen in the Figure, nearly all other lemmas are semantically related to the lemma 'festival'.

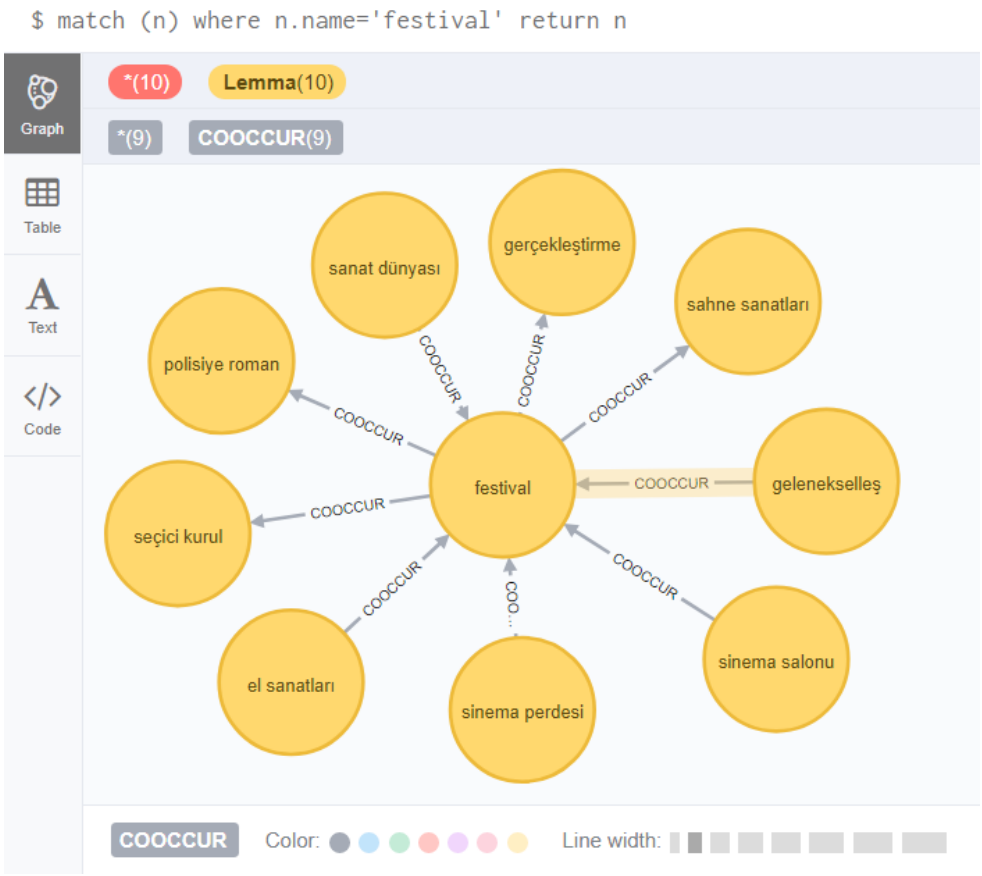


**Figure 1**. Lemma nodes connected to lemma node named 'festival' in semantic graph

### 3.2 *Disambiguation Methodology*

At the beginning of the disambiguation process, each test sentence is lemmatized and all alternative word sequences (permutation) are detected. An example sentence is introduced in Figure 2 which has 6 alternatives:

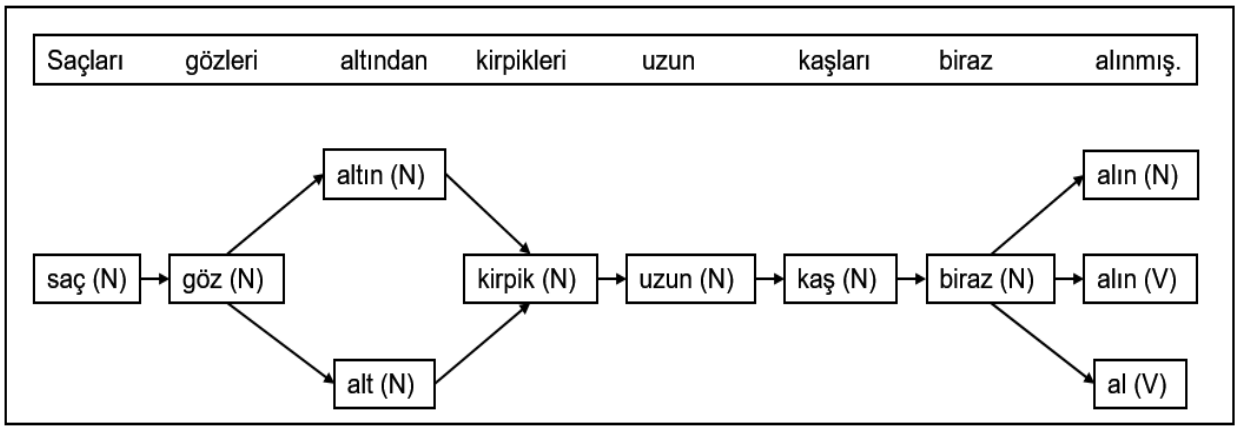


**Figure 2**. An example sentence of sequences

As seen in Figure 2 there are two lemma alternatives for the word 'altından' and three alternatives for the word 'alınmış'. When 3 is multiplied by 2 results is 6 representing the permutation count for this sentence.

Following the detection of the sequences, Naïve Bayes values for each lemma sequence are calculated using the lemma relation statistics obtained from the co-occurrence graph. The calculations are done as shown in Equations (1) and (2):

$$P(q_1^1, q_2^1) = \frac{f(q_1^1, q_2^1)}{f(q_1^1, q_2^1)} = 1 \qquad (q_1^1\text{=saç ve } q_2^1\text{=göz}) \tag{1}$$

$$P(q_1^1, q_3^1) = \frac{f(q_1^1, q_3^1)}{f(q_1^1, q_3^1) + f(q_1^1, q_3^2)} \qquad (q_1^1\text{=saç ve } q_3^1\text{=altın}) \tag{2}$$

In the preceding equations, $f$ represents the frequency value (relFreq) of the relation between $q_1^1$ and $q_2^1$ in co-occur graph. All the permutations of the example sentence in Figure 2 can be seen in Figure 3.

| | | | | | | | |
|---|---|---|---|---|---|---|---|
| saç (N) | göz (N) | altın (N) | kirpik (N) | uzun (N) | kaş (N) | biraz (N) | alın (N) |
| saç (N) | göz (N) | alt (N) | kirpik (N) | uzun (N) | kaş (N) | biraz (N) | alın (V) |
| saç (N) | göz (N) | altın (N) | kirpik (N) | uzun (N) | kaş (N) | biraz (N) | al (V) |
| saç (N) | göz (N) | alt (N) | kirpik (N) | uzun (N) | kaş (N) | biraz (N) | alın (N) |
| saç (N) | göz (N) | altın (N) | kirpik (N) | uzun (N) | kaş (N) | biraz (N) | alın (V) |
| saç (N) | göz (N) | alt (N) | kirpik (N) | uzun (N) | kaş (N) | biraz (N) | al (V) |

**Figure 3**. Six alternative sequences of the example sentence

Six Naive Bayes values are calculated for each sequence in Figure 3 as:

$$P(Q_1) = \prod_{i=1}^{N-1} \prod_{j=i+1}^{N} P(q_i, q_j) \tag{3}$$

## 4. Experimental Results

### *4.1. Training of the Semantic Graph*

Statistics of the semantic graph built by training all the sentences in the corpus are listed in Table 1:

**Table 1.** Statistics of the semantic graph

| | |
|---|---|
| Lemma node count | 79364 |
| Connected Lemma count | 18929 |
| Co-occur relationship count | 2121864 |
| Trained sentence count | 57K |

The 79K TLA lemmas listed in Table 1 are used for lemmatization. 18929 of these lemmas are connected to each other with at least one 'COOCCUR' relation type after training.

### *4.2. Preparation of the Test Sentences*

To obtain test sentences, at first, all ambiguous sentences from the sentence dataset are selected. The sentences which have fully inter-connected (detected by using the co-occurrence graph) lemmas are captured from the ambiguous sentences. The resulting sentences are the input to the disambiguation function as test sentences. The statistics for the test sentences are shown in Table 2:

**Table 2.** Test sentence statistics

| Sentence length < 150 | |
|---|---|
| Total sentence count | 30000 |
| Ambiguous sentence count | 13725 |
| Semantically connected sentence count | 180 |
| Ambiguity rate | 45.75 % |

As seen in Table 2, 30K portion of the 57K sentences is used to obtain test sentences. A sentence size of minimum 150 characters is applied as a filter to be able to select the sentences with at least a few words. Semantically connected sentences represent the sentences which include lemmas full-connected with at least one 'COOCCUR' relation in the semantic graph.

### *4.3. Test Results*

180 ambiguous sentences are subject to the disambiguation process. Since there are errors due to lemmatization nearly half of the test sentences are useless. The remaining sentences are considered in accuracy calculation, as shown in Table 3:

**Table 3.** Disambiguation test results

| | |
|---|---|
| Semantically connected sentence count | 180 |
| Permutations with equal value (ignored) | 72 |
| Incorrectly lemmatized sentences | 70 |
| Correctly disambiguated sentences | 26 |
| Success ratio | 68.42 % |

The test results are checked in a supervised fashion. The success ratio is 68.42% which can increase in value with more training. When the same test set is applied to a graph trained with 73K sentences there is one more correctly disambiguated sentence as shown in Figure 4:

```
1
2  Test output of a sentence trained with 57 K. sentences:
3  günün (günü) en (en) yüksek (yüksek) sıcaklıkları (sıcaklık)
4
5  Test output of a sentence trained with 73 K. sentences:
6  günün (gün) en (en) yüksek (yüksek) sıcaklıkları (sıcaklık)
```

**Figure 4.** Correct disambiguation with a larger train-set

As seen in Figure 4, the word 'günün' is selected as 'günü' lemma alternative (red frame). This erroneous selection is automatically corrected after the training with a larger data-set as the word 'gün'. This is because of the frequency increase between some re-occurring relations between some lemmas in the co-occurrence graph as training goes by.

For the disambiguation of Turkish language, (Sak et al., 2007)'s study improves the baseline study (93.61%) by providing an accuracy value of 96.80%. Statistics for the trigram models are provided by Markov method and Perceptron algorithm is used for training and ranking.

## 5. Conclusion

In this study, a disambiguation model is implemented on an unsupervised lemma graph database by using co-occurrence relations in-between. Co-occurrence frequency statistics are the main calculation parameter. A sentence with ambiguous words may have many alternative word sequences. Co-occurrence statistics are helpful in solving this kind of ambiguity.

When we consider the disambiguation of Turkish texts, features of words with their syntactical tags and root relationships are the main source of information in use. This study is different from (Sak et al., 2007)'s study, which is nearest in statistical means. We take the advantage of lemma-to-lemma relationships in a global context instead of trigram statistics of root-to-root relationships of words. Also we cannot profit from the syntactic features of words because of the nature of our algorithm. In our knowledge, there is not any work for morphological disambiguation of Turkish, exactly as the same of our methodology, which only relies on co-occurrence relationship of words in semantical means.

A dense training graph, composed of hundred thousands of words is needed to obtain more accurate results in the application of this methodology. More training will provide more clues in sentence disambiguation with the increased co-occurrence frequency values.

## Acknowledgements

This study is a part of the research programme with project number 212E256, which is financed by the Scientific and Technological Research Council of Turkey (TUBITAK).

## References

Ballesteros, L. and Croft, W.B., 1998. August. Resolving ambiguity for cross-language retrieval. In Proceedings of the 21st annual international ACM SIGIR conference on Research and development in information retrieval (pp. 64-71). ACM.

Beluga, S., Meštrović, A. and Martinčić-Ipšić, S., 2015. An overview of graph-based keyword extraction methods and approaches. Journal of information and organizational sciences, 39 (1), pp.1-20.

Borge-Holthoefer, J. and Arenas, A., 2010. Semantic networks: Structure and dynamics. Entropy, 12 (5), pp.1264-1302.

Duque, A., Stevenson, M., Martinez-Romo, J. and Araujo, L., 2018. Co-occurrence graphs for word sense disambiguation in the biomedical domain. Artificial intelligence in medicine.

Eryiğit, G., 2012. Biçimbilimsel Çözümleme. Türkiye Bilişim Vakfı Bilgisayar Bilimleri ve Mühendisliği Dergisi, 5 (2).

Fan, X., Wang, J., Pu, X., Zhou, L. and Lv, B., 2011. On graph-based name disambiguation. Journal of Data and Information Quality (JDIQ), 2 (2), p.10.

Hessami, E., Mahmoudi, J. and Jadidinejad, A.H., 2011. Unsupervised graph-based word sense disambiguation using the lexical relation of WordNet. Int. J. Comput. Sci. Issues (IJCSI).

Lahiri, S., Choudhury, S.R. and Caragea, C., 2014. Keyword and keyphrase extraction using centrality measures on collocation networks. arXiv preprint arXiv:1401.6571.

Litvak, M., Last, M., Aizenman, H., Gobits, I. and Kandel, A., 2011. DegExt—A language-independent graph-based keyphrase extractor. In Advances in Intelligent Web Mastering–3 (pp. 121-130). Springer, Berlin, Heidelberg.

Martinez-Romo, J., Araujo, L., Borge-Holthoefer, J., Arenas, A., Capitán, J.A. and Cuesta, J.A., 2011. Disentangling categorical relationships through a graph of co-occurrences. Physical Review E, 84 (4), p.046108.

Matsuo, Y., Ohsawa, Y. and Ishizuka, M., 2001. November. Keyword: Extracting keywords from document s small world. In International Conference on Discovery Science (pp. 271-281). Springer, Berlin, Heidelberg.

Mihalcea, R. and Tarau, P., 2004. Textrank: Bringing order into text. In Proceedings of the 2004 conference on empirical methods in natural language processing.

Minkov, E., Cohen, W.W. and Ng, A.Y., 2006. August. Contextual search and name disambiguation in email using graphs. In Proceedings of the 29th annual international ACM SIGIR conference on Research and

development in information retrieval (pp. 27-34). ACM.

Niwa, Y. and Nitta, Y., 1994. August. Co-occurrence vectors from corpora vs. distance vectors from dictionaries. In Proceedings of the 15th conference on Computational linguistics-Volume 1 (pp. 304-309). Association for Computational Linguistics.

Sak, H., Güngör, T. and Saraçlar, M., 2007, February. Morphological disambiguation of Turkish text with perceptron algorithm. In International Conference on Intelligent Text Processing and Computational Linguistics (pp. 107-118). Springer, Berlin, Heidelberg.

Sinha, R. and Mihalcea, R., 2007. Unsupervised graph-based word sense disambiguation using measures of word semantic similarity. In Semantic Computing, 2007. ICSC 2007. International Conference on (pp. 363-369). IEEE.

Tahiroğlu B.T. 2014, Türkçe Çevrim İçi Haber Metinlerinde Yeni Sözlerin (Neolojizm) Otomatik Çıkarımı. Derlem Dilbilim Uygulamaları, Özkan, B., Tahiroğlu, B. Tahir ve Özkan Ayşe Eda (Ed.), Karahan Kitabevi Yayınları, Adana, ss.1-22.

**GÜFBED/*GUSTIJ* (2018) CMES 2018 SEMPOZYUM EK SAYISI: 53-60**
DOI: 10.17714/gumusfenbil.436056 Araştırma Makalesi / *Research Article*

# Comparison of CoAP and CoCoA Congestion Control Mechanisms in Grid Network Topologies

## *Grid Ağ Topolojilerinde CoAP ve CoCoA Tıkanıklık Kontrol Mekanizmalarının Karşılaştırılması*

**Alper Kamil DEMIR*[a], Fatih ABUT[b]**
*Adana Science and Technology University, Faculty of Engineering, Computer Engineering Department, 01250, Adana*

• Geliş tarihi / *Received*: 24.06.2018 • Düzeltilerek geliş tarihi / *Received in revised form*: 20.09.2018 • Kabul tarihi / *Accepted*: 09.10.2018

**Abstract**
The Internet of Things (IoT) is a vision of the future Internet. Due to limited resources of IoT devices, a new generation of protocols and algorithms are being developed and standardized. The Constrained Application Protocol (CoAP) has been designed by the Internet Engineering Task Force (IETF) for application layer communication. CoAP is based on User Datagram Protocol (UDP), a simple transport layer protocol that does not handle congestion within the network. However, the phenomenon of congestion in IoT networks is also a major problem. Thus, the core CoAP specification offers a basic CoAP congestion control (CC) mechanism based on retransmission timeout (RTO) with binary exponential backoff (BEB). Default CoAP CC is insensitive to network conditions. Thus, to improve the default CoAP CC, CoAP Simple Congestion Control/Advanced (CoCoA), defined in a draft specification, is being standardized by the IETF CoRE working group. Nevertheless, comparison of default CoAP CC and CoCoA has not been sufficiently investigated in the literature. In this paper, we investigate and present comparison of default CoAP CC and CoCoA in terms of throughput (i.e. number of requests/second) by varying number of concurrent clients where each client continuously sends back-to-back traffic to servers residing in 1x6, 3x6 and 5x6 grid network topology. Our results show that CoCoA is not always better than default CoAP CC in terms of throughput in some scenarios. As a result, design and development of new CoAP CC mechanisms are open to research.

**Keywords**: Internet of Things, Congestion control, CoAP, CoCoA, Cooja, ContikiOS

***Öz***
*Nesnelerin İnterneti (IoT) geleceğin İnternet'inin bir vizyonudur. IoT cihazlarının sınırlı kaynakları nedeniyle yeni nesil protokoller ve algoritmalar geliştirilmekte ve standartlaştırılmaktadır. Kısıtlı Uygulama Protokolü (CoAP), uygulama katmanı iletişimi için Internet Mühendisliği Görev Gurubu (IETF) tarafından tasarlanmıştır. CoAP, ağ içinde tıkanıklığı karşılamayan basit bir taşıma katmanı protokolü olan Kullanıcı Datagram Protokolü (UDP) üzerine kurulmuştur. Bununla birlikte, IoT ağlarında tıkanıklık olayı da büyük bir sorundur. Bu nedenle, çekirdek CoAP spesifikasyonu, ikili üstel geri çekilme (BEB) ile yeniden iletim zaman aşımına (RTO) dayalı temel bir CoAP tıkanıklık kontrolü (CC) mekanizması sunar. Mevcut CoAP CC, ağ koşullarına duyarsızdır. Bu nedenle, mevcut CoAP CC'yi geliştirmek için IETF CoRE çalışma grubu tarafından taslak bir spesifikasyonda tanımlanan CoAP Simple Congestion Control/Advanced (CoCoA) mekanizması standartlaştırılmaktadır. Ancak mevcut CoAP CC ve CoCoA'nın karşılaştırılması literatürde yeterince araştırılmamıştır. Bu çalışmada, eşzamanlı istemcilerin sayısının değiştirilmesiyle her istemcinin sürekli olarak 1x6, 3x6 ve 5x6 grid ağ topolojilerinde yer alan sunuculara arka arkaya trafik gönderilerek mevcut CoAP CC ve CoCoA'nın performansları iş/zaman oranı (yani istek sayısı/saniye) açısından karşılaştırılmış ve sunulmuştur. Elde edilen sonuçlar, CoCoA'nın bazı senaryolarda mevcut CoAP CC'den iş/zaman oranı açısından her zaman daha iyi olmadığını göstermektedir. Sonuç olarak, yeni CoAP CC mekanizmalarının tasarımı ve geliştirilmesi araştırmaya açıktır.*

***Anahtar kelimeler****: Nesnelerin İnterneti, Tıkanıklık kontrolü, CoAP, CoCoA, Cooja, ContikiOS*

*a Alper Kamil DEMIR; akdemir@adanabtu.edu.tr; Tel: 0 (322) 455 0000 - 2081; [a] orcid.org/0000-0002-9256-0368
[b] orcid.org/0000-0001-5876-4116

## 1. Introduction

The Internet of Things (IoT) is a vision of the future Internet where the network of physical devices, embedded with electronics, software, sensors, actuators, and communication unit and protocols, enable to connect and exchange data about themselves and their surroundings within the existing Internet infrastructure. Experts forecast that the IoT will include about 30 billion physical devices and the global market value of IoT will reach $7.1 trillion by 2020 (Manjarekar et al., 2018). The IoT is bringing about new generation of applications such as smart factories, cities, homes, grids, power plants, automotive, transportation, aerospace, aviation, healthcare and agriculture (Bandyopadhyay and Sen, 2011; Li et al., 2015).

Due to constrained energy, computation, memory and communication capacities of IoT devices, a new generation of protocols and algorithms are being developed and standardized. The Constrained Application Protocol (CoAP) was constructed by the Internet Engineering Task Force (IETF) for the needs of IoT application layer communication (Shelby et al., 2014). The CoAP is a specialized web transfer protocol for use with these constrained physical devices. CoAP is based on User Datagram Protocol (UDP) to better fit the requirements of constrained physical devices. UDP is a very simple and lightweight transport layer protocol that does not handle congestion within the network. However, the phenomenon of congestion in IoT networks is also a major problem.

When the queuing and storing capacities of physical devices forming the IoT network are exceeded or generated traffic within IoT network gets close to the network capacity, network congestion is inevitably observed. Typical effect of network congestion results with queuing delay and packet loss. Congestion decreases the network utilization and can lead to congestive collapse. Congestion control and avoidance mechanisms are required to avoid congestive collapse. Thus, the core CoAP specification offers a basic CoAP congestion control (CC) mechanism based on retransmission timeout (RTO) with binary exponential backoff (BEB). Default CoAP CC is insensitive to network conditions.

Because default CoAP CC mechanism is conservative, rather than adjusting its behavior to network conditions, it may significantly underperform. Thus, CoAP specification encourages further CC mechanisms that leverage information related to current network condition. As a result, to improve the CoAP CC, CoAP Simple Congestion Control/Advanced (CoCoA) is being standardized by the IETF CoRE working group (Bormann et al., 2018). CoCoA uses round-trip time (RTT) measurements, dynamic RTO backoff computations, and RTO aging method to improve the performance of CoAP.

As far as we know, there exist some rare previous studies on comparing the performance of default CoAP CC and CoCoA (Betzler et al., 2014; Betzler et al., 2015; Ancillotti and Bruno, 2017) and comparing the performance of default CoAP CC, CoCoA and alternative CCs ( Jarvinen et al., 2015; Betzler et al., 2016; Lee et al., 2016). In (Betzler et al., 2014, 2015, 2016), the authors suggested CoCoA CC mechanism for CoAP and showed that CoCoA obtains better results than default CoAP CC in the larger part of considered cases. In (Jarvinen et al., 2015), two TCP-based RTO calculation methods, namely Linux RTO and Peak-Hopper RTO, are proposed for CoAP CC. The results show that all the alternatives of default CoAP CC operate more efficient particularly at higher congestion levels. In contrast, the authors in (Betzler et al., 2016) find out that Linux RTO and Peak-Hopper RTO underperform default CoAP CC under certain conditions. Hence, they do not recommend these two RTO calculation methods as CC mechanisms for CoAP. In (Lee et al., 2016), a new RTT-based adaptive CC mechanism is proposed. The results reveal that the proposed mechanism increases the throughput of default CoAP CC. In (Ancillotti and Bruno, 2017), as far as we know for the first time in literature, the authors reveal that CoCoA performs worse than default CoAP CC under burst and light traffic loads in grid network topologies.

Although the studies in (Betzler et al., 2014, 2015, 2016) show that performance of CoCoA is better than or in worst case similar to that of default CoAP CC, in (Ancillotti and Bruno, 2017) the authors showed that CoCoA does not perform the best in heavy and light traffic loads in grid topologies. In addtion to the results obtained in (Ancillotti and Bruno, 2017), in our work, we additively reveal that CoCoA also performs worse than default CoAP under moderate traffic loads besides heavy and light traffic loads in grid network topologies. We distinctly show that CoCoA does not consistently perform the best in different MAC protocol setups in grid topologies. Particularly, as being different from the rest of

previous studies, we considered three different congestion scenarios, namely lightly, moderately and heavily congested grid networks with two different MAC approaches including nullMAC and Carrier Sense Multiple Access (CSMA).

In this paper, we investigate and present comparison of default CoAP CC and CoCoA in terms of throughput (i.e. number of requests/second) by varying number of clients where each client continuously sends back-to-back traffic to servers residing in a 1x6, 3x6 and 5x6 grid network topology operated with nullMAC or CSMA. Our results show that CoCoA is not always better than default CoAP CC in our grid topologies and MAC protocol setups. As a result, design and development of new CoAP CC mechanisms are open to research.

This paper is organized as follows. Section 2 describes the default CoAP CC and CoCoA mechanisms. Sections 3 introduces the experimental setup and methodology used to compare the performance of CoCoA with default CoAP CC. Section 4 is devoted to results and discussion. Finally, Section 5 presents our conclusion.

## 2. CoAP Congestion Control Mechanisms

In this section, we first describe the default CoAP CC mechanism. Then, we introduce the new mechanisms leveraged by CoCoA.

### *2.1. Default CoAP Congestion Control*

CoAP specifies four types of messages: confirmable (CON), reset (RST), non-confirmable (NON) and acknowledgement (ACK) messages (Shelby et al., 2014). When a CON message is transmitted by a client, an ACK message is needed from the receiver. A CON message may maximally be retransmitted four times before the transmission is identified as failed. The initial RTO value is set to a random value between two and three seconds. This random initialization prevents synchronization issues. If RTO runs out and no ACK or response is obtained by the receiver, the client presumes that the CON message is lost. Hence, the client retransmits the CON message again. Consequently, for the next retransmission, the RTO value is doubled. This is known as BEB algorithm. Upon four retransmissions without any reply, the transmission is recognized as failed and the client can send a new CON request to the same receiver. Moreover, CoAP limits the number of parallel pending interactions to a single destination by NSTART parameter that is set to a conventional value of one by default. A pending interaction can be a CON or NON request that has not been replied yet.

### *2.2. CoAP Simple Congestion Control/Advanced (CoCoA)*

Default CoAP CC is insensitive to network conditions. Hence, CoCoA leverages adaptive RTO computations, a variable backoff factor (VBF), and RTO aging. An RTO for remote receiver (RTOoverall) is computed and updated in adaptive RTO computations. The RTO is computed adaptively by administering an exponentially weighted moving average (EWMA) of RTT and RTT-variation estimates. CoCoA keeps two RTO estimators for any remote receiver, referred to as the strong RTO estimator ($RTT_{strong}$) and the weak RTO estimator ($RTT_{weak}$). The RTTstrong preserves RTT information when no retransmission is obtained. On the other hand, the $RTT_{weak}$ preserves RTT information from retransmitted requests where the time is obtained between delivering the initial request and collecting the response. Succeeding equations represent RTTVAR and RTT where RTTVAR means the round-trip time variation, RTT means round-trip time, and X represents the strong or weak correspondingly when a new RTT ($RTT_{X\_new}$) is measured.

$$\begin{aligned} RTTVAR_X &= (1-\beta) \times RTTVAR_X + \beta \\ &\quad \times |RTT_X - RTT_{X_{new}}| \\ RTT_X &= (1-\alpha) \times RTT_X + \alpha \times RTT_{X\_new} \end{aligned} \quad (1)$$

In (1), default values for α and β are 0.25 and 0.125, respectively. Consequently, any update of RTTX results with an update of RTOX as

$$RTO_X = RTT_X + K_X \times RTTVAR_X, \quad (2)$$

where Kstrong=4 and Kweak=1. Finally, RTOoverall, which represents the total RTO value kept up for a remote receiver, is calculated as

$$RTO_{overall} = \gamma_X \times RTO_X + (1-\gamma_X) \times RTO_{overall}, \quad (3)$$

where γstrong=0.5 and γweak=0.25. RTOoveall is then utilized to decide the initial RTO (RTOinit). Contrary to the BEB used in default CoAP CC, CoCoA employs a VBF that sets the backoff value depending on the RTOinit. Additionally, to prevent the utilization of obsolete RTOoverall estimates that may have turned out to be

counterfeit after some time, CoCoA employs an aging method to the RTO estimation of remote receivers.

## 3. Experimental Setup and Methodology

For our experiments, we run varying number of clients and servers where the number of clients is always the same with the number of servers. Each client is programmed with Californium (Kovatsch et al., 2014) implementation of CoAP where default CoAP CC or CoCoA can be preferred as congestion control mechanism. On the other side, each server is programmed with Erbium implementation of CoAP in Cooja (Kovatsch et al., 2011) emulator of ContikiOS (Dunkels et al., 2004) toolset. The CoAP servers are programmed with ContikiOS that provide Erbium CoAP, UDP, uIPv6, RPL, SICSlowpan, nullMAC or CSMA based on nullRDC network stack over IEEE 802.15.4 physical layer.

Each client continuously sends back-to-back traffic to CoAP servers residing in a 1x6, 3x6 or 5x6 grid network topology for three minutes, as illustrated in Figure 1. Moreover, each client randomly selects a server. For 1x6 grid topology, the number of concurrent clients is varied as 2, 3, 4 and 5, whereas for 3x6 grid topology the number of concurrent clients is varied as 3, 5, 13 and 17. Finally, for 5x6 grid topology the number of concurrent clients is varied as 4, 6, 21 and 29. By starting each particular client-server scenario on 24 individual PCs simultaneously, we collected and evaluated the experimental results.

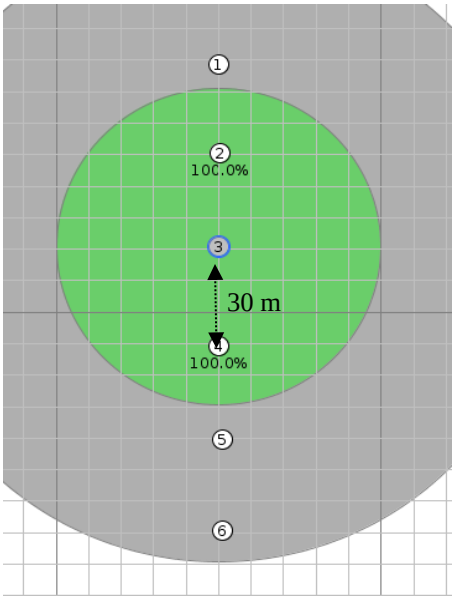


(a) 1x6 grid topology

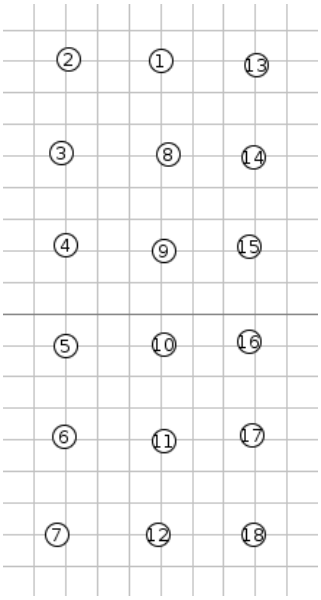


(b) 3x6 grid topology

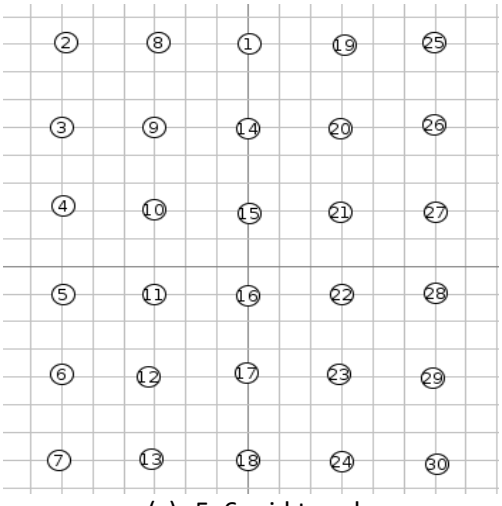


(c) 5x6 grid topology

**Figure 1.** Overview of experimental setup consisting of 1x6, 3x6 or 5x6 grid topologies. The nodes are 30 m apart from each other. The nodes with ID 1 represent the border gateways.

## 4. Results and Discussion

Table 1 and Table 2 show the throughput results of CoCoA compared to default CoAP CC using nullMAC and CSMA for 1x6, 3x6 and 5x6 grid topologies. In 1x6 topologies, where nullMAC is used as a medium access protocol, it is observed that CoCoA consistently outperforms default CoAP CC. Contrary, in 1x6 topologies where CSMA is used instead of nullMAC, the opposite case is observed, i.e. default CoAP CC performs better than CoCoA in terms of achieved throughput. In all other cases (i.e. in 3x6 and 5x6 topologies), where nullMAC is used as a medium access protocol, default CoAP CC performs better than CoCoA. In contrast, if CSMA is used instead of nullMAC, in some cases default CoAP CC performs better than CoCoA (i.e. in experiments with case ID's 7, 8, 10, 11 and 12), and in some other cases CoCoA outperforms default CoAP CC (i.e. in experiments with case ID's 5, 6 and 9).

**Table 1.** Comparison of default CoAP CC and CoCoA in terms of throughput using nullMAC

| Case ID | Number of clients | Topology | Default COAP CC (Requests/s) | CoCoA (Requests/s) |
|---|---|---|---|---|
| 1 | 2 | 1x6 | 3.653 | 4.704 |
| 2 | 3 | 1x6 | 3.375 | 3.391 |
| 3 | 4 | 1x6 | 1.793 | 2.066 |
| 4 | 5 | 1x6 | 1.412 | 1.506 |
| 5 | 3 | 3x6 | 3.195 | 2.888 |
| 6 | 5 | 3x6 | 3.206 | 3.046 |
| 7 | 13 | 3x6 | 1.087 | 0.956 |
| 8 | 17 | 3x6 | 0.748 | 0.628 |
| 9 | 4 | 5x6 | 3.829 | 3.353 |
| 10 | 6 | 5x6 | 3.008 | 2.483 |
| 11 | 21 | 5x6 | 0.920 | 0.905 |
| 12 | 29 | 5x6 | 0.747 | 0.695 |

**Table 2.** Comparison of default CoAP CC and CoCoA in terms of throughput using CSMA

| Case ID | Number of clients | Topology | Default COAP CC (Requests/s) | CoCoA (Requests/s) |
|---|---|---|---|---|
| 1 | 2 | 1x6 | 3.166 | 2.612 |
| 2 | 3 | 1x6 | 2.046 | 1.682 |
| 3 | 4 | 1x6 | 1.613 | 1.374 |
| 4 | 5 | 1x6 | 1.379 | 1.052 |
| 5 | 3 | 3x6 | 2.639 | 2.670 |
| 6 | 5 | 3x6 | 1.635 | 1.766 |
| 7 | 13 | 3x6 | 0.850 | 0.828 |
| 8 | 17 | 3x6 | 0.623 | 0.565 |
| 9 | 4 | 5x6 | 3.250 | 3.403 |
| 10 | 6 | 5x6 | 2.733 | 2.493 |
| 11 | 21 | 5x6 | 0.896 | 0.780 |
| 12 | 29 | 5x6 | 0.626 | 0.600 |

Figure 2 through Figure 4 illustrate the percentage increase or decrease rates in throughput of CoCoA compared to default CoAP CC using nullMAC and CSMA for 1x6, 3x6 and 5x6 grid topologies, respectively.

As illustrated in Figure 2, if CoCoA and default CoAP CC run with nullMAC in 1x6 topology, CoCoA outperforms default CoAP CC relatively improving the throughput ranging between 0.47% and 22.34%. In contrast, if CoCoA and default CoAP CC run with CSMA in 1x6 topology, CoCoA underperforms default CoAP CC

relatively worsening the throughput ranging between 17.39% and 31.08%.

According to Figure 3, if CoCoA and default CoAP CC run with nullMAC in 3x6 topology, CoCoA underperforms default CoAP CC relatively worsening the throughput ranging between 5.25% and 19.11%. Differently from the previous case, when CoCoA and default CoAP CC run with CSMA in the same topology, CoCoA outperforms default CoAP CC when the number of concurrent clients is 3 or 5 improving the throughput to 1.16% and 7.42%, respectively. When the number of concurrent clients is 13 or 17, CoCoA underperforms default CoAP CC relatively worsening the throughput to 2.66% and 10.27%, respectively.

Finally, in Figure 4, it is seen that independent of whether CoCoA and default CoAP CC run with nullMAC or CSMA (except the case where CoCoA and default CoAP CC run with CSMA and the number of concurrent clients is 4) in 5x6 topology, CoCoA consistently underperforms default CoAP CC relatively worsening the throughput ranging between 1.66% and 21.14%. In case where CoCoA and default CoAP CC run with CSMA and the number of concurrent client is 4, CoCoA outperforms default CoAP CC relatively improving the throughput to 4.50%.

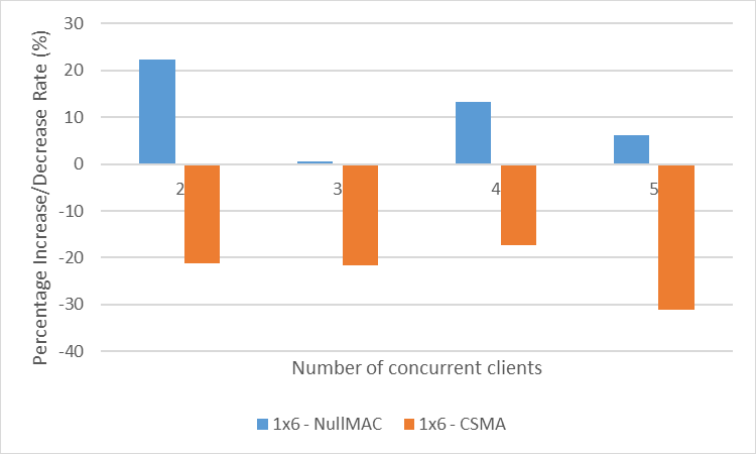


**Figure 2.** Percentage increase/decrease rates in throughput of CoCoA compared to default CoAP CC using nullMAC and CSMA for 1x6 topology

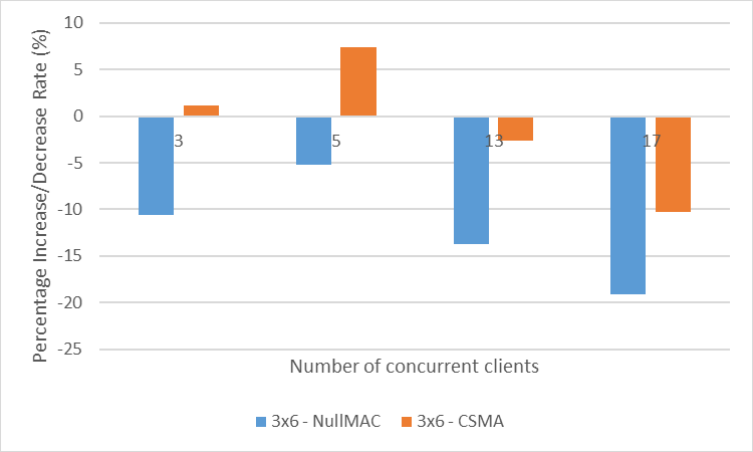


**Figure 3.** Percentage increase/decrease rates in throughput of CoCoA compared to default CoAP CC using nullMAC and CSMA for 3x6 topology

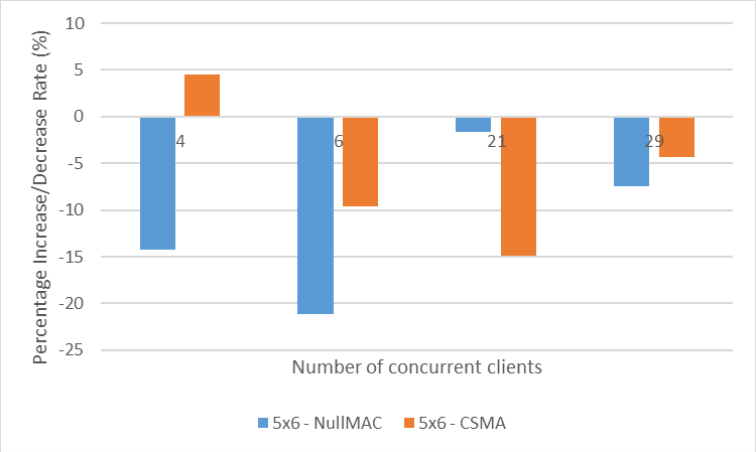


**Figure 4.** Percentage increase/decrease rates in throughput of CoCoA compared to default CoAP CC using nullMAC and CSMA for 5x6 topology

With these results, we demonstrate that MAC-level protocol setups influence the performance of the used CC mechanism. For example, in 1x6 topology, when nullMAC is used, CoCoA performs better than default CoAP CC in almost all traffic loads. On the other hand, in 1x6 topology, when CSMA is used, default CoAP CC performs better than CoCoA. Moreover, we investigated the performance of default CoAP CC and CoCoA in varying traffic loads, namely in lightly, moderately and heavily congested 1x6, 3x6 and 5x6 grid network topologies. Unlike other studies in the literature where CoCoA was shown to be superior to default CoAP CC under only heavy and light traffic loads, we observe and highlight that default CoAP CC outperforms CoCoA in almost all light, moderate and heavy traffic loads when CSMA, the most commonly used MAC protocol, is employed in considered grid networks.

The analysis of these results indicates that both CC mechanisms have their own shortcomings, and there is no generalizable superiority of one CC mechanism over the other that consistently performs well over all topologies, MAC protocols and varying traffic loads. Particularly, CoAP has the demerit of having a conservative retransmission timer which can cause long idle times before the lost packet is retransmitted during timeout period. On the other side, CoCoA can lead to unnecessary retransmissions, causing more congestion and resulting with reduced throughput. To overcome the shortcomings of CC mechanisms, one possible way would be to design enhanced CC mechanisms which may accurately adapt network conditions.

## 5. Conclusion

In this paper, we investigated and presented comparison of default CoAP CC and CoCoA in terms of throughput (i.e. number of requests/second) by varying number of concurrent clients where each client continuously sends back-to-back traffic to servers residing in 1x6, 3x6 and 5x6 grid network topologies. At the client-side, we configured 24 PCs to execute concurrent clients that use Californium implementation of default CoAP CC and CoCoA. At the server-side, we also used the same PCs to run varying number of servers that use Erbium implementation of CoAP in Cooja simulator of ContikiOS. Our results show that CoCoA is not always better than default CoAP CC in terms of throughput in some scenarios. As a result, design and development of new CoAP CC mechanisms are open to research.

## References

Ancillotti, E. and Bruno, R., 2017. Comparison of CoAP and CoCoA+ congestion control mechanisms for different IoT application scenarios. IEEE Symposium on Computers and Communications, Crete, Greece, pp. 1186–1192.

Bandyopadhyay, D. and Sen, J., 2011. Internet of Things: Applications and Challenges in Technology and Standardization. Wireless Personal Communications, 58(1), 49–69.

Betzler, A., Gomez, C., Demirkol, I. and Kovatsch, M., 2014. Congestion control for CoAP cloud services. IEEE Emerging Technology and Factory Automation, Barcelona, Spain, 1–6.

Betzler, A., Gomez, C., Demirkol, I. and Paradells, J., 2015. CoCoA+: An advanced congestion control mechanism for CoAP. Ad Hoc Networks, 33, 126–139.

Betzler, A., Gomez, C., Demirkol, I. and Paradells, J., 2016. CoAP congestion control for the internet of things. IEEE Communications Magazine, 54(7), 154–160.

Bormann, C., Betzler, A., Gomez, C. and Demirkol, I., 2018. CoAP Simple Congestion Control/Advanced, https://tools.ietf.org/html/draft-ietf-core-cocoa-03.

Dunkels, A., Gronvall, B. and Voigt, T., 2004. Contiki - a lightweight and flexible operating system for tiny networked sensors. 29th Annual IEEE International Conference on Local Computer Networks, Tampa, FL, USA, pp. 455–462.

Jarvinen, I., Daniel, L. and Kojo, M., 2015. Experimental evaluation of alternative congestion control algorithms for Constrained Application Protocol (CoAP). 2nd IEEE World Forum on Internet of Things, Milan, Italy, pp. 453–458.

Kovatsch, M., Duquennoy, S. and Dunkels, A., 2011. A Low-Power CoAP for Contiki. 8th IEEE International Conference on Mobile Ad-Hoc and Sensor Systems, Valencia, Spain, pp. 855–860.

Kovatsch, M., Lanter, M. and Shelby, Z., 2014. Californium: Scalable cloud services for the Internet of Things with CoAP. International Conference on the Internet of Things, Seoul, Korea, pp. 1–6.

Lee, J. J., Kim, K. T. and Youn, H. Y., 2016. Enhancement of congestion control of Constrained Application Protocol/Congestion Control/Advanced for Internet of Things environment. International Journal of Distributed Sensor Networks, 12(11) 1-13.

Li, S., Xu, L. Da and Zhao, S., 2015. The internet of things: a survey. Information Systems Frontiers, 17(2), 243–259.

Manjarekar, S., Rathod, S., Siddhiqi, R., Pathan, I. and Kale, M., 2018. IoT Based Home Security. International Journal of Advanced Research in Computer and Communication Engineering, 7(5), 47–50.

Shelby, Z., Hartke, K. and Bormann, C., 2014. Constrained Application Protocol. RFC 7252, https://tools.ietf.org/html/rfc7252.

**GÜFBED/*GUSTIJ* (2018) CMES 2018 SEMPOZYUM EK SAYISI: 61-66**
DOI: 10.17714/gumusfenbil.432685 Araştırma Makalesi / *Research Article*

# Electrical Analogue of Arterial Blood Pressure Signals

*Arteriyal Kan Basınç Sinyallerinin Elektriksel Analojisi*

**Sevcan EMEK*[1,a], Vedat EVREN[2,b], Şebnem BORA[3,c]**
[1]*Manisa Celal Bayar University, Department of Computer Engineering, 45140, Manisa*
[2]*Ege University, Department of Physiology,35100, İzmir*
[3]*Ege University, Department of Computer Engineering,35100, İzmir*

• Geliş tarihi / *Received*: 10.06.2018 • Düzeltilerek geliş tarihi / *Received in revised form*: 04.10.2018 • Kabul tarihi / *Accepted*: 24.10.2018

**Abstract**
In this study, we propose an electrical circuit model that will be useful for understanding of the mechanisms and dynamics of the human cardiovascular system, which is considered as a complex system in the field of physiology. The electrical circuit model, defined as the Windkessel model, plays an important role in the observation of the characteristic effect of the blood pressure on the arterial system. An electrical circuit model, which we have connected to the input terminals of the Windkessel model, ensures that the mean arterial blood pressure signals are observed within the expected range of values. The Windkessel circuit model that we have tried to develop in this study was constructed in a laboratory environment and the results were observed. It is thought that this study will contribute to the literature in terms of the development of the Windkessel model by increasing the number of parameters involved in the models of heart and arterial system.

**Keywords**: Arterial system, Mean arterial blood pressure, Windkessel model

***Öz***
*Bu çalışmada, fizyoloji alanında karmaşık bir sistem olarak kabul edilen insan kardiyovasküler sistemin sahip olduğu mekanizmaların ve dinamiklerinin anlaşılabilmesine fayda sağlayacak elektriksel bir devre modeli önerilmektedir. Windkessel model olarak tanımlanan elektriksel devre modeli, kalpten pompalanan kan basıncının arteriyel sistemdeki karakteristik etkisinin gözlemlenmesinde önemli rol oynamaktadır. Windkessel modelin girişine entegre ettiğimiz ayrı bir elektrik devre modeli, ortalama arteriyel kan basıncı sinyallerinin beklenen değer aralıklarında gözlemlenmesini sağlamaktadır. Bu çalışmada ele alınan ve geliştirmeye çalıştığımız Windkessel devre modeli laboratuvar ortamında kurulumu gerçekleştirilmiş ve sonuçları gözlemlenmiştir. Kalp ve arteriyel sistem ilişkisinde rol alan parametre sayılarının arttırılarak, Windkessel modelin geliştirilmesine bir alt yapı olması açısından bu çalışmanın literatüre katkı sağlayacağı düşünülmektedir.*

***Anahtar kelimeler:*** *Arteriyel sistem, Ortalama arteriyel kan basıncı, Windkessel modeli*

*[a] Sevcan EMEK; sevcan.emek@cbu.edu.tr; Tel: (0236) 201 10 00; Faks: (0236) 201 20 20; orcid.*org/0000-0003-2207-8418*
[b] orcid.org/0000-0003-0274-0427 [c] orcid.org/0000-0000-0000-0000

## 1. Introduction

Human physiology has a complex structure in terms of system dynamics. Direct computation or modeling of this structure is difficult. Using modeling techniques and technologies helps to the researchers to analyze and understand physiological systems. Modeling on physiological systems has become a popular research field in recent years with major contributions coming from a mix of physiologists, mathematicians, and engineers (Guyton et al., 1972; Khoo, 2000). Human physiology includes major systems that maintain vital functions. The human cardiovascular system (CVS) is one of the major systems of physiology that it consists of the heart and vascular system (Guyton and Hall, 2006; Bora et al., 2017). Various modeling techniques of different disciplines are used to explain dynamics of CVS, such as blood pressure, blood flow, blood flow velocity, blood volume, etc. Behavior of CVS is tried to be modeled by techniques, such as fluid mechanics (Olufsen, 2001), electrical circuit model (Westerhof et al., 2009; Fazeli and Hahn, 2012; Kokalari et al., 2013), computer based modeling (Bora et al, 2017; Al-Jaafreh et al., 2005), control theory (Wu et al., 2005), mathematical and numerical modeling (Quarteroni et al., 2002).

In comparison to several mathematical and electrical models of CVS, the researchers have used different approaches with the aim of providing better understanding and modelling of the vascular system dynamics and heart mechanism in the CVS (Abdolrazaghi et al., 2010). In this work, an electrical circuit model is defined to observe the arterial system dynamics. Windkessel model which is represented by electrical model of the arterial system is a mathematical model related to the relationship of between blood pressure and blood flow. In the literature, Windkessel model has been implemented for several numbers of compartment lumped parameters by using differential equations, laplace transforms, the equations of fluid dynamics, block diagrams, and conceptual formulation of the effects between the heart and systemic arterial system (De Pater and Van Den Berg, 1964). In this study, we use 3-elements Windkessel model. Unlike other studies, we have added a clamper circuit to the Windkessel model to observe the desired results in normal conditions, assuming the physical parameters of a healthy adult individual. This work contributes to the electrical analogue of the Windkessel model; thus we propose to extend the model with electronic components to improve the Windkessel model behavior. We plan to improve the model with integrated circuits in the future.

We have organized this paper as follows: Section 2 offers a detailed account of the arterial system. Details of the Windkessel model, the electrical circuit model of the arterial system, are described in Section 3. Proposed Windkessel model and its results are illustrated in Section 4. Evaluated of the results of this study and suggestions are given in the Conclusions section.

## 2. Arterial System

CVS can be described as a closed circuit model which consists of the heart (cardio) and blood vessels (vascular). CVS provides blood circulation within the body through the blood vessels (Guyton and Hall, 2006; Marieb and Hoehn, 2010; Bora et al., 2017). The heart is an important vital component of CVS. The blood is pumped from the heart to the blood vessels. Therefore, parameters such as blood pressure, blood flow, resistance, in terms of vascular system dynamics are important. Vascular system consists of the arterial system, capillary and venous system. The arterial system consists of arteries and arterioles which carry oxygen-rich blood away from the heart through the body. The aorta is the largest and main artery of the human body. Capillaries are the smallest vessels where diffusion occurs between blood and cells in tissues. Venous system involves veins, like the vena cava and pulmonary veins that carry oxygen-poor blood back to the heart (Guyton and Hall, 2006; Jahangir, 2016; Bora et al., 2017). The oxygen-rich blood pumped from the artery is transported to the tissues and organs through the capillaries from the arterial system, where the circulation of the oxygen-poor blood through the venous system is defined as systemic circulation (Figure 1).

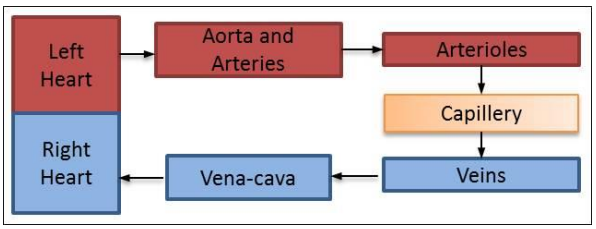


**Figure 1.** Systemic circulation

The left ventricle, defined as the left heart in Figure 1, is the only gate to the arterial system. The left ventricle pumps oxygen-rich blood under a certain pressure. Blood vessels are flexible and this flexibility significantly affects blood flow

dynamics (Capoccia, 2015). For example, the aorta has the highest elasticity due to its distinctive elastic layers (Guyton and Hall, 2006). The aorta has a significant dynamic structure when analyzing local blood flow characteristics such as pressure and blood flow fluctuations in the arterial system. The mechanism of a fluid in a straight pipe relative to hydrodynamic laws (Kinsky, 1982) has a similar meaning to the mechanism by which pressure is transmitted through the blood, which is a propelling force through the vessel (Oertel, 2005). This thrusting force arises from the energy difference between any two points of the vessel. This is actually Ohm's law, which is based on hemodynamics (Guyton and Hall, 2006). According to Ohm's law, the blood flow (F) in the vessel is calculated by equation (1). ΔP is pressure difference (pressure gradient) between the two endpoints of the vessel. R is resistance against the blood flow along the vessel.

$$F = \frac{\Delta P}{R} \quad (1)$$

The main purpose of hemodynamics is to deliver blood to the tissue capillaries at a sufficient pressure and to ensure the continuity of circulation through the mechanisms that will allow the oxygen-poor blood to return to the heart. The time from the heartbeat to the next beat is defined as a heart cycle. For this reason, blood pressure pumped from the heart can change as a function of time. The mean arterial blood pressure curve during a cardiac cycle is shown in Figure 2.

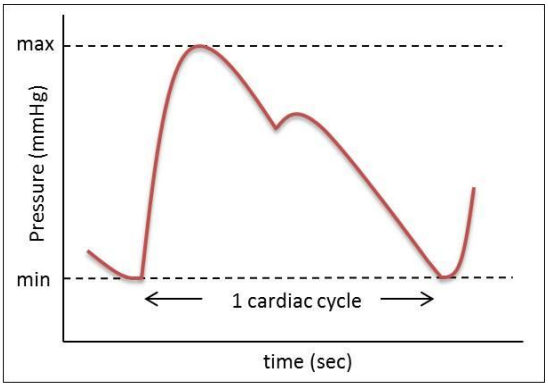


**Figure 2.** The mean arterial blood pressure (Guyton and Hall, 2006)

In Figure 2, the minimum pressure is between 60 and 89 mmHg and the maximum is between 100 and 140 mmHg (Bora et al., 2017).

There are various methods that are used in modeling the CVS (Creigen et al., 2007). The Windkessel model explained in Section 3 was included to the literature as an electrical analogue where the parameters of CVS were represented by electrical components in an electrical circuit model.

## 3. Electrical Circuit Model

The German physiologist Otto Frank (Frank, 1899) introduced the Windkessel model in his article. Frank has identified the heart and arterial system as a closed hydraulic circuit. This circuit consists of a water pump connected to an old type of firefighting mechanism, which is connected to a chamber filled with water except for some air. When the pump starts to work, water tries to push the water towards the outlet of the compartment by compressing the air (Westerhof et al., 2009; Mei et al., 2018). This mechanism can be represented as an electrical circuit model. In the electrical circuit model, the fluid defined as the water in the fluid spaces of the fluid mechanism corresponds to electric charges which describe all electrical phenomena: 1) electric force, i.e. potential difference (voltage) and 2) the motion of charge creating electric fluid, i.e. electric flow (current). The blood flow in the vessel in the CVS can be represented based on the relation of current, voltage and resistance in the electric circuits under Ohm's law. The electrical analogue of the CVS parameters is shown in Table 1 (URL-1, 2017).

**Table 1.** Electrical analogue of some CVS parameters

| CVS parameters | Electrical analogue |
|---|---|
| **Blood pressure (P)** | Potential difference (V) |
| **Blood flow (F)** | Current (I) |
| **Resistance (R)** | Resistance (R) |
| **Compliance (C)** | Capacitance (C) |
| 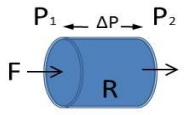  $F = \frac{P_1 - P_2}{R}$ |   $I = \frac{V_1 - V_2}{R}$ |

Hemodynamic parameters of the CVS exhibit the characteristic behavior of the blood vessel. The flow in the blood vessel is determined by two factors: (1) the pressure difference (ΔP) of the blood between the two ends of the vessel; (2) resistance to blood flow through the vessel, called vascular resistance. $P_1$ denotes the pressure at the

beginning of the vessel, and $P_2$ denotes the pressure at the other end of the vessel. Resistance is caused by friction along the entire inner surface of the vessel. The blood flow in the vessel can be calculated according to Ohm's law, as shown in equation (1). Ohm's law refers to the most important relationships that are necessary to understand circulatory hemodynamics. Transmission of the blood flow (F) to the tissues is caused by the pressure difference. The compliance (C) is related to flexibility and extensibility of the vessel. In electrical analogue of the capacitor, it means that it stores potential energy electrostatically in an electric field. Capacitance (C) means the effect of the capacitor. In physiology, we can define compliance as the total amount of blood that can be stored in response to an increase in pressure per mmHg in a given area of circulation.

In CVS, blood flow to the vascular system is achieved by pumping the heart under a certain pressure. The aortic valve opening into the arterial system from the left ventricle of the heart transmits the blood flow in a single direction. The blood that is pumped under high pressure from the left ventricle opens the aortic valve, causing the constriction and dilation of the vessel. The 3-element Windkessel model definition of this system is shown in Figure 3.

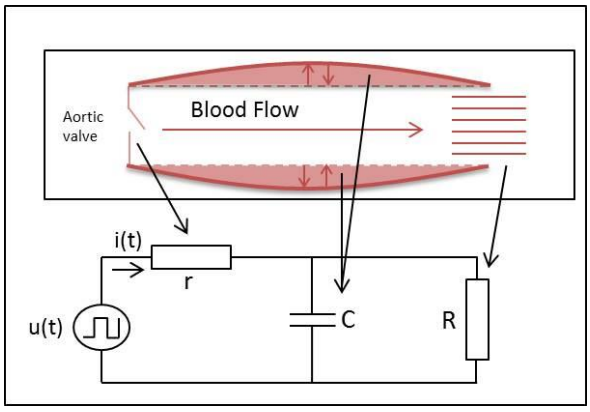


**Figure 3.** Representation of the arterial system along the aorta in the 3-element Windkessel model

In Figure 3, the input signal u(t) representing a blood pressure is applied to the circuit. The 1 kΩ resistor represents resistance of the aortic valve to the blood flow. A 1μF capacitor in the circuit defines the constriction and dilation of the vessel. The 10 kΩ resistor is defined as the resistance of arterial vessels to the blood flow.

The Windkessel model is a mathematical model with 2, 3 and 4 elements in the literature (Westerhof et al., 2009; Kokalari et al., 2013). This circuit model can be calculated by differential equations. In this study, 3-element Windkessel circuit model is observed in the laboratory by adapting to CVS parameter values.

## 4. Experimental Study

In this study, an electrical circuit was constructed in the laboratory environment so that we could observe the effect of the blood pressure on the arterial system. This circuit, which is defined as a 3-element Windkessel model, is shown in Figure 4.

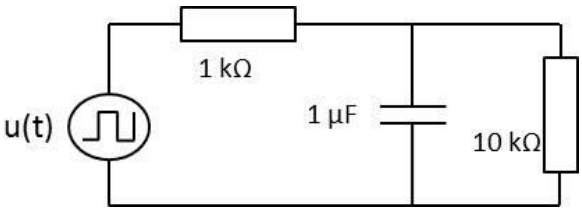


**Figure 4.** 3-element Windkessel model

When a square wave input of ± 5 volts 0.66 kHz is applied to the input of the circuit given in Figure 4, the input and output waveforms observed from the circuit are shown in Figure 5. Since the time constant τ (0.05 sec. with given a 10 kΩ resistor and a 1μF capacitor) is greater than the period of the input signal (0.0015 sec.), the capacitor does not charge to the peak of the input and it only has a potential to charge to a value of 2.5 volts. On the other hand, when the input voltage goes negative, the capacitor does not fully discharge and sinks down to -2.5 volts.

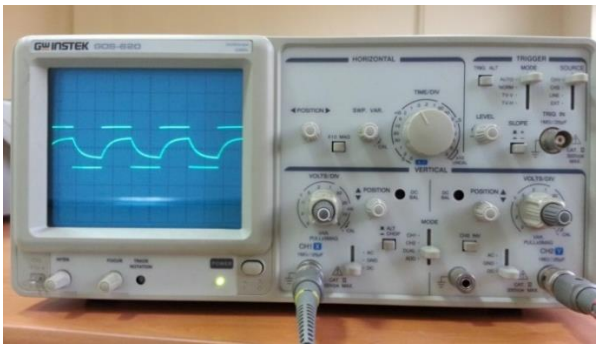

**Figure 5.** The square wave input signal applied to the 3-element Windkessel circuit model and the observed output signal

The signals observed in Figure 5 do not reflect the expected range of the mean arterial blood pressure. For this reason, a diode clamper is added

to the 3-element Windkessel model (Selek, 2017), which can provide the expected consistency of the results. This circuit clamps the AC signal to the DC level so that the arterial blood pressure remains at the minimum and maximum levels. This circuit is shown in Figure 6.

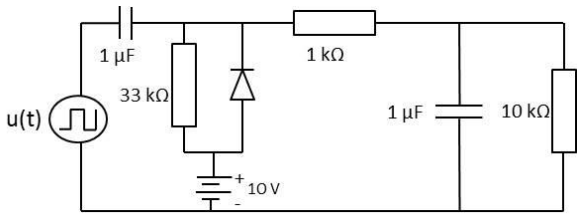


**Figure 6.** Windkessel circuit model and a clamper

In Figure 6, a square wave input of ± 5 volts 0,25 kHz is applied to the input of the circuit. This circuit can show the mean arterial pressure between 8 and 12 volts as in Figure 7.

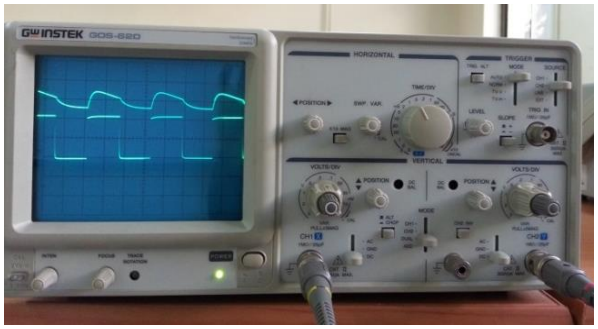

**Figure 7.** Input and output signals defined as the mean arterial pressure of the Windkessel model

Figure 8 shows an electrical circuit representing the arterial system, an experimental set-up providing input signal to the circuit and power supply, and an oscilloscope.

Blood pressure is a non-electrical biological signal. In order to be able to observe blood pressure signals in a circuit model, it is necessary to make some assumptions as in this study. Under normal circumstances, the average arterial blood pressure in an adult individual can be measured as between 80 and 120 mmHg (Guyton and Hall, 2006). These values were represented with the peaks of output voltages observed as 8 and 12 volts with the signal which was applied to the input of the circuit under laboratory conditions.

## 5. Conclusions

In this study, the electrical analogy of the basic parameters of the arterial system (blood flow, compliance and resistance) was examined. The characteristic behavior of the arterial system is described with the electrical circuit model known as the Windkessel model. This work has some limitations in defining of the model. We consider that Windkessel models consist of differential equations that relate the CVS dynamics. We do not make any calculations for the models we offer in this study. We present an experimental study which we interpret the dynamics of vessel behaviors by observing the results. In this study, it is expected that Windkessel model, which is supported by a separate circuit, achieves a suitable circuit potency to be further improved by increasing the system parameters.

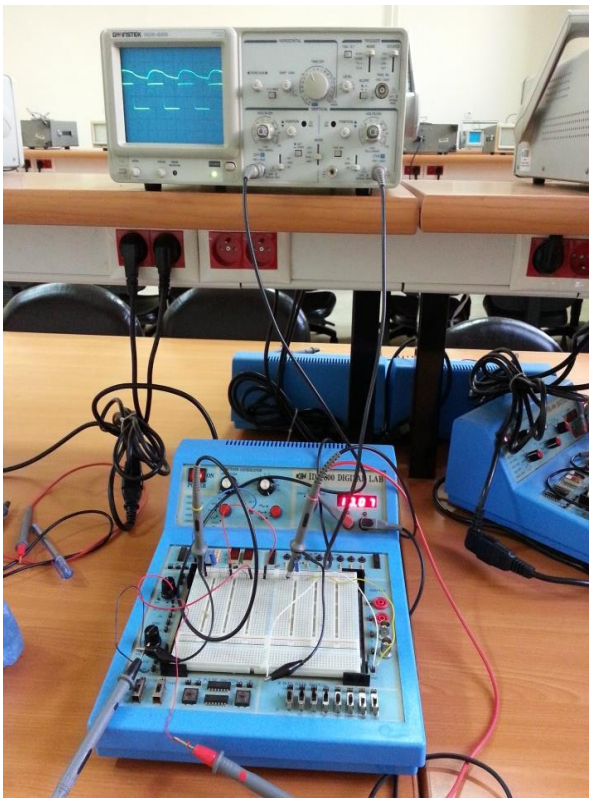

**Figure 8.** Electrical circuit representing the arterial system

## References

Abdolrazaghi, M., Navidbakhsh, M. and Hassani, K., 2010. Mathematical Modelling and electrical Analog Equilavent of the Human Cardiovascular System. Cardiovascular Engineering, 10, 45-51.

Al-Jaafreh, M. and Al-Jumily, A., 2005. Multi Agent System for Estimation of Cardiovascular Parameters. 1st International Conference on Computers, Communications, & Signal Processing with Special Track on Biomedical Engineering, pp. 269-299.

Bora, Ş., Evren, V., Emek, S. and Çakırlar, I., 2017. Agent-based modeling and simulation of blood vessels in the cardiovascular system, doi: 10.1177/0037549717712602.

Capoccia, M., 2015. Development and Characterization of the Arterial Windkessel and Its Role During Left Ventricular Assist Device Assistance, Artificial Organs, 39(8), 138-153.

Creigen, V., Ferracina, L., Hlod, A., Mourik, S., Sjauw, K., Rottschafer, V., Vellekoop, M. and Zegeling P., 2007, Modeling a Heart Pump, January 29th- February 2nd 2007, (Eds: Rob H. Bisseling, Karma Dajani, tammo jan Dijkema, Johan van de Leur, Paul A. Zegeling), Proceedings of the 58th European Study Group Mathematics with Industry, Utrecht, Netherlands, 115p.

De Pater, L. and Van Den Berg, J.W., 1964. An Electrical Analogue of the Entire Human Circulatory System. Medical Electronics and Biological Engineering, 2, 161-166.

Fazeli, N. and Hahn, J., 2012. Estimation of cardiac output and peripheral resistance using square-wave-approximated aortic flow signal, doi: 10.3389/fphys.2012.00298.

Frank, O., 1899. Die Grundform des arteriellen Pulses. Zeitschrift für Biologie, 37, 483-526.

Guyton, A.C. and Hall, J.E., 2006. Textbook of Medical Physiolog 11th Edition: Elseiver Inc, 1152p.

Guyton, A.C., Coleman, T.G. and Granger H.J., 1972. Circulation: Overall Regulation. Annual Review of Physiology, 34, 13-44.

Jahangir, M., 2016. Anatomy and Physiology for Health Professionals 2nd Edition: Jones & Barlett, ISBN-13 9781284036947, pp. 207-223.

Khoo, M.C.K., 2000. Physiological Control Systems: Analysis, Simulation, and Estimation: Hoboken, New Jersey, John Wiley & Sons, 344p.

Kinsky, R., 1982. Applied fluid mechanics: Sydney, McGraw-Hill, 182p.

Kokalari, I., Karaja, T. and Guerrisi, M., 2013. Review on lumped parameter method for modeling the blood flow in systemic arteris. Journal of Biomedical Science and Engineering, 6, 92-99, doi: 10.4236/jbise.2013.61012.

Marieb, E.N. and Hoehn, K., 2010. Human Anatomy and Physiology. 8th Edition: San Francisco, Benjamin Cummings, 1114p.

Mei, C.C., Zhang, J. and Jing, H.X., 2018. Fluid mechanics of Windkessel effect. Medical & Biological Engineering & Computing, 56(8), 1357-1366, doi: 10.1007/s11517-017-1775-y.

Oertel, H., 2005. Modelling the Human Cardiac Fluid Mechanics: Karlsruhe, University of Karlsruhe, ISBN 3937300821, 53p.

Olufsen, M.S., 2001. A One-Dimensional Fluid Dynamic Model of the Systemic Arteries. Computational Modeling in Biological Fluid Dynamics: New York, Springer, pp.167-187.

Quarteroni, A., Veneziani, A. and Zunino, P., 2002. Mathematical and Numerical Modeling of Solute Dynamics in Blood Flow and Arterial Walls. SIAM Journal on Numerical Analysis, 39(5), 1488-1511.

Selek, H.S., 2017. Elektronik-1 Analog Elektronik: Kocaeli, Seçkin Yayıncılık, pp.150-161.

URL-1, http://hyperphysics.phy-astr.gsu.edu/hbase/electric/watcir2.html. 1 Haziran 2018.

Westerhof, N., Lankhaar, J. and Westerhof B.E., 2009. The arterial Windkessel. Medical & Biological Engineering & Computing, 47, 131-141, doi: 10.1007/s11517-008-0359-2.

Wu, Y., Allaire, P., Tao, G. and Olsen, D., 2005. Modeling, Estimation and Control of Cardiovascular Systems with A Left Ventricular Assist Device, American Control Conference, June 2005, Portland, USA, pp.3841-3846.

**GÜFBED/*GUSTIJ* (2018) CMES 2018 SEMPOZYUM EK SAYISI: 67-78**
DOI: 10.17714/gumusfenbil.432582 Araştırma Makalesi / *Research Article*

# Semantic Relation's Weight Determination on a Graph Based WordNet

## *Çizge Tabanlı WordNet Ağı Üzerinde Anlamsal İlişki Ağırlıklarının Tespiti*

**Çağatay TÜLÜ*[1, a] Umut ORHAN[2,b], Erhan TURAN[3,c]**
[1]*Adana Science and Technology University, Information Technologies Department, Adana*
[2]*Çukurova University, Faculty of Engineering and Architecture, Computer Engineering Department, Adana*
[3]*Osmaniye Korkutata University, Faculty of Engineering, Computer Engineering Department, Osmaniye*

• Geliş tarihi / *Received*: 10.06.2018 • Düzeltilerek geliş tarihi / *Received in revised form*: 16.10.2018 • Kabul tarihi / *Accepted*: 24.10.2018

**Abstract**
Determination of semantic relatedness between two textual items is one of the crucial phases in many Natural Language Processing applications. In this study, a new approach to lexicon based semantic relation determination methods was experienced using WordNet 3.0 and Men's real-life similarity dataset. Men's test collection was used for the determination of the relation weights and determined weights were used in semantic relatedness computation. RG65 similarity dataset was used for a benchmark of the proposed method and Spearman correlation 0.81 was gained, taking into account that retrieving the relations weight using a large scale dataset and testing them with another real-life dataset promises new perspectives to the determination of the relations weight and to the relatedness computation.

**Keywords:** Natural language processing, Semantic relation, WordNet

***Öz***
*Birçok doğal dil işleme uygulamasında metinsel iki öğenin anlamsal ilişkisinin tespit edilmesi çok önemli bir aşamadır. Bu çalışmada WordNet 3.0 ve Men's veri seti kullanarak sözlük tabanlı anlamsal ilişki belirleme metodları için yeni bir yaklaşım sunulmaktadır. Anlamsal ağırlıkların hesaplanmasında Men's veriseti kullanılmış ve bulunan değerler anlamsal ağırlık hesaplanmasında kullanılmıştır. Önerilen metodun doğruluğunu ölçmek için RG65 benzerlik verisetі kullanılmış, kayıslama sonucunda 0.81 Spearman korelasyon değeri elde edilmiştir. Büyük boyutlu bir verisetinin geliştirme ve test için kullanılıp, diğer önemli bir verisetinin de kıyaslama amaçlı olarak anlamsal ilişki tiplerinin ağırlıklarının belirlenmesi ve anlamsal ilişkinin hesaplanmasında kullanılması anlamsal benzerlik ve anlamsal ilişki hesaplanmasına farklı bir bakış açısı getirmektedir.*

***Anahtar kelimeler:*** *Doğal dil işleme, Anlamsal ilişki, WordNet*

*[a] Çağatay TÜLÜ; cagataytulu@gmail.com; Tel: (0322) 4550010; https://orcid.org/0000-0002-4462-3707
[b] orcid.org/ 0000-0003-1882-6567 [c] orcid.org/0000-0002-2953-2698

## 1. Introduction

Scaling the relatedness of two different concepts always takes attention from the researchers, assigning a value to the relatedness of two concepts brings new research opportunities especially for expert systems, smart applications, automatic question answering systems, text summarization, short answer grading, and many other Natural Language Processing (NLP) applications. Developing a mathematical model for real-life problems enables to generate algorithm and helps to solve them easily and consistently by the machine. So it is very important to use tools and resources that are compatible with mathematical operations.

WordNet (Fellbaum, 1998) is a lexical semantic knowledge base designed for the English language. It is in a graph structure, so it can be adapted to perform mathematical operations. WordNet's core elements are concepts and relations. While concepts represent the unique semantic entities, relations are the semantic signs to address the relations between two concepts. There are twenty-six different type of relations defined in WordNet version 3.0. The most common relation is the Hypernym/Hyponym relations. Each concept is connected to neighbor concepts through relations. By these connections and concepts, WordNet can be represented as a graph network. Concepts are the nodes (vertex) of the graph and relations between concepts are the edges of the graph. This structure enables that relatedness between concepts in the graph network can be calculated using graph metrics. One of the important metrics is the path between two concepts. The path is the combination of nodes and edges. Relatedness can be measured by the length of the path. Type of the relation is important; WordNet-based semantic similarity measurement studies generally use hypernym/hyponym relation types, because they have well defined hierarchical structure. Hirst and St Onge (Hirst and St-Onge, 1998) have used direction change of the path in addition to path length, Wu and Palmer (Wu and Palmer, 1994) have used Lowest Common Subsumer (LCS) of the concepts and depth of the concepts from the top entity in the hierarchy.

A real-life dataset for the semantic relatedness consist of the word pairs (word1,word2) and relatedness value for each pair, they are evaluated by native English speakers, by the way, they give judgment of relatedness for a word pair (word1,word2), judgment can be made with numerical value or as true-false approach. There are several real-life datasets like RG65 (Rubenstein and Goodenough, 1965) consists of 65-word pairs, MC30 (Miller and Charles, 1991) with 30-word pairs, WordSim353 (Finkelstein et al, 2001) with 353-word pairs, Mens 3000 (Bruni et al, 2014) with 3000-word pairs.

In this study, we have focused on determining the weight of semantic relations which connects one concept to another in the WordNet as illustrated in Figure 1. Men's 3000 (Baroni et al, 2014) real-life dataset is used in the development phase of the proposed system. Using Men's 3000 real-life datasets in the proposed method, the weight of the relations in the WordNet is determined. Determined relations weights are applied to the real-life dataset RG65 simply multiplying the weights of the relations in the path and relatedness score is obtained. To evaluate the success of the found relatedness values in the RG65 real-life data set is used.

Rest of the paper is organized as follows; section 2 gives brief literature history of the semantic relatedness and semantic weight determination methods, section 3 presents detailed information about the method of the study, section 4 explains benchmark and evolution tests, section 5 is results and discussion part. And finally, section 6 is the conclusion of the study and gives a future aspect of the proposed method.

## 2. Related Works

Semantic relatedness, semantic similarity or semantic distance is the terms used for the same purposes, it aims to determine whether two textual items are related or not in a semantic manner. These textual items can be a single sense (concept), single words or short texts like sentences or paragraphs or documents. Relatedness of two textual items can be computed using several approaches; the first one is statistical approaches (Li et al, 2003; Sultan et al, 2014); it uses corpus statistics of the textual items and compares them according to retrieved statistical values from the corpus and generates relatedness score. The other one is knowledge-based approaches (Agirre and Soroa, 2009; Hughes and Ramage, 2007); it uses the features of hierarchical lexical knowledge bases. WordNet and conceptNet (Speer and Havasi, 2012) are the important ontology-based structured lexical knowledge bases. Wiktionary (en.wiktionary.org) are lexicon based free multilingual knowledge base developed collaboratively by people around the World and Babelnet (Navigli and Ponzetto,

2012) is another type of the knowledge base using multiple sources with cross-lingual structure. The last approach for relatedness is the hybrid approach(Meng et al, 2012) that combines knowledge-based and corpus-based approaches together.

Knowledge-based semantic relatedness computation methods use a resource that is consist of unique entities. These entities are called concepts. Each concept contains lexical or/and encyclopedic information about the concept and relation information to the other concepts. WordNet contains semantic relations among the concepts (known as synset) and their POS (Part of Speech) information. WordNet based methods are used for the semantic similarity measurement of short texts like senses, words, sentences and short paragraphs. Semantic relations in the WordNet are one of the key elements to the semantic relatedness computation. In the hierarchical structure of the WordNet, these relations provide the ability to reach from one concept to another. From originating synset to the destination synset in the WordNet, retrieving a path that consists of nodes and relations gives us the ability to make mathematical operations. Assigning a numerical value to the nodes and relations enables similarity calculation to be more accurate.

There are several studies in the literature about weighting the relations in the relatedness computation of WordNet concepts, one of older is the Hirst&St-Onge (Hirst G. and St-Onge D, 1998) method, in this method relatedness between two concepts in the WordNet is calculated using the path length and direction change of the path from originating to the destination concept. In this approach, relation type hypernym and autonomy are taken into account and only noun concepts are used and the weight of these relations are given as numerical value 1. Another approach is the Wu-Palmer (Wu Z., Palmer M., 1994) method that uses both path length and taxonomic depth of the concepts. Yang and Powers (Yang and Powers, 2005) have proposed edge counting techniques for the weight of the relation types. In this method, two kinds of searching methods in the graph are used, bidirectional depth-limit search (BDLS) and uni-directional bread-first search (UBFS), combining the metrics taken from this searches, similarity/relatedness value is generated. This method uses the relation type in three different level, the first one is an identical level where two concepts are identical relation weight is 1.0. The second one is synonym/antonym level where relation weight is taken as 0.9, this is also called intermediate level, lower level relation weight is taken as 0.85, relation types hypernym/hyponym and holonym/meronym are the examples of lower level relation types. Searching depth is another parameter in this method, and the value of searching depth depends on the type of relation. This method also covers the verb similarity. It has been tested in 28 noun pair dataset (Miller and Charles, 1991), and the correlation of this method to human judgment is found as 0.921.

The other important study about relation weighting has been performed by Ahsaee et al (Ahsaee et al, 2014) in which they suggested using the weight of an edge as 1.0 in the leaf nodes, and decreasing the weight of node according to proximity to the root. For example, a leaf node takes the weight as 1.0, one step up of the node to root is taken as 0.9, two steps upward are taken as 0.81. It is assumed that when a concept goes up from the leaf node to the root node, its subjectivity decreases and objectivity increases. This method also achieved high correlation in the RG65 dataset, this method takes hypernym/hyponym relation and cover just nouns.

Siblini and Kosseim (Siblini and Kosseim, 2013) have categorized the relations and assign a numerical weight into each category. Semantic categories are Similar, Hypernym, Sense, Gloss, Part, Other Instance. They have created a semantic network using the WordNet 3.1 as a source. In addition to the synsets in the created graph, they have defined node type word to point relation between synset and concept for the sense and gloss relation types. Sense relation from synset to the word is created for the different word forms of a synset and gloss relation from synset to the word is created for each keyword in the synset's definition. For example, synset (automobile) is connected to the car node with sense relation and Wheel node with gloss relation. Generated graph network in the mentioned study consists of around 265k node and around 2 million relations. In order to measure semantic relatedness of given two concepts, that have used path cost from originating to the destination node, the path cost is calculated using relation types and weights in the path and also some other constant parameters are used. This method had given a performance in a MC30 dataset with Pearson Correlation value=0.93, but it gives poor performance in WordSim353 dataset with correlation 0.5. In the other WordNet-based approach systems like PageRank (Brin and Page, 1998), weights of the relations are generally taken as numerical value 1.0. These methods generally

focus on other graph parameters than relation weights.

Machine-learned vector space model (Speer and Chin, 2016) has used which combines word embedding that is produced by GloVe (Pennington et al., 2014) and word2vec(Mikolov et al., 2013) using tightly structured semantic networks like conceptNet(Speer and Havasi, 2012). Kartsaklis et al (Kartsaklis et al, 2018) have proposed a method which maps the natural language texts to the knowledge-based entities, they have enhanced LTSM model with a dynamic disambiguation mechanism on the input word embeddings that address polysemy issue. This method has gained state of the art performance in many word-similarity evaluations.

## 3. Methodology

Initially, we have examined "The MEN Test Collection" (Bruni et al, 2014) relatedness dataset, it was prepared for the benchmark purposes of the similarity/relatedness studies. During the experiment, we have observed that relatedness between two concepts is mostly affected by the relation type and path length. Generally, relatedness and path length have a negative correlation. The shortest path between two concepts is the key parameter to prove the strength of relation in WordNet. But the strength of the relation of two concepts depends not only on the shortest path. Daily usage and cultural diversity imply the strength of the relations between two concepts in the human mind. Instead of a shortest path, all possible paths between two concepts are taken into account in this study, this approach is more close to human mind judgment.

Then we have decided to get all the paths between two concepts including shortest path, but retrieving all the paths between two concepts are time-consuming process for such a graph consist of the 117k node and more than 700k relations. So the length of the paths should be limited, we have performed tests on the graph DB and finally, we have determined path length interval as, interval more than 3 is getting the system into extreme CPU load and memory consumption that is causing in abnormal behavior and critical exceptions in the application. Query execution time is increased exponentially when path length is increased.

pathLenghtInterval=(shortestPath,shortestpath+3) (1)

We have collected all the paths between two words of each word pair in Men's dataset and retrieved paths are encoded with their relationship type, WordNet relation types and corresponding relation code can be found in Table 6. We have collected all paths of each word pair in Mens data collection. Path collection is performed as explained in the following example;

relatedness("*mushroom*", "*tomato")=0.74* given in Men's dataset.

As a first step, we find mushroom and tomato as nodes in WordNet graph db. Then we determined the shortest path length between this two node, the shortest path length is 3 and we retrieve all the path between mushroom and tomato nodes with *pathLenght=3+3=6*. Later we collected all the encoded paths and assign the value 0.74 to each of them as in the following;

*findAllPath("mushroom", "tomato")= [bcjbck, bcjbck, bcjbck, bcjbck, bjcckb, bjckbc, brsbbc, bccbc, bjck, bcc, bcccjb, bccjbc, bccjbc, bcjbbc, bccjbc, bcjbbc, bcjbbc, bcjbbc, bccbcj, bcjbc, bcjbc, bcjbc, bcjbc, bccj, bjc]=0.74*

All the paths in the above list are assigned with value 0.74, the same procedure is done all pairs in the Men's data, all dataset is consist of 3000-word pairs. Same paths with different relatedness score are grouped together and assigned a single score to show it as a relatedness score of that path. Consequently, we have assigned median and mean of the grouped values for a path. By the way, each path is represented with a numerical value between {0,1}, details of this process are explained in subsections of this section

We have filtered values of single length paths (pathLength=1) from the path list, then we have assigned these values to the relations, some relations are not found uniquely (as path length=1) their values are extracted from the paths. At this point, we have determined weights of each relation type. This phase is the first step of the relation weight determination process. In order to get strength the relation weights, we have calculated the path values using found relation weights in the first phase, in the second phase we have found many path values for a single word pair, then we have taken the nearest values to the real values of the relatedness. As in the above process, the unique path is taken directly as a relation weight and weight of the other relations are extracted using the weights found before.

### *3.1. Men's Data*

Mens data (Bruni et al, 2014) is taken as a trusted dataset for the development phase of the semantic relations weight determination phase. This data consists of 3000 pairs of words, there are words from all part of speech; nouns, verbs, adjectives, and adverbs. Word pairs are evaluated by fifty native English speakers, every pair of words was asked to the humans to give judgment whether they are related or not related. And relatedness score was given according to this result between 0-50, while 0 (zero) shows all evaluators have given "not related"judgment, and 50 shows all evaluators have given "related" judgment. In this study, these values are normalized between 0-1 by dividing them into 50.

### *3.2. WordNet 3.0*

WordNet 3.0 is another important component of the study. In this study, all the synsets and relations in WordNet are mapped into the graph network. In order to achieve this step a simple java application is developed, this application parses the data files from WordNet 3.0, and takes synset id, senses (literals of the sunset), pos type of a synset and creates a node in Graph database and assigns these values as a feature of the node, using the relation information; edges from source node to destination node are defined. A graph database is created in the Neo4j application (https://neo4j.com), graph network consists of around 117K nodes and 771K relations. All the relation types in WordNet are distributed in a graph network. Some relations were only unidirectional (for example, pertainym) in WordNet since proposed network to be bidirectional, these type of relations are converted into bidirectional type just by adding reverse relation, for example, reverse of the pertainym relation is converted to pertained pertainym<->pertainedBy. By the way, the bidirectional structure is completed.

### *3.3. Path Weight Determination Process for Each Path*

We have used Men's 3000 data as trusted data to develop proposed system. For each word pair (w1, w2) in Men's data, we have taken all the possible paths using some limitations. We have set maximum length parameter in the possible path lengths which are shortestPath+3, by the way, we have taken all the paths between w1 and w2 according to this limitation. We have encoded each relation type (edge) in these paths, for example, a path between w1 and w2 of the following in Figure 1, is encoded as "BBC" where b corresponds relation type Hypernym and c corresponds relation type Hyponym. All the relation type codes can be found in Table 6.

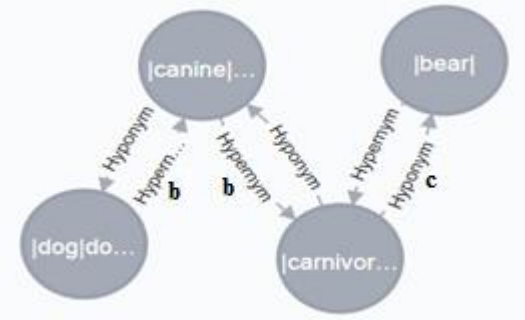


**Figure 1.** Sample path encoding between two concepts w1= "dog" and w2= "bear" in WordNet graph DB, encoded path= "BBC", all relation codes in the paths are given in Table 6.

By taking possible paths between each word pairs, we have gathered and encoded them into a text file, in that file we have collected more than 400k paths for the 3000-word pairs. We have assigned w1, w2 relatedness value to the all paths of two concept w1, w2.

For example, suppose *w1= "bedroom" and w2= "kitchen",* possible paths between them are taken in the following list;

*findAllPath ("bedroom", "kitchen")=[bcjk, bcjk, bcjk, bcjk, bcjk, bcjk, jkbc, jkbc, jkbc, jkbc, jkbc, bc, jk]*

According to Men's data *rel("bedroom", "kitchen")=0.6*, so we assign this value into each retrieved path list for this pair; taking into account using their number of occurrences as;

**Table 1.** Pathlist generated for *paths("bedroom","kitchen"), rel ("bedroom", "kitchen") = 0.6* is taken from Men's dataset.

| Path | Occurance | Importance factor | Value |
|---|---|---|---|
| bcjk | 6 | 1 | 0.6 |
| jkbc | 6 | 1 | 0.6 |
| bc | 1 | 16 | 0.6 |
| jk | 1 | 16 | 0.6 |

We have also taken into account that the short path is an important path, that is the reason that we have given importance factor in the path list table, this factor is calculated as;

$IF(path(\text{“bedroom”},\text{“kitchen”}))=n^{n-k}$ (2)
*(IF:importance factor)*

Where n is the length of the maximum length path in the path list of the word pair, k is the length of the current path in the list. n and k values are limited to 5, the even maximum path length is greater than 5 it is fixed to 5 because increasing maximum path length will increase the importance factor exponentially and looping it in the application, hangs the program and causing exceeded memory consumption and generate out of memory exception error.

For example, the importance factor for path “*bc*” in *paths(“bedroom”, “kitchen”);*

The first step is to find the maximum length path in the path list, so it is 4. Then path length of “*bc*” is 2, so Importance factor is faound as $4^{4-2} = 16$. Importance factor is used during the determination of the optimal path value.

### *3.4. Path Consolidation and Relation Weight Determination Process*

In this process, optimal path value is found for all paths in the generated path pool of the Men’s data. For each word pair, we have generated all possible paths including short path and assigned human judgment value to the all of the determined paths. Since there are 3k word pairs, we have collected 3k word pair list. These lists are consisting of paths in any size and any lengths. For the optimal path value determination for each path, we have grouped same paths with their corresponding human judgment values, occurrences and importance factors.

*findAllPath (“ceiling”, “wall”)= [jcjk, jkjk, jkjk, jjk, jk, jk]*

**Table 2.** Pathlist generated for paths("ceiling","wall"), value of rel(“ceiling”, “wall”)=0.7 taken from Men’s dataset.

| Path | Occurance | Importance factor | Value |
|---|---|---|---|
| jcjk | 1 | 1 | 0.7 |
| jkjk | 2 | 1 | 0.7 |
| jjk | 1 | 4 | 0.7 |
| jk | 2 | 16 | 0.7 |

Path consolidation is done to get optimal path value by combining each path. Consolidated paths and values for *final path(“bedroom”, “kitchen”) and final path(“ceiling”, “wall”)* are found as in Table 3.

**Table 3** Consolidated path and value list for *paths("bedroom","kitchen")&paths("ceiling","wall")*

| Path | ValueList(as ArrayList) |
|---|---|
| jcjk | [0.7] |
| jkbc | [0.6 0.6 0.6 0.6 0.6 0.6] |
| bcjk | [0.6 0.6 0.6 0.6 0.6 0.6] |
| jkjk | [0.7 0.7] |
| jjk | [0.7 0.7 0.7 0.7] |
| jk | [0.6…0.6(16 times 0.6) 0.7..0.7(32 times 0.7)] |
| bc | [0.6…0.6(16 times 0.6)] |

Values in *ValueList* are calculated for each path, for example in the Table 1 value for *jk=0.6* and *occuranceXimportance factor=1X16=16*, so we add 16 times 0.6 into value list of path *jk*, in the Table2 *jk* value 0.7 and *occuranceXimportance factor=2X16=32* so we add 32 times 0.7 into value list of path *jk*.

After determining the value list for each path, the next step is to get optimal value. For this process we have used some statistical methods, we have determined optimal value in two separated manner, one for mean and other for a median of the value list. After that, we have got paths and optimal values. By scanning all the paths we filter the paths with path length=1, this means that if there is a path with length=1, it means the weight of this relation type is determined because path with length=1 means a single relationship type is weighted.

### *3.5. Weight Determination of Missing Relations*

In the previous process, we have determined the weight of the single length paths (path length=1) in the path list. But there are some relations that are not found as a single path with path length=1, they have combined inside multiple length paths. For example, suppose there is no unique path for relation type “*x*”, but there are many paths with multiple lengths like “*a*”, “*jlx*”, “*MBA*”. In such a situation weight of the *x* determined using the known relations in the path, for example, if weight of relation *a=0.7* and value for path *xa=0.5* then value for x is found as *0.5/0.7=0.71*, if we can’t determine the value of the relation by using this method, relation weight is assigned manually and manual relation’s weight is given as 0.85. This value is taken from the edge counting technique of Yang and Powers (Yang and Powers, 2005). In that method, lower level relation weight is taken as 0.85.

With the above-explained processes we have extracted weight of each relation given in WordNet 3.0, just we have given manual value to the relation type *e(Instance_Hyponym)*, *s(Member_of_this_domain_USAGE)*, *q(Member_of_this_domain_REGION)*. That is 0.85, all other weights are determined by the algorithm.

### *3.6. Second Step in Relation Weight Determination*

As a second step of the relation weight determination process, we applied found weight values in the first step to the Men's collection dataset. We have calculated the possible path values list for each word pair. From this list, we have taken the nearest value to the real value (human judgment) of the word pair. So we determined the nearest path for each word pair. By the way, we had a 3k path for 3k word pair. Then we take the single length paths (path length=1), the same procedure is applied as explained in the previous subsection, and optimal weights are determined.
Consequently, we had two set of the relation weights determined from the first and second steps both given in Table7. In the next chapter, we will test both of these relation weights set and evaluate the determined scores with benchmark data.

### *3.7. Development Environment*

For the development of the proposed system, we have used the Java environment and Neo4j graph db. Using developed java codes, WordNet 3.0 data is imported into Neo4j DB in a graph structure. All queries are performed on the Neo4j database using cipher query language. Shortest paths between two nodes and all possible paths between two nodes have been determined through cipher queries. The operating system of the development environment is windows 7 professional 64-bit virtual machine with 2 core CPU and 8 GB memory.

## 4. Evaluation & Benchmark Tests

Using the determined weights of each relation, we tested RG65 real-world dataset, we have collected all possible paths for each word pair in this dataset, by the way we have got a list of the possible paths of each word pairs, and paths in a list are grouped using importance factor and number of occurrence for each path. We have calculated the value of each path in the list using given relation weights and then get the mean and median of the list one by one, found value from mean or average for each word pair that represents the relatedness value of the corresponding word pairs. In order to make a benchmark of the determined related values with the real RG65 values, we have used Spearman rank correlation because this method has used in most of the relatedness studies for the evaluation of the benchmark tests.

**Table 4.** Correlation values in the benchmark tests using RG65 data with mean and median of path value lists determined in step 1 and step 2.

| | Correlation using means of path value list | Correlation using the median of path value list |
|---|---|---|
| Relation weights determined in first step | 0.81 | 0.78 |
| Relation weights determined in second step | 0.79 | 0.74 |

We get 0.81 correlation using RG65 real values with relation weights found in the first step of the proposed method. In this step, we have statistically take the mean of the path values. In the first step, we take the median of the path values and we have found 0.79 correlation. Weights found in the second step are not better than the values found in the first step. We might comment that weights found in the first step are better promising. The second step of the method has performed in order to see whether we can get a better correlation. We get 0.78 correlation value using the relation weights found in the first step and taking the median of the path value list for each word pair. We continued testing the relation weight data taken in the second step. We get 0.79 correlation using the relation weights found in the second step and taking the mean of the path value list for each word pair. We get 0.74 value using the relation weights found in the second step and taking the median of the path value list for each word pair.

## 5. Results and Discussion

This study might give a new perspective to the relatedness computation of two concepts in WordNet; even success of this approach seems

not satisfied in comparison to the other WordNet-based approaches shown in Table 5. The method uses simple mathematical and statistical operations. Optimal path determination process and weight determination of missing relations are difficult in terms of algorithm generation and software development.

**Table 5.** Spearman Correlation values of several successful WordNet Based relatedness methods using RG65 dataset

| Method | Correlation |
|---|---|
| ADW (Pilehvar, Navigli 2015) | 0.868 |
| Hughes and Ramage (2007) | 0.838 |
| Agirre at al. (2009) | 0.830 |
| Wu and Palmer (1994) | 0.78 |

Given approach in this study is simple, only complex and time-consuming part is a determination of the possible paths between two concepts in the WordNet. In the Neo4j graph database, shortest path determination is easy using a cipher query language, but determining all the possible lengths in a limited path length takes several minutes for any two synsets because graph database is consist of the 117k node and more than 700k relations, querying in such a graph database takes time. This process takes more than ten hours for the 3k word pairs in Mens dataset which is used for the development of this study. After path determination, rest of the method is not time-consuming part, just we find the values of each path by multiplying the relation types in the path, then found results are put into array list and their mean or median is calculated easily.

Another aspect we have taken from this study for the future studies is that; we have generated path list and optimal values in the first phase of the study; by this approach, we might have a path database of the human judgments. We can extend this database using other real-life similarity datasets. In the new coming studies, we can detect the optimum path of two concepts and extract the optimum path value from this database, doing this makes the similarity/relatedness computation faster and more accurate.

Future studies about this approach might be done using other metrics, not only path length but also the depth of the concepts, depth of the lowest common subsumer (LCS) of the concepts. Contributions of such parameters to the relatedness computation might be in positive and this might increase the success of proposed method and bring it into the top of relatedness methods list is given in Table5. We set weight value 0.85 for the relation types that cannot be determined our algorithm, by changing this value in upward or downward we can observe the contributions of this coefficient to the method in a positive or negative way. Moreover, information content value that might be taken from an external corpus about the concepts and can be added to the nodes in the path. By the way, computation would be more complex; the success of this hybrid approach also might give promising results.

## 6. Conclusion

This study uses WordNet as source and takes the Men's data to determine the weights of the WordNet relations. Basic mathematical and statistical operations are used to determine and generalize the relation weights. Using these relations weights, the relatedness of the two concepts defined in WordNet is measured. Relatedness score is produced between [0,1]. Evaluated using RG65 that is a widely used benchmark dataset for semantic relatedness, found Spearman Correlation value is 0.81, in the literature, there are other methods outperforms this values. Most successful WordNet-based method's correlation value is 0.86 (Pilehvar and Navigli, 2015). By improving this method using some other features of WordNet's graph structure, this method might be improved and might generate more successful correlation values. It is a new approach for weighting all relation types instead of grouping or categorizing the relations. This study is measuring relatedness for two lexical items in any relation type in WordNet since most of the relatedness study uses limited relation types; this is the advantage of the study. Since most of the studies measure the relatedness of noun pairs, this study measures the lexical items without part of speech information; this is also another positive part of the study.

## Acknowledgment

This study is a part of the research programme with project number 212E526, which is financed by the Scientific and Technological Research Council of Turkey (TUBITAK).

**Table 6.** Relation type, relation code, and determined relation weight in each step

| Relation Type | Rel. Code | Determined Weight | |
|---|---|---|---|
| | | Step1 | Step2 |
| Antonym | a | 0.7 | 0.7 |
| Hypernym | b | 0.8 | 0.82 |
| Hyponym | c | 0.76 | 0.76 |
| Instance_Hypernym | d | 1.39 | 1.36 |
| Instance_Hyponym | e | 0.85 | 0.85 |
| Member_Holonym | f | 0.97 | 1.14 |
| Member_Meronym | g | 1.05 | 0.85 |
| Substance_Holonym | h | 1.07 | 1.1 |
| Substance_Meronym | i | 0.99 | 0.85 |
| Part_Holonym | j | 0.83 | 0.84 |
| Part_meronym | k | 0.78 | 0.8 |
| Attribute | l | 0.95 | 0.98 |
| Derivationally_related_form | m | 0.84 | 0.86 |
| Domain_of_synset_TOPIC | n | 0.90 | 1.02 |
| Domain_of_synset_REGION | p | 0.75 | 0.9 |
| Member_of_this_domain_REGION | q | 0.85 | 0.85 |
| Domain_of_synset_USAGE | r | 0.77 | 0.86 |
| Member_of_this_domain_USAGE | s | 0.85 | 0.85 |
| Entailment | t | 0.79 | 0.79 |
| Cause | u | 0.78 | 0.72 |
| Also_see | v | 0.82 | 0.95 |
| Verb_Group | x | 1.16 | 1.12 |
| Similar_to | w | 0.88 | 0.89 |
| Participle_of_verb | y | 1.44 | 0.85 |
| Pertainym | z | 1.48 | 1.30 |
| No_Path_Determined* | % | 0.21 | 0.21 |
| Synonym* | & | 0.84 | 0.79 |
| PertainedBy* | ! | 0.85 | 0.85 |

*This relation types are not given in WordNet 3.0, it is created by the algorithm.

**Table 7.** RG65 benchmark dataset and determined score by a proposed algorithm using relatedness weight determined in the first step with a mean of the path length values (Spearman rank correlation is 0.81).

| Word1 | Word2 | Rel Scr RG65 | Rel. Score By Our Method |
|---|---|---|---|
| cord | smile | 0.01 | 0.28 |
| rooster | voyage | 0.01 | 0.14 |
| noon | string | 0.01 | 0.25 |
| fruit | furnace | 0.01 | 0.26 |
| autograph | shore | 0.02 | 0.21 |
| automobile | wizard | 0.03 | 0.36 |
| mound | stove | 0.04 | 0.28 |
| grin | implement | 0.05 | 0.29 |
| asylum | fruit | 0.05 | 0.27 |
| asylum | monk | 0.10 | 0.24 |
| graveyard | madhouse | 0.11 | 0.16 |
| glass | magician | 0.11 | 0.30 |
| boy | rooster | 0.11 | 0.20 |
| cushion | jewel | 0.11 | 0.37 |
| monk | slave | 0.14 | 0.52 |
| asylum | cemetery | 0.20 | 0.24 |
| coast | forest | 0.21 | 0.46 |
| grin | lad | 0.22 | 0.35 |
| shore | woodland | 0.23 | 0.61 |
| monk | oracle | 0.23 | 0.34 |
| boy | sage | 0.24 | 0.25 |
| automobile | cushion | 0.24 | 0.62 |
| mound | shore | 0.24 | 0.41 |
| lad | wizard | 0.25 | 0.34 |
| forest | graveyard | 0.25 | 0.28 |
| food | rooster | 0.27 | 0.20 |
| cemetery | woodland | 0.30 | 0.30 |
| shore | voyage | 0.31 | 0.31 |
| bird | woodland | 0.31 | 0.33 |
| coast | hill | 0.32 | 0.48 |
| furnace | implement | 0.34 | 0.23 |
| crane | rooster | 0.35 | 0.30 |
| hill | woodland | 0.37 | 0.61 |
| car | journey | 0.39 | 0.43 |
| cemetery | mound | 0.42 | 0.34 |
| glass | jewel | 0.45 | 0.26 |
| magician | oracle | 0.46 | 0.59 |
| crane | implement | 0.59 | 0.35 |
| brother | lad | 0.60 | 0.33 |
| sage | wizard | 0.62 | 0.30 |
| oracle | sage | 0.65 | 0.39 |
| bird | crane | 0.66 | 0.57 |
| bird | cock | 0.66 | 0.76 |
| food | fruit | 0.67 | 0.41 |
| brother | monk | 0.69 | 0.62 |
| asylum | madhouse | 0.76 | 0.76 |
| furnace | stove | 0.78 | 0.65 |
| magician | wizard | 0.80 | 0.79 |
| hill | mound | 0.82 | 0.81 |
| cord | string | 0.85 | 0.75 |
| glass | tumbler | 0.86 | 0.76 |
| grin | smile | 0.87 | 0.79 |

**References**


Aguirre, E. and Soroa, A., 2009. Personalizing PageRank for Word Sense Disambiguation. Proceedings of the 12th conference of the European chapter of the Association for Computational Linguistics, March 2009, Athens, Greece, p. 34-41.

Ahsan, M.G., Naghibzadeh, M. and Naeini, S.E.Y., 2014. Semantic similarity assessment of words using weighted WordNet, Int. J. Mach. Learn. & Cyber, 5 (3), 479-490, https://doi.org/10.1007/s13042-012-0135-3.

Brin, S. and Page, L., 1998. The anatomy of a large-scale hypertextual web search engine. Computer Networks and ISDN Systems 30, 107-117.

Bruni, E., Tran, N. K. and Baroni, M., 2014. Multimodal Distributional Semantics. Journal of Artificial Intelligence Research, 49, 1-47, https://doi.org/10.1613/jair.413.

Fellbaum, C., 1998. WordNet: An Electronic Lexical Database. Cambridge, MA: MIT Press, 422p.

Finkelstein, L., Gabrilovich, E., Matia,S., Y., Rivlin, E., Solan, Z., Wolfman, G. and Ruppin, E., 2001. Placing search in context: The concept revisited. In WWW '01: Proceedings of the 10th international conference on World Wide Web, May 2001, Hong Hong, p. 406–414.

Hirst, G. and St-Onge, D, 1998, Lexical chains as representations of context for the detection and correction of malapropisms, in WordNet: An Electronic Lexical Database, MITP, p. 305–332.

Hughes, T. and Ramage, D., 2007. Lexical semantic relatedness with random graph walks. Proceedings of the Joint Conference on Empirical Methods in Natural Language Processing and Computational Natural Language Learning, EMNLP–CoNLL, June 2007, Prague, Czech Republic, p.581–589.

Kartsaklis D., Pilehvar M.T. and Collier N., 2018. Mapping Text to Knowledge Graph Entities using Multi-Sense LSTMs. EMNLP, Oct. 2018, Brussels, Belgium.

Li, Y., Zuhair, A. B. and McLean, D., 2003. An approach for measuring semantic similarity between words using multiple information sources, IEEE Trans. Knowledge and Data Eng., 15 (4), 871-882.

Meng, L., Gu, J. and Zhou, Z., 2012. A New Hybrid Semantic Similarity Measure Based on WordNet. In: Lei J., Wang F.L., Li M., Luo Y. (eds) Network Computing and Information Security. Communications in Computer and Information Science. 345, 739-744. https://doi.org/10.1007/978-3-642-35211-9_93.

Miller, G. A. and Charles, W. G., 1991. Contextual Correlates of Semantic Similarity. Language and Cognitive Processes, 6 (1), 1-28.

Mikolov T., Chen K., Corrado G. and Dean J., 2013. Efficient estimation of word representations in vector space. CoRR, abs/1301.3781.

Navigli R. and Ponzetto S., 2012. BabelNet: The Automatic Construction, Evaluation, and Application of a Wide-Coverage Multilingual Semantic Network. Artificial Intelligence, 193, P. 217-250.

Pennington J., Socher R. and Christopher D.M., 2014. GloVe: Global vectors for word representation. Proceedings of the Empiricial Methods in Natural Language Processing (EMNLP 2014), October 2014, Doha, Qatar, 12, 1532–1543.

Pilehvar, M. T. and Navigli, R., 2015. From Senses to Texts: An All-in-one Graph-based Approach for Measuring Semantic Similarity. Artificial Intelligence, 228, 95-128.

Rubenstein, H. and Goodenough, J.B., 1965. Contextual correlates of synonymy, Communications of the ACM, 8 (10), 627–633

Siblini, R. And Kosseim, L., 2013. Using a Weighted Semantic Network for Lexical Semantic Relatedness. Proceedings of Recent Advances in Natural Language Processing, Sept 2013, Hissar, Bulgaria, p.610-618

Speer R. and Chin J., 2016. An ensemble method to produce high-quality word embeddings. arXiv preprint arXiv:1604.01692

Speer, R. and Havasi C., 2012. Representing General Relational Knowledge in ConceptNet 5,. Proc. of LREC, May 2012, Istanbul Turkey, p. 3679-3686.

Sultan, A.M., Bethard, S. and Sumner, T., 2014. Back to basics for monolingual alignment: exploiting word similarity and contextual evidence, Trans. Assoc. Comput. Linguist., 2 (1), 219–230.

Wu, Z. and Palmer, M., 1994. Verb semantics and lexical selection. the 32nd Annual Meeting of the Association for Computational Linguistics, June 1994, New Mexico USA, p.133–138.

Yang, D. and Powers, M.V., 2005. Measuring semantic similarity in the taxonomy of WordNet. Proceeding of the 28th Australasian Computer Science Conference, Jan 2005, Newcastle, Australia, p. 315-332.

**GÜFBED/*GUSTIJ* (2018) CMES 2018 SEMPOZYUM EK SAYISI: 79-93**
DOI: 10.17714/gumusfenbil.428731 Araştırma Makalesi / *Research Article*

# Sandviç Kompozit Tabakalarında Mekanik Gerilmelerin Basınca Bağlı Olarak Ansys Yazılımı İle İncelenmesi

## *Investigation Of Mechanical Stresses On Sandwich Composite Layers According To The Pressure By Making Use Of Ansys Software*

**Kürşat KAYMAZ[1,a], Bilgin ZENGİN[*2,b], Muzaffer AŞKIN[2,c], Semih TAŞKAYA[3,d]**

[1]*İnşaat Mühendisliği Bölümü, Mühendislik Fakültesi, Üniversitesi Munzur, Tunceli*
[2]*Elektrik ve Elektronik Mühendisliği Bölümü, Mühendislik Fakültesi, Üniversitesi Munzur, Tunceli*
[3]*Metalurji ve Malzeme Mühendisliği Bölümü, Teknoloji Fakültesi, Üniversitesi Fırat, Elazığ*

• Geliş tarihi / *Received*: 30.05.2018 • Düzeltilerek geliş tarihi / *Received in revised form*: 15.10.2018 • Kabul tarihi / *Accepted*: 06.11.2018

***Öz***

Bu çalışmada; Ansys paket programında, 3 ara tabakadan oluşan, düz ve $7^0$'lik oryantasyon açısına sahip radyal geometrili 2 farklı model, x, y, z koordinat ölçülerine göre 3 boyutlu olarak tasarlanmıştır. Düz ve radyal geometriye sahip sandviç tabakaların 2 farklı testte, sağ ve sol mesnetlerden ankastre ve çizgisel olarak sabitlenerek 4 MPa basınç altında eksenlere göre mekanik gerilim analizleri yapılmıştır. Geometrik şekilleri aynı-mesnetleri farklı ve geometrik şekilleri farklı-mesnetleri aynı yapılar karşılaştırılarak incelenmiştir. Geometrik şekilleri aynı-mesnetleri farklı gerilim sonuçlarında, düz ankastreli mesnetin çekme oranlarının çizgisel mesnete göre artış gösterdiği ve sıkıştırma oranlarının ise azalış gösterdiği görülmüştür. Radyal ankastreli mesnetin çekme oranlarının çizgisel mesnete göre azalış gösterdiği ve sıkıştırma oranlarının ise x ekseninde arttığı, y ve z eksenlerinde azaldığı görülmüştür. Geometrik şekilleri farklı-mesnetleri aynı gerilim sonuçlarında ise, radyal ankastreli mesnetin düz mesnete göre hem çekme ve hem de sıkıştırma oranlarının y ekseninde arttığı, x ve z ekseninde azaldığı görülmüştür. Radyal çizgisel mesnetin düz mesnete göre, x ekseninde çekme ve sıkıştırma oranlarının azaldığı, y ekseninde arttığı, z ekseninde ise çekme oranının arttığı sıkıştırma oranının azaldığı görülmüştür.

**Keywords**: Ansys, Düz ve Radyal Tabaka, Mekanik Gerilim, Sandviç Kompozit.

**Abstract**

*In this study, in Ansys package program 2 different models of 3 intermediate layers, with a straight and 7° orientation angle, are designed as 3 dimensional according to x, y, z coordinate measurements. Sandwich plates with smooth and radial geometries were fixed in two different tests from their right and left supports, linearly and mechanical stresses were analyzed according to axes under 4 MPa pressure. Here, we mainly analysed two different structures by comparing features according to the cases that having same shape-different supports and different shapes-same support. It has been investigated that the compression ratios of straight anchorage support increase linearly as a function of linear meshes in the same geometry but different support stresses. The radial anchorage support draw ratio decreases with linear supports while the compression ratios increase with x axis and decrease with y and z axes. On the other hand, it is concluded that radial anchorage ratio for the structures having different shapes and same type supports increases in x axis and decreases in both y and z. Moreover, one can see that radial linear support has lower draw and compression ratios on the x axis, and also the quantity increases on the y axis while the compression ratio decreases on the z axis.*

***Anahtar kelimeler:*** *Ansys, Flat and Radial Layer, Mechanical Tension, Sandwich Composite.*

[*b] Bilgin ZENGİN; bilginzengin@munzur.edu.tr ; Tel 0 (428) 213 17 94; orcid.org/0000-0002-9355-8294
[a] orcid.org/0000-0002-8346-8260 [c] orcid.org/0000-0001-9172-6592 [d] orcid.org/0000-0003-1524-4537

## 1. Giriş

Son yıllarda azaltılmış ağırlık ve daha iyi mekanik performans ile karakterize edilen yapıları keşfetmeye yönelik artan çabalar, esas olarak kara ve deniz taşımacılığında sandviç yapıların geliştirilmesine ve istihdam edilmesine yol açmıştır (Atckinson, 1997). Yapısal bir sandviç, tek bir özelliği ile küresel yapı performansında işbirliği yapmak için bir araya getirilmiş farklı malzemelerin bir kombinasyonu ile karakterize edilen özel bir katmanlı kompozit tipidir. Bu yapıların tasarlanmasında ve doğrulanmasında asıl sorun, doğru modellemelerine izin vermeyen kendi içsel anizotropi ve homojen olmayan olmalarıdır. Günümüzde, doğru ve güvenilir bir tasarıma izin vermek için gerekli olan karmaşık yapıların mekanik özellikleri hakkındaki mevcut veriler yeterli değildir (Manning vd., 1993; Bannister vd., 1999). Sandviç yapıları, ağırlıkla ilişkili olarak önemli ölçüde sertlik ve yüksek mukavemet oranı gösteren hafif malzemelerdir. Sandviç panelin ana konsepti, dış yüzeylerin, bükülme (bükülme yükü ve sıkıştırma) nedeniyle oluşan yükleri transfer etmesidir. Buna göre, makroskopik olarak tarif edilen sandviç panelin çalışma modu, I-kiriş tarafından gerçekleştirilen görevlerle doğru bir şekilde karşılaştırılabilir (Muc vd., 2005; Ochelski vd., 2007; Campbell, 2010). Ganapathi vd. (2004) bu öğeyi, termal / mekanik yüklere maruz kalın lamine kompozit ve sandviç plakaların doğrusal olmayan dinamik analizini gerçekleştirmek için kullanmışlardır. Tawfik vd. (2002), aerodinamik ve termal yüklere maruz kalan gömülü şekil hafızalı alaşım ile izotropik panelin termal post-burkulması ve aeroelastik davranışlarını incelemek için von Karman gerilme-yer değiştirme ilişkilerine dayanan doğrusal olmayan sonlu elemanlar modelini kullanmışlardır. Natarajan vd. (2014), nem konsantrasyonu ve termal gradyanın, lamine kompozit plakaların serbest titreşim ve burkulma özelliklerine etkisini incelemek için birinci mertebe kesme deformasyon teorisine dayanan uzatılmış sonlu elemanlar yöntemini kullanmışlardır. Park vd. (2004), termal yüklere maruz kalan şekil hafızalı alaşım lifleri ile gömülmüş lamine kompozit plakalar için lineer olmayan sonlu eleman denklemlerini formüle etmek için birinci sıra kesme deformasyon teorisini kullanmış ve önceden bükülmüş ve post-toklaştırılmış bölgelerdeki plakaların titreşim karakteristiklerini araştırmışlardır. Vangipuram ve Ganesan (2007), termal yükler altında sıcaklığa bağlı viskoelastik çekirdek ile dikdörtgen kompozit viskoelastik sandviç plakaların serbest titreşim ve sönümleme özelliklerini incelemek için sonlu elemanlar yöntemini kullanmışlardır. Froud (1980), sandviç panellerin, avantajların ve göze çarpan özelliklerin temelini açıklamıştır. Ağırlık ve maliyet açısından optimum esneklik özelliklerini elde etmiştir. Ağırlık ve maliyet tasarrufu elde etmek için geometriyi seçerken tasarımcılar tarafından alınan güç, sertlik ve önlemlerin tasarım optimizasyonunun gerekliliğini vurgulamıştır. Panigrahi vd. (2007), FRP lamine kompozitlerin yapışkan lap makaslama birleştirmelerinde, delaminasyon hasar analizi üzerinde çalışmışlar ve yapışkan tabakadaki düzlem gerilimlerinden üç boyutlu sonlu eleman analizi gerçekleştirmişlerdir. Ara laminar kesme gerilmeleri ve delaminasyon mukavemetinin etkileri üzerinde durmuşlardır. Zhang (2013), deneysel alanda köpük çekirdekli sandviç panellerin, yarı statik üç noktalı eğilme hasar davranışı incelemişler ve sonra da FEM değerleri ile karşılaştırmışlardır. Çekirdek hasarı, yüz tabakası hasarı, arayüz hasarı, çekirdek çatlaması ve çekirdek kırma gibi bileşenlerde farklı hatalar, ABAQUS açık paketinin FEM simülasyonları ile açıklanmıştır. Swanson ve Kim (2003), CFRP kaplamaları ve köpük çekirdek sandviç yapılarının tasarımı üzerinde, deneysel ve FEM değerleri kullanarak bükülme etkisi ve sertlik gibi temas yükleri altında çalışmışlardır. Taşkaya (2017), St 37 levha çeliklerinde basınca bağlı levhaların mesnetlere göre tabakalarındaki mekanik gerilmelerin etkisini incelemiştir. Gür vd. (2017a), Ansys yazılımında farklı sıcaklık ve gerilme parametrelerinde Al malzemesi ile SİC metal matrisli kompozitin sürünme uzaması hareketi ile elastik gerilmeler arasındaki ilişkilendirmeleri araştırmışlardır. Taşkaya vd. (2018), Ansys yazılımında sonlu elemanlar yöntemine göre, St 70 çatı kafes çeliğinin St 37 çatı kafes çeliğine göre, kiriş eksenlerindeki hem kuvvet hem de moment etkisine göre deformasyon ve vektörel gerilmelerin arttığını gözlemlemişlerdir. Polat vd. (2017), elastik yarı sonsuz düzleme oturan ve rijit iki blok ile yüklenmiş fonsiyonel derecelendirilmiş sürekli temas probleminin sonlu elemanlar yöntemi ile analizini incelemişlerdir. Polat vd. (2018), elastik yarı sonsuz düzleme oturan ve rijit iki blok ile yüklenmiş homojen tabakada sürekli temas probleminin karşılaştırmalı analizini araştırmışlardır. Taşkaya (2018), izotropik bir çelik malzemeye sahip 3D kafes çatı modeline, farklı yük ve sabit basınç uygulayarak, kiriş eksenlerindeki, deformasyon, mekanik ve elastik gerilme analizlerini araştırmıştır. Gür vd. (2017b) izotropik bir çelik malzemeyi 3 boyutlu kafes çatı olarak tasarlayarak, sonlu elemanlar yöntemine göre farklı yükler doğrultusunda kiriş

eksenlerindeki mekanik gerilme etkilerini araştırmışlardır.

## 2. Materyal Ve Metot

### *2.1. Modelin Ankastre Mesnet Olarak Tanımlanmnası*

İlk adım olarak düz ankastre mesnetli sandviç kompozit malzemeyi Ansys 12.0 paket programına mekanik analiz yapılacağı için "structural"(yapı) olarak tanımlanır. Kompozit malzeme için element seçimi yapılır. Katı model çalışılacağı için Ansys programından "solid layered 46" elementi seçilir. Sonraki adım olarak sandviç kompozit malzemenin Tablo1'de gösterilen üst tabaka, alt tabaka ve çekirdek (köpük) tabakasının reel sabit numarası, tabaka sayısı, oryantasyon açısı ve kalınlığı girilir.

**Tablo 1.** Sandviç kompozit tabakaların parametreleri

| Malzeme Bölümü | Reel Sabit Numarası | Tabaka Sayısı | Oryantasyon Açısı | Kalınlık |
|---|---|---|---|---|
| Üst Tabaka | 1 | 1 | 0 | 500 mm |
| Alt Tabaka | 2 | 1 | 0 | 500 mm |
| Çekirdek (köpük) | 3 | 1 | 0 | 500 mm |

Sandviç kompozit malzemenin üst tabaka, alt tabaka ve çekirdek tabakasının Tablo 2'deki mekanik özellikleri Ansys 12.0 paket programına tanımlanır. Üst tabaka ve alt tabakalar ortotopik bir malzeme olduğu için sisteme malzemenin mekanik özellikleri tanımlanır. Çekirdek (köpük) tabakası izotropik malzeme olduğu için izotropik mekanik özellikler tanımlanır.

**Tablo 2**. Sandviç kompozit tabakaların mekanik özellikleri

| Malzeme Bölümü | Ex (MPa) | Ey (MPa) | Ez (MPa) | Prxy | Pryz | Prxz | Gxy (MPa) | Gyz (MPa) | Gxz (MPa) |
|---|---|---|---|---|---|---|---|---|---|
| Üst Tabaka | 23200 | 9000 | 9000 | 0.4 | 0.2 | 0.4 | 4000 | 4000 | 4000 |
| Alt Tabaka | 19750 | 8500 | 8500 | 0.15 | 0.2 | 0.15 | 4500 | 4500 | 4500 |
| Çekirdek (köpük) | 300 | | | 0.38 | | | | | |

Sandviç kompozit tabakasının sınır ölçüleri Tablo 3'deki gibi sisteme girilerek model oluşturulur.

**Tablo 3.** Sandviç kompozit tabakanın model sınır ölçüleri

| Malzeme Bölümü | $X_1$ (mm) | $X_2$ (mm) | $Y_1$ (mm) | $Y_2$ (mm) | $Z_1$ (mm) | $Z_2$ (mm) |
|---|---|---|---|---|---|---|
| Üst Tabaka | 0 | 500 | 10 | 15 | -150 | 150 |
| Alt Tabaka | 0 | 500 | -12.9 | -15 | -150 | 150 |
| Çekirdek (köpük) | 0 | 500 | -12.9 | 10 | -150 | 150 |


**Şekil 1.** Sandviç kompozit tabakanın modellenmesi

Ansys yazılımında, modelin mekanik özelliklerini birbirine yapıştırma komutu olarak "Glue Volumes" modülü kullanılır. Sonraki işlem adımı olarak sistem başlangıcında Tablo 2'deki model parametrelerini üst tabaka, alt tabaka ve çekirdek tabakasını tek tek seçerek modele tanımlama işlemi yapılır.

### *2.2. Meshleme (Ağ örtüsü) İşlemi*

Sandviç kompozit malzeme modelinin ilk önce üst tabaka, sırasıyla alt tabaka ve çekirdek tabaka seçilerek mesh tanımlama işlemi yapılır ve ağ örtüsü sağlanmış olur. Buradaki amaç, mekanik simülasyon dağılımların birbirleriyle teması sağlanarak çözümleme yapılır.

### *2.3. Mesnetleme ve sandviç tabakaya basınç uygulama işlemi*

Sandviç kompozit modelin sağ ve sol mesnetlerden üst, alt ve çekirdek tabakanın tamamı seçilerek ankastre mesnetleme şeklinde model sabitlenir ve üst tabakadan 4 MPa basınç altında bir yük uygulanarak model çözümlendirilir (Şekil 3).

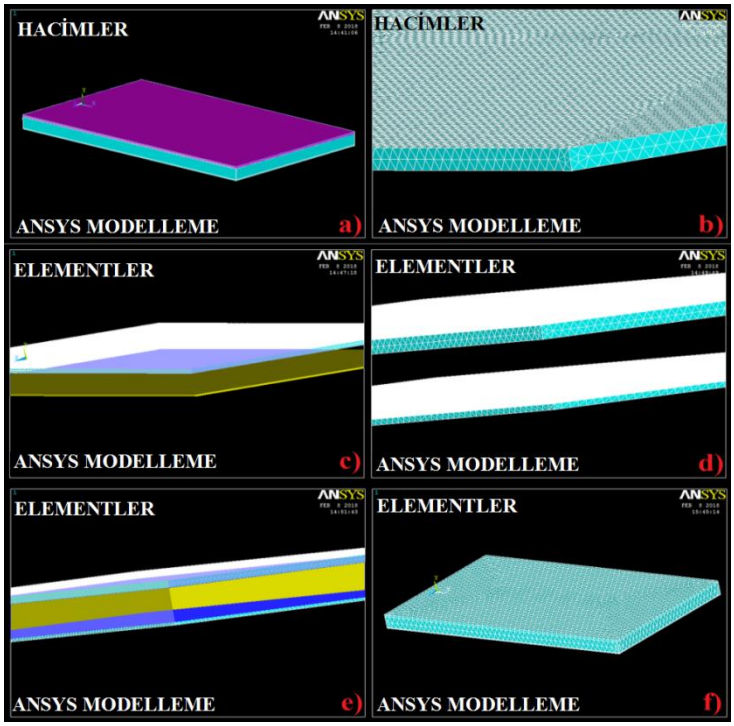


**Şekil 2.** Sandviç kompozit tabakanın meshleme aşamaları a) Üst tabakanın mesh ağının tanımlanması, b) Üst tabakanın mesh ağı, c) Alt tabakanın mesh ağının tanımlanması, d) Alt tabakanın mesh ağı, e) Çekirdek tabakasının mesh ağının tanımlanması ve f) Çekirdek tabakanın mesh ağı

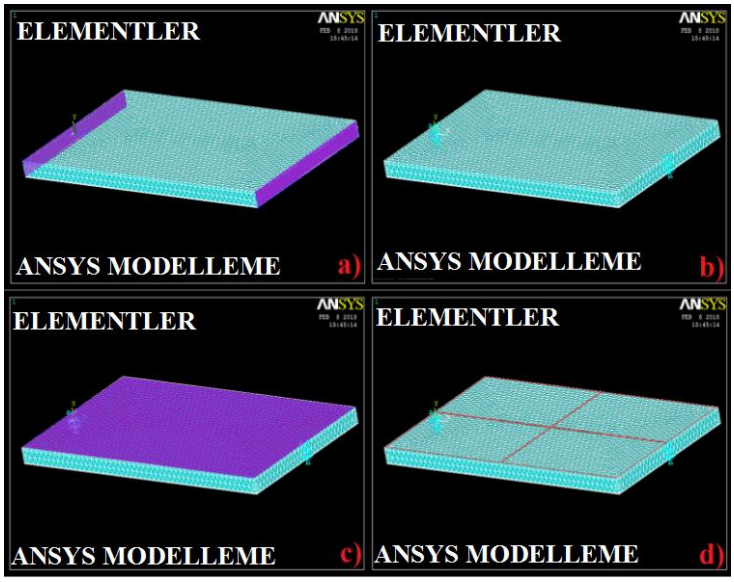


**Şekil 3.** Sandviç kompozit tabakanın a ve b) sağ ve sol mesnetlerden ankastre mesnet tanımlaması, c ve d) Üst tabakaya basınç uygulama işlemi

### *2.4. Modelin çizgisel mesnetlenmesi*

Sandviç kompozit modelin çizgisel olarak mesnetlenmesi işleminde düz ankastre modeldeki işlemlerin aynısı sırasıyla Ansys programına tanımlanır. Sadece model oluşturulduktan sonra mesnetleme işlemine gelindiğinde Şekil 4'de gösterildiği gibi sağ ve sol üst tabaka kenar çizgileri seçilerek model çizgisel olarak mesnetlenmiş olur ve üst plakaya aynı şekilde 4 MPa basınç uygulanarak çizgisel mesnetli model çözümlendirilir.

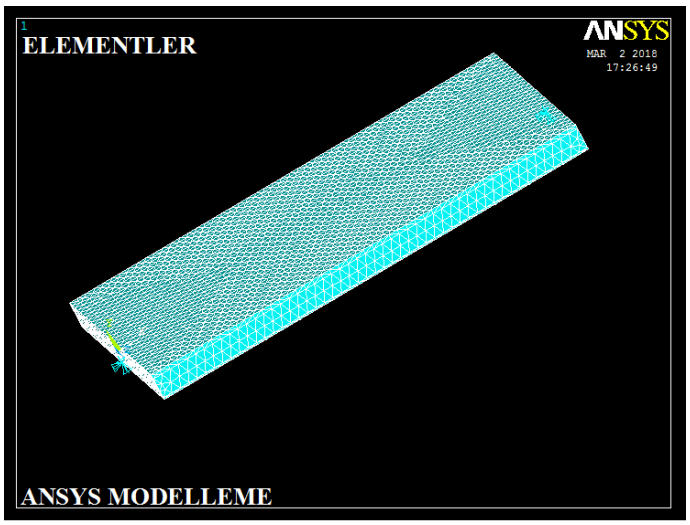


**Şekil 4.** Sandviç kompozit tabakanın çizgisel mesnetlenmesi

### *2.5. Sandviç kompozit tabakanın radyal modellenmesi ve meshleme işlemi*

Radyal ankastre mesnetli sandviç modelin oluşturulmasındaki işlemler düz ankastre mesnetli plakalı sandviç kompozit modelin aşamalarındaki gibi Tablo 1 ve Tablo 2 parametreleri ve mekanik özellikleri Ansys programına tanımlanır. Model oluşumunda sınır koşulları radyal model olduğu için belirlenen ölçüler doğrultusunda Tablo 4'e göre sisteme tanımlanır ve $7^0$'lik oryantasyon açısına sahip radyal model oluşturulur (Şekil 5). Daha sonra modele düz plakalı sandviç modelde olduğu gibi ayrı ayrı tabakalara ağ yapısı tanımlanarak meshleme işlemi yapılır (Şekil 6).

**Tablo 4.** Radyal tabakalı sandviç kompozit modelin sınır parametreleri

| Malzeme Bölümü | Dış yarıçap | İsteğe bağlı iç yarıçap | $Z_1$ koordinatı | $Z_2$ koordinatı | Başlangıç açısı | Bitiş açısı |
|---|---|---|---|---|---|---|
| **Üst Tabaka** | 4005 | 4000 | 0 | 500 | 0 | 7 |
| **Alt Tabaka** | 4030 | 4027.9 | 0 | 500 | 0 | 7 |
| **Çekirdek (köpük)** | 4027.9 | 4005 | 0 | 500 | 0 | 7 |

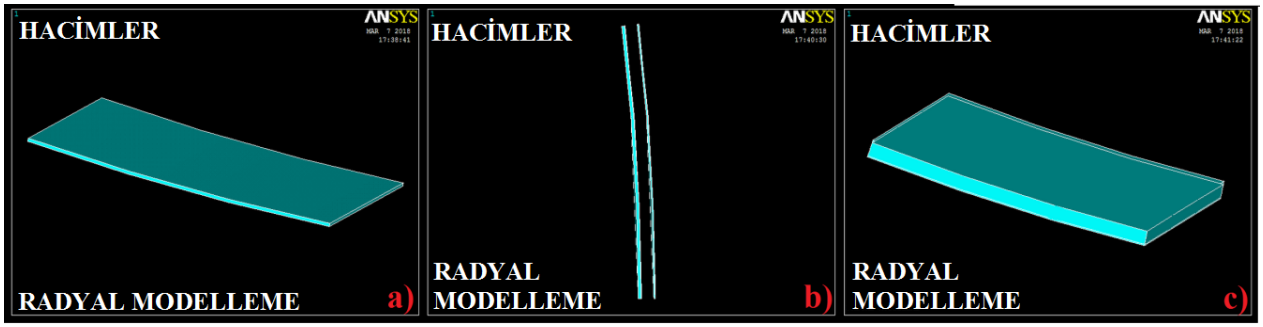


**Şekil 5.** Radyal tabakanın modellenmesi a) üst tabaka, b) alt tabaka ve c) çekirdek tabaka ve modelin bütün hali

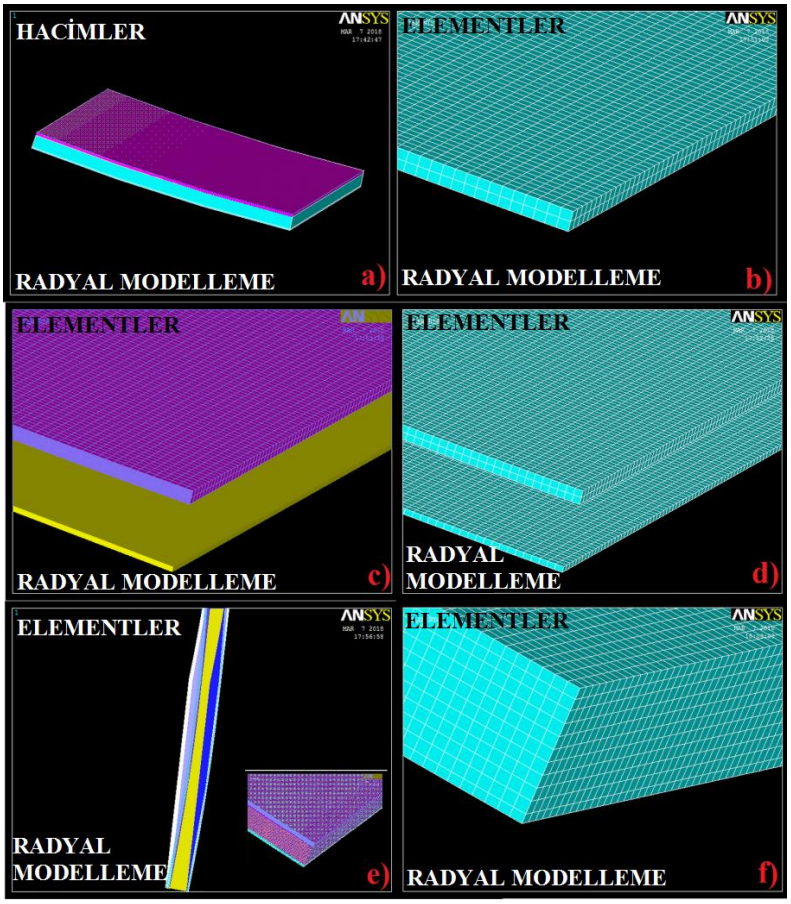


**Şekil 6.** Radyal tabakanın meshlenmesi a ve b) Üst radyal tabakanın mesh ağının tanımlanması ve mesh işlemi, c ve d) Alt radyal tabakanın mesh ağının tanımlanması ve mesh işlemi, e ve f) Çekirdek radyal tabakanın mesh ağının tanımlanması ve mesh işlemi, modelin bütün hali

### *2.6. Mesnetleme ve radyal sandviç tabakaya basınç uygulama işlemi*

Radyal sandviç kompozit modelin ankastre olarak mesnetlenmesi işleminde düz ankastre sandviç kompozit modeldeki işlemlerin aynısı sırasıyla Ansys programına tanımlanır. Model izotropik görünümden sağ ve sol üst, alt ve çekirdek tabakaların hepsi seçilerek ankastre mesnetlenmiş olur ve üst plakaya aynı şekilde 4 MPa basınç uygulanarak model çözümlendirilir (Şekil 7).

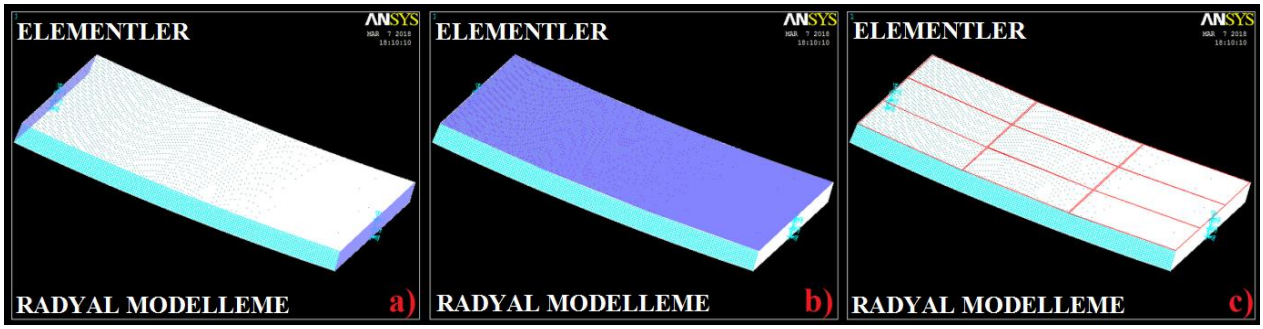


**Şekil 7.** Radyal sandviç tabakanın a) Sağ ve sol mesnetlerden ankastre mesnetlenmesi, b) Üst tabakaya basınç tanımlama ve c) Üst tabakaya basıncın uygulanması

### *2.7. Radyal modelin çizgisel mesnetlenmesi*

Radyal sandviç modelin çizgisel olarak mesnetlenmesi işleminde düz çizgisel modeldeki işlemlerin aynısı sırasıyla Ansys programına tanımlanır. Sadece model oluşturulduktan sonra mesnetleme işlemine gelindiğinde Şekil 8'de görüldüğü gibi sağ ve sol üst tabaka kenar çizgileri seçilerek model çizgisel olarak mesnetlenmiş olur ve üst plakaya aynı şekilde 4

MPa basınç uygulanarak çizgisel mesnetli model çözümlendirilir.

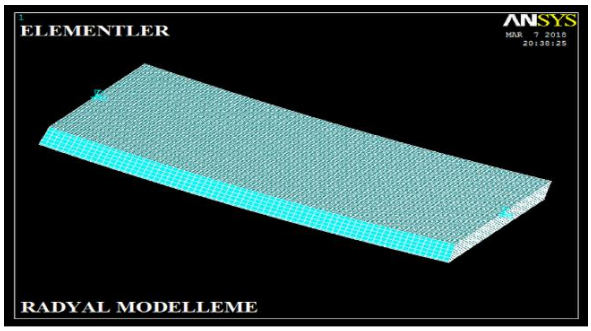


**Şekil 8.** Radyal sandviç kompozit tabakanın çizgisel mesnetlenmesi

## 3. Bulgular ve Tartışma

### *3.1. Düz ankastreli sandviç kompozitin çözümlenmesi*

Düz ankastreli sandviç kompozit tabakanın basınca bağlı olarak çözümlenmesi sonucunda 52891 eleman ve 10882 node (düğüm sayısı) sayısı oluşmuştur. Şekil 9'da sandviç tabakanın deformasyon şekil değişimi ve vektör analizi incelenmiştir. Şekil 10'da ise eksenlere bağlı stres gerilim analizleri yapılmıştır.

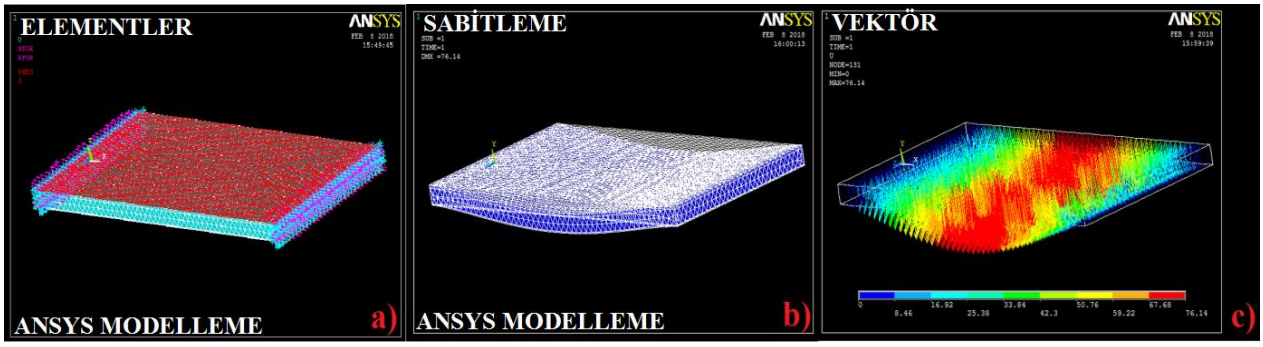


**Şekil 9.** Düz ankastreli sandviç kompozit tabakanın a) Modelin çözümlenmesi, b) Deformasyon şekil değişimi ve c) Bileşke vektör analizi

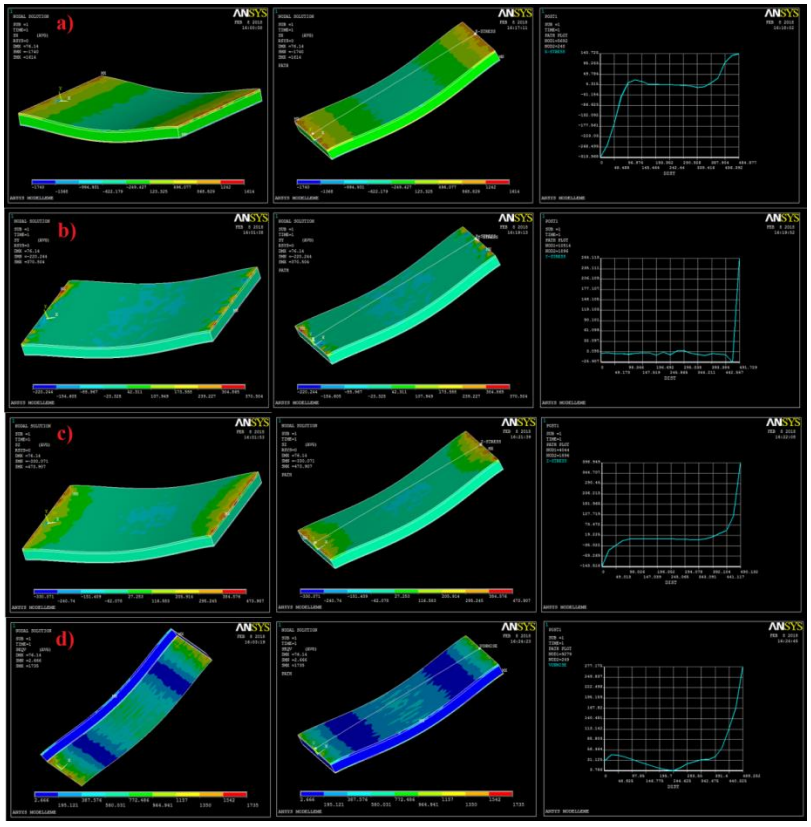


**Şekil 10.** Düz ankastreli sandviç kompozit tabakanın a) X eksenindeki stress gerilim analizi, b) Y eksenindeki stress gerilim analizi, c) Z eksenindeki stress gerilim analizi ve d) Von mises gerilim analizi

Şekil 11'de sandviç tabakada meydana gelen toplam mekanik gerilim dağılımları simulize edilmiştir. Burada meydana gelen gerilimler grafik analizlerle incelenmiştir.

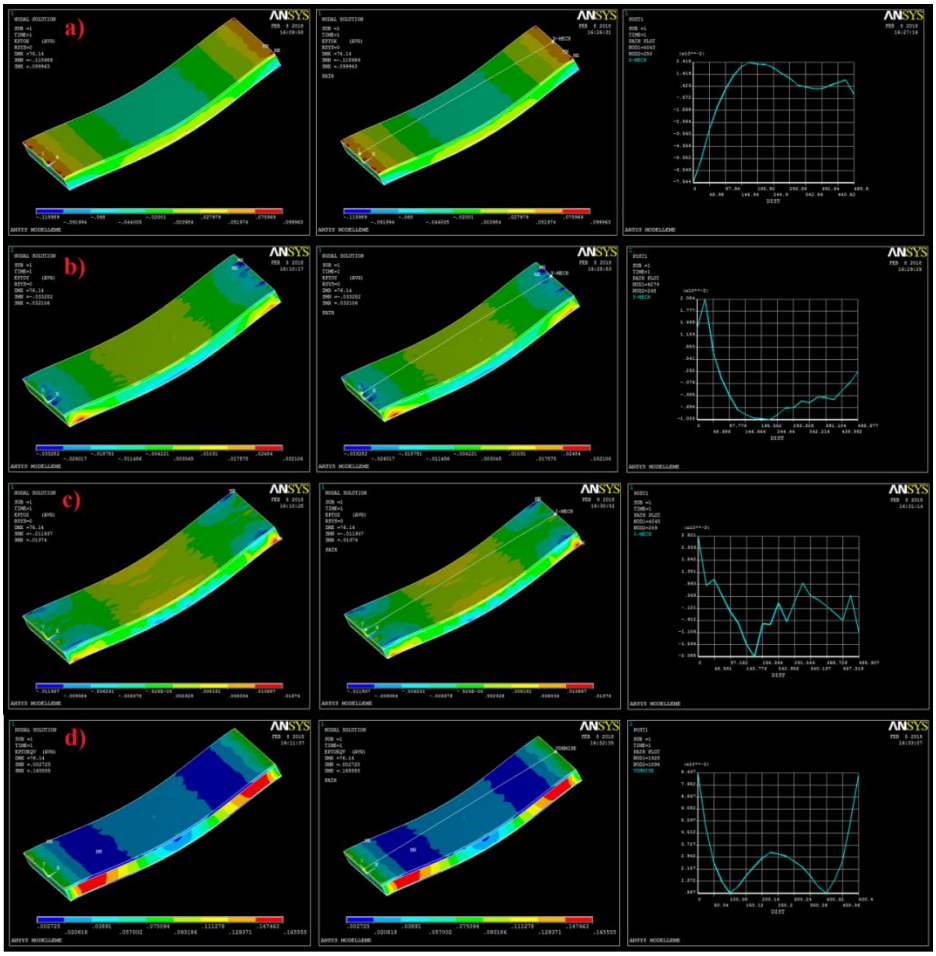


**Şekil 11.** Düz ankastreli sandviç kompozit tabakanın a) X eksenindeki toplam mekanik gerilim analizi, b) Y eksenindeki toplam mekanik gerilim analizi, c) Z eksenindeki toplam mekanik gerilim analizi ve d) Von mises toplam mekanik analizi

### *3.2. Düz çizgisel sandviç kompozitin çözümlenmesi*

Düz çizgisel sandviç kompozit tabakanın basınca bağlı olarak çözümlenmesi sonucunda Şekil 12'de sandviç tabakanın deformasyon şekil değişimi ve vektör analizi incelenmiştir. Şekil 13'de ise eksenlere bağlı stres gerilim analizleri yapılmıştır. Şekil 14'de sandviç tabakada meydana gelen toplam mekanik gerilim dağılımları simulize edilmiştir. Burada meydana gelen gerilimler grafik analizlerle incelenmiştir.

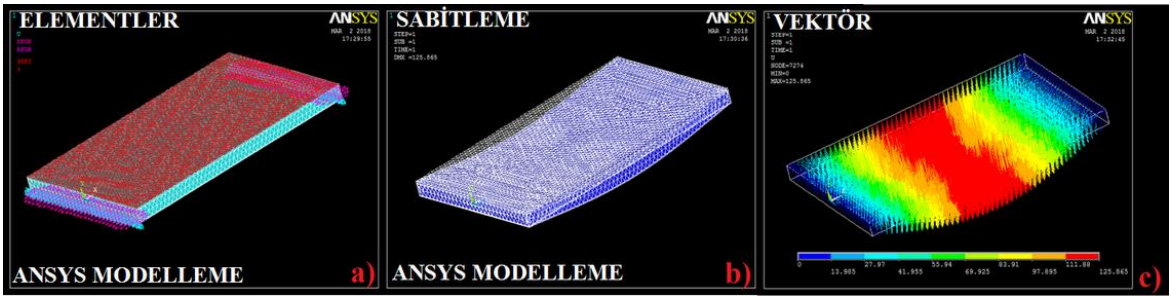


**Şekil 12.** Düz çizgisel sandviç kompozit tabakanın a) Modelin çözümlenmesi, b) Deformasyon şekil değişimi ve c) Bileşke vektör analizi

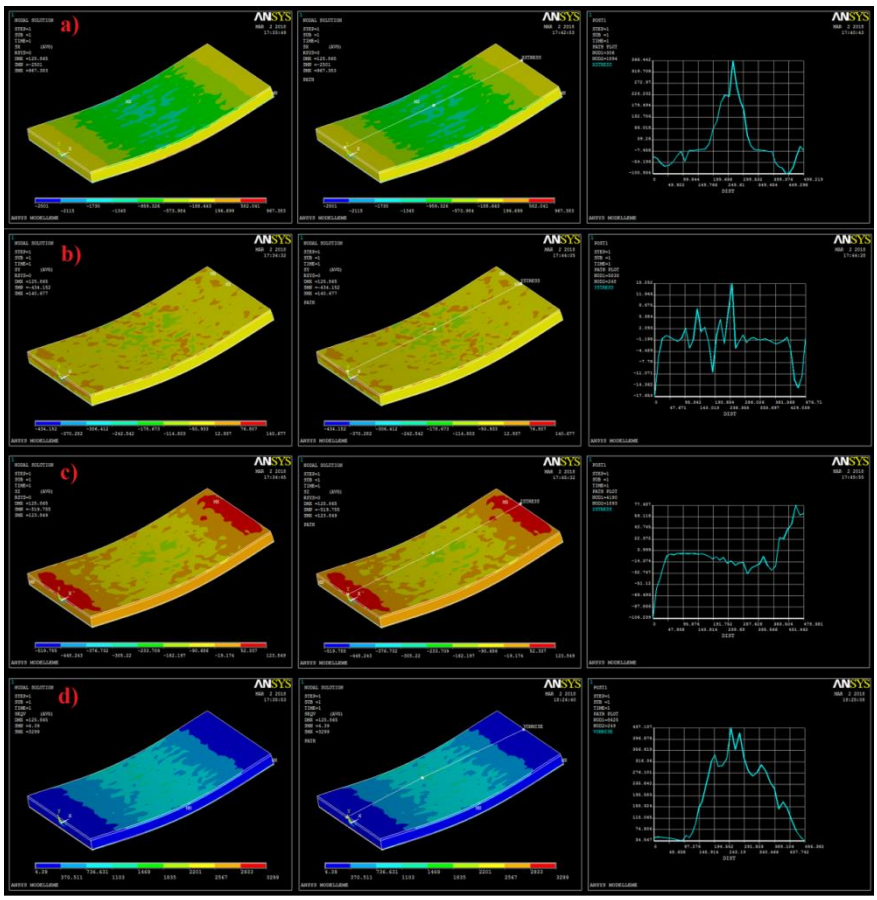


**Şekil 13.** Düz çizgisel sandviç kompozit tabakanın a) X eksenindeki stress gerilim analizi, b) Y eksenindeki stress gerilim analizi, c) Z eksenindeki stress gerilim analizi ve d) Von mises gerilim analizi

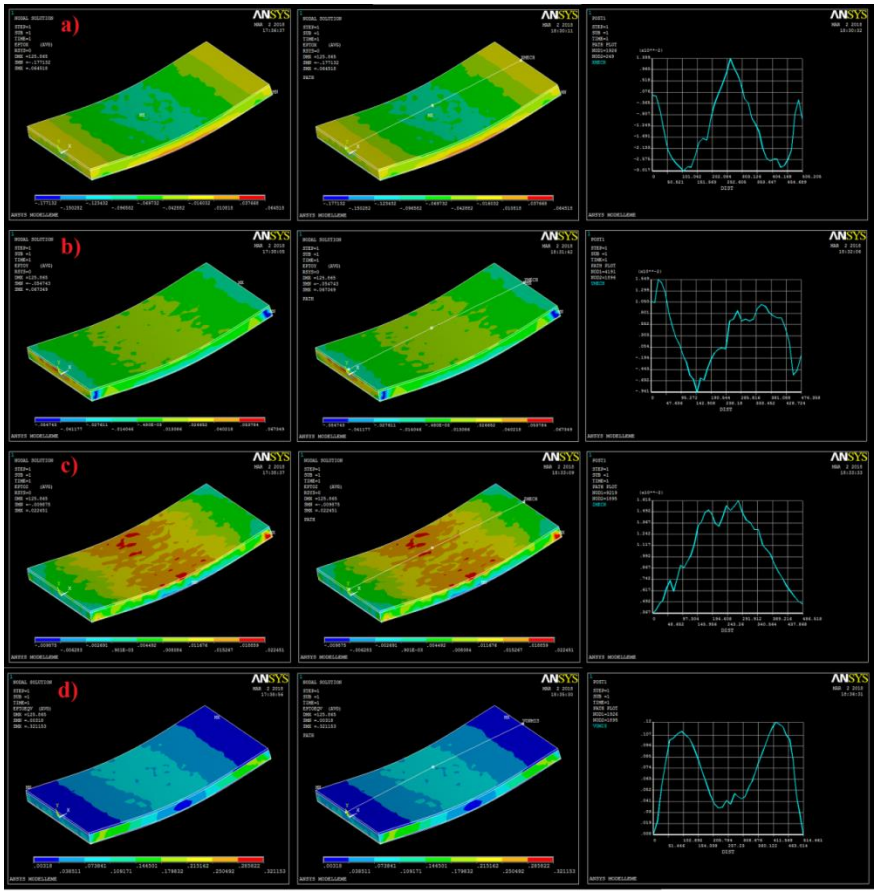


**Şekil 14.** Düz çizgisel sandviç kompozit tabakanın a) X eksenindeki toplam mekanik gerilim analizi, b) Y eksenindeki toplam mekanik gerilim analizi, c) Z eksenindeki toplam mekanik gerilim analizi ve d) Von mises toplam mekanik analizi

### *3.3. Radyal ankastre sandviç kompozitin çözümlenmesi*

Radyal ankastreli sandviç kompozit tabakanın basınca bağlı olarak çözümlenmesi sonucunda 30672 eleman ve 36792 node (düğüm sayısı) sayısı oluşmuştur. Şekil 15'de sandviç tabakanın deformasyon şekil değişimi ve vektör analizi incelenmiştir. Şekil 16'da ise eksenlere bağlı stres gerilim analizleri yapılmıştır.

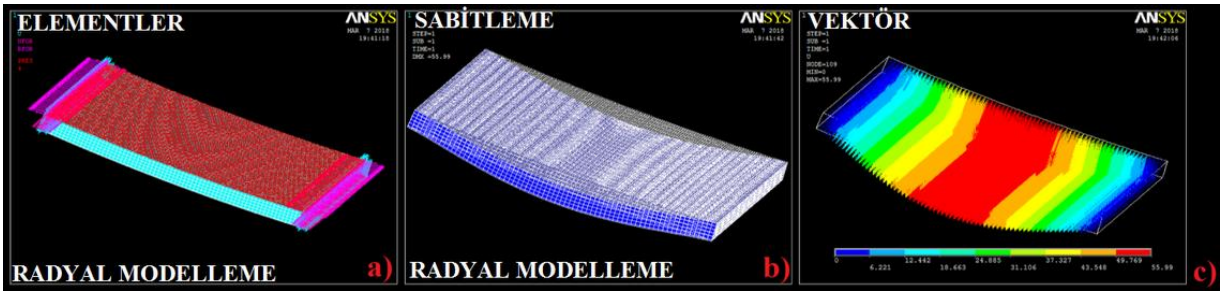


**Şekil 15.** Radyal ankastre sandviç kompozit tabakanın a) Modelin çözümlenmesi, b) Deformasyon şekil değişimi ve c) Bileşke vektör analizi

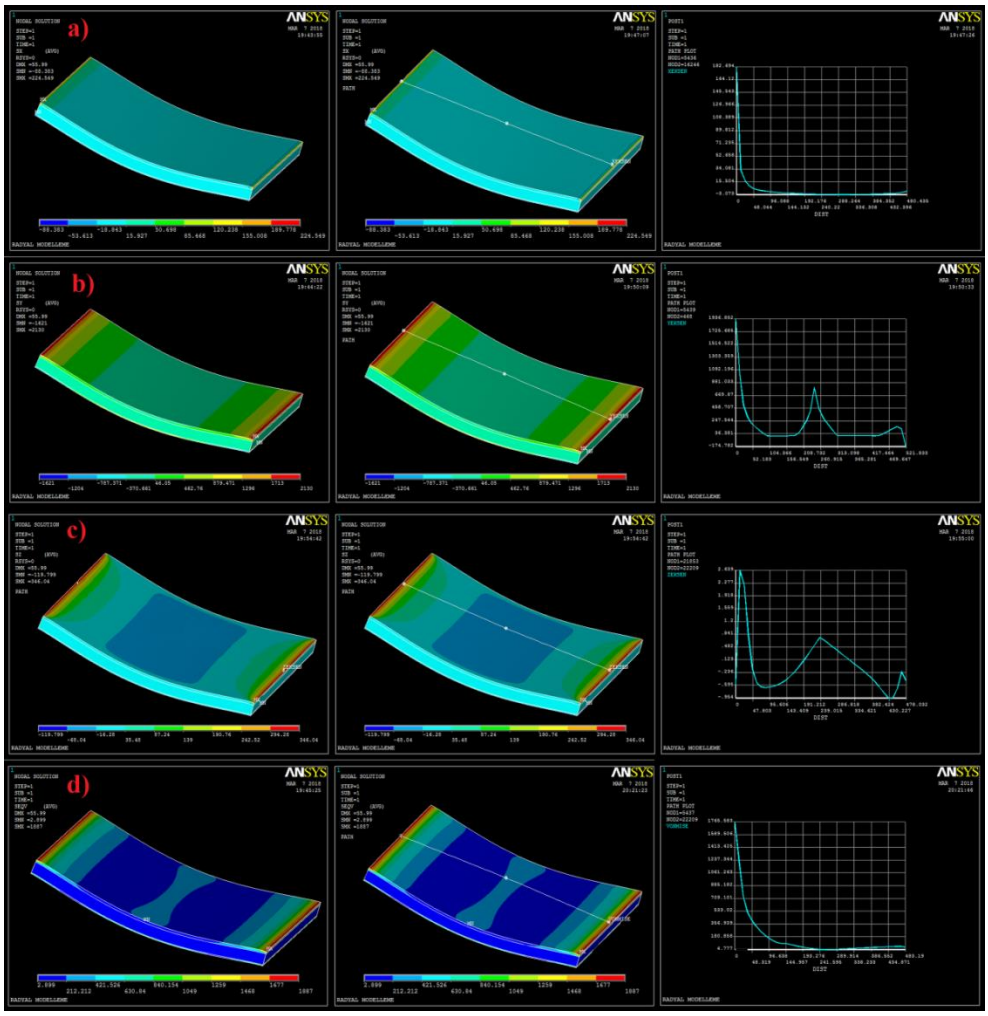


**Şekil 16.** Radyal ankastre sandviç kompozit tabakanın a) X eksenindeki stress gerilim analizi, b) Y eksenindeki stress gerilim analizi, c) Z eksenindeki stress gerilim analizi ve d) Von mises gerilim analizi

Şekil 17'de sandviç tabakada meydana gelen toplam mekanik gerilim dağılımları simulize edilmiştir. Burada meydana gelen gerilimler grafik analizlerle incelenmiştir.

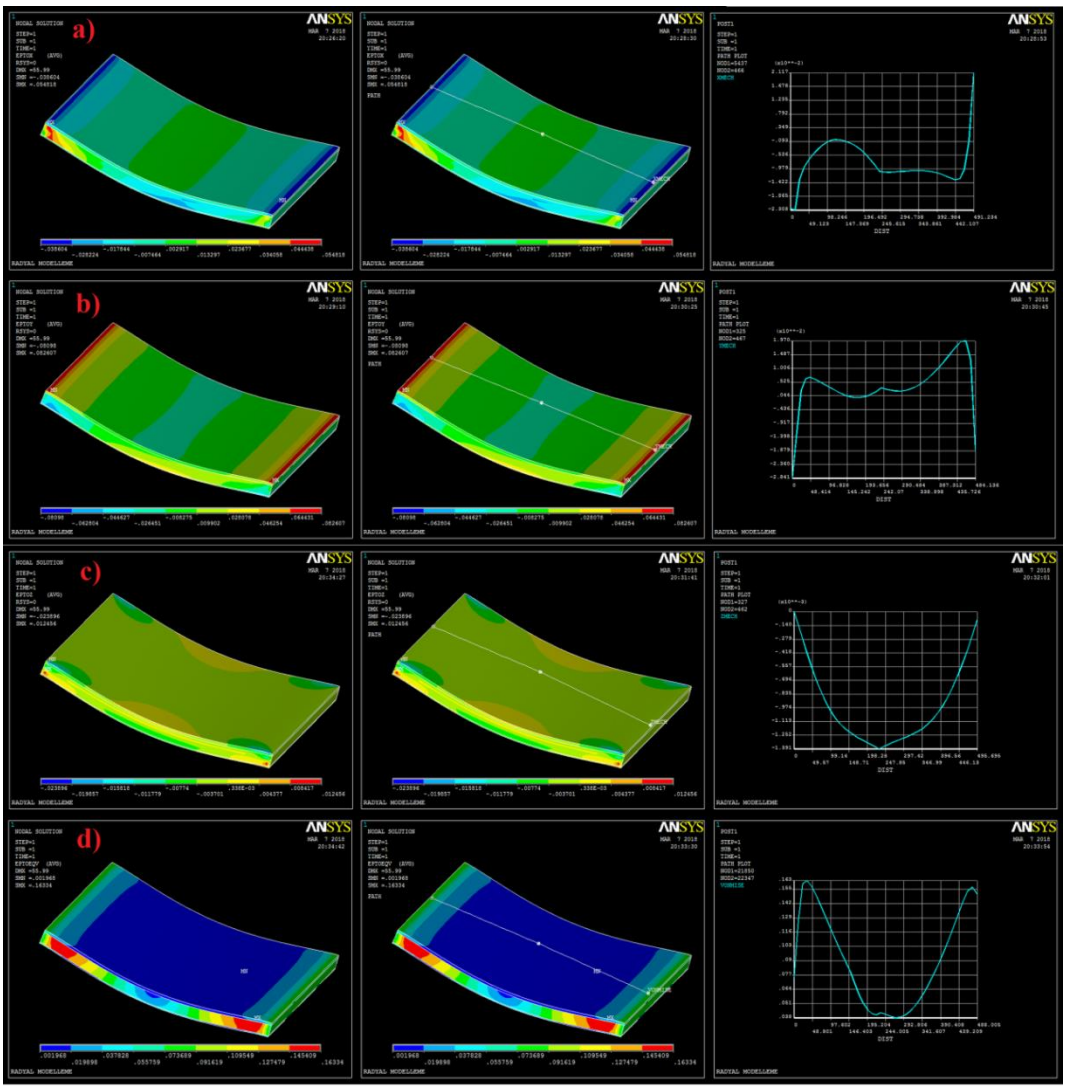


**Şekil 17.** Radyal ankastre sandviç kompozit tabakanın a) X eksenindeki toplam mekanik gerilim analizi, b) Y eksenindeki toplam mekanik gerilim analizi, c) Z eksenindeki toplam mekanik gerilim analizi ve d) Von mises toplam mekanik analizi

### *3.4. Radyal çizgisel sandviç kompozitin çözümlenmesi*

Radyal çizgisel sandviç kompozit tabakanın basınca bağlı olarak çözümlenmesi sonucunda Şekil 18'de sandviç tabakanın deformasyon şekil değişimi ve vektör analizi incelenmiştir. Şekil 19'da ise eksenlere bağlı stres gerilim analizleri yapılmıştır.

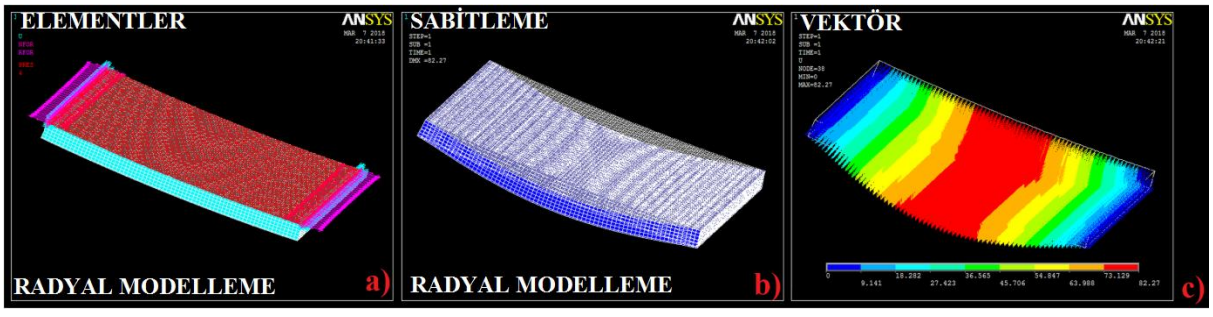


**Şekil 18.** Radyal çizgisel sandviç kompozit tabakanın a) Modelin çözümlenmesi, b) Deformasyon şekil değişimi ve c) Bileşke vektör analizi

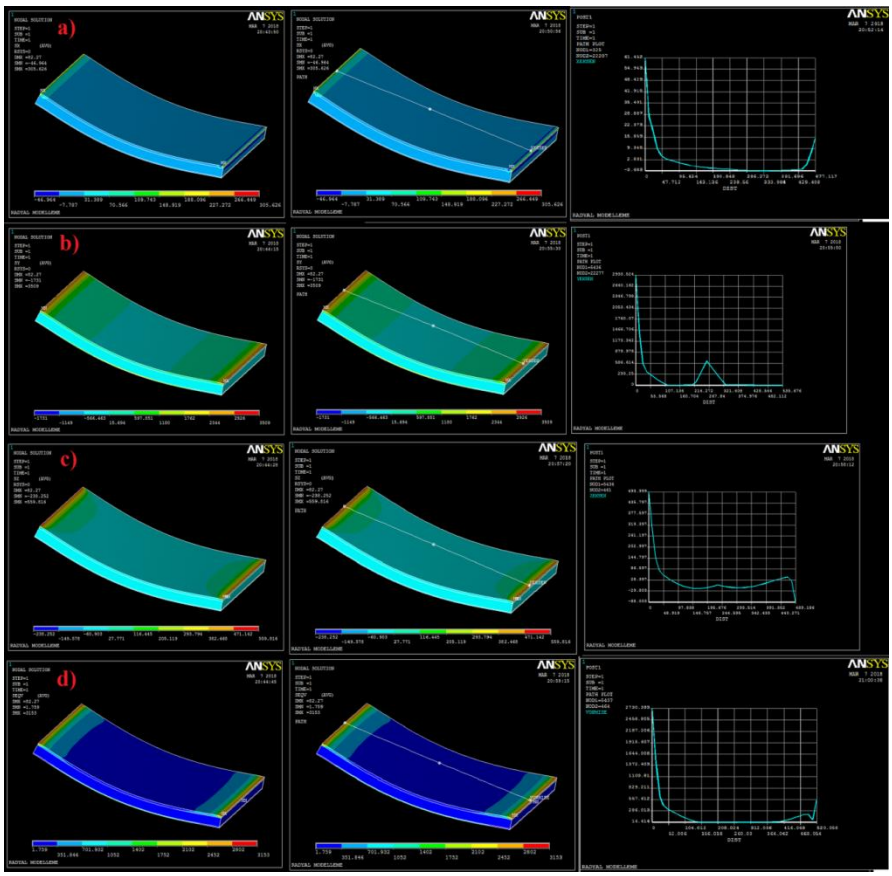

**Şekil 19.** Radyal çizgisel sandviç kompozit tabakanın a) X eksenindeki stress gerilim analizi, b) Y eksenindeki stress gerilim analizi, c) Z eksenindeki stress gerilim analizi ve d) Von mises gerilim analizi

Şekil 20'de sandviç tabakada meydana gelen toplam mekanik gerilim dağılımları simulize edilmiştir. Burada meydana gelen gerilimler grafik analizlerle incelenmiştir.

Tablo 5'de sandviç tabakalarda meydana gelen stres gerilim analizlerin simülasyon dağılım sonuçları verilmiştir.

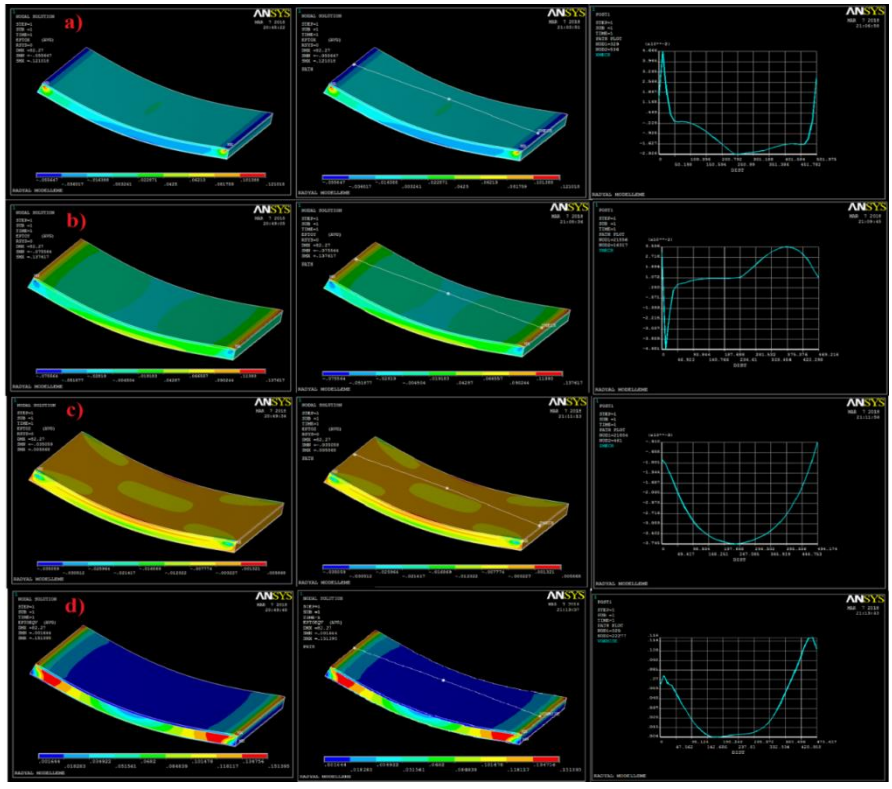

**Şekil 20.** Radyal çizgisel sandviç kompozit tabakanın a) X eksenindeki toplam mekanik gerilim analizi, b) Y eksenindeki toplam mekanik gerilim analizi, c) Z eksenindeki toplam mekanik gerilim analizi ve d) Von mises toplam mekanik analizi

## 4. Genel Sonuçlar ve Öneriler

Analiz sonuçları 2 şekilde kıyaslandığı zaman;

- Geometri şekilleri aynı, mesnetleri farklı stres gerilim skala sonuçlarında, düz ankastreli mesnetin çeki oranlarının çizgisel mesnete göre artış gösterdiği ve bası oranlarının ise azalış gösterdiği incelenmiştir. Radyal ankastreli mesnetin çeki oranlarının çizgisel mesnete göre azaldığı fakat bası oranlarının ise x ekseninde arttığı, y ve z eksenlerinde azaldığı görülmüştür.
- Geometri şekilleri farklı, mesnetleri aynı stres gerilim skala sonuçlarında ise, radyal ankastreli mesnetin düz mesnete göre hem çeki ve hem de bası oranlarının y ekseninde arttığı, x ve z ekseninde azaldığı görülmüştür. Radyal çizgisel mesnetin düz mesnete göre, x ekseninde çeki ve bası oranlarının azaldığı, y ekseninde arttığı, z ekseninde ise çeki oranının arttığı bası oranının azaldığı görülmüştür. Bu sandviç kompozit tabakalar arasındaki mesafeye bağlı mekanik grafiksel gerilimler üst, orta ve alt düğüm noktalarından alınmıştır. Hem stres hem de toplam mekanik mesafeye bağlı gerilim grafiksel sonuçlar kıyaslandığı zaman, sandviç kompozitlerin yapısı gereği gerilimlerin anizotropi (Manning vd., 1993; Bannister vd., 1999) yani değişik farklı yönlenmelerin olduğu artış ve azalış yani titreşimli gerilmeler gözlemlenmiştir.

Sandviç tabakaların mesafeye bağlı toplam mekanik gerilim skala sonuçları mukayese edildiği zaman;

Geometri şekilleri aynı, mesnetleri farklı toplam mekanik skala gerilim sonuçlarında, düz ankastreli mesnetin çizgisel mesnete göre x eksenindeki çeki oranının arttığı, y ve z eksenlerinde ise azaldığı, bası oranlarının x, y eksenlerinde azaldığı, z ekseninde ise arttığı gözlemlenmiştir. Radyal ankastreli mesnetin çeki oranlarının çizgisel mesnete göre x, y eksenlerinde azaldığı, z ekseninde ise arttığı, fakat bası oranlarının x, z eksenlerinde azaldığı, y ekseninde ise arttığı gözlemlenmiştir.

**Tablo 5.** Sandviç kompozit tabakaların stres simülasyon dağımların sonuçları

|  | **σx (MPa )** | **σy (MPa )** | **σz (MPa )** | **Von Mises Gerilme (MPa )** | **Vector analizi** |
|---|---|---|---|---|---|
| 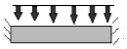 (Düz Tabaka, Ankastre Mesnet) | 1614 Mpa (Çeki)<br>1740 Mpa (Bası) | 370.504 Mpa (Çeki )<br>220.244 Mpa (Bası ) | 473.907 Mpa (Çeki )<br>330.071 Mpa (Bası ) | 1735 Mpa (Çeki)<br>2.666 Mpa (Bası) | 76.14 (çeki)<br>0<br>(bası) |
| 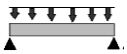 (Düz Tabaka, Çizgisel Mesnet) | 967.383 Mpa (Çeki)<br>2501 Mpa (Bası) | 140.677 Mpa (Çeki )<br>434.152 Mpa (Bası ) | 123.849 Mpa (Çeki )<br>519.755 Mpa (Bası ) | 3299 Mpa (Çeki)<br>4.39 Mpa (Bası) | 125.865 (çeki)<br>0<br>(bası) |
|  (Radyal Tabaka, Ankastre Mesnet) | 224.549 Mpa (Çeki)<br>88.383 Mpa (Bası) | 2130 Mpa (Çeki)<br>1621 Mpa (Bası) | 346.04 Mpa (Çeki )<br>119.799 Mpa (Bası ) | 1887 Mpa (Çeki)<br>2.899 Mpa (Bası) | 55.99 (çeki)<br>0<br>(bası) |
|  (Radyal Tabaka, Çizgisel Mesnet) | 305.626 Mpa (Çeki)<br>46.964 Mpa (Bası) | 3509 Mpa (Çeki)<br>1731 Mpa (Bası) | 559.816 Mpa (Çeki)<br>238.252 Mpa (Bası ) | 3153 Mpa (Çeki)<br>1.759 Mpa (Bası) | 82.27 (çeki)<br>0<br>(bası) |

- Geometri şekilleri farklı, mesnetleri aynı toplam mekanik skala gerilim sonuçlarında ise, radyal ankastreli mesnetin düz mesnete göre x, z eksenlerinde azaldığı, y ekseninde ise arttığı, bası oranlarının ise x ekseninde azaldığı, y, z eksenlerinde ise arttığı görülmüştür. Radyal çizgisel mesnetin düz mesnete göre, z ekseninde azaldığı, x, y eksenlerinde arttığı, bası oranlarının ise radyal ankastreli mesnetin düz mesnete göre bası oranlarıyla aynı sonuçlarda tespit edildiği yani x ekseninde azaldığı, y, z eksenlerinde ise arttığı görülmüştür. Bu sonuçlar, sandviç kompozit tabakaların konstrüktif açıdan iyi olduğunu göstermektedir. Farklı paket programları kullanarak (ABAQUS, Apex, Nastran gibi) benzer analizler yapılabilir ve birbirleriyle mukayese edilebilir (Taşkaya vd., 2018; Taşkaya, 2018).

- Farklı modelli geometriler, farklı alan ölçüleri, oryantasyon açıları, malzeme türü, farklı çekirdek tabakası, element türü, mesh türü, yük miktarı, mesnetleme şekli değiştirilerek çözüm yaptırılıp, malzemeler birbirleriyle kıyaslanabilinir. Uygulama alanındaki karmaşık geometriye sahip malzemeler, farklı sonlu elemanlar simülasyonlar programları sayesinde (ABAQUS, Apex, Nastran gibi) en basit hale dönüştürülerek prototipler oluşturulabilir ve sonuçları birbirleriyle karşılaştırılabilinir. Bu sayede basit geometrili modellerden birçok test analizleri (yapı, termal, titreşim, mekanik, statik, dinamik gibi) yapılabilir. Uygulama sanayisinde hafiflik ve rijitlik istenen (otomotiv, havacılık, uçak sanayi gibi) alanlarda kaplama malzemesi kullanılan bu modellemeler sandviç konstrüksiyon tekniği ile üretilip, bu gibi sonlu elemanlar simülasyon programları ile farklı tip analizler uygulanabilir (Taşkaya vd., 2018; Taşkaya, 2018).

## Teşekkür

Bu çalışmanın sadeleştirilmiş özet bildirimi 4-6/05/2018 tarihinde Girne, K.K.T.C.'de düzenlenen "3rd International Conference on Computational Mathematics and Engineering Sciences (CMES'2018)-(Turkish Republic of Northern Cyprus)" kongresinde sözlü sunum olarak sunulmuş olup, kongre üyelerine teşekkür ederiz.

## Kaynaklar

Atckinson, R., 1997. Innovative uses for sandwich constructions. Reinforced Plastics, 41(2), 30-33.

Bannister, M.K., Braemar, R. ve Crothers, I.P., 1999. The mechanical performance of 3D woven sandwich composites, Composite Structure, 47, 687-690.

Campbell, F.C., 2010. Structural Composite Materials: Novelty, Ohio, ASM International, 612p.

Froud, G.R., 1980. Your Sandwich order,Sir? Composites, 11(3), 133-138.

Ganapathi, M., Patel, B.P. ve Makhecha, D.P., 2004. Nonlinear dynamic analysis of thick composite/sandwich laminates using an accurate higher-order theory. Composites Part B: Engineering, 35, 345-355.

Gür, A.K., Taşkaya, S., Katı, N. ve Yıldız, T., 2017a. 3D Kafes çatı modelinin Ansys yöntemiyle mekanik gerilmelerinin incelenmesi, 2nd International Conference on Material Science and Technology in Cappadocia (IMSTEC'17), Ekim 2017 Nevşehir, Türkiye, s. 11-15.

Gür, A.K., Taşkaya, S., Yıldız, T. ve Katı, N., 2017b. Metal Matrisli Kompozit Malzemelerde Sıcaklığın Etkisiyle Sürünme ve Elastik Özelliklerin Ansys Yöntemiyle İncelenmesi, 2nd International Conference on Material Science and Technology in Cappadocia (IMSTEC'17), Ekim 2017 Nevşehir, Türkiye, s. 171-177.

Manning, JA., Crosky, AG. ve Bandyopadhay, S., 1993. Flexural and impact properties of sandwich panels used in surfboard construction. In: Proceedings of the International Conference on Advanced Composites, February 1993, Wollongong, Australia, pp.123–128.

Muc, A. ve Nogowczyk, R., 2005. Formy zniszczenia konstrukcji sandwiczowych z okładzinami wykonanymi z kompozytów. Composites, 5(4), 31–36.

Natarajan, S., Deogekar, P.S., Manickam, G. ve Belouettar, S., 2014. Hygrothermal effects on the free vibration and buckling of laminated composites with cutouts. Composite Structure, 108, 848-855.

Ochelski, S. ve Niezgoda, T., 2007. Kompozytowe konstrukcje pochłaniające energię uderzenia. Przegląd Mechaniczny, 1, 21–28.

Panigrahi, S.K. ve Pradhan, B., 2007. Delamination damage analyses of adhesively bonded lap shear joints in laminated frp composites. International Journal of Fracture Mechanics, 148, 373-385.

Park, J.S., Kim, J.H. ve Moon, S.H., 2004. Vibration of thermally post-buckled composite plates embedded with shape memory alloy fibers. Composite Structure, 63, 179-188.

Polat, A., Kaya, Y. ve Özşahin, T.Ş., 2017. Fonksiyonel derecelendirilmiş tabakada sürekli temas probleminin sonlu elemanlar yöntemi ile analizi. 20. Ulusal Mekanik Kongresi, Eylül 2017, Bursa, Türkiye, s.332-341.

Polat, A., Kaya, Y. ve Özşahin, T.Ş., 2018. Elastik yarı sonsuz düzlem üzerine oturan ağırlıklı tabakanın sonlu elemanlar yöntemi kullanılarak sürtünmesiz temas problemi analizi. Düzce Üniversitesi Bilim ve Teknoloji Dergisi, 6, 357-368.

Swanson, S.R. ve Kim, J.M., 2003. Design of sandwich structures under contact loading. Composite Structures, 59, 403-413.

Taşkaya, S., 2017. St 37 çeliğinin Ansys programında basınca bağlı olarak mekanik gerilmelerin incelenmesi. The Journal of International Manufacturing and Production Technologies, 1(1), 39-46.

Taşkaya, S., 2018. Investigation of mechanical and elastic stresses in Ansys program by finite elements method of 3D lattice roof model. Mugla Journal of Science and Technology, 4(1), 27-36.

Taşkaya, S., Zengin, B. ve Kaymaz, K., 2018. Investıgatıon of force and moment effect of St 37 and St 70 roof lattıce steels in Ansys program. Middle East Journal of Science, 4(1), 23-35.

Tawfik, M., Ro, J.J. ve Mei, C., 2002. Thermal post-buckling and aeroelastic behaviour of shape memory alloy reinforced plates. Smart Materials and Structure, 11, 297-307.

Vangipuram, P. ve Ganesan, N., 2007. Buckling and vibration of rectangular composite viscoelastic sandwich plates under thermal loads. Composite Structure, 77, 419-429.

Zhang, F., Ramadan M., Baozhong, S. ve Bohong, G., 2013. Damage behaviors of foam sandwiched composite materials under quasi static three point bending. Applied Composite Materials, 20, 1231-1246.

**GÜFBED/*GUSTIJ* (2018) CMES 2018 SEMPOZYUM EK SAYISI: 94-98**
DOI: 10.17714/gumusfenbil.439669 Araştırma Makalesi / *Research Article*

# On Optimal Control of the Initial Status in a Hyperbolic System

*Hiperbolik Bir Sistemde Başlangıç Konumunun Optimal Kontrolü Üzerine*

**Seda İĞRET ARAZ***
*Siirt University, Faculty of Education, Department of Mathematics Education, Siirt*

• Geliş tarihi / *Received*: 02.07.2018 • Düzeltilerek geliş tarihi / *Received in revised form*: 01.11.2018 • Kabul tarihi / *Accepted*: 06.11.2018

**Abstract**
In this study, optimal control problem governed by a hyperbolic problem with Dirichlet conditions is considered. It is demonstrated that the optimal solution for the considered optimal control problem is exist and unique and it is obtained adjoint problem. Derivative of the cost functional is calculated utilizing from adjoint problem. Finally, necessary optimality conditions for hyperbolic system are derived.

**Keywords:** Frechet Derivative, Hyperbolic Equations, Optimal Control

***Öz***
*Bu makalede Dirichlet koşuluna sahip hiperbolik sistem ile yönetilen optimal kontrol problem göz önüne alınır. Optimal çözümün var ve tek olduğu kanıtlanır ve eşlenik problem elde edilir. Eşlenik problemden yararlanılarak amaç fonksiyonunun gradyeni hesaplanır. Hiperbolik sistem için gerekli optimallik şartları türetilir.*

**Anahtar kelimeler***: Frechet Türev, Hiperbolik Denklemler, Optimal Kontrol*

*Seda İĞRET ARAZ; sedaaraz@siirt.edu.tr; Tel: (0484) 212 11 11 dâhili: 3135; orcid.org/0000-0002-7698-0709

## 1. Introduction

### *1.1. Formulation of the Problem*

As it is known, hyperbolic partial differential equations can be used to describe many physical phenomena. Some of them are heat conduction, vibration of elastic material, diffusion-reaction processes, population systems, and many others. However, there has been much attention to studies related with optimal control problems involving hyperbolic equation in recent years. It has been found too many researches about these problems using various control functions in literature. When these researches are analyzed, it has been seen that the control function is at the right hand side of equation, in the coefficient or on boundary for hyperbolic equation. But, there are too little researches about the initial control for hyperbolic problem.

Some of these important studies can be summarized as follows.

The problem of controlling the coefficient function has been studied for linear hyperbolic equation using the cost functional in (Tagiyev, 2012). The coefficient function has controlled for nonlinear hyperbolic equation using the functional involved in (Kröner, 2011). In (Bahaa, 2012), various optimal boundary control problems for linear infinite order distributed hyperbolic systems involving constant time lags are considered. It has been studied optimal control problems for the hyperbolic equations with a damping term involving p-Laplacian in (Ju ve Jeong, 2013). In (Hwang ve Nakagiri 2006), it has been examined optimal control problems for the equation of motion of membrane with strong viscosity. The tensions of end points for the vibration problem have been controlled using the cost functional in (Subaşı vd., 2017). Similar problems with different controls and cost functionals have been examined in (Lions, 1971; Yeloğlu ve Subaşı, 2010; Bahaa, 2011).

In this study, we handle the following hyperbolic system

$$u_{tt}-u_{xx}+q(x)u=F(x,t),\quad (x,t)\in\Omega \tag{1}$$

$$u(x,0)=\varphi(x),\quad u_t(x,0)=\psi(x),\quad x\in(0,l) \tag{2}$$

$$u(0,t)=0,\quad u(l,t)=0,\quad t\in(0,T) \tag{3}$$

defined on the domain $\Omega:=(x,t)\in(0,l)\times(0,T)$. We control the initial status minimizing the cost functional

$$J_\alpha(\varphi)=\iint_\Omega\left[u(x,t)-y_1(x,t)\right]^2dxdt + \int_0^l\left[u_t(x,T)-y_2(x)\right]^2dx+\alpha\|\varphi\|^2_{W_2^1(0,l)} \tag{4}$$

on the set $\phi$ which is closed, convex subset of $W_2^1(0,l)$.

Namely, aim of this study is to deal with the problem of

$$\inf_{\varphi\in\phi} J_\alpha(\varphi) \tag{5}$$

assuming that the conditions $\varphi(x)\in W_2^1(0,l),\ \psi(x)\in L_2(0,l)$ are hold.

For cost functional, $y_1(x,t)\in L_2(\Omega)$ is the state function to which $u(x,t)$ must be close enough and $w(x)\in L_2(0,l)$ is the final speed to which $u_t(x,T)$ must be close enough. $\alpha>0$ is regularization parameter.

In brief, in this study, we show that the initial status of the system can be controlled for hyperbolic problem by minimizing the cost functional $J_\alpha(\varphi)$.

In literature, there is no much research on optimal control of the initial status for hyperbolic system. So, this study is important in view of making the contribution on the initial control for theoretical and numerical investigations.

We introduce the spaces used in this article.

The space $L_2(\Omega)$ describes space of square integrable functions. The norm and inner product on this space are given by

$$\langle u,v\rangle_{L_2(\Omega)}=\iint_\Omega(u.v)dxdt\ ,$$

$$\|u\|_{L_2(\Omega)}=\sqrt{\langle u,u\rangle_{L_2(\Omega)}}.$$

The space $W_2^1(\Omega)$ is a space consisting of all elements $L_2(\Omega)$ with generalized derivatives of first.

$$\langle f,g\rangle_{W_2^1(\Omega)} = \iint_\Omega \left( f.g + \frac{\partial f}{\partial x}\cdot\frac{\partial g}{\partial x} + \frac{\partial f}{\partial t}\cdot\frac{\partial g}{\partial t}\right)dxdt,$$

$$\|f\|_{W_2^1(\Omega)} = \sqrt{\langle f,f\rangle_{W_2^1(\Omega)}}.$$

We organize this paper as follows. Firstly, we introduce some definitions and preliminary results. Then, we show that the weak solution and optimal solution is exist and unique. Later, we obtain the adjoint problem for the considered problem and calculate Frechet derivative of the cost functional. Also, we establish necessary optimality conditions for optimal solution.

## 2. Material and Method

### *2.1. Existence and Uniqueness Theorem*

Firstly, we show that the weak solution of hyperbolic problem is exist, unique and continuous dependence according to initial data under some conditions.

The generalized solution of the problem (1)-(3) is the function $u \in \overset{o}{W}{}_2^1(\Omega)$ satisfying the following integral equality;

$$\begin{aligned}&\iint_\Omega \left[-u_t\eta_t + u_x\eta_x + q(x)u\eta\right]dxdt = \\ &\iint_\Omega F(x,t)\eta dxdt + \int_0^l \psi(x)\eta(x,0)dx\end{aligned} \tag{6}$$

for $\forall\ \eta \in \overset{o}{W}{}_2^1(\Omega),\ \ \eta(x,T)=0.$

It can be seen in (Ladyzhenskaya, 1985) that weak solution is exist, unique and satisfies the inequality

$$\|u\|^2_{W_2^1(\Omega)} \le c_0\left(\|\varphi\|^2_{W_2^1(0,l)} + \|\psi\|^2_{L_2(0,l)} + \|F\|^2_{L_2(0,l)}\right) \tag{7}$$

Here $c_0$ is independent from $\varphi$ and $\psi$.

Let give an increment $\delta\varphi(x) \in W_2^1(0,l)$ to the control function $\varphi(x)$ such as $\varphi+\delta\varphi \in \phi$. Then the difference function $\delta u = \delta u(x,t) = u(x,t;\varphi+\delta\varphi) - u(x,t;\varphi)$ is the solution of the following difference initial-boundary problem;

$$\delta u_{tt} - \delta u_{xx} + q(x)\delta u = 0 \tag{8}$$

$$\delta u(x,0) = \delta\varphi, \quad \delta u_t(x,0) = 0 \tag{9}$$

$$\delta u(0,t) = 0, \ \ \delta u(l,t) = 0 \tag{10}$$

It can easily be seen from (7) that the solution of above difference initial-boundary problem holds the inequality

$$\|\delta u(.,t)\|^2_{L_2(0,l)} \le c_1\|\delta\varphi\|^2_{W_2^1(0,l)}, \ \ \forall t\in[0,T] \tag{11}$$

Here $c_1$ is independent from $\delta\varphi$.

We will benefit from Goebel's theorem in order to demonstrate the existence and the uniqueness of optimal solution for problem (1)-(5) (Goebel, 1970).

**Theorem (Goebel Theorem) :** Let $H$ be a uniformly convex Banach space and the set $\phi$ be a closed, bounded and convex subset of $H$. If $\alpha>0$ and $\beta\ge 1$ are given numbers and the functional $J(\varphi)$ is lower semi continuous and bounded from below on the set $\phi$ then there is a dense set $G$ of $H$ that the functional

$$J_\alpha(\varphi) = J(\varphi) + \alpha\|\varphi\|^\beta_H \tag{12}$$

takes its minimum on the set $\phi$. If $\beta>1$ then minimum is unique.

Now, we can show that optimal solution is exist and unique using this theorem.

The set $W_2^1(0,l)$ is a uniformly convex Banach space (Yosida, 1980), the set $\phi$ is a closed, bounded and convex subset of $W_2^1(0,l)$.

On the other hand, for the increment of the functional $J(\varphi)$, the following inequality is valid;

$$|\delta J(\varphi)| \le c_2\left(\|\delta\varphi\|_{W_2^1(0,l)} + \|\delta\varphi\|^2_{W_2^1(0,l)}\right) \tag{13}$$

From this inequality, we can say that this functional is also lower semi continuous and bounded from below on the set $\phi$. So, $J_\alpha(\varphi)$ has minimum on the set $\phi$. Namely, the optimal solution is exist.

Finally, since $\beta=2$, the optimal solution is unique.

## 3. Main Results

### *3.1. Adjoint Problem and Derivative of the Functional*

In this section, we write the Lagrange functional used for finding adjoint problem, before we show that the cost functional $J_\alpha(\varphi)$ is Frechet differentiability on the set $\phi$. Augmented functional for the problem is

$$\begin{aligned}\tilde{J}_\alpha(u,\varphi,\eta)&=\iint_\Omega\left[u(x,t)-y_1(x,t)\right]^2dx+\int_0^l\left[u_t(x,T)-y_2(x)\right]^2dxdt+\alpha\|\varphi\|^2_{W_2^1(0,l)}\\&+\int_0^T\int_0^l\left[u_{tt}-u_{xx}+q(x)u-F(x,t)\right]\eta_t dxdt\end{aligned}\tag{14}$$

The first variation of this functional is obtained such as;

$$\begin{aligned}\delta\tilde{J}_\alpha(\varphi)&=\int_0^l\int_0^T\left[2u(x,t)-2y_1(x,t)-\eta_{tt}+\eta_{xx}-q(x)\eta+\delta u(x,t)\right]\delta u(x,t)dxdt\\&+\int_0^l\left[2u_t(x,t)-2y_2(x)-\eta_t(x,T)+\delta u_t(x,T)\right]\delta u_t(x,T)dx\\&-\int_0^l\eta_x(x,0)\delta u_x(x,0)dx-\int_0^l\eta(x,0)\delta u(x,0)dx\\&+\alpha\int_0^l\left(2\varphi\delta\varphi+2\varphi_x\delta\varphi_x+\varphi_x^2\right)dx\end{aligned}\tag{15}$$

By means of stationary condition $\delta\tilde{J}_\alpha=0$, the following adjoint boundary value problem is found;

$$\eta_{tt}-\eta_{xx}+q(x)\eta=2\left[u(x,t)-y_1(x,t)\right]\tag{16}$$

$$\eta_x(x,T)=0,\quad \eta_t(x,T)=2\left[u_t(x,T)-y_2(x)\right]\tag{17}$$

$$\eta(0,t)=0,\quad \eta(l,t)=0\tag{18}$$

For $\forall\gamma\in\overset{o}{W}{}_2^1(\Omega)$, the function $\eta\in C^1\left([0,T],L_2(0,l)\right)\cap C^0\left([0,T],W_2^1(0,l)\right)$ which satisfies the following equality

$$\begin{aligned}\int_0^T\int_0^l\left[-\eta_t\gamma_t+\eta_x\gamma_x+q(x)\eta\gamma-2\left[u(x,t)-y_1(x,t)\right]\gamma\right]dxdt&=\int_0^l\eta_t(x,0)\gamma(x,0)dx\\&-\int_0^l2\left[u_t(x,T)-y_2(x)\right]\gamma(x,T)dx\end{aligned}\tag{19}$$

is the solution of adjoint boundary value problem (16)-(18).

From the conditions of the difference problem, we rewrite the equality (1.15) as follows;

$$\begin{aligned}\delta J_\alpha(\varphi)&=\int_0^l\left(-\eta(x,0)\delta\varphi-\eta_x(x,0)\delta\varphi_x+2\alpha\varphi\delta\varphi+2\alpha\varphi_x\delta\varphi_x\right)dx+o\left(\|\delta\varphi\|^2_{W_2^1(0,l)}\right)\\&=\left\langle-\eta(x,0)+2\alpha\varphi,\delta\varphi\right\rangle_{W_2^1(0,l)}+o\left(\|\delta\varphi\|^2_{W_2^1(0,l)}\right).\end{aligned}$$

So, we obtain the derivative of the cost functional from definition of Frechet derivative such as;

$$J'_\alpha(\varphi)=-\eta(x,0)+2\alpha\varphi\tag{20}$$

### *3.2. Condition for Optimal Solution*

After calculating the derivative of the functional, it can be said that the derivative $J'_\alpha(\varphi)$ is continuous on the set $\phi$. The fact that the functional $J_\alpha(\varphi)$ is continuously differentiable on the set $\phi$ and the set $\phi$ is convex, in that case the following inequality is valid according to theorem in (Vasilyev, 1981);

$$\left\langle J'_\alpha(\varphi^*), \varphi - \varphi^* \right\rangle_{W_2^1(0,l)} \geq 0, \quad \forall \varphi \in \phi \tag{21}$$

Therefore, necessary condition for optimal solution is given by the following inequality;

$$\left\langle -\eta(x,0) + 2\alpha\varphi^*, \varphi - \varphi^* \right\rangle_{W_2^1(0,l)} \geq 0, \quad \forall \varphi \in \phi \tag{22}$$

## 4. Conclusion

This study presents the optimality conditions for an optimal control problem involving hyperbolic equation. The initial status has been chosen as the control function in this paper. We obtain an adjoint problem for problem (1)-(3) and calculate derivative of the cost functional via adjoint problem on the space $W_2^1(0,l)$. The derivative of the functional is highly important for obtaining a control which converges optimal solution. Therefore, this study leads to numerical investigations related to obtaining an optimal solution.

## References


Bahaa, G.M. and Tharwat, M.M., 2011. Optimal control problem for infinite variables hyperbolic systems with time lags. Archieves of Control Sciences, 21 (4), 373-393.

Bahaa, G.M., 2012. Boundary Control Problem of Infinite Order Distributed Hyperbolic Systems Involving Time Lags**.** Intelligent Control and Automation, 3, 211-221.

Goebel, M., 1979. On Existence of Optimal Control. Mathematische Nachrichten, 93, 67-73.

Hwang, J. and Nakagiri, S., 2006. Optimal control problems for the equation of motion of membrane with strong viscosity. Journal of Mathematical Analysis and Applications, 321 (1) 327-342.

Ju, EY. and Jeong, J.M., 2013. Optimal control problems for hyperbolic equations with damping terms involving p-Laplacian. Journal of Inequalities and Applications, 92.

Kröner, A., 2011. Adaptive Finite Element Methods for Optimal Control of Second Order Hyperbolic Equations. Computational Methods in Applied Mathematics, 214-240.

Ladyzhenskaya, O.A., 1985. Boundary Value Problems in Mathematical Physics. Springer-Verlag, 322 p, New York.

Lions, J.L., 1971. Optimal Control of Systems Governed by Partial Differential Equations. Springer, 273-291 p, Berlin.

Subaşı, M., Güngör, H. and Araz, İ.S., 2017. On the Control of End Point Tensions in a Vibration Problem. International Journal of Modeling and Optimization, 7 (2) 74-77.

Tagiyev, R.K., 2012. On Optimal Control of the Hyperbolic Equation Coefficients. Automation and Remote Control, 1145-1155.

Vasilyev, F.P., 1981. Ekstremal problemlerin çözüm metotları, Nauka, 400.

Yeloğlu, T. and Subaşı, M., 2010. Simultaneous control of the source terms in a vibrational string problem. Iranian Journal of Science & Technology, Transaction A, 34, A1.

Yosida, K., 1980. Functional Analysis, Springer-Verlag, 624 p, New York.

**GÜFBED/*GUSTIJ* (2018) CMES 2018 SEMPOZYUM EK SAYISI: 99-105**
DOI: 10.17714/gumusfenbil.437302 Araştırma Makalesi / *Research Article*

# Concircular Curvature Tensor on Generalized Kenmotsu Manifolds

*Genelleştirilmiş Kenmotsu Manifoldları Üzerinde Concircular Eğrilik Tensörü*

**İnan ÜNAL*[1,a], Ramazan SARI[2,b], Aysel TURGUT VANLI[3,c]**
[1]*Munzur Üniversitesi, Mühendislik Fakültesi, Bilgisayar Mühendisliği Bölümü, Tunceli*
[2]*Amasya Üniversitesi, Gümüşhacıköy Hasan Duman Meslek Yüksekokulu, Amasya*
[3]*Gazi Üniversitesi Fen Fakültesi Matematik Bölümü, Ankara*

• Geliş tarihi / *Received*: 26.06.2018 • Düzeltilerek geliş tarihi / *Received in revised form*: 08.10.2018 • Kabul tarihi / *Accepted*: 07.11.2018

**Abstract**
The aim of the present paper is to study on concircular curvature tensor on generalized Kenmotsu manifolds. Concircular flat and φ-concircular flat generalized Kenmotsu manifolds are examined. Also some results are given about φ-semi symmetric and φ -concircular semi symmetric generalized Kenmotsu manifolds.

**Keywords**: Concircular curvature tensor, Generalized Kenmotsu manifolds, φ-semi symmetric, φ-concircular semi symmetric

***Öz***
*Bu çalışmanın amacı genelleştirilmiş Kenmotsu manifoldları üzerinde concircular eğrilik tensörünün çalışılmasıdır. Concircular düz ve φ-concircular düz genelleştirilmiş Kenmotsu manifoldları incelenmiştir. Ayrıca φ-semi simetrik ve φ-concircular semi simetrik genelleştirilmiş Kenmotsu manifoldları üzerine bazı sonuçlar verilmiştir.*

***Anahtar kelimeler:*** *Conircular eğrilik tensörü, Genelleştirilmiş Kenmotsu manifoldları, φ-semi simetrik, φ-concircular semi simetrik*

*[a] İnan ÜNAL; inanunal@munzur.edu.tr; Tel: (0428) 2131794 ; *orcid.org/0000-0003-1318-9685*
[b] *orcid.org/0000-0002-4618-8243* [c] orcid.org/0000-0001-9793-7366

## 1. Introduction

Contact geometry is an important branch of geometry. One can dived into two part this notion: real and complex. The complex contact geometry studied since 1959 and there several works in literature (Blair, 2010; Turgut Vanlı and Unal, 2017). Real contact geometry is studying widely by scientists and has lots of applications to other areas of mathematics and theoretical physics (Kholodenko, 2013). There are several classes of contact manifolds. One of them Kenmotsu manifolds which is called for honor of Katsuei Kenmotsu who was introduced the notion. Kenmotsu proposed to study the properties of warped product of the complex space with real line. This product is one of the three classes in classification was given by S. Tanno (Tanno, 1969). So this problem appears naturally at that time. Kenmotsu obtained some results and gave characterization for this third classes of Tanno's classification. The importance of Kenmotsu manifolds comes from some different properties of these spaces. On of them is that a n almost contact manifold which is satis- fied being Sasakian condition is not Sasakian. Also the contact distribution of any Kenmotsu manifolds is always integrable. A Kenmotsu manifold is not compact and has negative sec- tional curvature, for details see (Pitiş, 2007).

A manifold with the almost contact Riemann structure $(\varphi,\xi,\eta,g)$ is an almost Kenmotsu manifold if the following conditions are satisfied

$$d\eta = 0,\ d\Omega = 2\eta\wedge\Omega$$

$$\varphi^2 = -I+\sum_{i=1}^{s}\eta^i\otimes\xi_i,\ \ \eta^i(\xi_j)=\delta_{ij},\varphi\xi_i = 0,\ \ \eta^i\circ\varphi = 0 \tag{1}$$

$$g(\varphi X,\varphi T) = g(X,T)-\sum_{i=1}^{s}\eta^i(X)\eta^i(T) \tag{2}$$

then we recall $M$ is $f$-manifold (Goldberg and Yano,1971). In addition we get

$\eta^i(X) = g(X,\xi_i),\ \ g(X,\varphi T) = -g(\varphi X,T).$

The fundamental second form of the contact structure is defined by $\Phi(X,T) = g(X,\varphi T)$.

If we denote $\mathcal{L} = \{X:\eta^\alpha(X)=0, 1\le\alpha\le s\}$ and $\mathcal{M} = sp\{\xi_1,\xi_2,...,\xi_s\}$ then we can write $TM = \mathcal{L}\oplus\mathcal{M}$ Let $U$ be a coordinate neighborhood and $E_1$ be a unit vector field on $U$ orthogonal to the structure vector fields. $M$ has local an orthonormal basis

$$\{E_1,\ldots,E_n,\varphi E_1,\ldots,\varphi E_n,\xi_1,\ldots,\xi_s\}.$$

A metric $f$-manifold is normal if $[\phi,\phi]+2\sum_{i=1}^{s}d\eta^i\otimes\xi_i = 0$, where $[\varphi,\varphi]$ is the Nijenhuis tensor of $\varphi$. A 2-form $\Phi$ on $M$ such that $\eta^1\wedge...\wedge\eta^s\wedge\Phi^n\neq 0$ then $M$ is called an almost s-contact metric manifold. A normal almost s-contact metric manifold is called an s-contact metric manifold.

**Definition 2.1** Let $\left(M^{(2n+s)},\varphi,\xi^i,\eta^i\right), s\ge 1,$ be an almost $s-$contact metric manifol. If for all $1\le i\le s,$ are closed and $d\Phi = 2\sum_{i=1}^{s}\eta^i\wedge\Phi$ then M is called generalized almost Kenmotsu manifol.

where $\Omega$ is second fundamental form of almost contact structure and defined by $\Omega(X,Y) = g(\varphi X,Y)$ for X, Y ∈ Γ(T M). In 2006, M. Falcitelli and A. M. Pastore introduced Kenmotsu $f.pk$ -manifold (Falciletti and Pastore, 2006). An $f.pk$ -manifold M is (2n+ s)-dimensional manifold with an $f$ –structure with parallelizable kernel. A normal -manifold $\left(M,\varphi_i,\xi_i,\eta_i,g\right)$ is called Kenmotsu if 1-forms $\eta^i$ are closed and $d\Omega = 2\eta^1\wedge\Omega$.

Two of presented authors introduced generalized Kenmotsu manifolds obtained some results on curvature properties (Turgut Vanlı and Sari, 2016). Also same authors studied on invariant submanifolds of generalized Kenmotsu manifold (Turgut Vanlı and Sari, 2015a,b). In 2017 Srikantha and Venkatesha examined this kind of submanifolds by certain conditions (Srikantha and Venkatesha, 2017). In this article we studied on concircular curvature tensor on generalized Kenmotsu manifolds. We gave some results on flatness conditions and symmetric conditions.

## 2. Preliminaries

Let $M$ be a $(2n+s)-$dimensional differentiable manifold. If, for $(1,1)$ type tensor field $\varphi$, $s-$ differentiable vector fields $\xi_1,\ldots,\xi_s$ (called structure vector fields), $s-$ differentiable 1-forms $\eta^1,\ldots,\eta^s$, a Riemannian metric $g$ and vector fields $X,T\in\Gamma(TM)$ on $M$ we have

If, in addition, M is normal, then it is called a generalized Kenmotsu manifold.
Let $R$ be Riemannian curvature tensor of $M$ which is defined as:

$$R(X,Y)W = \nabla_X \nabla_Y W - \nabla_Y \nabla_X W - \nabla_{[X,Y]} W \quad (3)$$

for $X, Y, W$ vector fields on $M$. The Riemann curvature of a generalized Kenmotsu manifold have following equations (Turgut Vanli and Sari, 2016)

$$R(X,T)\xi_i = \sum_{j=1}^{s} \{\eta^j(T)\varphi^2 X - \eta^j(X)\varphi^2 T\} \quad (4)$$

$$R(X,\xi_i)T = \sum_{j=1}^{s} \{\eta^j(T)\varphi^2 X - g(X,\varphi^2 T)\xi_j\} \quad (5)$$

$$R(X,\xi_j)\xi_i = \varphi^2 X, \qquad R(\xi_k,\xi_j)\xi_i = 0 \quad (6)$$

$$\eta^i(R(X,T)W) = \sum_{j=1}^{s} \{\eta^j(T)g(X,W) - \eta^j(X)g(T,W)\}. \quad (7)$$

Also for $X, Y, T \in \Gamma(TM)$ we get

$$R(X,Y)\varphi T - \varphi R(X,Y)T = g(Y,T)\varphi X - g(X,T)\varphi Y - g(Y,\varphi T)X + g(X,\varphi T)Y, \quad (8)$$

$$R(\varphi X,\varphi Y)T = R(X,Y)T + g(Y,T)X - g(X,T)Y + g(Y,\varphi T)\varphi X - g(X,\varphi T)\varphi Y, \quad (9)$$

$$R(\varphi X,Y)T = \varphi R(X,Y)T + g(Y,T)\varphi X - g(X,T)\varphi Y - g(\varphi X,\varphi T)\varphi Y - g(\varphi Y,\varphi T)\varphi X. \quad (10)$$

For the Ricci curvature $S$ of $M$ we have

$$S(X,\xi_i) = -2n\sum_{j=1}^{s} \eta^j(X), \quad S(\xi_k,\xi_i) = -2n. \quad (11)$$

The notion of curvature is one of important tools for understanding Riemannian geometry of manifolds. Some geometric features of structure on manifolds could be restricted from curvature tensors. One of the important curvature tensor is concircular curvature tensor which is invariant under concircular transformations (Yano and Kon, 1984). If concircular curvature tensor vanishes then we recall the manifold concircularly. Concircular curvature tensor on a $(2n+s)-$ dimensional generalized Kenmotsu manifold is given by

$$Z(X,Y)T = R(X,Y)T - \frac{r}{(2n+s)(2n+s-1)}[g(Y,T)X - g(X,T)Y]. \quad (12)$$

where $r$ is the scalar curvature of $M$. Yano proved that a concircular flat Riemann manifold is space of constant curvature (Yano, 1940). Also an Einstein space is invariant under concircular transformation. We can express that this tensor measure the difference the manifold from being space forms. In order to brevity we take $A = \frac{r}{(2n+s)(2n+s-1)}$.

From the definition of concircular curvature tensor on a generalized Kenmotsu manifold $M$ we have

$$Z(\xi_k,\xi_j)\xi_i = 0 \quad (13)$$

$$Z(X,\xi_j)\xi_i = -X + \sum_{\alpha=1}^{s} \eta^\alpha(X)\xi_\alpha - A\eta^j(X)\xi_i \quad (14)$$

$$Z(X,\xi_i)Y = \sum_{j=1}^{s} \left(g(X,Y)\xi_j - \eta^j(Y)X\right) + A(g(X,Y)\xi_i - \eta^i(Y)X) \quad (15)$$

$$Z(X,Y)\xi_i = \sum_{j=1}^{s} (\eta^j(X) - \eta^j(Y)X) + A(\eta^i(X)Y - \eta^j(Y)X) \quad (16)$$

for all $X,Y \in \Gamma(TM)$ and $1 \le i, j, \alpha \le s$.

In the contact geometry $\eta-$ Einstein metric has important position. This metric is the generalization of Einstein metric. Let $\lambda, \mu$ some functions and $X,T$ be vector fields on $M$ if the Ricci tensor of a generalized Kenmotsu manifold satisfies

$$S(X,T) = \lambda g(X,T) + \mu \sum_{i=1}^{s} \eta^i(X)\eta^i(T)$$

then $M$ is called $\eta-$Einstein generalized Kenmotsu manifold. Since $TM = \mathcal{L} \oplus sp\{\xi_1, \xi_2, ..., \xi_s\}$ we can write

$$X = X_0 + \sum_{i=1}^{s} \eta^i(X)\xi_i \quad \text{and} \quad T = T_0 + \sum_{i=1}^{s} \eta^i(T)\xi_i$$

where $X_0, T_0 \in \mathcal{L}$. Then we get

$$S(X,T) = S(X_0,T_0) - 2n \sum_{i=1}^{s} \eta^i(X)\eta^i(T). \quad (17)$$

There we get that if $S(X_0,T_0) = \alpha g(X_0,T_0)$ then $M$ is $\eta-$Einstein.

By similar consideration for sectional curvature of a generalized Kenmotsu manifold we have

$$\begin{aligned} k(X,T) = k(X_0,T_0) &+ \sum_{\alpha,\beta=1}^{s} \eta^\alpha(T)\eta^\beta(T)k(T_0,\xi_\alpha) + \sum_{\alpha,\beta=1}^{s} \eta^\alpha(X)\eta^\beta(X)k(X_0,\xi_\alpha) \\ &+ \sum_{\alpha,\beta=1}^{s} [\eta^\alpha(X)\eta^\beta(T)]^2 k(\xi_\alpha,\xi_\beta). \end{aligned} \quad (18)$$

## 3. Flatness Of Generalized Kenmotsu Manifold Via Concircular Curvature Tensor

As we know any concircular flat Riemann manifold is space of constant curvature. There is also a similar results for generalized Kenmotsu manifold. By an easy and direct computation;

**Theorem 3.1** Any concircularly flat generalized Kenmotsu manifold is Einstein.

**Definition 3.2** Let $M$ be a generalized Kenmotsu manifold. For $X,Y,W \in \Gamma(TM)$ if

$$\phi^2(Z(\varphi X, \varphi Y)\varphi W) = 0 \quad (19)$$

then $M$ is called $\varphi-$concircularly flat.

**Theorem 3.3** $\varphi-$concircularly flat generalized Kenmotsu manifold is $\eta-$Einstein.

**Proof** Let $M$ be a $\varphi-$concircularly flat generalized Kenmotsu manifold. From the definition of concircular curvature tensor and by using (10) for $X,Y,U \in \Gamma(TM)$ we get

$$\begin{aligned} &Z(\varphi X, \varphi Y,)\varphi U = \varphi R(X,Y)U + g(Y,U)\phi X - g(X,U)\varphi Y \\ &+(1+A)g(\varphi X, \varphi U)\phi Y - (1+A)g(\varphi Y, \varphi U)\varphi X. \end{aligned}$$

Since $M$ is $\varphi-$concircularly flat by applying $\varphi^2$ to this equation we have

$$\begin{aligned} 0 = &-\varphi R(X,Y)U - g(Y,W)\phi X + g(X,U)\varphi Y - (1+A)g(\varphi X, \varphi U)\varphi Y \\ &+(1+A)g(\varphi Y, \varphi U)\varphi X. \end{aligned}$$

Let apply $\varphi$ again to last equation and from (1),(2) and (7) we obtain

$$\begin{aligned} R(X,Y)U = &\sum_{\alpha=1}^{s}\sum_{j=1}^{s}\{\eta^j(X)g(Y,U) - \eta^j(Y)g(X,U)\}\xi_\alpha \\ &-\{g(Y,U) - (1+A)g(\varphi Y, \varphi U)\}\phi^2 X + \{g(X,U) - (1+A)g(\varphi X, \varphi U)\}\phi^2 Y. \end{aligned} \quad (20)$$

Let choose $Y = U = E_i$ , $X = X_0, T = T_0$ for $X_0, T_0 \in \mathcal{L}$ and taking sum over $i$ to $2n+s$ for the basis $\{E_1, \ldots, E_n, \varphi E_1, \ldots, \varphi E_n, \xi_1, \ldots, \xi_s\}$ from (20) we get

$$\sum_{i=1}^{s} g(R(X_0,E_i),E_i,T_0) = -\sum_{i=1}^{s}\{\{g(E_i,E_i)-(1+A)g(\phi E_i,\phi E_i)\}g(\phi^2 X_0,T_0)\}$$

$$+\sum_{i=1}^{s}\{\{g(X_0,E_i)-(1+A)g(\phi X_0,\phi,E_i)\}g(\phi^2 E_i,T_0)\}$$

and thus we have

$$\sum_{i=1}^{s} g(R(X_0,E_i),E_i,T_0) = -(2n+s)g(\phi^2 X_0,T_0)-(1+A)2ng(\phi^2 X_0,T_0)+g(\phi^2 X_0,T_0)$$

$$-(1+Ag(\phi^2 X_0,\phi^2 T_0)).$$

Therefore we get

$$S(X_0,T_0) = (4n+s+(2n-1)A)g(X_0,T_0)$$

and from (17) we have

$$S(X,T) = (4n+s-(2n-1)A)g(X,T)+(-6n-s+(2n-1)A)\sum_{j,\alpha=1}^{s}\eta^{\alpha}(X)\eta^{\alpha}(T)$$

for arbitrary vector fields $X,T$ on $M$. So this shows that $M$ is $\eta-$Einstein.

**Definition 3.4** Let $M$ be a generalized Kenmotsu manifold. For $X,Y,W\in\Gamma(TM)$ if

$$g\left(Z(\phi X,Y)T,\phi W\right)=0 \qquad (21)$$

then $M$ is called pseudo-concircularly flat.

**Theorem 3.5** Let $M$ be pseudo-concircularly flat generalized Kenmotsu manifold then the Riemannian curvature of $M$ has the following form:

$$R(T,W)X = -g(W,\phi X)T-g(T,\phi X)W-g(W,X)\phi T+g(T,X)\phi W$$

$$+A\left(g(\phi X,W)T-g(\phi X,T)\phi W\right)+\sum_{\alpha=1}^{s}\{\eta^{\alpha}(R(T,W)X)+g(W,\phi X)\eta^{\alpha}(T) \qquad (22)$$

$$+g(T,\phi X)\eta^{\alpha}(W)\}\xi_{\alpha}$$

where $T,W,X\in\Gamma\left(TM\right)$.

**Proof** Let $M$ be pseudo-concircularly flat generalzed Kenmotsu manifold. For $X,Y,T,W\in\Gamma(TM)$ from (12), (8) we get

$$\phi R(T,W)X = -g(W,\phi X)\phi T+g(T,\phi X)\phi W-g(W,X)T-g(T,X)W$$
$$+A(g(\phi X,W)T-g(\phi X,T)W. \qquad (23)$$

By applying $\varphi$ to the (23) and from (1), (7) we obtain (22).

From this theorem we have following corollary;

**Corollary 3.6** Let $M$ be a pseudo-concircularly flat generalized Kenmotsu manifold for $X_0,T_0\in\Gamma(\mathcal{L})$ and $\xi_{\alpha}\in\Gamma(\mathcal{M})$ the sectional curvature of a pseudo-concircularly flat generalized Kenmotsu manifold is given $k(X_0,T_0)=k(X_0,\xi_{\alpha})=k(\xi_{\alpha},\xi_{\beta})=0.$

Thus from (18) also we get;

**Corollary 3.7** The sectional curvature of a pseudo-concircularly flat generalized Kenmotsu manifold vanishes.

**Corollary 3.8** The $\varphi-$sectional curvature of a pseudo-concircularly flat generalized Kenmotsu manifold $M$ is equal to 1.

## 4. Some Symmetry Properties of a Generalized Kenmotsu Manifold

The notion of symmetry has the important position to study the Riemannain geometry of manifolds. Locally symmetry of a Riemann manifold could state by curvature tensor.

For a $S$ tensor $R(X,Y).S$ is defined by

$$R(X,Y).S = \nabla_X\nabla_Y S-\nabla_Y\nabla_X S-\nabla_{[X,Y]}S.$$

Also if $R.\mathcal{T}=0$ then the manifold is called $T-$ semi symmetric. For a Riemannian manifold if $R.R=0$ then the manifold is called locally symmetric. Locally symmetric generalized Kenmotsu manifold studied by Turgut Vanli and Sari (Turhut Vanlı and Sarı, 2016). They proved that $\varphi-$sectional curvature of any semi symmetric $(2n+s)$-dimensional generalzed Kenmotsu manifold $\left(M,\varphi,\xi_i,\eta^i,g\right)$ is equal to $-s$. Same authors also studied on Ricci-semi symmetric generalized Kenmotsu manifolds. In 2005 Blair, Kim and Tripathi studied on concircular curvature tensor of a contact metric manifold (Blair vd., 2005). They classify the special class of contact $N(k)$ manifolds by concircularly symmetric (which means $\nabla\mathcal{Z}=0$) condition. The concircular geometry has interesting results in the contact geometry. In this section we study on generalized Kenmotsu manifold via symmetry condition with these tensor.

Let $M$ be a generalized Kenmotsu manifold. If $R(X,Y).\varphi=0$ then $M$ is called $\varphi-$semi symmetric. For $X,Y,U\in\Gamma(TM)$ $R(X,Y).\varphi$ is given by

$$(R(X,Y).\phi)U=R(X,Y)\phi U-\phi R(X,Y)U.$$

Similarly if $\mathcal{Z}(X,Y).\varphi=0$ then the manifold is called $\varphi-$concircular semi symmetric. For $X,Y,W\in\Gamma(TM)$ $\mathcal{Z}(X,Y).\varphi$ is given by

$$(Z(X,Y).\varphi)W=Z(X,Y)\varphi W-\varphi Z(X,Y)W.$$

Also for arbitrary vector fields $X,Y,Z,T,U$ and $W$ on $M$ we have

$$(R(X,Y).Z)(T,U)W=R(X,Y)Z(T,U)W-Z(R(X,Y)T,U)W-Z(T,R(X,Y)U)W-Z(T,U)R(X,Y)W.$$

A genarlized Kenmotsu manifold with $R.\mathcal{Z}=0$ is called concircular semi symmetric.

In this section we give some results on symmetry properties with related to concircular curvature tensor of generalized Kenmotsu manifold.

**Theorem 4.1** A genarlized Kenmotsu manifold is $\varphi-$concircular semi symmetric if and only if the scalar curvature $r\neq-(2n+s)(2n+s-1)$ and the manifold is $\varphi-$semi symmetric.

**Proof** Let $M$ be a $\varphi-$semi symmetric generalzed Kenmotsu manifold. From the definition and by using (8), (9) we get

$$0=(1+A)(g(Y,W)\varphi X-g(X,U)\varphi Y-g(Y,\varphi U)X+g(X,\varphi U)Y).$$

If $1+A\neq0$ i.e $r\neq-(2n+s)(2n+s-1)$ we get

$$(g(Y,U)\varphi X-g(X,U)\varphi Y-g(Y,\varphi U)X+g(X,\varphi U)Y=0.$$

This means $M$ is $\varphi-$semi symmetric. Conversely let $M$ be a $\varphi-$semi symmetric generalzed Kenmotsu manifold and $r\neq-(2n+s)(2n+s-1)$ then we get

$$(Z(X,Y)\varphi)U=-A(g(Y,\varphi U)X-g(X,\varphi U)Y-g(Y,U)\varphi X+g(X,U)\varphi Y).$$

So the manifold $M$ is $\varphi-$concircular semi symmetric.

**Theorem 4.2** The Riemannian curvature tensor $R$ of the a concircularly semi symmetric generalized Kenmotsu manifold is

$$R(T_0,U_0)Y_0=(s-2A)g(Y_0,T_0)U+(1+A)g(Y_0,U)T_0 \tag{24}$$

where $Y_0,U_0,T_0$ are vector fields orthogonal to $\xi_i$ on $M$.

**Proof** Let choose $X=W=\xi_i$ and $Y_0,U_0,T_0$ orthogonal to $\xi_i$ then we get

$$R(\xi_i,Y_0)Z(T_0,U_0)\xi_i-Z(R(\xi_i,Y_0)T_0,U)\xi_i-Z(T_0,R(\xi_i,Y_0)U)\xi_i-Z(T_0,U_0)R(\xi_i,Y_0)\xi_i=0.$$

From equalities (4) ,(5), (6), (14), (15) and (16) and by some computations we get (24).

For vector field $V_0$ is orthogonal to $\xi_i$ from (24) we get

$$g(R(T_0,U_0)Y_0,V_0)=(s-2A)g(Y_0,T_0)g(U_0,V_0)+(1+A)g(Y_0,U_0)g(T_0,V_0)$$

and by choosing $U_0 = V_0 = E_i$ , taking sum from $i$ to $2n$ we obtain

$$S(T_0, Y_0) = (2n + s - 1 - (2n-1)A)g(T_0, Y_0).$$

Then from (18) for arbitrary vector fields $T, Y \in \Gamma(TM)$ we get

$$S(T,Y) = (2n + s - 1 - (2n-1)A)g(T,Y) - (-4n - s - 1 + (2n-1)A)\sum_{\alpha=1}^{s} \eta^{\alpha}(Y)\eta^{\alpha}(Y).$$

Thus we have proved following corollary.

**Corollary 4.3** A concircularly semi symmetric generalized Kenmotsu manifold is $\eta-$Einstein.

**Corollary 4.4** The sectional curvature of a generalized Kenmotsu manifold for unit ant mutually orthogonal vector field $T, W \in \Gamma(TM)$ is given by

$$k(T,W) = (1+A)\left(1 + \sum_{\alpha,\beta=1}^{s}\left(\eta^{\alpha}(T)\eta^{\beta}(T) + \eta^{\alpha}(W)\eta^{\beta}(W) + \left(\eta^{\alpha}(T)\eta^{\beta}(W)\right)^2\right)\right).$$

## 4. References


Blair, D.E., 2010. Riemannian geometry of contact and Symplectic Manifolds: Boston, Birkhauser, 360p.

Blair, D. E., Kim, J. S. and Tripathi, M., 2005. On the concircular curvature tensor of a contact metric manifold. Journal of the Korean Mathematical Society, 42(5), 883-892.

Falcitelli, M. and Pastore, A.M., 2006. f-structures of Kenmotsu Type. Mediterranean Journal of Mathematics, 3(3-4), 549-564.

Goldberg, S.I. and Yano, K., 1971. Globally framed f-manifolds. Illinois Journal of Mathematics, 15, 456-474.

Kholodenko, A.L., 2013. Applications of Contact Geometry and Topology in Physics: Singapore, World Scientific Publishing Co., 492p.

Pitiş G., 2007. Geometry of Kenmotsu manifolds: Braşov, Publishing House of Transilvania University of Braşov.

Srikantha, N. and Venkatesha, 2017. On Invariant Submanifolds of a Generalized Kenmotsu Manifold Satisfying Certain Conditions. International Journal of Mathematics and Mathematical Sciences, 13(1), 17-25.

Tanno, S., 1969. The automorphism groups of almost contact Riemannian manifolds. Tohoku Mathematical Journal, 21, 21-38.

Turgut Vanli, A. and Sari, R., 2015a. On Semi-Invariant Submanifolds of a Generalized Kenmotsu Manifold Admitting a Semi-Symmetric Metric Connection. Acta Universitatis Apulensis, 43, 79-92.

Turgut Vanli, A. and Sari, R., 2015b. On Semi-Invariant Submanifolds of a Generalized Kenmotsu Manifold Admitting a Semi-Symmetric Non-Metric Connection. Pure and Applied Mathematics Journal, 4(1-2), 14-18.

Turgut Vanli, A. and Sari, R., 2016. Generalized Kenmotsu Manifolds. Communications in Mathematics and Applications, 7(4), 311-328.

Turgut Vanli, A. and Unal, I., 2017. Conformal, concircular, quasi-conformal and conharmonic flatness on normal complex contact metric manifolds. International Journal of Geometric Methods in Modern Physics, 14(05), 1750067.

Yano, K. and Kon, M., 1984. Structure on manifolds, In: Series in Pure Mathematics: Volume 3: Singapore, World Scientific, 520p.

Yano, K., 1940. Concircular geometry I. Concircular transformations. Proceedings of the Imperial Academy, 16(6), 195-200.

**GÜFBED/*GUSTIJ* (2018) CMES 2018 SEMPOZYUM EK SAYISI: 106-111**
DOI: 10.17714/gumusfenbil.437467 Araştırma Makalesi / *Research Article*

# Betonun Mekanik Özelliklerinin Çarpma Dayanımına Etkisi

*The effect of mechanical properties of concrete on ımpact strength*

**Kürşat KAYMAZ[*1,a], Erdinç ARICI[2,b]**
[1]*Munzur Üniversitesi, Mühendislik Fakültesi, İnşaat Mühendisliği Bölümü, Tunceli, Türkiye*
[2]*Fırat Üniversitesi, Teknoloji Fakültesi, İnşaat Mühendisliği Bölümü, Elazığ, Türkiye*

• Geliş tarihi / *Received*: 27.06.2018 • Düzeltilerek geliş tarihi / *Received in revised form*: 03.11.2018 • Kabul tarihi / *Accepted*: 07.11.2018

**Öz**
Bu çalışmada; betonun mekanik özelliklerinden olan basınç, eğilmede çekme ve yarmada çekme dayanımlarının çarpma dayanımı üzerindeki etkileri incelenmiştir. Bu amaç doğrultusunda maksimum agrega çapı 4, 8 ve 16 mm, su/çimento (S/Ç) oranı ise 0.50 ve 0.55 olan altı seri numuneleri hazırlanmıştır. Hazırlanan numuneler üzerinde basınç, eğilme, yarma ve Charpy darbe dayanımları belirlenmiştir. Yapılan deneysel çalışmalar sonucunda; betonun mekanik özelliklerini agrega çapındaki artış olumlu etkilerken S/Ç oranındaki artış olumsuz yönde etkilemiştir. Betonun çarpma dayanımındaki değişim de aynı şekilde olmuştur. Fakat çarpma dayanımı S/Ç oranındaki artıştan daha az etkilenmiştir.

**Anahtar kelimeler:** Basınç Dayanımı, Beton, Charpy Deneyi, Çarpma Dayanımı, Çekme Dayanımı.

***Abstract***
*In this study, impact stregth of concrete is investigated with the effect of mechanical properties such as compressive strength, flexural tensile strength and splitting tensile strength. For this purpose, six serial specimens with three different maximum aggregate diameter (4, 8 and 16 mm) and whose water/cement (w/c) ratio of 0.50 to 0.55 were prepared. The compressive, bending, splitting and impact strength of the prepared specimens were determined. As a result of study; The mechanical properties of the concrete were positively effected by the increase in the aggregate size, while the icrease in the W/C ratio adversely effected. The change in the impact strength of concrete has also been the same. But the impact strength is less effected than the increase in W/C ratio.*

***Keywords:*** *Compressive Strength, Concrete, Charpy Experiment, Impact Strength, Tensile Strength.*

*[a] Kürşat KAYMAZ; kkyamaz@munzur.edu.tr ; Tel: 0 (4248) 213 17 94; orcid.org/ 0000-0002-8346-8260
[b] orcid.org/0000-0002-6153-5805

## 1. Giriş

Değişik türdeki yapılarda kullanılmakta olan betonun üzerine değişik yönlerde etki yapan statik veya dinamik yükler gelebilmektedir. Beton, bu yükleri taşıyabilmek için direnç göstermektedir. Doğal olarak, üzerine gelen yükün etkisiyle betonda bir miktar şekil değişikliği meydana gelmektedir. Üzerine gelen yüklerin büyüklüğü arttıkça, hem betondaki şekil değişikliğinin miktarı artmakta, hem de bu yükleri taşıyabilmek için daha çok direnç gerekmektedir. Eğer meydana gelen yükleme betonun taşıma kapasitesinden daha fazla boyutlarda oluşursa, betonda şekil değişikliğiyle birlikte betonun kırılmasına neden olmaktadır (Mather, B., 1994). Betonun üzerine değişik yönlerde uygulanan yükler, değişik etkiler yaratabilmektedir. Basınç, çekme, eğilme ve kayma etkisi yaratacak yükler altında betonun şekil değiştirmeye ve kırılmaya karşı göstereceği direnme kabiliyeti sırasıyla; basınç dayanımı, çekme dayanımı, eğilme dayanımı, kayma dayanımıdır (Erdoğan, 2003). Özellikleri en az bilinen ve incelenmiş yüklemelerden biri de çarpma yüklemesidir (Murtiadi, 1999). Çarpma yüklemesinde anlık yüksek değerlerdeki şiddet etkiyle meydana gelen gerilmeler diğer yükleme değerine göre daha fazladır. Çarpma sonucu oluşan dinamik etki, statik yüklemelere göre yapıda yüksek oranlarda ani gerilme artışları meydana getirmektedir. Bu gerilme artışları yapı elemanlarında anlık çatlamalara sebep olarak yapı güvenliğini olumsuz yönde etkilemektedir. Çarpma kuvvetlerinin oluşturduğu gerilmelerin yapı elemanları üzerindeki etkileri belirleyecek kesin bir yöntem olamaması ise bu konu üzerinde yapılan çalışmaların en büyük sorunudur. Kullanım amaçlarına göre beton ve betonarme yapı elemanları çarpma etkisi altında kalabilirler. Örneğin birçok beton ve betonarme yapılardan; döşeme kaplamaları, hava alanları, yollar, kazık ve palplanş başlıkları çarpma tesirine maruz kalabilmektedir. Bir malzeme üzerinde çarpma etkisi, yüzeyine bir cismin belirli yükseklikten düşmesi yolu ile olacağı gibi aniden uygulanan kuvvetler şeklinde de olabilir. Çarpma sonucunda bir cisimde gerilmeler çok kısa sürede büyük değerlere ulaşabilmekte, gerilme ve deformasyonlar karmaşık hale geldiği için teorik olarak irdelemesi zor olmaktadır. (Arıcı vd., 2007). Teknolojik gelişmelerle birlikte çelik ve beton gibi temel yapı malzemelerinin çarpma yükleri altında gösterdikleri davranış biçimi daha da önem kazanmıştır. Örneğin nükleer santrallerde reaksiyonlar sırasında ortaya çıkan yükler kısa sürede çok büyük değerlere ulaşabilmektedir (Kantar vd., 2011). Çarpma deneyleri yakın tarihimize kadar temel yapı malzemelerinden olan çelik üzerinde yoğunlaşmıştır. Fakat betonun aktif kullanımı yaygınlaştıkça, çarpma etkisi altında davranışı önem kazanmaya başlamıştır. Bu güne kadar yapılan çalışmalarda deney metotları ve prosedür hakkında herhangi bir standart oluşturulamamıştır (Arıcı vd., 2007; Selvi, 2008). Çarpma deneyleri, malzeme şekline ve cinsine bağlı olarak farklı şekillerde yapılabilmektedir. Bunlar;

a. Hareketli Sarkaç – Charpy (Edgington vd., 1974; Johnston, 1974) İzod (Arıcı, E., 2010).
b. Düşen Top – Düşme makinesinin farklı tipleri ise sabit yükseltideki düşüş veya değişken yükseltideki düşüş (Verhagen, 1978; Jamrozy vd., 1979).
c. Kesin bir yükseklikten düşürülen yapısal elemanlar (Barb vd., 1974).
d. Patlayıcı Maddeler (Verhagen, 1978; Jamrozy vd., 1979; Williamson, G. R., 1965) ‘dir.

Malzemelerin çarpma dayanım değerlerini tespiti etmek amacıyla malzemenin cinsine göre farklı deney metotlarını içeren standartlar mevcuttur. Çarpma dayanımının belirlenmesine yönelik son zamanlarda farklı çalışmalarda Charpy darbe deneyi üzerinde araştırmalar yapılmıştır (Arıcı, 2010). Darbe testinde dinamik bir yüklemeyle numunelerin kırılması için gerekli enerji belirlenir. Bu enerji miktarları numunelerin kesit alanına bölünerek darbe direnci değeri olarak çarpma dayanımını elde edilmektedir. Enerjinin korunumunun temel prensibindeki Charpy düzeneğinde; sarkaca belli bir yükseklikte enerji kazandırılır, sarkaç serbest bırakıldığında enerjinin bir kısmı numuneyi kırmada harcanırken geri kalanı ile sarkaç bir miktar daha yükselir. Şekil 1’deki Charpy deney düzeneğinde ağırlığı G olan sarkaç, $h_0$ yüksekliğinde potansiyel enerjisi ($Gxh_0$) yükseklikte maximum düzeydedir. Sarkaç bu yükseklikten serbest bırakıldığında, düşey bir doğrultuda salınarak numuneyi kırma işleminden sonra bir h yüksekliğine çıkmaktadır. Böylece bu kırılma işlemi sonrasındaki sarkaçta kalan potansiyel enerji (Gxh) yüksekliğindedir. Şekil 1’de gösterilen Charpy deney düzeneğinde enerjinin korunumu kanununda faydalanılarak hesaplamalar yapılmaktadır.

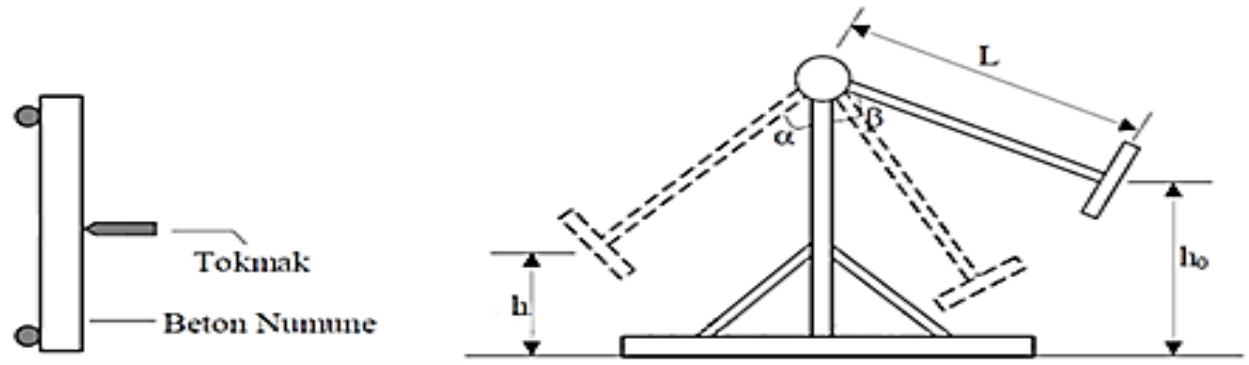


**Şekil 1.** Charpy Deney Düzeneği

Numunenin kırılmasında, sarkaçtaki tokmağın numune ile temas ettiği noktadaki enerjisi ile numunenin kırılma sonrasındaki sarkaçta kalan potansiyel enerjisi farkı o numunenin kırılması için gerekli enerjiyi göstermektedir. Bu formülle şu şekilde gösterilebilir.

$$U = G(h_0 - h) = GL(cos\beta - cos\alpha) \quad (1)$$

Burada, sarkaç tokmağının ilk ve son konum noktalarındaki potansiyel enerji farklarından elde edilen değerler bulunur ve bu değerler numunenin kesit alanları da hesaba katılarak çarpma mukavemeti formülle elde edilir.

$$Ç = \frac{U}{A} = \frac{G(h_0 - h)}{A} \quad (2)$$

## 2. Materyal ve Metot

Deneylerde kullanılan agrega, Elazığ ili, Palu ilçesinden temin edilmiştir. Mineralojik olarak nehir kumu niteliğinde olan agreganın özellikleri Tablo 1'de verilmiştir. Çimento olarak; Tablo 2'deki fiziksel ve kimyasal özelliği verilen Ergani Çimento Sanayi T.A.Ş 'nin üretimindeki CEM IV 32.5 R tipi kullanılmıştır. Deney numuneleri TS 802' ye göre hazırlanmış (Williamson, 1965) ve Tablo 3'de bu veriler gösterilmiştir. Numunelerin seri özeliklerine göre, maksimum dane çapları 4, 8 ve 16 mm olarak alınmıştır. Granülometrik bir karışım oluşturulması amacıyla TS 706'daki sınır değerlere uygun olarak ayarlanmıştır.

**Tablo 1.** Karışıma giren agregaya ait genel özellikler

| Özgül ağırlık ($gr/cm^3$) | Su emme (%) | Aşınma kaybı (%) | Kil miktarı (%) | Donma kaybı (%) |
|---|---|---|---|---|
| 2.48 | 4 | 16.6 | 2.0 | 1.83 |

**Tablo 2**. CEM IV 32.5 R Tipi çimentonun fiziksel ve kimyasal analizleri

| $SiO_2$ | $Al_2O_3$ | $Fe_2O_3$ | CaO | MgO | $SO_3$ |
|---|---|---|---|---|---|
| 26.86 | 8.09 | 5.18 | 45.88 | 3.64 | 2.41 |

| 45µ | Blaine | Priz b. | Priz s. | Öz. ağ. | Yoğunluk | H. gen. | 2 gün |
|---|---|---|---|---|---|---|---|
| 1.9 | 4326 | 2.35 | 3.45 | 2.98 | 925 | 4 | 16.9 |

Serilerin karışım hesaplamalarında, max. agrega çapı 4, 8 ve 16 mm., S/Ç (su/çimento) oranı ise 0.50 ve 0.55 olarak alınmıştır.

**Tablo 3.** Karışıma giren malzeme miktarları

| $D_{max}$ (mm) | S/Ç | Çimento (kg) | Su (kg) | Agrega (mm) | | |
|---|---|---|---|---|---|---|
| | | | | 0-4 | 4-8 | 8-16 |
| 4 | 0.50 (Seri 1) | 400 | 200 | 1564 | - | - |
| | 0.55 (Seri 2) | 357 | 197 | 1609 | - | - |
| 8 | 0.50 (Seri 3) | 380 | 190 | 1142 | 489 | - |
| | 0.55 (Seri 4) | 345 | 190 | 1162 | 498 | - |
| 16 | 0.50 (Seri 5) | 334 | 167 | 963 | 350 | 437 |
| | 0.55 (Seri 6) | 304 | 167 | 976 | 355 | 443 |

Basınç deneyleri 150x300 mm. lik silindir numunelerle, eğilmede çekme deneyleri 100x100x500 mm. lik kiriş numunelerde, yarma deneyleri 100x200 mm. lik silindir numunelerde ve Charpy darbe deneyleri ise 100x100x500 mm. lik numunelerde yapılmıştır. Betonun mekanik özellikleri ile çarpma dayanımları arasındaki ilişkinin belirlenmesi amacıyla, çarpma dayanım değerleri sırasıyla basınç dayanımının karekökü, eğilmede çekme dayanımı ve yarmada çekme dayanımları ile bölünerek "q" değeri elde edilmiştir.

$$q = \frac{Ç}{\sqrt{\sigma}} \quad (3)$$

Ayrıca $D_{max}$ (max. agrega çapı) ve S/Ç (su / çimento) oranlarına bağlı olarak dayanım değerlerindeki değişim oranları hesaplanmıştır. Aşağıda Tablo 4 ve Tablo 5'de bu değerler gösterilmektedir.

**Tablo 4**. Serilerin dayanım değerleri

| Seri No | Çarpma Dayanımı (Ç) (N.mm) | Basınç Dayanımı ($\sigma$) ($N/mm^2$) | $q_\sigma$ ($Ç/\sqrt{\sigma}$) | Eğilmede Çekme Dayanımı ($\sigma_E$) ($N/mm^2$) | $q_{\sigma E}$ ($Ç/\sigma_E$) | Yarma Dayanımı ($\sigma_ç$) ($N/mm^2$) | $q_{\sigma ç}$ ($Ç/\sigma_Ç$) |
|---|---|---|---|---|---|---|---|
| **S1** | 3.84 | 25.49 | 0.76 | 4.41 | 0.87 | 3.50 | 1.10 |
| **S2** | 3.65 | 20.63 | 0.80 | 3.39 | 1.08 | 2.79 | 1.31 |
| **S3** | 4.10 | 27.11 | 0.79 | 4.78 | 0.86 | 3.94 | 1.04 |
| **S4** | 3.92 | 23.48 | 0.80 | 4.55 | 0.97 | 3.09 | 1.25 |
| **S5** | 4.69 | 31.86 | 0.83 | 5.34 | 0.88 | 4.35 | 1.08 |
| **S6** | 4.49 | 28.84 | 0.84 | 4.64 | 0.97 | 3.47 | 1.30 |

**Tablo 5.** Agrega çapı ve S/Ç oranına göre dayanımlarındaki azalma yüzdeleri

| $D_{max}$ | S/Ç | Basınç Dayanımı | | Eğilme Dayanımı | | Yarma Dayanımı | | Çarpma Dayanımı | |
|---|---|---|---|---|---|---|---|---|---|
| | | N/mm$^2$ | % | N/mm$^2$ | % | N/mm$^2$ | % | N/mm$^2$ | % |
| **4** | 0.50<br>0.55 | 25.49<br>20.63 | 23.56 | 4.41<br>3.39 | 30.09 | 3.50<br>2.79 | 25.45 | 3.84<br>3.65 | 5.21 |
| **8** | 0.50<br>0.55 | 27.11<br>23.48 | 15.46 | 4.78<br>4.01 | 19.20 | 3.94<br>3.09 | 27.51 | 4.10<br>3.88 | 5.67 |
| **16** | 0.50<br>0.55 | 31.86<br>28.84 | 10.47 | 5.34<br>4.64 | 15.09 | 4.35<br>3.47 | 25.36 | 4.69<br>4.49 | 4.45 |

## 3. Sonuç ve Öneriler

Yapılan deneysel çalışmalardan elde edilen sonuçlar şunlardır.

a) Basınç dayanımı, eğilmede çekme ve yarmada çekme dayanımı değerleri agrega çapının büyümesine bağlı olarak artmıştır. Bu artış çarpma dayanımını da olumlu yönde etkilemiştir.
b) S/Ç oranının artışı ile basınç, eğilmede çekme, yarmada çekme ve çarpma dayanımları azalmıştır.
c) S/Ç oranındaki artış; basınç, eğilmede çekme ve yarmada çekme dayanımlarında aşırı derecede bir düşüşe sebep olurken, çarpma dayanımındaki düşme oranı % 5 gibi küçük bir değerde kalmıştır.
d) S/Ç oranı ve agrega çapındaki değişimle beraber dayanım değerlerindeki % değişimlerine bakıldığında; basınç ve eğilmede çekme dayanımlarında değişim geniş bir aralıkta olmasına karşın yarmada çekme dayanımı ve çarpma dayanım değişimleri ortalama olarak aynı değerlerde (% 25 ve % 5) kalmıştır.
e) Çarpma dayanımı hesaplandıktan sonra çekme dayanımı ile arasındaki ilişkinin belirlenmesi amacıyla çarpma dayanımı ile çekme dayanımı arasındaki oran (q) hesaplanmıştır. Bu değerlerden görüleceği üzere $d_{max}$ değerinin büyümesiyle beraber q değerinde de artış olmuştur. Aynı şekilde S/Ç oranının artması ile beraber q değerindeki artış devam etmiştir. Bunun sebebi S/Ç oranındaki artış, basınç, eğilme ve yarma dayanımlarını çok fazla düşürmesine karşın, çarpma dayanımındaki düşme miktarının daha küçük olmasıdır.

Charpy düzeneğinde deney esnasında bir miktar hesapta olmayan enerji kaybı meydana gelmektedir, bu kayıp deney sonuçlarına etki etmektedir. Fakat bütün deneyler aynı şartlar altında yapıldığından ve bu enerji kaybı değeri çok küçük olduğundan dolayı ihmal edilmiştir. Daha sağlıklı sonuçların elde edilmesi için, bu kayıp oranlarının tam olarak belirlenip, sonuç üzerinde etki ettirilmesi daha uygun olacaktır. Ayrıca yarma dayanımı ile çarpma dayanımı arasındaki ilişkinin daha net incelenmesi yararlı olacaktır.

## Kaynaklar

Arıcı, E., Dursun, R. ve İnce, R., 2007. Determination of Impact Strength of Concrete. 8th International Fracture Conference, November 2007, İstanbul, Turkey, 628-633.

Arıcı, E., 2010. Effect of Compressıve Strength on Impact Strength of Concrete. Journal of Technical, 9 (1), 1-9.

Barb, S., Hanson, D., 1974. Investigation of Fiber Reinforced Breakwater Armour Units. Fiber Reinforced Concrete Publication SP-44, American Concrete Institute, Detroit, 434 p.

Edgington, J., Hannant, D. J. ve Williams, G.I.T., 1974. Steel Fibre Reinforced Concrete. Building Research Establishment Current Paper, The Establishment, 46p.

Erdoğan, T.Y., 2003. Beton. ODTÜ Geliştirme Vakfı Yayıncılık ve İletişim A.Ş Yayınları, Ankara, 446p.

Jamrozy, Z. ve Swamy, R.N., 1979. Use of Steel Fibre Reinforcement for Impact Resistance and Machinery Foundations. International Journal of Cement Composites, 1 (2), 65-75.

Johnston, C. D., 1974. Steel Fiber Reinforced Mortar and Concrete. A Review of Mechanical Properties Fiber Reinforced Concrete, Publication SP-44, American Concrete Institute.Detroit, 127-142.

Kantar, E., Arslan, A. ve Anıl, Ö., 2011. Effect of Concrete Compressive Strength Variation on Impact Behaviour. Engineering Architecture Faculty journal Gazi University, 26 (1), 115-123.

Mather, B., 1994. Cement and Concrete Terminology. American Concrete Institute, 116 (R-90), 1-68.

Murtiadi, S., 1999. Behavior of High-Strength Concrete Plates under Impact Loading. Master Thesis, Faculty of Engineering and Applied Science Mernorial University of Newfoundland, 17p.

Selvi, M., 2008. Beton Dayanımındaki Değişimin Çarpma Dayanımına Olan Etkisinin Deneysel ve Sonlu Elemanlar Yöntemiyle İncelenmesi. Yüksek Lisans Tezi, Gazi Üniversitesi Fen Bilimleri Enstitüsü. Ankara,119 s.

Verhagen, A. H., 1978. Impact Testing of Fibre Reinforced Concrete: Reflection on Possible Test Methods, Testing and Test Methods of Fibre Cement Composites RILEM Symposium Edited by R. N. Swamy, The Construction Press Ltd., Hornby, p.99-105.

Williamson, G. R., 1965. Fibrous Reinforcements for Portland Cement Concrete. Technical Report. 1, 1-500.

**GÜFBED/*GUSTIJ* (2018) CMES 2018 SEMPOZYUM EK SAYISI: 112-118**
DOI: 10.17714/gumusfenbil.456858 Araştırma Makalesi / *Research Article*

# Para Kenmotsu Manifoldun Skew Semi İnvaryant Altmanifoldları

*Skew Semi Invariant Submanifolds of Para Kenmotsu Manifold*

**Ramazan SARI[*1,a], İnan ÜNAL[2,b], Elif AKSOY SARI[3,c]**
[1]*Gümüşhacıköy Hasan Duman Vocational Schools, Amasya University, Amasya, TURKEY*
[2]*Department of Computer Engineering, Munzur University, Tunceli, TURKEY*
[3]*Merzifon Vocational Schools, Amasya University, Amasya, TURKEY*

• Geliş tarihi / *Received*: 03.09.2018 • Düzeltilerek geliş tarihi / *Received in revised form*: 09.11.2018 • Kabul tarihi / *Accepted*: 15.11.2018

**Öz**
Bu çalışmada para Kenmotsu manifoldlaırn skew semi invaryant altmanifoldları çalışıldı. Bir örnek verildi ve distribüsyonların integrallenebilirlik şartları elde edildi. Para Kenmotsu space formun bu tür altmanifoldları incelendi ve bazı eğrilik özellikleri elde edildi. Son olarak para Kenmotsu manifoldların bir total geoedezik skew semi invaryant altmanifoldunun $\eta$-Einstein olduğu ispatlandı.

**Anahtar kelimeler:** Para Kenmotsu manifold, Para Kenmotsu uzay form, Skew semi invariant altmanifold

***Abstract***
*In this paper skew semi invariant submanifolds of para Kenmotsu manifold are studied. An example is given and integrability conditions of distributions are obtained. This kind of submanifolds of para Kenmotsu space form are examined and some curvature properties are obtained. Finally it is proved that a totally geodesic skew semi invariant submanifold of para Kenmotsu manifold is $\eta$-Einstein.*

***Keyword**: Para Kenmotsu manifold, Para Kenmotsu space form, Skew semi invariant submanifolds*

*[a] Ramazan SARI; ramazan.sari@amasya.edu.tr; Tel: (0536) 431 64 30; orcid.org/0000-0002-4618-8243
[b] [c]

## 1. Introduction

Para complex geometry is the geometry which is related to the algebra of para complex numbers (Cruceanu et al, 1996). The para complex structures is defined on a smooth manifold $M$ with the endomorphism $J: \Gamma(TM) \to \Gamma(TM)$, $J^2 = I$ such that the 1-eigen distributions are integrable and has the same dimension. There are some differences between para complex geometry and complex geometry. The product of two manifolds $M_+ \times M_-$ of the same dimension is the natural example of para complex manifold. These manifolds also have some applications in physics, they are related to supersymmetric field theories with Euclidean space time (Zamkovoy, 2009).

In 1985 Willams and Kaneyuki studied the almost para contact structure on $(2n+1)$-dimensional pseudo-Riemannian manifold $M$ and showed the almost paracomplex structure on the product manifold of $M$ and real line $\mathbb{R}$ (Kaneyuki and Willams, 1985). Also Zamkovoy (Zamkovoy, 2009) studied an almost paracontact metric manifold and their subclasses. Similar to contact manifolds some classes of para contact manifolds are defined and this notion studied by geometers. One of them is para Kenmotsu manifolds and we focused on this notion in this paper.

The almost semi invariant submanifold of a Sasakian manifold was studied by Bejancu and Papaghuic (Bejancu and Papaghuic, 1984). They also gave a classification for submanifold classes of a Sasakian manifold. Ronsse defined skew CR-submanifolds of Kaehler manifold, such a generalization of bi slant submanifold (Ronsse, 1990). After this notion is studied by several authors (Lui and Shao, 1999; Şahin, 2010).

Our aim in the present work is to extend the study of skew semi invariant submanifolds to the setting of a para Kenmotsu manifold. After giving fundamental facts about para Kenmotsu manifolds we examine the submanifolds of them. We recall the definition of skew semi invariant submanifold and we give an example. Morover we obtain integrability conditions of distributions. Then we give some curvature properties of skew semi invariant submanifold of para Kenmotsu space form. Finally we prove that a totally geodesic skew semi invariant submanifold of para Kenmotsu manifold is $\eta$-Einstein.

## 2. Preliminaries

**Definition 1** Let $\bar{M}^{(2n+1)}$ differentiable manifold and $\varphi$, $\eta$, $\xi$ ,g is (1,1)-tensor field, 1-form, a vector field and a pseudo-Riemannian metric on $\bar{M}$, respectively. If for all $W, Y \in \Gamma(T\bar{M})$ following conditions are satifeied then $\bar{M}$ called almost para contact metric manifold:

$$\varphi^2 W = \mu(W - \eta(W)\xi), \quad \eta(\xi) = 1 \tag{1}$$

$$g(\varphi W, \varphi Y) = -\mu(g(W, Y) - \varepsilon\eta(W)\eta(Y)) \tag{2}$$

where $\mu, \epsilon = \pm 1$. In addition, we have

$$\varphi(\xi) = 0, \ \ \eta o \varphi = 0, \ \eta(W) = \varepsilon g(W, \xi). \tag{3}$$

By this definition $\bar{M}$ is an almost contact metric manifold if $\mu = -1$. For an almost contact metric manifold by setting $\varepsilon = 1$ we get the signature of metric is equal to *2p*, and by setting $\varepsilon = -1$, the signature of metric is equal to $2p + 1$. Also $\bar{M}$ is an almost paracontact metric manifold if $\mu = 1$. In this case the signature of metric is equal to $n$ by setting $\varepsilon = 1$, or $n + 1$ by setting $\varepsilon = -1$ (Olszak, 2013).

**Definition 2** An almost para contact metric manifold $\bar{M}$ is normal if
$[\varphi, \varphi](W, Y) - 2d\eta(W, Y)\xi = 0$
for all $W, Y \in \Gamma(T\bar{M})$ ,where
$[\varphi, \varphi](W, Y) = \varphi^2[W, Y] + [\varphi W, \varphi Y] - \varphi[\varphi W, Y] - \varphi[W, \varphi Y]$ (Olszak, 2013).

**Proposition 1** On an almost para contact metric manifold for any $W, Y, U \in \Gamma(T\bar{M})$ we have

$$\begin{aligned} 2g\big((\bar{\nabla}_W \varphi)Y, U\big) = {} & 3d\Phi(W, \varphi Y, \varphi U) \\ & - 3d\Phi(W, Y, U) \\ & + g(N(Y, U), \varphi W) \\ & + \mu N^2(Y, U)\eta(W) \\ & + 2\mu d\eta(\varphi Y, W)\eta(U) \\ & - 2\mu d\eta(\varphi U, W)\eta(Y) \end{aligned}$$

where $\bar{\nabla}$ is Levi-Cevita connection on $\bar{M}$ and $N^2(W, Y) = 2d\eta(\varphi W, Y) - 2d\eta(\varphi Y, W)$.

**Definition 2** An almost para Kenmotsu manifold is an almost para contact metric manifold which has closed 1-form $\eta$ and $d\Phi = 2\eta \wedge \Phi$. If $\bar{M}$ is also normal then we call $\bar{M}$ is called a para Kenmotsu manifold.

**Theorem 1** M is para Kenmotsu manifold if and only if

$$(\bar{\nabla}_W \varphi)Y = g(\varphi W, Y)\xi - \eta(Y)\varphi W \tag{4}$$

for all $W, Y \in \Gamma(T\bar{M})$.

**Proof.** Let $\bar{M}$ be a para Kenmotsu manifold. From Proposition 1, $\forall\, W, Y \epsilon \Gamma(T\bar{M})$ we have

$$\begin{aligned} 2g((\bar{\nabla}_W \varphi)Y, U) = {} & 3d\Phi(W, \varphi Y, \varphi U) \\ & - 3d\Phi(W, Y, U)) \end{aligned}$$

From the definition of second fundamental form we get

$$g((\overline{\nabla}_W\varphi)Y,U) = -\eta(W)g(\varphi Y,\varphi^2U) + \eta(W)g(Y,\varphi U) - \eta(Y)g(U,\varphi W) - \eta(U)g(W,\varphi Y).$$

Therefore from (1) and (2) we obtain (4).
Conversely using (4), we get $\varphi\overline{\nabla}_W\xi = g(\varphi W,\xi)\xi - \eta(\xi)\varphi W$ and therefore $\overline{\nabla}_W\xi = \varphi^2 W$.
On the other hand for $\eta$ 1-form we have

$$d\eta(W,Y) = \frac{1}{2}\{g(Y,-\varphi^2W) - g(W,-\varphi^2Y)\} = 0$$

and this shows 1-form $\eta$ is closed. In addition since

$$3d\Phi(W,Y,U) = g(Y,(\overline{\nabla}\varphi)U) - g(U,(\overline{\nabla}_Y\varphi)W) - g(W,(\overline{\nabla}_U\varphi)Y)$$

and from (4), we have

$$\begin{aligned}3d\Phi(W,Y,U) = {} & \{g(\varphi W,U)g(Y,\xi) - \eta(U)g(Y,\varphi W) - g(\varphi Y,U)g(X,\xi) \\ & +\eta(U)g(W,\varphi Y) + g(\varphi U,Y)g(X,\xi) - \eta(Y)g(W,\varphi U)\} \\ = {} & 2\{\Phi(U,W)\eta(Y) + \Phi(W,Y)\eta(U) + \Phi(Y,U)\eta(W)\}\end{aligned}$$

Thus we get $d\Phi = 2\eta\wedge\Phi$. Moreover, the Nijenhuis tensor of $\varphi$ is

$$N_\varphi(W,Y) = \varphi(-\{g(\varphi W,Y)\xi - \eta(Y)\varphi W\} + \{g(\varphi Y,W)\xi - \eta(W)\varphi Y\}) + \{g(\varphi^2W,Y)\xi - \eta(Y)\varphi^2W\} - \{g(\varphi^2Y,W)\xi - \eta(W)\varphi^2Y\} = 0$$

Hence, $\overline{M}$ is normal. The proof is completed.
By above theorem we get following corollary.
**Corollary 1** For a para Kenmotsu manifold with $(M,\varphi,\xi,\eta,g)$ and $W,Y\in\Gamma(T\overline{M})$ we have

$$\overline{\nabla}_W\xi = \varphi^2W. \tag{5}$$

## 3.Submanifolds of Para Kenmotsu Manifold

Let $M^n$ be a submanfold of a para Kenmotsu manifold $\overline{M}^{(2n+1)}$. The fundamental equations of the submanifold theory for *M* are given by

$$\overline{\nabla}_W Y = \nabla_W Y - h(W,Y) \text{ (Gauss Equation)} \tag{6}$$

$$\overline{\nabla}_W V = -A_V W + \nabla^\perp_W V \text{ (Weingarten Equaiton)} \tag{7}$$

where $W,Y\in\Gamma(TM)$ and $V\in\Gamma(TM)^\perp$. In this equations *h* is denoting the second fundamental form, $\nabla^\perp$ is denoting the normal bundle connection and $A_V$ is shape operator associated with *V*. *A* and *h* related by

$$g(h(W,Y),V) = g(A_VW,Y)\,. \tag{8}$$

The mean curvature tensor *H* is defined by

$$H = \frac{1}{m}\sum_{k=1}^{m} h(e_k,e_k) \tag{9}$$

where $\{e_1,\dots,e_m\}$ is a local orthonormal basis of *TM*.

For every tangent vector field $W$ on $M$ we can write

$$\varphi W = TW + NW \tag{10}$$

where $TW$ (resp. $NW$) denotes the tangential (resp. normal) component of $\varphi W$ and for every normal vector field $V$ we can state

$$\varphi V = tV + nV \tag{11}$$

where $tV$ in the tangental component of $\varphi V$ and $nV$ is the normal one.
Now, for later use, we establish some results for a submanifold para Kenmotsu manifold.

**Proposition 2** On $M^n$ we have

$$(\nabla_W T)Y = A_{NY}W + th(W,Y) + g(TW,Y)\xi - \eta(Y)TW \tag{12}$$

$$(\nabla_W N)Y = nh(W,Y) - h(W,TY) - \eta(Y)NW \tag{13}$$

for all $W,Y\in\Gamma(TM)$
**Proof.** For any $W,Y\in\Gamma(TM)$ we have

$$(\overline{\nabla}_W\varphi)Y = \overline{\nabla}_W\varphi Y - \varphi\overline{\nabla}_W Y$$

Then, using (4), (6) and (7) we get

$$\begin{aligned}g(TW+NW,Y)\xi - \eta(Y)(TW+NW) &= \overline{\nabla}_W(TY+NY) - \varphi(\nabla_W Y + h(W,Y)) \\ &= \nabla_W TY + h(W,TY) - A_{NY}W + \nabla^\perp_W NY - T\nabla_W Y - N\nabla_W Y - th(W,Y) - nh(W,Y) \\ &= (\nabla_W T)Y + (\nabla_W N)Y + h(W,TY) - A_{NY}W - th(W,Y) - nh(W,Y)\end{aligned}$$

and thus we obtain

$$\begin{aligned}(\nabla_W T)Y + (\nabla_W N)Y &= g(TW+NW,Y)\xi - \eta(Y)TW - \eta(Y)NW \\ &\quad -h(W,TY) + A_{NY}W + th(W,Y) - nh(W,Y).\end{aligned}$$

By cosider tangent and normal components in this equation, (12) and (13) is obtanied.

## 4. Skew Invariant Submanifolds of Para Kenmotsu Manifold

In 1990, Ronsse defined skew semi invariant submanifold of a contact metric manifold. In this chapter we use this definition for para Kenmotsu manifolds.

**Definition 3** Let $(\bar{M}^{(2n+1)}, \varphi, \xi, g)$ be a para Kenmotsu manifold and $M^n$ be a submanifold of $\bar{M}$ which is tangent to $\xi$. For s distinct functions $\mu_1, \mu_2, \dots, \mu_s$ defined on M with values in the open interval $(0,1)$ such that TM is decomposed as $T-$ invariant and mutually orthogonal differentiable distributions given by

$TM = D^0 \oplus D^1 \oplus D^{\mu_1} \oplus \dots \oplus D^{\mu_s} \oplus \{\xi\}$

then M is called almost skew semi invairant submanifold of $\bar{M}$. For each $x \in M$, the distributions are ${D^0}_x = \ker(N)$, ${D^1}_x = \ker(T)$ and ${D^{\mu_i}}_x = \ker(T^2 + {\mu_i}^2 I)$, where I is the identity transformation and $\mu(x)$ belongs to closed real interval [0,1] such that $-\mu^2(x)$ is an eigenvalue of $T^2(p)$ (Ronsse,1990). Moreover if each $\mu_i$ is constant, then M is called a skew semi invariant submanifold.

An known example of para Kenmotsu manifold is $(\mathbb{R}^{2n+1}, \varphi, \xi, \eta, g)$. Now, we give a skew semi invairant submanifold example of $(\mathbb{R}^{2n+1}, \varphi, \xi, \eta, g)$.

**Example 1**

The para Kenmotsu structure on canonic contact manifold $(\mathbb{R}^{2n+1}, \varphi, \xi, \eta, g)$ is given by

$$\varphi(U_1, \dots, U_n, V_1, \dots, V_n, \xi) = (V_1, \dots, V_n, -U_1, \dots, -U_n)$$

$$\xi = \frac{\partial}{\partial z}, \qquad \eta = dz$$

$$g = e^{-2z} \sum_{i=1}^{n} [dx_i \otimes dx_i + dy_i \otimes dy_i] - \eta \otimes \eta$$

where $U_i, V_i, 1 \le i \le 2n$ are vector fields on $\mathbb{R}^{2n+1}$ (Olszak, 2013). Let consider a submanifold of $\mathbb{R}^9$ defined by

$$M = X(u, v, k, l, s, w, t) = (u, 0, k, s, v, l, \cos w, \sin w, t).$$

Then we have a local frame of TM by

$$e_1 = \frac{\partial}{\partial x_1}, \quad e_2 = \frac{\partial}{\partial y_1}, \quad e_3 = \frac{\partial}{\partial x_3}, \quad e_4 = \frac{\partial}{\partial y_2}, e_5 = \frac{\partial}{\partial x_4}$$
$$e_6 = \sin w \frac{\partial}{\partial y_3} + \cos w \frac{\partial}{\partial y_4}, \quad e_7 = \xi = \frac{\partial}{\partial z}$$

and

$${e_1}^* = \frac{\partial}{\partial x_2}, {e_2}^* = \frac{\partial}{\partial y_3}$$

from a basis of $T^{\perp}M$. We determine $D^0 = Sp\{e_1, e_2\}, D^1 = Sp\{e_3, e_4\}$ and $D^{\mu} = Sp\{e_5, e_6\}$. Thus we get $TM = D^0 \oplus D^1 \oplus D^{\mu}$ and M is a skew semi invariant submanifold of $\mathbb{R}^9$.

Now, let $M^n$ be an skew semi invariant submanifold of para Kenmotsu manifold $\bar{M}$. The projection morphisms of TM to the distributions $D^0, D^1$ and $D^{\mu}$ are denoted respectively by $P_0, P_1$ and $P_2$. Then for each $W \in \Gamma(TM)$ we have

$W = P_0 W + P_1 W + P_2 W + \eta(W)\xi.$ (14)

Thus from (10) we get $TW = TP_0 W + TP_2 W$ and $NW = NP_1 W + NP_2 W$.

By using (5), (6) and (14) and several computations we obtaion following propositions.

**Proposition 3** On M for $Y \in \Gamma(TM)$ we have

$$g(P_0 W, Y) = g(W, P_0 Y), \text{ for any } W, Y \in \Gamma(D^0) \quad (15)$$

$$g(P_1 W, Y) = g(W, P_1 Y), \text{ for any } W, Y \in \Gamma(D^1) \quad (16)$$

$$g(P_2 W, Y) = g(W, P_2 Y), \text{ for any } W, Y \in \Gamma(D^{\mu}) \quad (17)$$

$$g(P_i W, Y) = g(W, P_j Y), \text{ for any } W, Y \in \Gamma(TM), i \neq j \text{ and } i, j \in \{0,1,2\} \quad (18)$$

$$\nabla_W \xi = P_0 W, \ h(W, \xi) = 0 \text{ for any } W \in \Gamma(D^0) \quad (19)$$

$$\nabla_W \xi = 0, \ h(W, \xi) = P_1 W \text{ for any } W \in \Gamma(D^1) \quad (20)$$

$$\nabla_W \xi = \varphi T P_2 W, \ h(W, \xi) = \varphi N P_2 W \text{ for any } W \in \Gamma(D^{\mu}) \quad (21)$$

**Theorem 2** Let $M^n$ be skew semi invariant submanifold of para Kenmotsu manifold $\bar{M}$. The distrbution $D^0$ is not integrable.

**Proof** For all $W, Y \in \Gamma(D^0)$ and from equation (19)

$$\begin{aligned} g([W,Y],\xi) &= g(\nabla_W Y,\xi) - g(\nabla_Y W,\xi) \\ &= -g(Y,\nabla_W\xi) + g(W,\nabla_Y\xi) \\ &= g(Y,P_0W) - g(W,P_0Y) \\ &= 2g(W,P_0Y). \end{aligned}$$

Thus $D^0$ is integrable if and only if $g(W,P_0Y) = 0$. From (15) the proof is completed.

**Theorem 3** Let $M^n$ be skew semi invariant submanifold of para Kenmotsu manifold $\bar{M}$. The distribution $D^1$ is always integrable.

**Proof** for all $W, Y \in \Gamma(D^1)$, from (20)

$$\begin{aligned} g([W,Y],\xi) &= -g(Y,\nabla_W\xi) + g(W,\nabla_Y\xi) \\ &= -g(Y,\varphi TP_2W) + g(W,\varphi TP_2Y) \\ &= g(\varphi P_2Y, TP_2W) - g(\varphi P_2W, TP_2Y) \\ &= g(TP_2Y, TP_2W) - g(TP_2W, TP_2Y) \\ &= 0. \end{aligned}$$

**Theorem 5** Let M be skew semi invariant submanifold of para Kenmotsu manifold $\bar{M}$. The distrbution $D^0 \oplus \{\xi\}$ is always integrable if and only if $h(W,\varphi Y) = h(Y,\varphi W)$.

**Proof** For all $W, Y \in \Gamma(D^0 \oplus \xi\})$

$$\begin{aligned} \varphi([W,Y]) &= \varphi\bar{\nabla}_W Y - \varphi\bar{\nabla}_Y W \\ &= \bar{\nabla}_W\varphi Y - (\bar{\nabla}_W\varphi)Y - \bar{\nabla}_Y\varphi W - (\bar{\nabla}_Y\varphi)W \\ &= \nabla_W\varphi Y - h(W,\varphi Y) - g(\varphi W,Y)\xi - \eta(Y)\varphi W \\ &\quad + \nabla_Y\varphi W - h(Y,\varphi W) - g(\varphi Y,W)\xi - \eta(W)\varphi Y. \end{aligned}$$

Then we give $[W,Y] \in \Gamma(D^0 \oplus \xi\})$ if and only if $h(W,\varphi Y) = h(Y,\varphi W)$, where $\varphi([W,Y])$ shows the component of $\nabla_W Y$ from ortogonal complementary distribution of $D^0 \oplus \{\xi\}$ in M.

**Corollary 2** Let M be skew semi invariant submanifold of para Kenmotsu manifold $\bar{M}$. The distribution $D^1 \oplus \{\xi\}$ is always integrable if and only if $A_{\varphi Y}W = A_{\varphi W}Y$.

**Theorem 6** Let M be skew semi invariant submanifold of para Kenmotsu manifold $\bar{M}$. The distribution $D^0 \oplus D^1$ is not integrable.

**Proof** For all $W, Y \in \Gamma(D^0 \oplus D^1)$

$$\begin{aligned} g([W,Y],\xi) &= -g(Y,\nabla_W\xi) + g(W,\nabla_Y\xi) \\ &= g(Y,P_0W + P_1W) - g(W,P_0Y + P_1Y) \\ &= 2g(Y,P_0W) - 2g(W,P_1Y). \end{aligned}$$

Thus $D^0 \oplus D^1$ is integrable if and only if $g(Y,P_0W) = g(W,P_1Y)$. From (18) the proof is completed.

**Corollary 3** Let M be skew semi invariant submanifold of para Kenmotsu manifold $\bar{M}$. The distribution $D^0 \oplus D^\mu$ and $D^1 \oplus D^\mu$ is not integrable.

## 5. Skew Invariant Submanifolds of Para Kenmotsu Space Form

One of the special classes of contact manifolds is contact space form which has constant $\varphi$ −sectional curvature. In this section we study on skew semi invariant submanifolds of para Kenmotsu space forms. The Riemannian curvature of a submanifold of para Kenmotsu space form $\bar{M}$ is given by

$$\begin{aligned} R(W,Y,U,V) &= \frac{c+3}{4}\big(g(Y,U)g(W,V) - g(W,U)g(Y,V)\big) \\ &\quad + \tfrac{c-1}{4}(g(Y,\varphi U)g(\varphi W,V) - g(W,\varphi U)g(\varphi Y,V) - 2g(W,\varphi Y)g(\varphi U,V) \\ &\quad + g(W,U)\eta(Y)\eta(V) - g(Y,U)\eta(W)\eta(V) + g(Y,V)\eta(W)\eta(U) \\ &\quad - g(W,V)\eta(Y)\eta(U)) + g\big(h(W,U),h(Y,V)\big) - g(h(Y,U),h(W,V)). \end{aligned} \tag{22}$$

for all $W, Y, U, V \in \Gamma(TM)$, where c is constant $\varphi$ −sectional curvature of $\bar{M}$. Now, we define a local field of orthonormal frames $\{e_1, \dots, e_{2p}, e_{2p+1}, \dots, e_{2q}, e_{2q+1}, \dots e_{2r}, e_{2r+1}\}$ on skew semi invariant submanifold M. Then we have

$D^0 = sp\{e_1, \dots, e_{2p}\}$, $D^1 = sp\{e_{2p+1}, \dots, e_{2q}\}$, $D^2 = sp\{e_{2q+1}, \dots e_{2r}, e_{2r+1}\}$, $\xi = sp\{e_{2r+1}\}$

where $\dim D^0 = 2p, \dim D^1 = 2q$ and $\dim D^2 = 2r$.

**Corollary 4** For a skew semi invariant submanifold of para Kenmotsu space form we have

$$R(W,Y,U,V)=\frac{c+3}{4}\big(g(Y,U)g(W,V)-g(W,U)g(Y,V)\big)$$
$$+\frac{c-1}{4}(g(Y,\varphi U)g(\varphi W,V)-g(W,\varphi U)g(\varphi Y,V)-2g(W,\varphi Y)g(\varphi U,V)$$
$$+g\big(h(W,U),h(W,V)\big)-g(h(Y,U),h(W,V))$$

for all $W,Y,U,V\epsilon\Gamma(D^0)$.

**Proof** For all $W\epsilon\Gamma(D^0)$, from $\eta(W)=0$. Using (22), the desired equality is obtained.

**Theorem 7** Let M be skew semi invariant submanifold of para Kenmotsu space form $\bar{M}$ and $D^1$ be totally geodesic. Then M is flat if and only if $c=-3$.

**Proof** For all $W,Y,U,V\epsilon\Gamma(D^1)$ from (22) we have

$$R(W,Y,U,V)=\frac{c+3}{4}\big(g(Y,U)g(W,V)-g(W,U)g(Y,V)\big)+g\big(h(W,U),h(Y,V)\big)-g\big(h(Y,U),h(W,V)\big).$$

Since $D^1$ be totally geodesic then $h=0$ and so

$$R(W,Y,U,V)=\frac{c+3}{4}\big(g(Y,U)g(W,V)-g(W,U)g(Y,V)\big).$$

Thus M is flat if and only if $c=-3$.

**Theorem 8** Let M be a skew semi invariant submanifold of para Kenmotsu space form $\bar{M}$. If M is totally geodesic, then it is η-Einstein.

**Proof** Let M be totally geodesic skew semi invariant submanifold of para Kenmotsu space form $\bar{M}$. For all $W,Y\in\Gamma(TM)$ by using (22) the Ricci tensor is

$$S(W,Y)=\sum_{i=1}^{2p}R(W,E_i,E_i,Y)+\sum_{j=2p+1}^{2q}R\big(W,E_j,E_j,Y\big)+\sum_{k=2q+1}^{2r}R(W,E_k,E_k,Y)+R(W,\xi,\xi,Y)$$
$$=\Big(\frac{c+3}{4}(2p-1)-3\frac{c-1}{4}\Big)g(Y,U)+\sum_{i=1}^{2p}\{g\big(h(W,Y),h(E_i,E_i)\big)-g\big(h(E_i,Y),h(W,E_i)\big)\}$$
$$+\Big(\frac{c+3}{4}(2q-1)-3\frac{c-1}{4}\Big)g(Y,U)$$
$$+\textstyle\sum_{j=2p+1}^{2q}\{g\Big(h(W,Y),h\big(E_j,E_j\big)\Big)-g\Big(h\big(E_j,Y\big),h\big(W,E_j\big)\Big)\}$$
$$+\Big(\frac{c+3}{4}(2r-1)-3\frac{c-1}{4}\mu^2\Big)g(Y,U)+\sum_{k=2q+1}^{2r}\{g\big(h(W,Y),h(E_k,E_k)\big)$$
$$-g\big(h(E_k,Y),h(W,E_k)\big)\}+g(W,Y)-\eta(W)\eta(Y).$$

thus since $h=0$ we get

$$S(W,Y)=\Big(\tfrac{c+3}{4}(2p+2q+2r-3)-3\tfrac{c-1}{4}(2+\mu^2)+1\Big)g(W,Y)-\eta(W)\eta(Y).$$

**Corollary 5** Let M be an skew semi invariant submanifold of para Kenmotsu space form $\bar{M}$. Then the scalar curvature $\tau$ of M is given by

$$\tau=\Big(\frac{c+3}{4}(2p+2q+2r-3)-3\frac{c-1}{4}(2+\cos^2\theta)+1\Big)(2p+2q+2r+1)-1$$
$$+\tfrac{1}{(2p+2q+2r+1)^2}\|H\|^2+\|h\|^2.$$

**Acknowledgements**

This paper is supported by Amasya University research project (FMB-BAP 17-0284)

**References**

Bejancu, A. and Papaghiuc, N., 1984. Almost Semi Invariant Submanifolds of a Sasakian

Manifold. Bulletin Mathematique de la Societe des Sciences, 28(76), 13-30.

Cruceanu, V., Fortuny, P. and Gadea, P.M., 1996. A survey on paracomplex geometry. Rocky Mountain Journal of Mathematics, 26(1), 83-115.

Kaneyuki, S. and Willams, F.L., 1985. Almost paracontact and parahodge structures on manifolds. Nagoya Mathematical Journal, 99, 173-187.

Lui, X. and Shao, F.M., 1999. Skew Semi Invariant Submanifolds of a Locally Product Manifold. Portugaliae Mathematica, 56, 319-327.

Olszak, Z., 2013. The Schouten-Van Kampen Affine Connection Adapted to an Almost Para Contact Metric Structure. Publications De L'Institut Mathematique, 94(108), 31-42.

Ronsse, G.S., 1990. Generic and Skew CR-Submanifolds of a Kaehler Manifold. Bulletin of the Institute Mathematics Academia Sinica, 18, 127-141.

Şahin, B., 2010. Skew CR-waped product submanifolds of a Kaehler Manifolds. Mathematical Communications, 15, 189-204

Zamkovoy, S. 2009, Canonical connections on para contact manifolds. Annals of Global Analisis and Geometry, 36(1), 37-60.

**GÜFBED/*GUSTIJ* (2018) CMES 2018 SEMPOZYUM EK SAYISI: 119-124**
DOI: 10.17714/gumusfenbil.427696 Araştırma Makalesi / *Research Article*

# Hybrid DE - HS Algorithm with Randomized Parameters

*Rastgele Değişkenli Melez DG-HA Algoritması*

**Ezgi DENİZ ÜLKER***
*European University of Lefke, Engineering Faculty, Computer Engineering Department, Mersin-10, TURKEY.*

• Geliş tarihi / *Received*: 28.05.2018 • Düzeltilerek geliş tarihi / *Received in revised form*: 21.11.2018 • Kabul tarihi / *Accepted*: 23.11.2018

**Abstract**
The evolutionary algorithms and their hybrid methods are quite efficient and accurate in terms of solution quality of optimization. In this study, a new hybrid algorithm is generated by merging Differential Evolution (DE) and Harmony Search Optimization (HS) algorithms which is called DES. The core steps of the algorithms are used without any modifications, but the main control parameters which directly affect the performance are randomized. The experimental study is done by comparing DE, HS and their hybrid method DES. According to the results, it is found that DES algorithm has improved the performances of original algorithms for the selected test problems.

**Keywords:** Differential evolution, Evolutionary algorithms, Harmony search, Hybridization, Random parameters

***Öz***
*Evrimsel algoritmalar ve onları kullanarak yaratılan melez algoritmalar optimizasyon problemlerini çözmede etkili ve doğru sonuçlar üretirler. Bu çalışmada, Diferansiyel Gelişim (DG) algoritması ve Harmoni Arama (HA) algoritması birleştirilerek yeni bir melez algoritma oluşturulmuştur. Birleştirilen algoritmaların ana basamakları herhangi bir performans yükseltme yapılmadan kullanılmıştır, ancak performans üzerinde doğrudan etkisi olduğu bilinen ana kontrol değişken değerleri için rastgele seçim yapılmıştır. Deneysel çalışma, birleştirilen DG ve HA algoritmaları ile onların oluşturduğu DES algoritması arasında yapılmıştır. Elde edilen sonuçlara göre melez algoritma DES, diğer iki algoritmaya göre daha iyi bir performans göstermiştir.*

***Anahtar kelimeler:*** *Diferansiyel gelişim, Evrimsel algoritmalar, Harmoni arama, Melezleme, Rastgele değişkenler*

*Ezgi DENİZ ÜLKER; eulker@eul.edu.tr; Tel: (0392) 660 20 00; orcid.org/0000-0002-9642-7301

## 1. Introduction

In past, optimization problems were handled by researchers using large variety of algorithms (Sama et al., 2016; Ülker, 2017; 2017, Şimşek and Şimşek, 2017). Solving a complex optimization problem is quite challenging, since there are more than one design variables. Moreover, the algorithm generally focuses on finding the global optimum point, but it may be trapped into one of the local optimum points of given problems. Therefore, classical methods may not be efficient by alone for solving complex optimization problems.

Also, as it is known from *No Free Lunch* theorem, some optimization algorithms are quite effective for solving some problems, while ineffective for other problems or in other words there is no optimization algorithm that is able to to solve all kinds of problems (Wolpert and William, 1997). Instead of proposing new optimization methods, by using the advantages of previously introduced and proved to be effective ones can be used in the process of optimization.

Among the large variety of algorithms; DE and HS have the significant performance for solving complex problems from different areas (Qui et al., 2016; Kukkonen and Carlos, 2017). DE has distinctive attributes which provide some advantages in optimization with respect to classical methods. DE uses mutation and crossover operations to generate a new vector by using the existing ones. It uses crossover rate (CR) and differential weight (F) as main control parameters to avoid from local optima and to explore better areas in the search space (Qui et al., 2016). Additionally, HS algorithm can produce noticeable results by using its advantages. It optimizes a problem by generating a new vector which is derived from existing ones with its control parameters. The algorithm has an easy implementation with less number of steps. Besides the remarkable advantages of DE and HS, it is studied that both of the algorithms have high parameter dependency (Tvrdik, 2006; Chen et al., 2012; Gao et al., 2015; Chellaswamy et al., 2016; Qui et al., 2016; Wang et al., 2016; Roy et al., 2016). DE and HS need to optimize their control parameters for every problem to be handled. The algorithms DE and HS are designed in a way that a balance between exploration and exploitation characteristics is attained by applying the best combinations of their control parameters. It is seen that main control parameters effect the performance of the algorithms by controlling exploration and exploitation abilities. Therefore, there is a direct link between the selection of control parameters and the convergence rate of an algorithm. In this paper, DE and HS algorithms are hybridized to solve complex optimization problems by minimizing the disadvantages which are caused by control parameters tuning. In order to observe the improvement on the performance of the hybridized DE/HS algorithm (DES), it is compared with the original algorithms that is derived from. The experimental analysis is done by performing some complex benchmark functions.

The rest of the paper is organized as follows; section 2 shows the hybrid algorithm DES with its main steps. Section 3 describes some of the complex optimization tasks and the experimental results achieved. Lastly, section 4 gives the concluding remarks of this paper.

## 2. Hybrid DE/HS Algorithm (DES)

DE algorithm is known as a metaheuristic algorithm (Storn and Price, 1997) which tries to optimize the given problem in a large search space by avoiding local optimum points. It mainly considers two control parameters differential weight (F) and crossover rate (CR) which have great influence on the performance of DE. HS algorithm simply mimics the process of composers, when they compose a melody in a harmony. It produces a new solution vector after considering present vectors. This feature helps HS to obtain the optimum solution at a reasonable time. However, likewise DE algorithm, HS algorithm needs to perform fine tuning of its control parameters (Geem et al., 2001; Wang et al., 2013). The performance of HS generally relies on its main control parameters which are pitch adjusting rate (par), fretwidth (fw) and harmony memory considering rate (HMCR).

Based on the facts above, it can be said that both of the algorithms can produce remarkable results, if their control parameters are optimized for each task. However, finding the best combination values of control parameters for each task is not a time efficient process. Therefore, the control parameters are optimized in the given intervals defined in the literature.

In order to have their great potentials in solving problems, both of the algorithms are merged without any modifications on their main steps in hybrid algorithm DES. Additionally, the algorithm uses an equal random selection process

to select the steps of DE an HS. Therefore, neither DE nor HS algorithm manipulate the process of optimization by alone. There are similar methods of hybridization which considers DE and HS algorithms in literature (Chakraborty et al., 2009; Wang et al., 2009), but DES algorithm can be distinguished from the others as giving an equal chance to the main steps of the algorithms without any modifications and as randomizing main control parameters of the algorithms. It is aimed to have a hybrid DES algorithm which is not sensitive to the set of control parameters with good convergence rate. The main steps of hybridized DES algorithm are shown in Figure 1.

Selection of DE part in DES algorithm relies on 3 main functions:

$$V_i = X_a + F(X_b + X_C) \quad (1)$$

where $V_i$ is the mutant vector and $a$, $b$ and $c$ are the distinct members in the population. $F$ is a control parameter for DE in the interval [0-2].

$$U_{ij} = \begin{cases} V_{ij} & if\ \ r_j \le CR \\ X_{ij} & Otherwise \end{cases} \quad (2)$$

where $U_{ij}$ is the trial vector which is generated by crossover of $X_{ij}$ and $V_{ij}$. $r_j$ is a uniformly distributed random number for each member in the population and $CR$ is a control parameter for DE in the interval [0-1].

$$X_{ij} = \begin{cases} U_i & if\ \ f(U_i) \le f(X_i) \\ X_i & Otherwise \end{cases} \quad (3)$$

where $X_{ij}$ is the member which will survive for the next generation.

Selection of HS part in DES algorithm depends on 2 main functions:

$$X_{ij} = \begin{cases} selection\ from\ candidate\ population, & if\ \ r_1 < HMCR \\ randomly\ generation\ of\ a\ candidate, & Otherwise \end{cases} \quad (4)$$

where $r_1$ is a random number between (0-1) and *HMCR* is a control parameter of HS in the interval [0-1].

$$X_{ij} = \begin{cases} X_i + rand * fw, & if\ \ r_2 < par \\ X_i, & Otherwise \end{cases} \quad (5)$$

where $r_2$ is a random number between (0-1) and *fw* and *par* are the control parameters of HS in the intervals 0.01*range and [0-1], respectively.

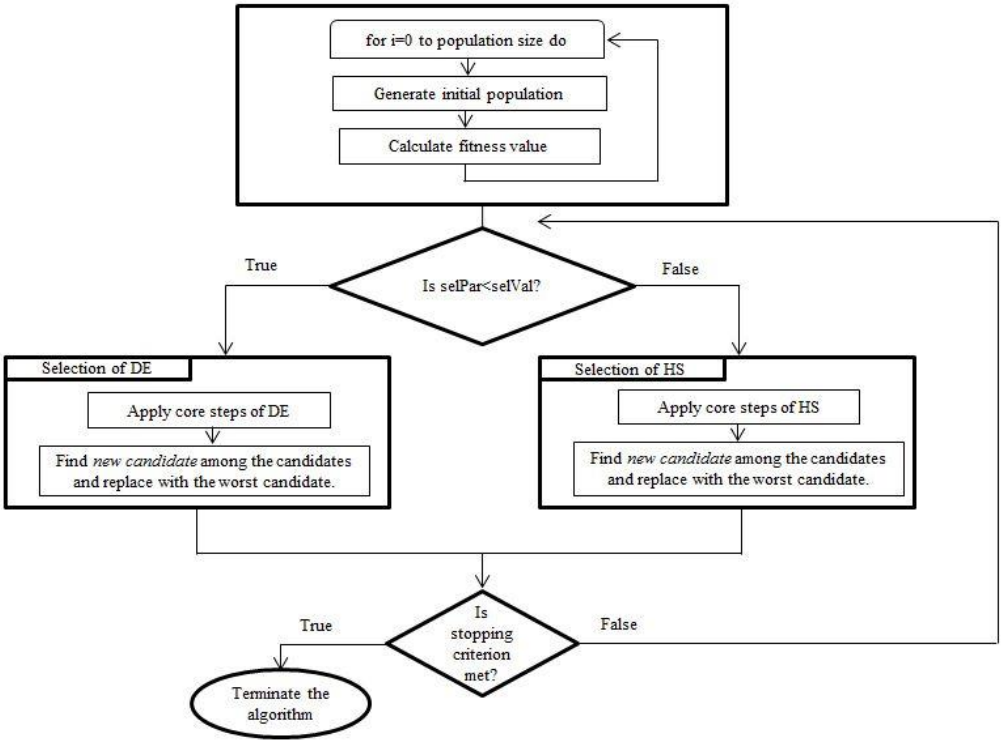


**Figure 1.** Main steps of hybrid DES algorithm.

The algorithm starts by initializing the population *X* by generating random values in the search space. Then, the selection process performed among the core steps of DE and HS algorithms. The hybrid DES algorithm gives an equal probability of selecting the steps of DE and HS. In the selection step, DES algorithm uses two selection parameters; *selPar* and *selVal*. The randomized paradigm is again considered for these control parameters. *selPar* and *selVal* are randomized in the range [0-1]. The performance of the algorithm relies on the frequency of use of the algorithms DE and HS. However, in this experiment the same chance of use is given to both of the algorithms. According to the selection done, the population is updated either by DE or HS at a time. Both of the algorithms uses their control parameters to obtain the global optimum value by avoiding local optimum points. The fine-tuning of these parameters is eliminated by assigning random values in predefined ranges. The algorithm repeats its steps until the stopping criterion is satisfied. At the end, the algorithm returns the optimal solution with a corresponding function value.

## 3. Experimental Results and Discussions

The hybridized algorithm DES and its originals DE and HS are compared by using some optimization problems taken from literature (Mahdavi et al., 2007). The optimization problems are selected in a way that they have multiple constraints and unknowns which show the effectiveness of the selected algorithms. The optimization problems selected for this experiment and the known optimum values are shown in Table 1 (Mahdavi et al., 2007).

**Table 1.** Information of test problems.

| Problem description | Problem formulation | Optimum value |
|---|---|---|
| Pressure Vessel Design | $f(x) = 0.6224x_1x_3x_4 + 1.7781x_2{x_3}^2 + 3.1661{x_1}^2x_4 + 19.84{x_1}^2x_3$<br>$g_1(x) = -x_1 + 0.0193x_3 \le 0,$<br>$g_2(x) = -x_2 + 0.00954x_3 \le 0,$<br>$g_3(x) = -\pi{x_3}^2x_4 - \frac{4}{3}\pi{x_3}^3 + 1296000 \le 0,$<br>$g_4(x) = x_4 - 240 \le 0.$ | 5849.76169 |
| Constrained function V | $f(x) = ({x_1}^2 + x_2 - 11)^2 + (x_1 + {x_2}^2 - 7)^2$<br>$g_1(x) = 4.84 - (x_1 - 0.005)^2 - (x_2 - 2.5)^2 \ge 0,$<br>$g_2(x) = {x_1}^2 + (x_2 - 2.5)^2 - 4.84 \ge 0,$<br>$0 \le x_1 \le 6, \quad 0 \le x_2 \le 6.$ | 13.590841 |
| Unconstrained function I | $f(x) = \exp\left\{\frac{1}{2}({x_1}^2 + {x_2}^2 - 25)^2\right\} + sin^4(4x_1 - 3x_2) + \frac{1}{2}(2x_1 + x_2 - 10)$ | 1.0000 |

For all of the algorithms in this experiment, the random values are assigned to the control parameters between the predefined intervals in each iteration found in the literature. The population size and dimension are fixed to 100 and 50. The maximum number of iterations is selected as a stopping criterion and is assigned to 500,000 for each algorithm. The results are tabulated in Table 2 which are averaged over 30 trials.

**Table 2.** A comparative table obtained by DES and its originals.

| Problem description | DES | DE | HS |
|---|---|---|---|
| Pressure Vessel Design | 5997.7542 | 6112.1128 | 6349.3427 |
| Constrained function V | 13.590843 | 13.591062 | 13.590950 |
| Unconstrained function I | 1.000 | 0.99998 | 0.99997 |

For the first problem, it is aimed to minimize the objective function by considering four design variables; $x_1$, $x_2$, $x_3$ and $x_4$, four constraints; $g_1(x)$, $g_2(x)$, $g_3(x)$ and $g_4(x)$. Due to the complexity of this test function, the results obtained by the originals are slightly far from the global optimum value. However, using the advantages of originals together in DES provides better result. According to the best $f(x)$ value; the values for $x$ [0.8036, 0.3972, 41.6392, 182.4120] and the $g(x)$ values [3.65E-05, 3.79E-05, -1.5914, -57.5879] are obtained.

For the second problem, the objective function is needed to be minimized with two design variables; $x_1$ and $x_2$, two constraints; $g_1(x)$ and $g_2(x)$, and also four boundary conditions. The problem can be stated as complex because of the presence of constraints. According to the best $f(x)$ value; the values for $x$ [2.25, 2.38] and the $g(x)$ values [0.00, 0.22] are obtained. All of the algorithms approached to the optimum value of the given problem, but it is seen that the hybrid algorithm DES has more precise value of objective function than the others.

For the third problem, the objective function has two design variables $x_1$ and $x_2$ without any constraints. The original algorithms DE and HS find the global optimum value of given problem, but in terms of accuracy DES algorithm provides a better solution than the originals. According to the best $f(x)$ value; the values for $x$ [3.00, 3.99] are obtained.

## 4. Conclusions

The paper has presented a hybridized version of DE and HS algorithms which has an advantage over the originals in terms of solution quality. The control parameters have strong impacts on the performance of the algorithms. In hybridized algorithm DES, it is aimed to reduce undesirable effects that are directly related to the selecting or tuning the control parameters. On the other hand, DES does not underestimate the positive effects of control parameters in terms of exploration and exploitation characteristics of an algorithm. Therefore, the control parameters are not neglected both in the originals and their hybrid version DES. The hybrid algorithm DES can be differentiated from the other hybridization techniques by randomizing control parameters and by giving an equal chance to the originals in merging process without altering them.
The original algorithms and hybrid DES algorithm are compared for some test functions. DES algorithm achieves efficient results as well as its originals in finding global optimum by using its main control parameters. However, in terms of solution quality the results by DES are more efficient and accurate for the selected test functions. As a future work, different probability values of selecting original algorithms can be studied and the effects can be obtained on the performance of DES.

## References

Chakraborty, P., Roy, G.G., Das, S., Jain, D. and Abraham, A., 2009. An Improved Harmony Search Algorithm with Differential Mutation Operator, Fundamenta Informaticae, 95, 401-426.

Chellaswamy, C. and Ramesh, R., 2016. Parameter Extraction of Solar Cell Models Based on Adaptive Differential Evolution Algorithm, Renewable Energy, 97, 823-837.

Chen, J., Pan, Q.K. and Li, J.Q., 2012. Harmony Search Algorithm with Dynamic Control Parameters, Applied Mathematics and Computation, 219, 592-604.

Delice, Y., Aydoğan, E.K., Özcan, U. and İlkay, M.S., 2017. A Modified Particle Swarm Optimization Algorithm to Mixed-Model Two-sided Assembly Line Balancing, Journal of Intelligent Manufacturing, 28, 23-36.

Gao, X.Z., Govindasamy, V., Xu, H., Wang, X. and Zenger, K., 2015. Harmony Search Method: Theory and Applications, Computational Intelligence and Neuroscience,1-10.

Geem, Z.W., Kim, J.H. and Loganathan, G.V, 2001. A New Heuristic Optimization Algorithm: Harmony search, Simulation, 76, 60-68.

Kukkonen, S.and Carlos, A.C., 2017. Generalized Differential Evolution for Numerical and Evolutionary Optimization, Springer International Publishing, 253-279.

Mahdavi, M., Fesanghary, M.and Damangir, E., 2007. An Improved Harmony Search Algorithm for Solving Optimization Problems, Applied mathematics and computation, 188, 1567-1579.

Qui, X., Xu, J.K., Tan, K.C. and Abbas, H.A., 2016. Adaptive Cross-Generation Differential Evolution Operators for Multiobjective Optimization", IEEE Transactions on Evolutionary Computation, 20, 232-244.

Roy, N., Ghosh, A.and Sanyal, K., 2016. Normal Boundary Intersection Based Multi-objective Harmony Search Algorithm for Environmental Economic Load Dispatch problem, IEEE International Conference on Power Systems, 1-6.

Sama, M., Pellegrini, I, P., D'ariana, A., Rodriguez, J. and Pacciarelli, D., 2016. Ant Colony Optimization for the Real-Time Train Routing Selection Problem, Transportation Research Part B: Methodological, 85, 89-108.

Storn, R. and Price, K., 1997. Differential Evolution–A Simple and Efficient Heuristic for Global Optimization Over Continuous Spaces", Journal of global optimization, 11, 341-359.

Şimşek, B. and Şimşek E.H., 2017. Assessment and Optimization of Thermal and Fluidity Properties of High Strength Concrete via Genetic Algorithm, An international journal of optimization and Control: Theories&Applications (IJOCTA), 7 , 90-97.

Tvrdik, J., 2006. Competitive Differential Evolution and Genetic Algorithm in GA-DS Toolbox, Technical Computing Prague, Praha, Humusoft, 99-106.

Ülker, E.D., 2017. A PSO/HS Based Algorithm for Optimization Tasks, IEEE Xplore Computing Conference Proceedings 2017, London, 117-120.

Ülker, E.D., 2018. An Elitist Approach for Solving the Traveling Salesman Problem using an Animal Migration Optimization Algorithm, Turkish Journal of Electrical Engineering & Computer Sciences, 1, 605-617.

Wang, G.G., Gandomi, A.H., Zhao, X. and Chu, H.C.E., 2016. Hybridizing Harmony Search Algorithm with Cuckoo Search for Global Numerical Optimization, Soft Computing, 20, 273-285.

Wang, L. and Lingp-Po, L., 2013. An Effective Differential Harmony Search Algorithm for the Solving Non-convex Economic Load Dispatch Problems, International Journal of Electrical Power & Energy Systems, 44, 832-843.

Wolpert, D.H. and William, G. M., 1997. No Free Lunch Theorems for Optimization,1997, IEEE Transactions on Evolutionary Computation, 1, 67-87.

## 1. KAPSAM ve GENEL BİLGİ

Gümüşhane Üniversitesi Fen Bilimleri Enstitüsü Dergisi (GUFBED), Gümüşhane Üniversitesi Fen Bilimleri Enstitüsü'nün yayın organıdır. Dergi kapsamında bütün Fen, Teknoloji, Mühendislik, Tarım ve Mimarlık Alanlarında daha önce başka yerlerde yayınlanmamış, özgün, araştırma makaleleri, derlemeler ve editöre mektuplar yayınlanır (Anket çalışmaları dergimizin konu kapsamına uygun değildir). Dergi ***bilimsel ve hakemli*** bir dergi olup, Ocak ve Temmuz aylarında olmak üzere yılda iki kez çevrimiçi ortamda yayımlanır.

Derginin amacı araştırma ve geliştirme faaliyetlerinin bilimsel yayına dönüştürülmesi, ulusal ve uluslararası indekslere girerek evrensel bilime katkı sağlamaktır.

## 2. YAYIN DİLİ ve ANLATIM

Dergide yayınlanacak tüm yazılar için yayın dili 2018'den itibaren olmak üzere Türkçe ve İngilizce'dir. Anahtar kelimeler alfabetik sıralamaya uygun olarak verilir. İngilizce anahtar kelimeler (Keywords) ise yine bu sıralama dikkate alınarak yazılır.

Makale içerisinde yazar tarafından gerçekleştirilen çalışmalara yönelik (Deneysel çalışmalar, analizler vb) anlatımlarda **üçüncü şahıs kullanılmaya özen gösterilmelidir.**

## 3. ELEKTRONİK ORTAMDA BAŞVURU

Dergi ile ilgili ***tüm yazışmalarda*** DergiPark tarafından sağlanan arayüz kullanılmalıdır. Dergi ***yazım kurallarına uygun olarak hazırlanmış*** makaleler, basılı kopyaya gerek olmaksızın, Ulakbim Dergipark üzerinden http://dergipark.ulakbim.gov.tr/gumusfenbil adresi kullanılarak gönderilmelidir. Dergiye makale göndermek isteyen yazarların yazım kuralları ile birlikte "**Gönderi Kontrol Listesi"**ndeki her maddeyi de kontrol etmeleri gerekmektedir. Makaledeki bilgilerin doğruluğunun sorumluluğu yazar(lar)a aittir.

Yayınlanacak makalelerde, araştırma ve yayın etiğine uygunluk esastır. **"Makale Gönderimi ve Telif Hakkı Devir Formu"** doldurulup bütün yazarlar tarafından imzalanmalıdır. Yayın ile ilgili işlemler bu formun tesliminden sonra başlar. Bu formun farklı kopyaları başka şehirlerde yaşayan yazar(lar) tarafından ayrı ayrı imzalanıp gönderilebilir.

Hayvanların veya zararlı maddelerin kullanıldığı araştırmalarda "**Etik Kurul İzin Belgesi**"nin makaleye eklenmesi gerekir. İnsanların denek olarak kullanıldığı araştırma sonuçlarını içeren makalelerde yazar(lar), "insan denemeleri üzerinde yetkili kurul" etik standartlarına ve gözden geçirilmiş Helsinki bildirgesi 1983'e uygunluğunu belgelemeleri gerekir.

## 4. DEĞERLENDİRME SÜRECİ

Gümüşhane Üniversitesi Fen Bilimleri Enstitüsü Dergisi'ne iletilen yazılar öncelikle dergi baş editörünün yönlendireceği bölüm editörü tarafından konu başlığı ve anahtar kelimelere dayanılarak biçimsel açıdan değerlendirilir. Bu ön kontrol aşamasında öncelikle intihal tespit yazılımları kullanılarak benzerlik raporları oluşturulur. Aday yayının benzerlik raporu toplamda %30, tek bir kaynaktan ise %5 oranından fazla olmamalıdır. Daha sonra incelenecek yayının dergi formatına uygun olup olmadığına karar verilir. "Makale Gönderimi ve Telif Hakkı Devir Formu" olmayan veya eksik olan aday yayınlar ile benzerlik oranı sınırlarını aşan aday yayınlar ön incelemeye alınmaz. Dergi yazım kurallarına uygun hazırlanmayan makaleler düzeltilmek üzere yazara geri gönderilir.

Formata uygun olarak hazırlanan yazılar dergi baş editörü tarafından inceleme sürecinin gerçekleştirilmesi için ilgili bölüm editörüne yönlendirilir.

Bölüm editörü bilimsel içerik bakımından değerlendirilmek üzere aday yayını, konusuna uygun olarak en az üç hakeme yönlendirir. Hakem seçiminde öncelikle konu ile ilgili dergi yayın danışma kurulu üyelerinden ya da alanında uzman başka bir bilim insanından yararlanılır. Hakemler değerlendirmeleri sonucunda, uygun, düzeltilerek yayınlanabilir, düzeltildikten sonra tekrar görmek isterim, istediğim düzeltmelerin kontrolünü derginin uzman bilimsel ekibi tarafından yapılması uygundur veya yayınlanamaz şeklinde kararları verebilirler.

Düzeltme istenen yazılarla ilgili olarak yazar gerekli düzeltmeleri yapar. Ayrıca katılmadığı hususlarla ilgili olarak gerekçeli yazısını dergiye gönderir.

Hakem kurulu tarafından farklı türde değerlendirilen yazılar için bölüm editörü kendi görüşünü de ekleyerek değerlendirmenin sonuçlandırılması için baş editöre iletir. Değerlendirmede son karar baş editöre aittir. Baş editör gerekli görürse yeni bir hakem tayin eder veya yazı ile ilgili kararını sonuçlandırır.

Tüm değerlendirmeler sonucunda kabul ya da red kararı gerekçeleri ile birlikte DergiPark üzerinden yazışmadan sorumlu yazara iletilir.

Değerlendirme sonucu kabul edilen makaleler dergi sekreteryası tarafından esasa bağlı kalınarak yayına uygun formata dönüştürülür.

Dergide yayımlanan makaleler başka hiç bir yerde yayımlanamaz veya bildiri olarak sunulamaz. Kısmen veya tamamen yayımlanan makaleler kaynak gösterilmeden hiçbir yerde kullanılamaz. Dergiye gönderilen makalelerin içerikleri özgün, daha önce herhangi bir yerde yayımlanmamış veya yayımlanmak üzere gönderilmemiş olmalıdır. Değerlendirmeye sunulacak çalışmaların bir başka dergiye gönderilmediği veya basılmadığı ön yazı ile belirtilmelidir.

Makale basım için kabul edilmezse “Makale Gönderimi ve Telif Hakkı Devir Formu” nun yasal bir önemi kalmaz ve hükümsüz olarak kabul edilir. Bu Form’un imzalanması ile yazarlar, makalenin “GÜMÜŞHANE ÜNİVERSİTESİ FEN BİLİMLERİ ENSTİTÜSÜ DERGİSİ” dergisi ve web sayfasında yayınlamasına ilaveten makalenin tamamı veya bir kısmının yasal olarak çoğaltılması ve dağıtılması hakkını Gümüşhane Üniversitesi Fen Bilimleri Enstitüsü’ne devrederek, kendi haklarından feragat etmektedirler.

## 5. MAKALE TÜRLERİ

**Dergide yayınlanan farklı yayın formatları ile ilgili bilgiler ve yazı türlerine göre yazarların dikkat etmeleri gereken hususlar şu şekildedir:**

**5.1 Araştırma Makaleleri:** Türkçe Başlık, İngilizce Başlık, Yazarlar, Adresler, Türkçe Öz, Türkçe Anahtar Kelimeler, İngilizce Öz, İngilizce Anahtar Kelimeler, Giriş, Amaç, Gereç ve Yöntem, Bulgular, Tartışma ve Sonuçlar, gerekli ise Etik konular, Katkı Belirtme ve Teşekkür, Kaynaklar, Şekil ve Tablolarla ilgili açıklamalar içermelidir. Makale konunun uzmanları tarafından tekrarlanabilecek şekilde yeterli bilgiyi içermelidir. **Bu tür makalelerde ana metin 3500-4000 kelime arası olmalı, kaynak sayısı 40’ı aşmamalıdır.**

**5.2 Derlemeler:** Yazar(lar)ın uzmanlık alanında yapılmış eski araştırmaların derlenip eleştirel bir şekilde yorumlanıp ortaya yeni bir görüş ileri süren çalışmaları kapsamalıdır. **Bu tür makale öneren yazar(lar)ın en az 10 SCI-Expanded makalesi bulunmalı ve bunların en az 5 tanesi derleme yaptığı alanda olmalıdır.** Derlemeler, Türkçe Başlık, İngilizce Başlık, Yazarlar, Adresler, Türkçe Öz, Türkçe Anahtar Kelimeler, İngilizce Öz, İngilizce Anahtar Kelimeler, Giriş, Ana Bölümler, Alt Bölümler, Sonuç, Katkı Belirtme ve Teşekkür, Kaynaklar, Şekil ve Tablolarla ilgili açıklamalar içermelidir. **Ana metin en fazla 5000 kelime olup kaynak sayısında bir kısıtlama yoktur.**

**5.3 Editöre Mektup:** Dergide yayınlanmış makaleler hakkında veya ilgili diğer konularda soru sormak, görüş bildirmek isteyenlerin yazıları bu türde değerlendirilir. Bu tür yazılarda kapsam ve etik kavramlar göz önünde bulundurulur. **Ana metin en fazla 1000 kelime olup kaynak sayısı 10’u geçmemelidir.**

## 6. MAKALENİN HAZIRLANMASI

•***Sayfa boyutu, sayısı ve kenar boşlukları:*** A4 formatında, en fazla 15 sayfa olmalıdır. Tüm kenarlardan 2 cm boşluk bırakılmalıdır.

•***Sayfa numaraları:*** Sayfa numaraları sayfa altında ve ortada verilmelidir. Sayfa numarası Times New Roman yazı tipinde ve 11 punto olmalıdır.

•***Satır numaraları:*** Satır numaraları makalenin ilk sayfasından itibaren başlayarak ve "sürekli" olarak numaralandırılmalıdır (her sayfada yeniden başlat ve/veya her bölümde yeniden başlat özellikleri kullanılmamalıdır).

•***Satır boşlukları:*** Bütün satır boşlukları Times New Roman karakterinde ve 11 punto olmalıdır.

• ***Gövde Metni*****:** Ana metin "Times New Roman" karakterinde "11 punto" ile "iki yana yaslı" ve anahtar düzeyi "gövde metni" olarak ayarlanmalı, sağ ve sol satır girintisi olmamalı, metinden önceki ve sonraki aralık değerleri 0nk olmalı ve satır aralık değeri tek (1) olarak yazılmalıdır. Noktalama işaretlerinden (nokta, virgül, noktalı virgül vb.) sonra bir karakter boşluk bırakılmalıdır. Her paragraf arasında bir satır boşluk bırakılmalı, paragraf başlarında içerden başlanmamalıdır (ilk satır girintisi veya Tab tuşu kullanılmamalıdır).

• ***Makale başlığı (Türkçe ve İngilizce):*** Sayfa başından 1 satır boşluk bırakıldıktan sonra, Türkçe başlık Times New Roman, 14 punto, koyu, tek satır aralıklı ve ortalı olarak yazılmalıdır. Türkçe başlıktan sonra 1 satır boşluk bırakılmalıdır. Daha sonra İngilizce başlık Times New Roman, 13 punto, italik, tek satır aralıklı ve ortalı olarak yazılmalıdır. Başlıklarda yer alan her kelimenin ilk harfi büyük olacak şekilde yazılmalı, otomatik başlık stilleri kullanılmamalıdır.

• ***Yazar adı veya adları:*** İngilizce başlıktan sonra 2 satır boşluk bırakılarak, unvan belirtilmeden, Adın ilk harfi büyük olacak şekilde tüm harfleri ve soyadın tamamı büyük harfle yazılmalıdır. Birden fazla yazarlarda aralarına virgül konularak, Times New Roman, 11 punto, kalın ve sayfaya ortalanarak yazılmalıdır. Sorumlu yazar isminde üst simge yıldız sembolü olmalıdır.

• ***Yazarın/ların adresi/leri ve ORCID bilgisi:*** Yazar adının hemen altına boşluk bırakılmadan, Times New Roman, 10 punto ve *italik* olarak yazılmalıdır. Adresleri aynı olan yazarlar için tek adres, farklı yazar adresleri alt alta boşluk bırakılmadan yazılmalıdır. Yayında yer alan tüm yazarların ORCID bilgileri mutlaka verilmelidir.

• ***İletişim yazarının bilgileri:*** Unvansız Ad soyad, e-mail adresi, telefon numarası (Tel: (xxx) xxx xx xx.) aralarına virgül konularak 1. sayfanın altına dipnot olarak, (*) sembolü ile belirtilmelidir, Times New Roman, 10 punto ile yazılmalıdır.

• ***Türkçe Öz*****:** Adres/ler den 2 satır boşluk bırakıldıktan sonra, ***Öz*** kelimesi Times New Roman yazı karakterinde, 11 punto, ***koyu*** ve sola dayalı olarak yazılmalıdır. Özetin gövde metni ise Times New Roman yazı karakterinde, 11 punto, iki yana yaslı, tek satır aralıklı ve girinti olmadan yazılmalıdır. Özet metninin 250 kelimeyi geçmemesine özen gösterilmelidir. Öz başlığı ile özetin gövde metni arasında boşluk bırakılmamalıdır.

• ***İngilizce Öz (Abstract):*** Türkçe anahtar kelimelerin altına 2 satır boşluk bırakılarak, **Abstract,** kelimesi Times New Roman yazı karakterinde, 11 punto, ***koyu,*** *italik,* tek satır aralıklı ve sola dayalı olarak yazılmalıdır. Abstract gövde metni Times New Roman yazı karakterinde, 11 punto, tek satır aralıklı ve *italik* olarak yazılmalıdır. Abstract metninin 250 kelimeyi geçmemesine özen gösterilmelidir. Abstract kelimesi ile abstract metni arasında boşluk bırakılmamalıdır.

• ***Anahtar kelimeler / Keywords:*** *"Anahtar kelimeler"* Türkçe özetin altına bir satır boşluk bırakılarak Times New Roman, 11 punto ve tek satır aralıklı yazılmalıdır. En az 3 en fazla 6 adet anahtar kelime verilmeli, "Anahtar kelimeler" yazısı **koyu**, verilen diğer kelimeler ise koyu olmadan yazılmalıdır. Her kelimenin ilk harfi büyük ve aralarına virgül konularak verilmeli ve alfabetik sıralamaya uygun olarak sıralanmalıdır. "*Keywords"* kelimesi İngilizce özetin altına bir satır boşluk bırakılarak Times New Roman, 11 punto, tek satır aralıklı, *italik* ve **koyu** yazılmalıdır.

İngilizce anahtar kelimeler (Keywords), Türkçe anahtar kelimelerde verilen sıralama dikkate alınarak yazılmalı, kelimeler koyu olmamalıdır.

• ***Ana başlıklar:*** Ana Başlıklar sırasıyla numaralandırılmalıdır (**1. Giriş 2. Amaç, Gereç ve Yöntem** gibi). ***Tüm başlıklar*** sola dayalı Times New Roman, 11 punto **koyu** ve her kelimenin ilk harfi büyük yazılmalıdır. Ana başlıklardan önce ve sonra 1 satır boşluk bırakılmalıdır. ***Alt başlıklar,*** ana başlık numarasına uygun olarak numaralandırılmalıdır. ***Tüm alt başlıklar*** sola dayalı Times New Roman, 11 punto, ***koyu*** ve ***italik*** olarak her kelimenin ilk harfi büyük olacak şekilde yazılmalıdır (***2.1. Malzeme 2.2. Deney Numunelerinin Hazırlanması,*** gibi). Alt başlıklardan önce ve sonra tek satır boşluk bırakılmalıdır. Başlıkları yazarken otomatik başlık stili, madde işaretleri, çok düzeyli liste gibi biçimler kullanılmamalı, düz metin şeklinde yazılmalıdır.

• ***Şekiller, Resimler ve Fotoğraflar:*** Sayfa sınırlarını asmayacak şekilde ortalanarak, net ve okunaklı olmalıdır. Sıra ile numaralandırılmalıdır. Şekil no ve adları şeklin altında şeklin sol alt kenarına yaslanarak ve sadece ilk kelimenin ilk harfi büyük olarak verilmelidir. Şekiller ya bir çizim programı ile çizilmiş olmalı ya da en az 300 dpi çözünürlükte taranmış olmalıdır. Şekil olarak gösterilen grafik, resim ve metin kutularında yer alan yazı ve sayıların büyüklüğü makale içinde Times New Roman karakteri ile yazılmış 9 punto boyutundaki bir yazının büyüklüğünden az olmamalıdır. Şekilden önce, şekil adından önce ve sonra birer satır boşluk bırakılmalıdır. **Şekiller metin içine yerleştirilirken mutlaka şekilden önce atıfta bulunulmalıdır. Şekil yazılarında (metin içerisinde ve ilgili şekillerin altında) otomatik şekil yazısı stili kullanılmamalı, düz metin şeklinde yazılmalıdır.**

• ***Tablolar:*** Sayfa sınırlarını aşmayacak şekilde ortalanarak konulmalıdır. Sıra ile numaralandırılmalıdır. Tablo no ve adları, tablonun sol üstünde tek satır boşluk ile sadece ilk kelimenin ilk harfi büyük olacak şekilde yazılmalıdır. Tablo adı yazılırken üstte ve altta birer satır, tablodan sonra yine bir satır boşluk bırakılmalıdır. **Tablolara tablodan önce mutlaka metin içerisinde atıfta bulunulmalıdır.** Tablo satır ve sütunlarındaki rakam ve yazılar Times New Roman 11 punto ile yazılmalıdır. Ancak zorunlu kalınan durumlarda yazı boyutu yazı sınırlarını geçmeyecek şekilde en az 9 puntoya kadar düşürülebilir. **Tablo yazılarında (metin içerisinde ve ilgili tabloda) otomatik şekil yazısı stili kullanılmamalı, düz metin şeklinde yazılmalıdır.**

• ***Denklemler:*** Metin içerisine yazılacak denklemler, Word yazım programındaki denklem editörü veya MathType editörü ile sola dayalı olarak yazılmalı ve eşitliklere sağa dayalı olarak parantez içerisinde sıra ile numara verilmelidir.

• ***Semboller:*** Makale çok sayıda sembol içeriyor ya da makaledeki sembollerin açıklanması gerekiyorsa uluslararası standarda uygun olarak, semboller, kaynaklardan önce, Times New Roman 11 punto ile *italik* yazılmalıdır. Makalede ondalık gösterimde nokta kullanılmalı, binlikleri ayırırken virgül kullanılmalıdır.

• ***Kaynaklar:*** Kaynaklar tez içerisinde "**soyadı ve tarih sistemine**" göre yazılmalıdır. Her kaynak kendi orijinal dilinde verilmelidir. Kaynak eserin yazımının bir satırdan daha uzun olması halinde ikinci satır ve diğer satırlar, ***değinilen ilk eserin yazar ilk adının baş harfi hizasından başlayarak yazılmalıdır (yazar soyadının uzun olması durumunda ikinci satır 1 cm içeriden başlamalıdır). Takip eden kaynaklar, ilk kaynağın ikinci satır hizasından başlamalıdır.*** Dergi adları ise kısaltma yapılmadan ve altı çizili olarak yazılır. Kaynaklar aşağıda verilen yönergelere göre yazılmalıdır:

**1- Metin içerisindeki referanslara atıfta bulunma**

1.1. Cümle içerisinde atıf verilen yazar ismine değinildiği durumlarda yıl parantez içerisinde yazılmalıdır.

"Popüler bir çalışmada Harvey (1992) konu ile ilgili olarak ……"

"David ve Clifford'a (2003) göre ..."

"Matthews ve Jones (1997) yapmış oldukları çalışmalarda …"

1.2. Cümle içerisinde atıf verilen ancak yazar ismine değinilmeyen durumlarda hem yazar ismi hem de yıl parantez içerisinde yazılmalıdır. Birden çok atıf verilmiş ise iki atıf arası noktalı virgül ile ayrılmalıdır.

"Daha yeni bir çalışma (Stevens, 1988) göstermiştir ..."

"Doğu Pontidler, 'Kuzey Zon' ve 'Güney Zon' olmak üzere iki bölüme ayrılarak tanımlanmıştır (Özsayar vd., 1981; Güven, 1993)."

1.3. İki ve daha fazla atıf verilmiş ise sıralama yıl temel alınarak geçmişten günümüze doğru yazılmalıdır.

"Eosen ve sonrası gelişmiş volkanik aktiviteler sonucu meydana gelmiştir (Adamia vd., 1977; Şengör ve Yılmaz, 1981; Akıncı, 1984; Arslan vd., 1997; Arslan ve Aslan, 2006; Aslan, 2010)."

1.4. Aynı yazarın birden fazla eserine atıf verilmiş ise, eserlerin yılı dikkate alınarak geçmişten günümüze doğru yazılmalıdır.

"Derinoba ve Kayadibi granitleri (Kaygusuz vd., 2012a,b, 2013), Özdil Granitoyidi, Soğuksu ve Seslikaya granitleri (Kaygusuz vd., 2013, 2016) oluşturmaktadır."

"Birkaç yazar tarafından tartışıldığı gibi (Smith, 1993, 2003; Brown, 1995; Smith ve Jones, 1997; Green, 2004)…"

1.5. Metin içerisinde yazarı belli olmayan internet kaynaklarına atıf yapılırken, büyük harflerle URL-sıra numarası (,), yıl şeklinde yazılmalıdır.

Örneğin: (URL-4, 2003), (URL 1 ve 2, 2003)

1.6. Kaynakların yazılması sırasında literatürde yaygın olarak bilinen periyodik dergilerin adları açık olarak yazılmalıdır.

Örneğin: Mineralogy and Petrology, Journal of Geology and Mining Research, Journal of Food Engineering, Gondwana Research.

**2- Kaynaklar (Referanslar) Bölümünün Hazırlanması**

**2.1. Ulusal ve Uluslararası Makaleler:**

Gücer, M.A., Arslan, M., Sherlock, S. ve Heaman, L.M., 2016. Permo-Carboniferous granitoids with Jurassic high temperature metamorphism in Central Pontides, Northern Turkey. Mineralogy and Petrology, 110, 943-964.

Le Breton, N. ve Thompson, A.B., 1988. Fluid-absent (dehydration) melting of biotite in metapelites in the early stages of crustal anatexis. Contributions to Mineralogy and Petrology, 99, 226-237.

Gücer, M.A., Aydınçakır, E., Yücel, C. ve Akaryalı, E., 2017. Tersiyer Yaşlı Altınpınar Hornblendli Andezitlerinin (Torul-Gümüşhane) Petrografisi, Mineral Kimyası ve P-T Kristalleşme Koşulları. Gümüşhane Üniversitesi Fen Bilimleri Enstitüsü Dergisi. 7 (2), 236-267, doi: 10.17714/gumusfenbil.310263.

Kabul edilmiş ancak sayı almamış veya baskı aşamasındaki makaleler:

Çimen, O., Göncüoğlu, M.C., Simonetti, A. ve Sayıt, K., 2017. Whole rock geochemistry, Zircon U-Pb and Hf isotope systematics of the Çangaldağ Pluton: Evidences for Middle Jurassic Continental Arc Magmatism in the Central Pontides, Turkey. Lithos, doi: 10.1016/j.lithos.2017.06.020.

Hoffman, H.J. ve Masson, M., 1994. Archean stromatolites from Abitibi greenstone belt, Quebec, Canada. Geological Society of America Bulletin, 106 (baskıda).

### 2.2. Kitaplar:

Hem, J.D., 1989. Study and Interpretation of the Chemical Characteristics of Natural Waters: USGS Professional Paper, 2254, US Gov. Print. Office, 263p.

Postel, S., 2000. Son Vaha, Su Sıkıntısıyla Karşı Karşıya, (çev: F. Şebnem Sözer), TUBİTAK-TEMA VAKFI yayınları, ISBN 975-403-188-6, Ankara, 218s.

Twiss, R.J., ve Moores, E.M., 1992. Structural geology: New York, W.H. Freeman and Company, 532 p.

Burchfiel, B.C., Hodges, K.V. ve Royden, L.H., 1992. The South Tibetan detachment system, Himalayan orogen: Extension contemporaneous with and parallel to shortening in a collisional mountain belt: Geological Society of America, Special Paper, 269, 41p.

### 2.3. Tezler:

Dağ, S., 2007. Çayeli (Rize) ve Çevresinin İstatistiksel Yöntemlerle Heyelan Duyarlılık Analizi. Doktora Tezi, Karadeniz Teknik Üniversitesi Fen Bilimleri Enstitüsü. Trabzon, 241s.

Tezcan, L., 1993. Karst Akifer Sistemlerinin Trityum İzotopu Yardımıyla Matematiksel Modellemesi, Doktora Tezi, Hacettepe Üniversitesi Fen Bilimleri Enstitüsü. Ankara, 125s.

### 2.4. Raporlar:

Aslaner, M., 1972. Çayeli-Madenköy Cu-Pb-Zn Aramaları Hakkında Kısa Not, MTA Maden Etüd Rap. No. 118.

Baran, I. ve Kasparek, M., 1989. Marine Turtles of Turkey; Status Survey 1988 and Recommendations for Conservation and Management: WWF Report, Heidelberg, 123p.

IAEA, 1992. Statistical Treatment of Data on Environmental Isotopes, Technical Reports Series No.331, IAEA Vienna, 781p.

Akartuna, M., 1953. Çaycuma-Devrek Yenice-Kozcağız Bölgesinin Jeolojisi Hakkında Rapor: MTA Rap. No. 2059 (yayımlanmamış), Ankara.

Altun, İ.E., Şengün, M., Keskin, H., Akçaören, F., Sevin, M., Deveciler, E. ve Akat, M.U., 1990. 1/100.000 Ölçekli Açınsama Nitelikli Türkiye Jeoloji Haritaları Serisi, Kastamonu-B17 Paftası: MTA Gen. Müd. Jeoloji Etütleri Dairesi, Ankara.

### 2.5. Editörlü Kitaplar:

Zuber, A., 1986. Mathematical models for the interpretation of environmental radioisotopes in groundwater systems. Handbook of Environmental Isotope Geochemistry. Fritz, P. and Fontes, J.Ch. (Eds.), Elsevier, Amsterdam. pp. 1-59.

Akıncı, Ö.T., 1984. The Eastern Pontide volcano-sedimentary belt and associated massive sulphide deposits, in: Dixon, J.E., Robertson, A.H.F. (Eds), The Geological Evolution of the Eastern Mediterranean: Geological Society, London, Special Publications 17(1), 415-428.

Aydın, M., Demir, O., Özçelik, Y., Terzioğlu, N. ve Satır, M., 1995. A geological revision of Inebolu, Devrekani, Ağlı and Küre areas: new observations in Paleotethys-Neotethys sedimentary successions, in: Erler, A., Ercan, T., Bingöl, E., Örçen, S. (Eds.), Geology of the Black Sea region. MTA, Ankara, Special Publication, pp. 33-38.

Boynton, W.V., 1984. Cosmochemistry of the rare earth elements; meteorite studies, in: Henderson, P. (Eds.), Rare earth element geochemistry. Elsevier Science Publishing Co., Amsterdam, pp. 63-114.

Hippolyte, J.C., Müller, C., Kaymakçı, N., Sangu, E., 2010. Dating of the Black Sea basin: New Nannoplankton ages from its inverted margin in the Central Pontides (Turkey), in: Stephenson, R.A., Kaymakci, N., Sosson, M., et al. (Eds). Sedimentary basin tectonics from the Black Sea and Caucasus to the Arabian Platform. Geological Society London Special Publications 340, 113-136.

**2.6. Bildiriler Kitabı:**

Sualtı Günleri-1999, Türkiye'de Sualtı Görüntüleme, Belgeleme ve Arşivleme Çalışmalarının Günümüzdeki Durumu, 26-27 Şubat 1999, Bildiriler Kitabı (editörler: B. Akınoğlu, M. Draman), Sualtı Araştırmaları Derneği, Ankara, 84s.

**2.7. Bildiri Özeti:**

Tezcan, L., Gunay, G., Hotzl, H., Reichert, B. ve Solomon, K., 1997. Hydrogeology of the Kirkgozler Springs, Antalya, Turkey. International Conference on Water Problems in the Mediterranean Countries, 17-21 November 1997, Near East Technical University, Nicosia, North Cyprus. p.76.

Bayarı, C.S., Kurttaş, T. ve Tezcan, L., 1998b. Köyceğiz Gölü Karışım Dinamiği: Çevresel Izotoplar ve Üç Boyutlu Yerinde Yoğunluk Ölçümleri. MTA Cumhuriyetin 75. Yıldönümü Yerbilimleri ve Madencilik Kongresi Bildirileri, 2-6 Kasım 1998, Ankara, s.104-106.

Gücer, M.A. ve Aslan, Z., 2011. Evaluation of diagenesis and metamorphism relationship by using clay mineral indices in the Yoncayolu (Üzümlü, Erzincan) area. International European Clay Conference, Antalya, Book of abstracts, s. 281.

Akaryalı, E., Aydınçakır, E., Atay, U., Gücer, M.A. ve Türk, E., 2015. Mass change calculation of hydrothermal alteration in Kaletaş-Söğütağıl area (Gümüşhane, NE Turkey). The World Multidisciplinary Earth Sciences Symposium (WMESS), Prague, Abstracts, p. 232.

**2.8. Tam Metni Basılı Bildiriler:**

Hamarat, S., Ülkenli, H. ve Türe, G., 1998. Türkiye kıyıları Aydıncık-Taşucu Deniz Mağaraları Sualtı Araştırmaları, Sualtı Bilim ve Teknoloji Toplantısı, Aralık 1998, İstanbul, Türkiye, s.105-111.

**2.9. Aktüel Dergi ve Gazete Haberi:**

Corliss, Richard, 1993. Sept. 13, Pacific Overtures. Time 142(11), 68-70.

Feder, Barnaby J, 1993. December 18, For Job Seekers, a Toll-Free Gift of Expert Advice. New York Times 30 (late ed.).

**2.10. İnternet Kaynakları:**

Başaran, A., Yıldırım, N. ve Gülal, Z. (2000, 14 Ekim). Depreme karşı nasıl bir bina yapmalı? Cumhuriyet Bilim Teknik, http://bilimteknik.cumhuriyet.com.tr-/w/b08.-html.

OCMIP, 2000., Ocean Carbon-Cycle Model Intercomparison Project, IGBP, Global, Analysis, Interpretation And Modeling Task Force, Http:/www.lpsl.jussieu.-fr/OCMIP.

URL-1, www.tdk.gov.tr/TR/Genel/BelgeGoster. 05 Ağustos 2011.

GÜMÜŞHANE ÜNİVERSİTESİ FEN BİLİMLERİ ENSTİTÜSÜ DERGİSİ
GÜMÜŞHANE UNIVERSITY JOURNAL OF SCIENCE AND TECHNOLOGY INSTITUTE
GÜMÜŞHANE ÜNİVERSİTESİ / GÜMÜŞHANE UNIVERSITY